Characterisation and Regulation of a Novel Lysyl Hydroxylase, JMJD7

By Charlotte Devon Eaton

A thesis submitted to the College of Medical and Dental Sciences, the University of Birmingham, for the degree of

DOCTOR OF PHILOSOPHY

Institute of Cancer and Genomic Sciences

College of Medical and Dental Sciences

University of Birmingham

February 2019

Abstract

Post-translational modifications (PTMs) are found throughout cell biology and are essential for normal cell growth and survival. Hydroxylation is a PTM that is generally catalysed by a family of enzymes known as 2-oxoglutarate (2OG) oxygenases. A sub-family of 2OG oxygenases with a 'Jumonji-C' (JmjC) catalytic domain have important regulatory functions in gene expression control and are often deregulated in disease. However, within this family of enzymes there remain a number of uncharacterised "orphan" enzymes, whose substrates remain unknown and potential roles in disease is not yet investigated. One of these orphan enzymes is Jumonji-C Domain 7 (JMJD7). Here, we contribute to the first biochemical characterisation of JMJD7, which is an active 2OG oxygenase with lysyl hydroxylase activity towards the Developmentally Regulated GTP binding Proteins, DRG1 and DRG2. Furthermore, we investigate a role for JMJD7 and pathway components in cancer, with our findings indicating potential tumour suppressive functions, including in gastric cancer. Cancer mutation analysis identified "hot-spots" within the JMJD7 gene which may be of functional importance. One cancer mutation hot-spot centres around a conserved N-terminal threonine phosphorylation site, indicative of a potential novel regulatory domain. However, the role of phosphorylation in regulating JMJD7 function and the kinase responsible for this modification were not known. Our work demonstrates that JMJD7 phosphorylation contributes to its role in growth, is cell cycle regulated, and may be catalysed by a cyclin-dependent kinase. Finally, we discuss the outcomes in the wider context and look towards the future directions of this project.

Acknowledgments

First and foremost I would like to thank my supervisor Dr Mat Coleman, for his continual guidance and support over the past 4 years, for being a friend when I needed and for being an excellent academic mentor.

I would also like to thank all other members of the Tumour Oxygenase Group, both past and present specifically: Uncaar Bora for cloning help and the early morning pep-talks; Dr Qinqin Zhuang for JMJD7 support; Dr Sally Fletcher, Charlotte Hall, Eline Hendrix, Dr Athanasios Ploumakis and Dr Helen Smith;

The “Awesome Foursome”: Kyle Connolly, Matt ‘Tuti’ Taylor and James Bundred for financially crippling me through mass caffeine consumption and consoling me over a strong beverage.

To my funders, The University of Birmingham and the AE Hills Scholarship.

Finally to my parents, Su and John Eaton, for financially assisting my caffeine dependence and their endless support.

Table of Contents

Table of Figures

Chapter 3:

Exploring the Potential for Deregulation of the JMJD7 Pathway in Cancer

Chapter 4:

Investigating the Role of Phosphorylation in Regulating the Biological Function of JMJD7

Chapter 5:

JMJD7 phT37 Regulation and Kinase ID

Chapter 6:

Final Discussion

Table of Tables

List of Abbreviations

2OG - 2-oxoglutarate

3' - 3 prime end of DNA

5' - 5 prime end of DNA

AcyC - Adenoid Cystic Carcinoma

Adeno -Adenocarcinoma

ARD -Ankyrin Repeat Domains

ARID - AT-rich interaction domain

ATM - Ataxia-Telangiectasia Mutated

ATP - Adenosine Triphosphate

ATR - Ataxia Telangiectasia and Rad3-related

AurkB - Aurora Kinase B

CAK - CDK Activating Kinase

CCLE - Cancer Cell Line Encylopedia

CDK - Cyclin Dependant Kinase

CDKL - Cyclin Dependant Kinase-like

CEP192 - Centrosomal Protein 192

ChIP - Chromatin Immunoprecipitation

CMGC Kinases - Kinase family named after members: CDK, MAPK, GSK, CDKL

COSMIC - Catalogue of Somatic Mutations in Cancer

CPM - Counts per Million

CRTAP - Cartilage-associated Protein

CS - Carcinosarcoma

CTD - C-terminal Transactivation Domain

Cyc - Cyclin

CypB - Cytophilin B

Da –Dalton

DAPI - 4′,6-diamidino-2-phenylindole

DFRP – DRG Family Regulatory Proteins

DLBCL - Diffuce Large B-Cell Lymphoma

DMOG – Dimethyl oxalyglycine

DMSO - DiMethyl SulfOxide

DNA – Deoxyribonucleic Acid

Dox – Doxycycline

DRG - Deveopmentally regulated GTP-binding Protein

DSBH - Double Stranded Beta Helix

DYRK - Dual-specificity Tyrosine Regulated Kinase

ECM - Extra Cellular Matrix

emPAI - Exponentially Modified Protein Abundance Index

EMT - Epithelial Mesenchymal Transition

ER – Endoplasmic Reticulum

eRF1 - Eukaryotic Release Factor 1

EV – Empty Vector

FACS – Fluorescence Assisted Cell Sorting

FIH - Factor Inhibiting HIF

G1 phase - Gap 1 phase

G2 phase - Gap 2 phase

GFP – Green Fluorescence Protein

GSK - Glycogen Synthase Kinase

GTP - Guanosine Triphosphate

HA-tag – Hemagglutinin tag.

HCLK2 - Human Biological Clock Protein 2

HEK293T – Human Embryonic Kidney 293 expressing large T

HIF - Hypoxia Inducible Factor

HIPK - Homeo-domain Interacting Protein Kinase

HNSCC - Head and Neck Squamous Cell Carcinoma

HR - Hairless Protein

HRE - HIF Responsive Element

HTH - Helix-Turn-Helix

IP - immunoprecipitate

JmjC – Jumonji Cupin domain

JMJD7 –Jumonji Domain Containing protein 7

KDa – Kilodalton,

KDM - Lysine Demethylase

LH - Lysyl Hydroxylase

M phase – Mitosis phase

MAPK - Mitogen Activateed Protein Kinase

MINA53 - Myc Induced Nuclear Antigen, 53 kDa

MS – Mass Spectrometry

MT - Methyltransferase Domain]

MTS - 3-(4,5-Dimethylthiazol-2-yl)-5-(3-carboxymethoxyphenyl)-2-(4-sulfophenyl)-2H-tetrazolium, inner salt

NCL-60 - National Cancer Institute mixed cell lines

NEPC - Neuroendocrine Prostate Cancer

NES – Nuclear Export Sequence

NLS – Nuclear Localisation Sequence

NO66 - Nucleolar Protein 66kDa

NSCLC - Non-small Cell Lung Cancer

OGFOD - 2-oxoglutarate and Fe(II) dependent oxygenase Domain

OHyW - Hydroxywybutosine

OSX -Osterix

P3H - Proline-3 Hydroxylase

P4H - Proline-4 Hydroxylase

PBS - Phosphate Buffered Saline Solution

PCR - Polymerase Chain Reaction

PDI - Protein disulphide isomerase

PHF - Plant Homeodomain Finger

PHD - Prolyl Hydroxylase Domain

phT37 - Phosphorylated Threonine 37 on JMJD7

PKA - Protein Kinase A

PLA2G4B – Phospholipase A2 beta

PTM – Post-translational Modification

Rb - Retinoblastoma Protein

RFP – Red Fluorescence Protein

RNA – Ribonucleic Acid

RNAi - RNA interference

RRM - RNA Recognition Motif

S phase - Synthesis phase

S5D2L - Ribosomal Protein S5 2-like

SDS – Sodium dodecyl sulfate

shRes –shRNA resistant

TBS - Tris-Buffered Saline

TGS Domain - Domain found in ThrRSs, GTPase, Spot proteins

TRAFAC - Translation Factor

TSS - Transcriptional Start Site

U2AF65 - U2 Small Nuclear Ribonucleoprotein Auxillary Factor 65kDa

UPR - Unfolded Protein Response

Uterine CEC - Corpus Endometrial Carcinoma

UTR – Untranslated Region

UTX - Ubiquiously Transcribed telopeptide repeat X Chromosome protein

UTY - Ubiquiously Transcribed telopeptide repeat Y Chromosome protein

VHL - von Hippel Lindau

WT – Wildtype

Wy - Wybutosine

XLID - X-linked Intellectual Disability

Chapter 1
Introduction

In this thesis I investigate a previously uncharacterised 2-oxoglutarate oxygenase, JMJD7. I have contributed to the basic characterisation of the enzyme and explored how JMJD7 is regulated by cancer mutation and phosphorylation. I have begun to identify the JMJD7 kinase and to investigate how phosphorylation modulates JMJD7 function. This Introduction will therefore aim to provide an overview of the current literature surrounding the 2OG oxygenase enzyme family, with a focus on protein hydroxylases most closely related to JMJD7.

1.1 Post-translational Modifications

The human genome encodes approximately 25,000 genes. However, due to post-transcriptional and post-translational processing this number increases to ~1.8 million protein species, partly due to ~200 different types of 'post-translational modifications' (PTMs) (Jensen, 2004, International Human Genome Sequencing, 2004, Kho et al., 2004): (Khoury et al., 2011). Generally, PTMs involve the covalent attachment of a molecule to a protein (the top 10 most frequent PTMs proven experimentally are shown in Table 1.1). These modifications are present in a broad spectrum of cellular processes and can have diverse consequences, including on; protein localisation, activity, function, degradation and substrate specificity (Knorre et al., 2009). In fact, >60% of all PTMs reside within protein-protein interaction domains, and are therefore thought to modulate protein complexes (Duan and Walther, 2015). The PTM network is extremely mulitfaceted and can involve independent events or cross-talk between modifications (Duan and Walther, 2015). For example, ubiquitin is typically associated with cross-talk between other modifications and modifying enzymes (Pickart, 2004). As such, there are reports of ubiquitin cross-talk with sumoylation,

acetylation, phosphorylation, hydroxylation and methylation, among others (Zhao et al., 2014, Cockman et al., 2000).

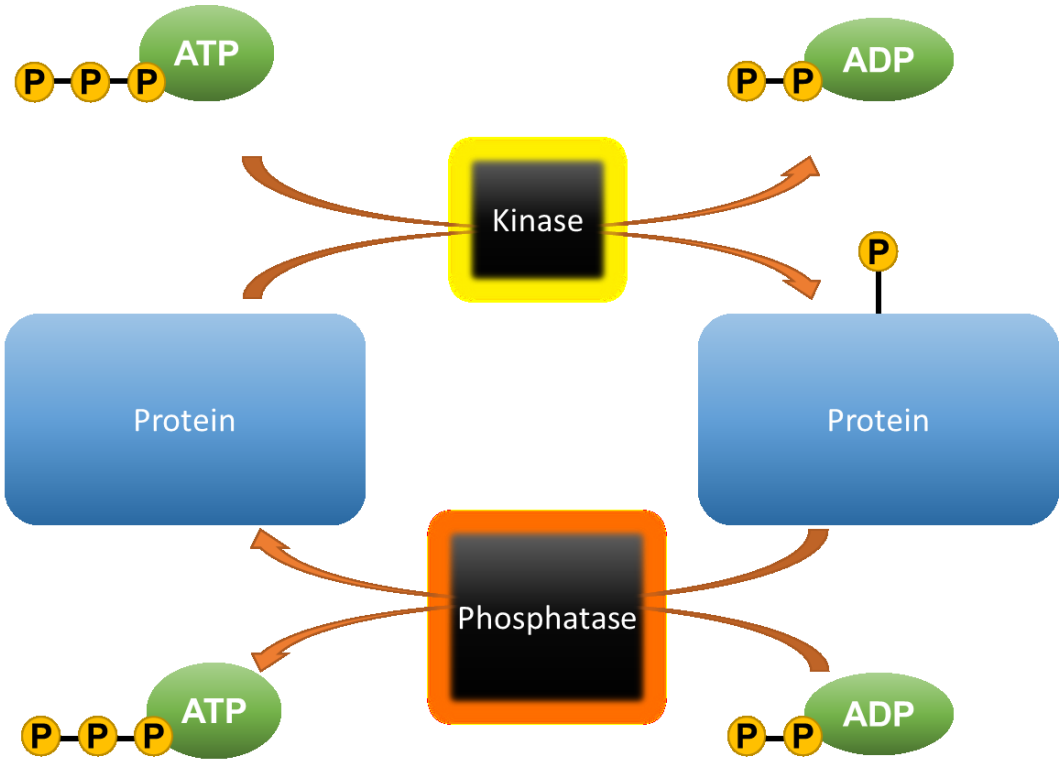

Figure 1.1 Protein phosphorylation and dephosphorylation. Kinases catalyse protein phosphorylation. During the reaction the kinase transfers one phosphate group from the bound adenosine triphosphate (ATP) to its substrate protein, generating adenosine diphosphate (ADP). The reverse is true for dephosphorylation, a phosphatase removes the phosphate group bound to the protein which generates ATP from ADP.

Table 1.1 List of Top 10 experimentally proven PTMs with description and example. Total numbers correct as of September 2018.

Type of modification	Description	Example Ref	Total number (Khoury et al., 2011)
Phosphorylation	Addition of a phosphate group (80Da, PO_4) to Serine, Threonine or Tyrosine residues.	(Baba et al., 2011)	58,383
Acetylation	Attachment of an acetyl group from Acetyl Coenzyme A onto either: - Amino group of the N-terminus - Amino group of Lysine	(Kuhns et al., 2018)	6751
N-linked glycosylation	Addition of a carbohydrate to the nitrogen of an asparagine. Occurs in in the endoplasmic reticulum.	(Sareneva et al., 1995)	5526
Amidation	Oxidation of a glycine which is then cleaved into two products, including N-term or C-term amidated peptide.	(Merkler, 1994)	2844
Hydroxylation	Addition of a hydroxyl group onto the side chain of an amino acid. Types include: lysine, arginine, aspartic acid, asparagine, histidine, proline.	(Markolovic et al., 2018)	1619
Methylation	Addition of a methyl group (CH_3) (15Da) on to a Lysine or Arginine.	(Clarke et al., 2017)	1523
O-linked glycosylation	Addition of a carbohydrate to the oxygen of a serine or threonine. Occurs in the golgi apparatus.	(Harvey and Haltiwanger, 2018)	1133
Ubiquitination	The addition of a small (8kDa) ubiquitin protein. Lysine residues within the ubiquitin peptide can also be ubiquitinated. Polyubiquitin chains convey varying functions.	(Hwang et al., 2018)	878
Pyrrolidone Carboxylic Acid	Lactam derivative of glutamic acid.	(Moro et al., 2018)	826
Sulfation	Addition of a sulfo group (SO_3H).	(Mueller et al., 2018)	504

Phosphorylation

Phosphorylation is the reversible attachment of an 80 Da phosphate group (PO_4) to another molecule. Although protein phosphorylation is the most abundant type, other molecules can also be phosphorylated i.e. lipids. On proteins, enzymes known as kinases catalyse the phosphorylation of specific amino acid side chains including serine, threonine or tyrosine, and phosphatases reverse the reaction (Figure 1.1). There are over 500 kinases in the genome making this the largest family of enzymes (Johnson, 2009, Knorre et al., 2009). Phosphorylation involves transferring the gamma-phosphate group from adenosine triphosphate (ATP) to a protein substrate, yielding a phospho-protein and adenosine diphosphate (ADP) (Figure 1.1) (Cheng et al., 2011). The activation of kinases generally requires phosphorylation of a conserved tyrosine residue within an 'activation loop', sometimes by autophosphorylation (e.g. DYRKs, HIPKs), in a tightly regulated process that often involves multiple feedback loops (Himpel et al., 2001, Harvey et al., 2005, Lolli and Johnson, 2005). The addition of a small phosphate group leads to a significant change in the local biochemistry due to the addition of a negative charge, which can trigger changes in protein conformation and protein-protein interactions through electrostatic attraction and repulsion. Experimental studies have shown that the addition of negative charge by substituting the phosphorylated site to aspartic acid (D) or glutamic acid (E) can sometimes be used as an effective tool to mimic protein phosphorylation (Yang et al., 2013, Guerra-Castellano et al., 2016).

Protein phosphorylation can act as a molecular switch between functional states. As such it has been observed throughout many aspects of cell biology, including (but not limited to); protein translocation, substrate specificity, enzyme activation, targeting for peptidyl-isomerase activity, mediating protein:protein interactions, and priming for

further PTMs (Harreman et al., 2004, Ortmann et al., 2016, Baba et al., 2011, Estey et al., 2013, Cole et al., 2006, Nishi et al., 2011). The biology surrounding phosphorylation is complex, tightly regulated and often overlapping. As such, several kinases may target the same residue on a substrate and conversely, one kinase may target multiple residues on the same protein. For example, both Dual-specificity Tyrosine Regulated Kinase 2 (DYRK2) and Homeodomain Interacting Protein Kinase 2 (HIPK2) target p53 Ser46 in response to DNA damage. Furthermore, both 'Ataxia Telangiectasia Mutated' (ATM) and 'ATM- and RAD3-related' (ATR) target multiple sites on BReast CAncer susceptibility gene (BRCA) 1 (Taira et al., 2007, Puca et al., 2009, Miller and Turk, 2018, Tibbetts et al., 2000).

One significant example of phosphorylation that is essential for growth is the Mitogen Activated Protein Kinase (MAPK) pathway. MAPKs are involved in almost all cellular processes via signalling from the cell surface into specific regulatory pathways (Chang and Karin, 2001). This pathway is primarily formed of three tiers: the MAPK kinase kinases (MAPKKK), the MAPK kinases (MAPKK) and the MAPKs (Dhillon et al., 2007). As their names might suggest, the MAPKKKs reside at the top of the pathway and respond to extra-cellular signalling to activate the MAPKKs, and in turn the MAPKs. Activation of different MAPKs will have varying effects on cellular function (Gutkind, 2000). Most protein kinases have specific substrate recognition motifs (Biondi and Nebreda, 2003). As such, MAPKs rely on a 'docking site' for substrate recognition which is separate from the phosphorylation site (Holland and Cooper, 1999). This docking sequence allows stringent substrate specificity by providing a site for the kinase to bind before phosphorylation occurs. For the MAPKs, this recognition motif is [R/K]-[X_{2-6}]-[I/L]-X-I/L and mutation of either the basic or

hydrophobic residues in this sequence can negatively affect kinase binding (Bardwell et al., 2003). Taken together, it is clear that interplay between protein modifying enzymes is complex and is an important area of molecular biology to consider in functional studies.

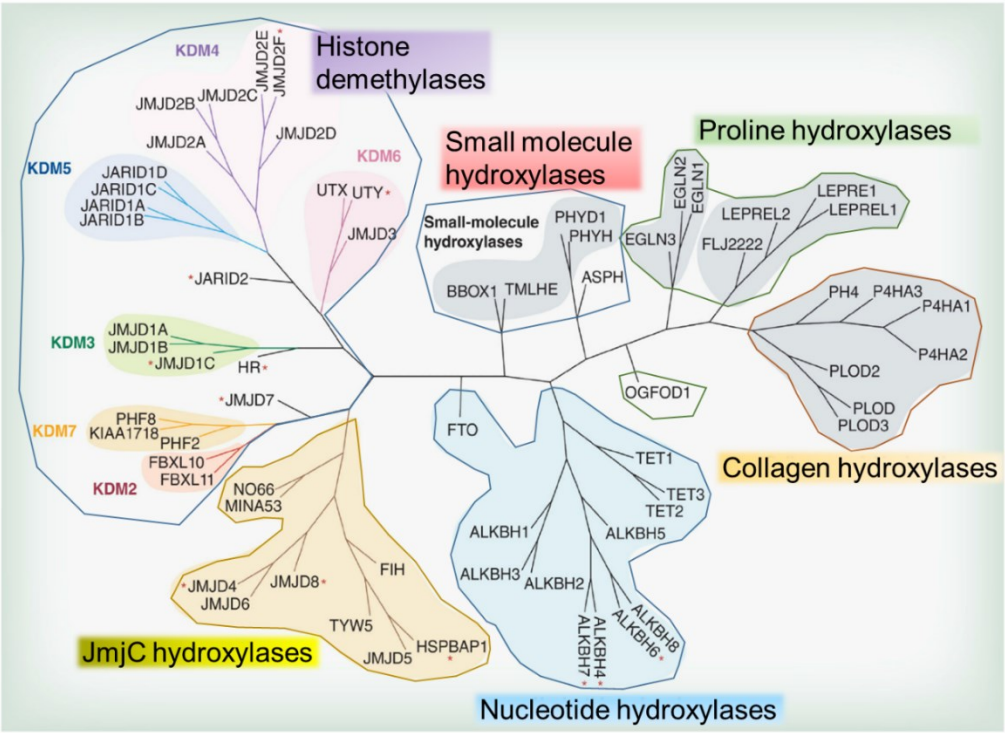

Figure 1.2 Phylogenetic tree of 2OG oxygenases. Highlights the six main families of 2OG oxygenases; histone demethylases, proline hydroxylases, collagen hydroxylases, nucleotide hydroxylases, small molecule hydroxylases and JmjC hydroxylases. Figure used from: Figure 1, (Johansson et al., 2014)

1.2 2-Oxoglutarate Oxygenases

In contrast to phosphorylation, protein hydroxylation is a relatively new area of PTM research. Protein hydroxylation is the covalent modification of an amino acid side chain by an oxygen atom to form an alcohol group. It is generally catalysed by a family of enzymes known as '2-oxoglutarate (2OG) oxygenases' (Figure 1.2) (Johansson et al., 2014). The first 2OG oxygenases were identified as collagen prolyl- and lysyl- hydroxylases in 1967 and were found to be essential for proper collagen extra-cellular fibril formation (discussed in more detail below) (Kivirikko and Prockop, 1972). Since then, it has become clear that 2OG oxygenases can catalyse hydroxylation of other amino acids in addition to proline and lysine, including histidine, asparagine, aspartate and arginine.

As their name suggests, 2-oxoglutarate (2OG) oxygenases require the Kreb's cycle intermediate 2-oxoglutarate (also known as α-ketoglutarate) as a cofactor for catalysis, in addition to Fe(II) and oxygen (Figure 1.3a). 2OG oxygenases are a family of ~70 enzymes (Johansson et al., 2014) which are conserved throughout evolution, suggesting that hydroxylation serves a fundamental role in biology (McDonough et al., 2010). These enzymes catalyse the hydroxylation or demethylation of their substrate. In such cases of demethylation, the hydroxylated methyl group results in an unstable hydroxy-methyl group which, in turn, produces a demethylated substrate, and formaldehyde (Figure 1.3b). Due to the requirement for 2OG, oxygen and Fe(II), 2OG oxygenases have the potential to function as intracellular nutrient sensors (Webb et al., 2009, Schofield and Ratcliffe, 2004). The 2OG oxygenases can be broadly sub-divided into groups according to their biochemical specificities, which include histone and DNA demethylation and RNA,

DNA and protein hydroxylation (Ploumakis and Coleman, 2015). Importantly, although the substrate specificity of these enzymes can differ, the catalytic mechanism is conserved. Briefly, the catalytic domain, present in all 2OG oxygenases, consists of a double-stranded β-helix (DSBH) made of two 4-stranded anti-parallel β-sheets which, when folded, provides a substrate binding pocket (Martinez and Hausinger, 2015). Within this catalytic domain lies an essential Fe(II) binding motif known as the HxD/E…H facial triad that lies at the open end of the binding pocket. Theoretically, however, Asn, Cys, His, Gln and Tyr residues may also coordinate Fe(II) in the absence of the conserved HxD/E…H facial triad (McDonough et al., 2010).

The mechanism for hydroxylation by 2OG oxygenases is complex and currently not fully understood (Markolovic et al., 2015). Illustrated in Figure 1.3b, a solvent-exposed Fe(II) is coordinated to the 2OG oxygenase with octahedral geometry by the HxD/E…H facial triad. Catalysis occurs when 2OG displaces two coordinating water molecules and binds to the Fe(II) via the C1 carboxyl group and ketone. Binding of the prime substrate to the enzyme, but not directly to Fe(II), displaces the remaining Fe(II)-bound water molecule, allowing O_2 to bind in its place. Binding of this oxygen initiates the oxidative decarboxylation of 2OG, releasing CO_2 and generating a succinate bound to a ferryl intermediate. It is suggested that the presence of this ferryl-oxo group promotes the formation of a radical intermediate on the substrate, which then facilitates hydroxylation (Martinez et al., 2015) (McDonough et al., 2010). Some 2OG oxygenases require ascorbate as an additional cofactor, and although its exact purpose remains unknown, it is thought to act as a reducing agent upon Fe(II) (Kuiper and Vissers, 2014).

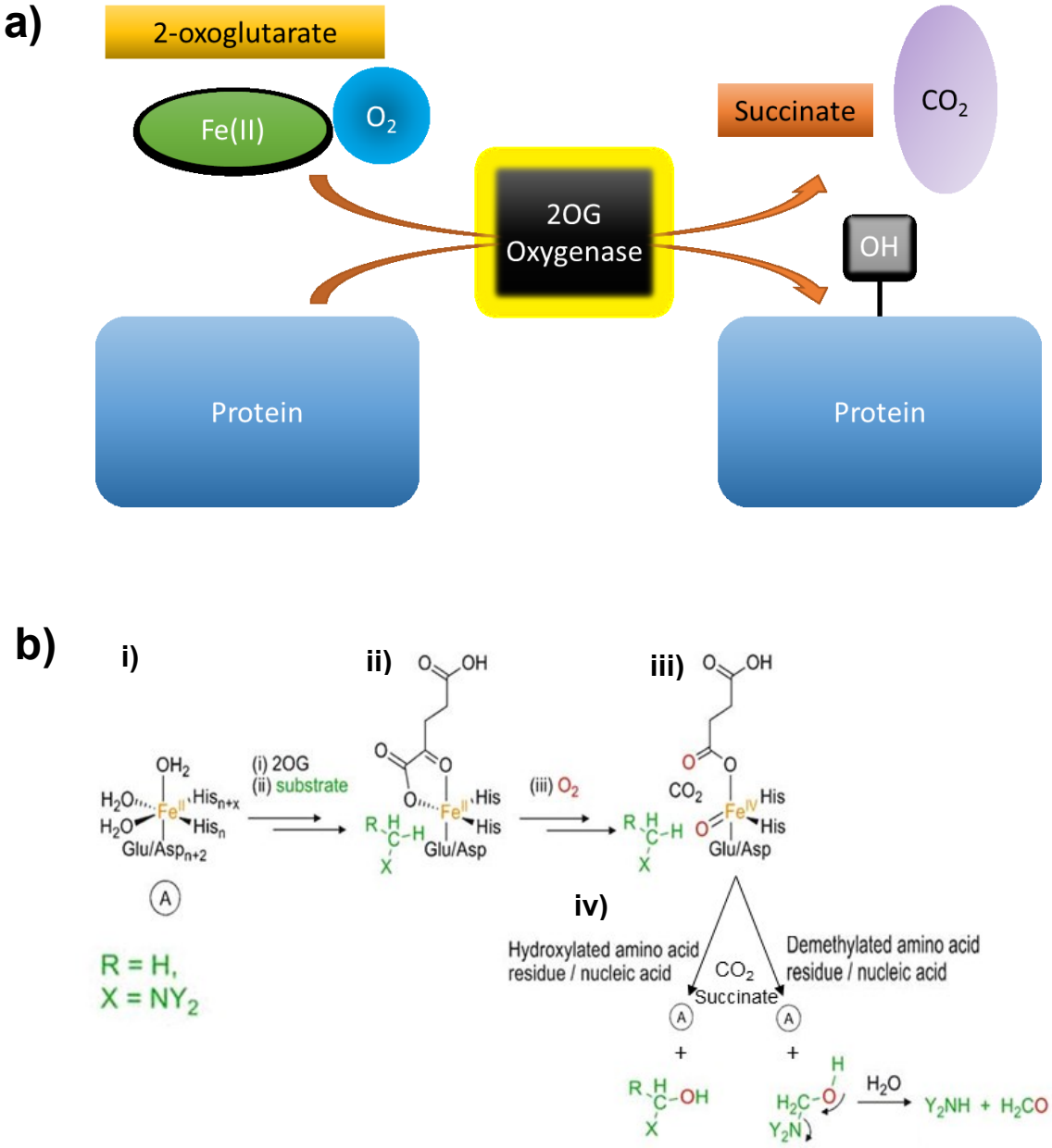

Figure 1.3 The Hydroxylation reaction catalysed by 2OG oxygenases. (a) Basic schematic of protein hydroxylation as catalysed by 2OG oxygenases. 2OG, Fe(II) and oxygen are co-factors. After hydroxylation of the substrate, succinate and CO_2 are produced as by-products. (b) i) The Fe(II) is bound to the enzyme with octahedral geometry. Two water molecules are displaced from Fe(II) upon 2OG binding (ii), and a third is displaced by binding of the prime substrate, providing a docking site for oxygen (iii). Oxidative decarboxylation of 2OG yields succinate, CO_2 and a ferryl-oxo species. Hydroxylation occurs (iv) via a reaction between the prime substrate and the ferryl-oxo species. Demethylation happens when the resulting hydroxylation creates an unstable hydroxy-methyl-lysine, which fragments into formaldehyde and a demethylated lysine. Figure adapted from: Figure 1, (McDonough et al., 2010).

Almost all 2OG oxygenases have been implicated in disease, particularly cancer (Ploumakis and Coleman, 2015). Although cancer is widely known as the unstoppable proliferation of cells, there are six key characteristics (Figure 1.4), or hallmarks, which distinguish a cancer cell from a normal cell (Hanahan and Weinberg, 2011) these will be described below.

Indeed, "*Sustaining Proliferative Signalling*" is arguably the most important trait which the cell needs to acquire in order to continue dividing and progress through the cell cycle. Under normal conditions, cell surface receptors signal for cell cycle progression which initiates a cascade of signals to prompt the cell out of senescence and into G1. However, when a cell becomes a cancer cell deregulation of these signals result in sustained and uncontrolled proliferation. This can be enhanced by cancer cells increasing the number of receptors on their cell surface, thereby promoting sensitivity to extra-cellular signals. Furthermore, cancer cells can signal to surrounding cells to stimulate proliferation of normal cells. Deregulation of this extent would normally trigger a cellular response by tumour suppressors, but another hallmark of cancer: the "*Evasion of Growth Suppressors*" highlights that tumour suppressors often become deregulated. For example, RetinoBlastoma protein (RB), Merlin and P53 are *bona fide* tumour suppressors which are inactive in the majority of cancers. Inactivation of such essential proteins provides an uninhibited environment for proliferating cells.

When normal cells become abnormal they can activate pathways which lead to cell death for example, apoptosis, autophagy and necrosis. A cancer cell, however, is programmed to resist such mechanisms. The hallmark "*Resisting Cell Death*" describes how can cells can upregulate the expression of anti-apoptotic and

pro-survival genes while increasing the expression of anti-survival and pro-apoptotic factors. Furthermore, cancer cells which enter into an autophagic state can enter into a reversible dormancy which enables survival of late stage tumours. Moreover, necrotic cells release regulatory factors which initiate proliferation of proximal cells.

Cells which have gained the ability to sustain prolonged proliferation must also be able to consistently and successfully replicate its genome. The fourth hallmark of cancer (Hanahan and Weinberg, 2011) "*Enabling Replicative Immortality*" highlights the importance of genome integrity to the immortal cell. Telomerase is essential for this process because it is an enzyme required for the maintenance of structures located at the end of telomeric DNA known as the telomere repeats. As normal cells divide telomere repeats shorten thereby limiting the number of times a cell can replicate its genome. In immortalised cells telomerase is expressed at a significantly higher level than in normal cells which enables sustained DNA replication of the proliferating cells.

Malignant tumour cells require the transportation of nutrients both into and out of the cell, similar to a normal cell. Therefore, the fifth hallmark of cancer is "*Inducing Angiogenesis*" (Hanahan and Weinberg, 2011). Angiogenesis, the formation of new vessels, provides a highway in which the tumour can receive the oxygen and other nutrients it requires to continue proliferating, and to excrete wastes such as carbon dioxide.

Finally, malignant tumours can "*Activate Invasion and Metastasis",* the sixth hallmark of cancer (Hanahan and Weinberg, 2011). The process of tumour invasion and metastasis starts with the local invasion of tumour cells within the same

microenvironment. This progresses into intravasation where the malignant cells enter and travel along nearby blood and lymphatic vessels. The cancer cells then disperse into the lymphatic and haematogenous systems before exiting into the parenchyma of the invading tissue.

These six hallmarks of cancer are fundamental characteristics for the progression of most cancer types.

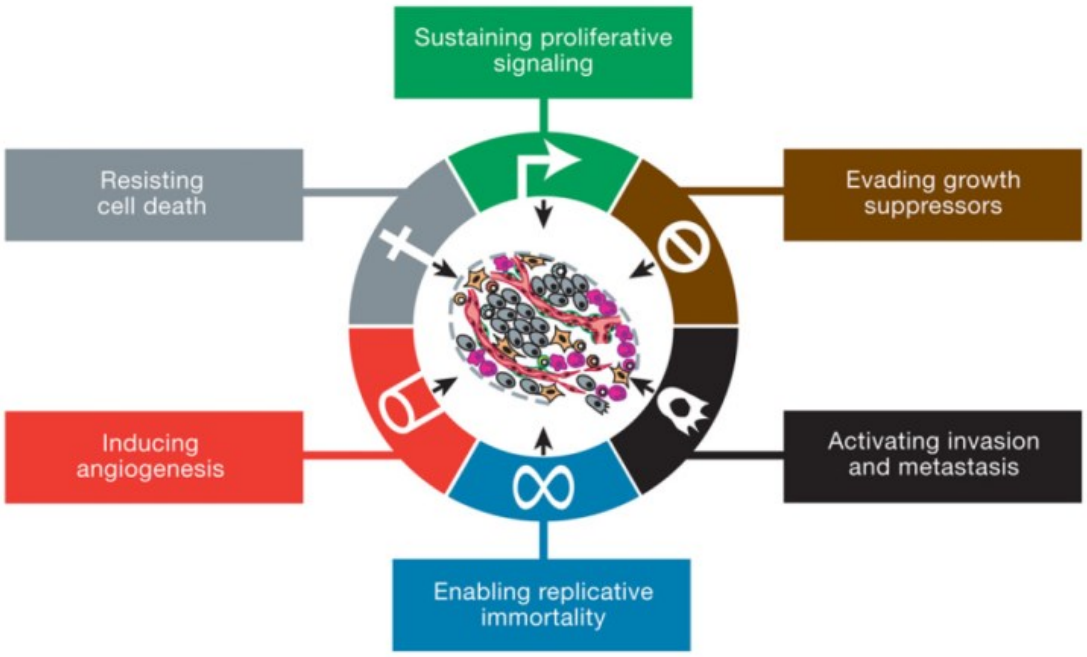

Figure 1.4. The Six Hallmarks of Cancer. Cancerous cells display six characteristics which distinguish them from normal cells. These hallmarks are required for cancer progression and are involved in prognosis. Figure from (Hanahan and Weinberg, 2011)

1.2.1 Nucleotide Hydroxylases

2OG oxygenases with assigned nucleotide hydroxylase activity so far consist of the ALKBH sub-family, the TET enzymes and TYW5 (Figure 1.2) (TYW5 will be discussed later). Between them, they catalyse the hydroxylation of double stranded and single stranded DNA and RNA.

ALKBH enzymes

There are nine ALKBH enzymes (ALKBH1-8 and Fat Mass and Obesity-associated protein (FTO)), which have evolved from an *E.coli* orthologue, AlkB. AlkB is involved in the repair of alkylated nucleotides through demethylation of 1-methyladenine (1-meA) and 3-methylcytosine (3-meC) (Trewick et al., 2002). Although ALKBH1 is the most structurally similar to AlkB (sharing 18.5% sequence identity), the function of ALKBH1 remains controversial (Westbye et al., 2008). Initial studies suggested ALKBH1 is a mitochondrial DNA and RNA demethylase with specificity towards 3-methylcytosine (3-meC) (Westbye et al., 2008). In contrast, ALKBH1 has also been reported as a nuclear histone demethylase targeting histone H2A with functions in neuronal differentiation (Ougland et al., 2012). More recently however, ALKBH1 was identified as a tRNA demethylase regulating translation via positive control of methionine tRNA ubiquitination (Liu et al., 2016).

ALKBH2 and ALKBH3, on the other hand, are *bona fide* DNA and RNA demethylases with similar function to *E. coli* AlkB. Both ALKBH2 and ALKBH3 localise to the nucleus and function as 1-meA and 3-meC demethylases in RNA, single-stranded DNA (ssDNA) and double-stranded DNA (dsDNA) (Fu et al., 2015). The alkylated nucleotides, 1-meA and 3-meC, inhibit DNA replication and are known to be cytotoxic (Sedgwick, 2004). Therefore, ALKBH2 and ALKBH3 function is important in the DNA damage repair pathway. In contrast, ALKBH4 and ALKBH7 are

speculated to be involved in protein modification because their acidic nature does not allow for association with a negatively charged nucleic acid backbone (Bjornstad et al., 2012). In line with this, a study investigating global gene regulation showed that ALKBH7 regulates genes involved in the cell cycle and spermatogenesis, possibly due to an effect on histone methylation status. Although ALKBH4 showed similar effects, these were less striking (Bjornstad et al., 2012). ALKBH5 and FTO are, within the ALKBH family, the most structurally similar. They both localise to nuclear speckles and share a conserved mRNA N^6-methyladensoine (m^6A) demethylase function (Zheng et al., 2013, Jia et al., 2011). Studies have shown that mRNA m^6A demethylation promotes mRNA stability via the m^6A reader protein, YTHDF1, demonstrating the emergence of an additional layer to gene regulation (Wang et al., 2015b, Fu et al., 2014). Knockdown of ALKBH5 results in viable but infertile mice (Zheng et al., 2013, Landfors et al., 2016). The function of ALKBH6 remains elusive, however it likely functions as an iron-dependent 2OG oxygenase since it contains the conserved HxD/E…H iron binding facial triad (The UniProt, 2017).

The final ALKBH enzyme, ALKBH8, contains an RNA recognition motif (RRM) and a SAM-dependant methyltransferase domain (MT). Interestingly, ALKBH8 is thought to have an opposing role to its demethylase homologues, ALKBH2 and ALKBH3, by functioning as a tRNA methyltransferase (Fu et al., 2010). Acting in the DNA damage repair pathway, ALKBH8 promotes the generation of 5-carboxymethyl-uridine (mcm^5U) at the wobble codon of tRNA, the final step in tRNA biogenesis (Songe-Moller et al., 2010, Fu et al., 2010). Interestingly, depletion of ALKBH8 results in sensitivity to DNA damaging agents and high expression is associated with bladder cancer progression (Ohshio et al., 2016, Fu et al., 2010, Shimada et al., 2009).

TET enzymes

TET1, TET2 and TET3 are orthologues of *Trypanosoma* 2OG oxygenases, JBP1 and JBP2. They were first described as 5-methylcytosine (5meC) hydroxylases by Tahiliani et al. (2009) and later as enzymes involved in the formation of 5-formylcytosine (5fC) and 5-carboxylcytosine (5caC) during DNA demethylation at CpG sites. The exact role that 5-hydroxymethylcytosine (5hmeC) plays in mammalian DNA demethylation is yet to be fully elucidated (Ito et al., 2011, Kafer et al., 2016). Currently, there are two distinct theories on the mechanisms by which DNA demethylation occurs (Rasmussen and Helin, 2016). Firstly, active DNA demethylation begins with the formation of 5hmeC from 5meC, which is sequentially oxidised into 5fC, and then the carboxylic acid derivative, 5caC by the TET enzymes: 5fC and 5caC moieties are removed by the base excision repair pathway and replaced with an unmodified cytosine. Alternatively, 5hmC may also interfere with the activity of DNA methyltransferase 1 and 2 (DNMT1 and DNMT2) which in turn reduces DNA methylation (Ito et al., 2011, Maiti and Drohat, 2011).

1.2.2 Collagen Prolyl Hydroxylases

Collagen is the most abundant protein in humans and constitutes a third of all proteins in the human body. Mature collagen is found in the extra cellular matrix (ECM) and is essential for growth in human tissues (Gelse et al., 2003). Collagen is composed of three left handed polypeptide chains which coil around one another to form one right handed super coil (Shoulders and Raines, 2009). The α-chain triple helix is at the centre of the peptide, at each end lies a (N-terminal or C-terminal) propeptide, and a telopeptide (proximal to the propeptide). Collagen biosynthesis involves many types of PTMs including 3-hydroxyproline (3-HyP), 4-hydroxyproline (4-HyP), hydroxylysyine (Hyl), galactosylhydroxylysyine and

glucosylgalactosylhydroxylysine. Together, these modifications stabilise collagen strands, thus supporting collagen excretion into the ECM and function in fibril formation (Figure 1.5) (Gjaltema and Bank, 2017). Here, we describe the families of 2OG oxygenases that catalyse collagen proline hydroxylation and summarise why each modification is important for the efficient production of mature collagen.

Hydroxylation of collagen is performed by three groups of 2OG oxygenases: Prolyl-3-hydoxylases (P3Hs), Prolyl-4-hydroxylases (P4Hs) and lysyl hydroxylases (LHs).

P4Hs

The first 2OG oxygenases implicated in collagen biosynthesis were proline-4-hydroxylase alpha I, II and III (P4HA1, P4HA2 and P4HA3, respectively). Human P4HA1 and P4HA2 share 64% amino acid sequence identity but only 35% and 37% with P4HA3, respectively (Kukkola et al., 2003). They all localise to the lumen of the endoplasmic reticulum (ER) and hydroxylate immature collagen chains in the C-4 position of proline in the sequence X-Pro-Gly, prior to the formation of the triple helix. In cells, they each form a $\alpha_2\beta_2$ tetramer where the β subunit is the protein disulfide isomerase (PDI), also known as P3HB, and the α-subunit is one of P4HA1, 2 or 3 (Kivirikko and Myllyharju, 1998, Kukkola et al., 2003, Gjaltema and Bank, 2017). If the α-subunit is unable to bind to the β-subunit, it will form aggregates and be catalytically inactive (Gjaltema and Bank, 2017). In this $\alpha_2\beta_2$ complex, an N-terminal substrate binding domain is responsible for substrate recognition. After hydroxylation of the substrate the PDI subunits perform disulphide isomerase activity upon the substrate before returning the complex to the rough endoplasmic reticulum (rER) via a C-terminal Lys-Asp-Glu-Leu (KDEL) retention signal (Wilkinson and

Gilbert, 2004). The 4-HyP residues are essential for proper formation of the collagen triple helices via intramolecular hydrogen bonding (Myllyharju, 2003). Interestingly, in humans there have been no mutations found in the coding regions of the P4HA genes, suggesting that any mutation may be fatal to the human embryo (Gjaltema and Bank, 2017).

The P4Hs have been studied in the context of physiology and disease. P4HA1 has been identified as a potential target for glioblastoma treatment due to its function in pro-neovascularisation via regulation of vascular endothelial growth factor isoform, VEGF165b, to promote the formation of blood vessels. Furthermore, in the same study mouse xenograft models also showed delayed growth in P4HA1 knockdown tumours compared to control (Zhou et al., 2017).

P4HA2 is upregulated in pancreatic ductal carcinoma patients with “short” survival consistent with it supporting tumourigenesis (Hu et al., 2018). Moreover, other studies have found P4HA2 to be a reliable prognostic marker in breast cancer stem cells, triple negative breast cancer, Diffuse Large B-Cell Lymphoma (DLBCL) and functions associated with invasion and metastasis (Moon et al., 2015, Xiong et al., 2014, Jiang et al., 2018, Liu et al., 2018b, Hu et al., 2018). Less is known about P4HA3, but similar to P4HA2 it has also been identified as a potential negative prognostic marker in breast cancer (Winslow et al., 2016).

P3Hs

There are three functionally active P3H enzymes, P3H1, P3H2 and P3H3 (also known as Leprecan-1, Leprecan like protein-1, and Leprecan like protein-2, respectively: see Figure 1.2). They catalyse the hydroxylation of proline in the Y position of the Y-4HyP-Gly sequence on collagen strands, subsequent to

hydroxylation by the P4H enzymes (Johansson et al., 2014). All P3H enzymes have an N-terminal endoplasmic reticulum (ER) retention sequence and are therefore localised to the lumen of the ER and golgi (Tiainen et al., 2008). P3H1 forms a 1:1:1 complex with cartilage-associated protein (CRTAP) and cytophilin B (CypB) to target the fibril forming type I collagen for 3-prolyl hydroxylation (Vranka et al., 2004). This complex performs several functions in the formation of procollagen fibrils. These include prolyl hydroxylation (functioning as a molecular chaperone), peptidyl prolyl isomerase activity, and a role in the prevention of premature aggregates of immature collagen in the rough ER (rER) (Ishikawa et al., 2009b, Morello et al., 2006). On the other hand, P3H2 has a preference for hydroxylating type IV collagen strands, although it also maintains capacity to hydroxylate other non-type I fibril forming collagens (Tiainen et al., 2008, Fernandes et al., 2011). Interestingly, two independent P3H2 null mouse models show conflicting phenotypes, where one resulted in embryonic lethality at E6.5 due to blood clots forming around the embryo, whereas the other study observed no significant phenotype (Hudson et al., 2015, Pokidysheva et al., 2014). Hudson et al. (2015) speculated that the difference between the observed phenotypes is likely due to additional, off target effects caused by the retention of the neo cassette after recombination of the FLP-FRT sites by Pokidysheva et al. (2014), a phenomenon also observed and reviewed by Olson et al. (1996). Finally, P3H3 acts in a complex along with a CRTAP family member, SC65, and the collagen lysyl hydroxylase LH1 (LH's will be discussed below) (Heard et al., 2016, Hudson et al., 2017). Interestingly, although knockdown of SC65 and P3H3 resulted in a loss of lysyl hydroxylation of LH1 targets in collagen, the same was not observed for any known 3-hydroxyproline collagen residues, leaving the

identification of P3H3 enzymatic substrates open for future research (Heard et al., 2016, Hudson et al., 2017).

Mutations in collagen modifying enzymes often result in profound effects on human development, predominantly bone development. (Homan et al., 2014). Furthermore, recent evidence suggests that mutations in P3H2 can cause structural abnormalities in the eye leading to progressive myopia (Mordechai et al., 2011, Hudson et al., 2015).

In the context of cancer, P3H enzymes appear to play a predominantly tumour suppressive role with evidence to suggest they could also function as oncogenes in certain contexts. For example, down-regulation of P3H2 has been observed in primary breast cancer samples and in immortalised breast cancer cell lines via hypermethylation of the CpG island (Shah et al., 2009). Similarly, P3H3 gene methylation is found in primary breast cancer samples and a range of cancer cell lines. Furthermore, downregulation of P3H3 has been reported in lung tumours and hepatocellular carcinomas, and loss of all P3H enzymes was observed in lymphoma (Wang et al., 2013, Li et al., 2018, Hatzimichael et al., 2012, Shah et al., 2009). Taken together, P3H2 and P3H3 may be acting as tumour suppressors in these tissue types. Consistent with this, other studies have found that exogenous P3H3 expression in lung cancer cells leads to cell cycle arrest at the G2/M transition and altered expression of cell cycle related proteins, and that knockdown of P3H3 enhanced the invasion and migration of cancer cells (Li et al., 2018). On the other hand, P3H3 is upregulated in some bladder and thyroid cancer cell lines, perhaps indicative of an oncogenic role (Di Maro et al., 2014, Ho et al., 2012).

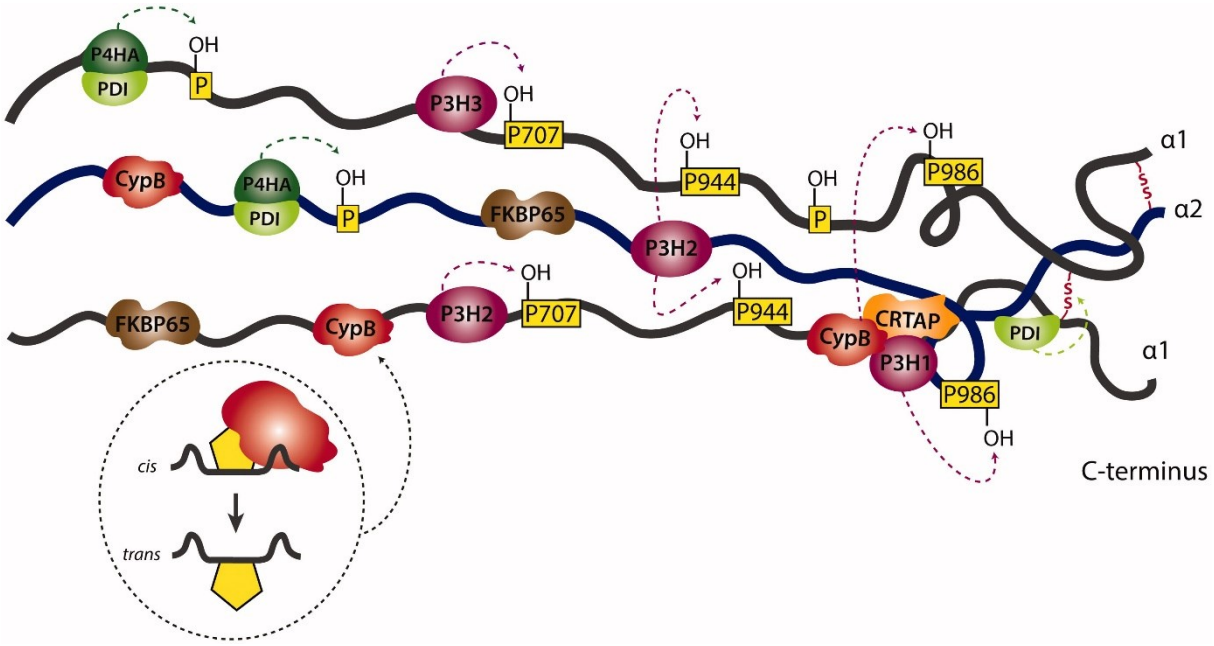

Figure 1.5 Proline hydroxylation of collagen by 2OG oxygenases. The first 2OG oxygenases to act upon collagen are the P4HA enzymes. They form a complex with PDI (green, top and middle chain) and hydroxylate immature collagen chains at the C-4 position in the sequence Xxx-Pro-Gly. The P3H hydroxylases have individual functions in the formation of mature collagen. P3H1 forms a complex with CRTAP and CypB to hydroxylate fibril forming collagen strands and performs *cis/trans* isomerisation to prevent premature association of the chains. P3H1 and P3H2 also have collagen hydroxylase activity. Adapted from Figure 3 (Gjaltema and Bank, 2017)

1.2.3 Lysyl Collagen Hydroxylases

The importance of lysine hydroxylation in cellular and extracellular processes was initially demonstrated by the lysyl hydroxylase (LH) family of enzymes, (coded by the PLOD genes) (Kivirikko and Prockop, 1972, Passoja et al., 1998). This group is comprised of three enzymes, LH1, LH2 and LH3, where LH2 is alternatively spliced into two variants known as LH2α and LH2β (Yeowell and Walker, 1999). Together they share approximately 60% overall sequence identity at the amino acid level. Hydroxylation catalysed by the LH enzymes mostly occurs in collagen within the

helical and telopeptide regions (Gjaltema and Bank, 2017). The recognition sequences for helical lysyl hydroxylation is different from that in the telopeptide regions. In the triple helix, only the C5 on the side chain of lysine residues found in the sequence Gly-Xxx-Lys sequence are hydroxylated (Figure 1.6) (Hautala et al., 1992). Similar to MINA53 and FIH (described below), dimerisation of all LH enzymes is required for full enzymatic activity (Chen et al., 2017). In the case of LH2 the peptidyl prolyl-isomerase, FKBP65, aids in the formation of the dimer (Chen et al., 2017). LH2 is responsible for the hydroxylation of the telopeptides. After hydroxylation, the hydroxyl-lysine (Hyl) residues are converted into the lysine derrivatives, allysine or hydroxyallysine, which enable crosslinking with residues in the α-helix of another strand (van der Slot et al., 2003, Yeowell and Walker, 1999). Similarly, the aforementioned LH1:P3H3:SC65 complex promotes LH1 dimerisation and subsequent α-helix lysyl hydroxylation (Heard et al., 2016, Hudson et al., 2017). Hydroxylation of lysine in the helical domains supports a docking mechanism for carbohydrates to bind, an essential step in the triple helical intermolecular crosslinks (Heikkinen et al., 2000). The main differences between the substrate specificity of LH1 and LH3 are the types of collagen targeted: Through studies on patients with Ehlers–Danlos syndrome (a syndrome characterised by mutations in collagen modifying enzymes) and Bruck syndrome, it has been shown that LH1 specifically targets lysines within α-helices in collagen type I, II and III, whereas LH3 specifically targets collagen type IV and V. Furthermore, LH3 is the only known enzyme capable of glucosyltransferase activity on galactosylhydroxylysyl within collagen strands. In addition to collagen, LH3 also hydroxylates ~10 other proteins with similar sequences (Heikkinen et al., 2000).

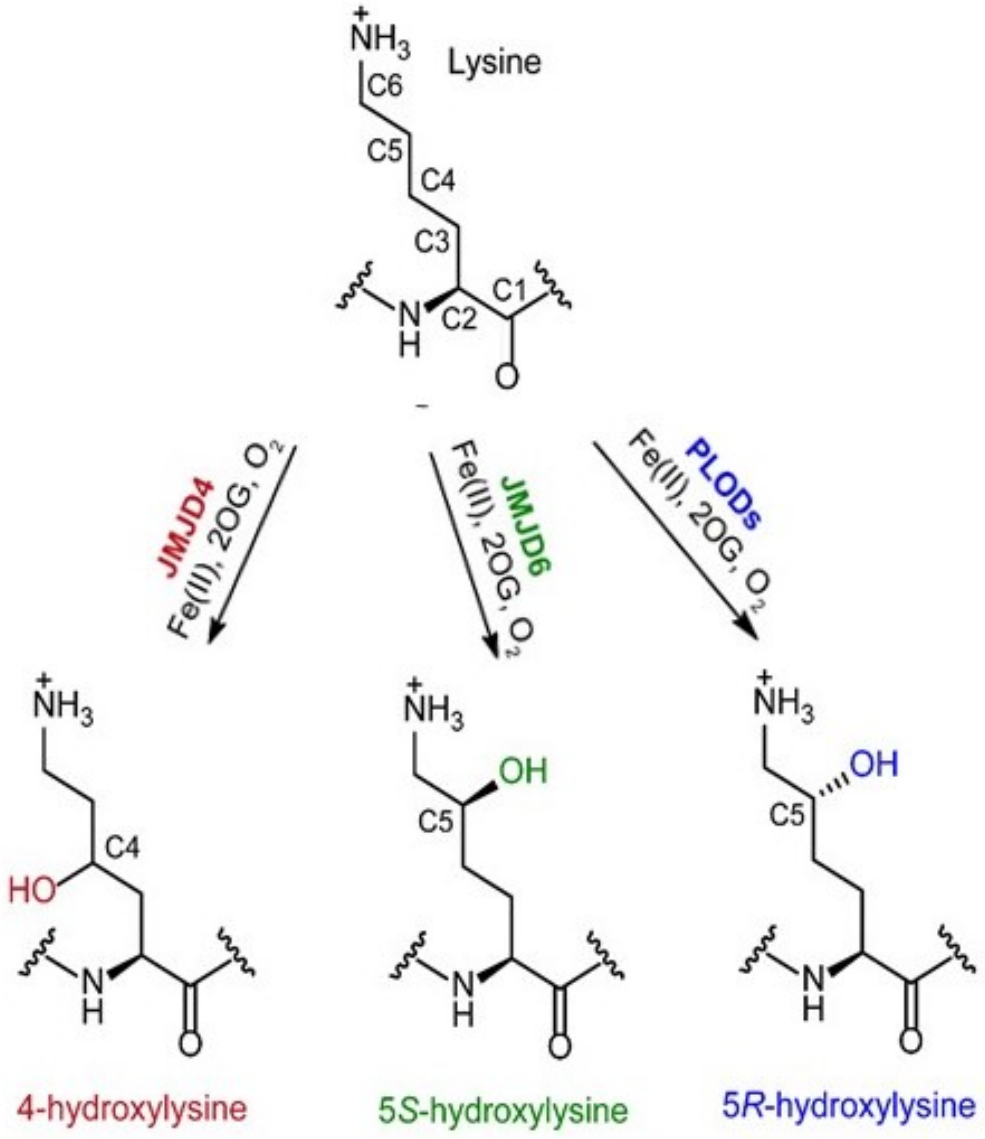

Figure 1.6 Types of lysine hydroxylation. Three type of lysine hydroxylation have been characterised: hydroxylation catalysed by the LH enzymes (PLODs) is C5 in the *R* geometry. Similarly, JMJD6 also catalyses the C5 lysine hydroxylation however, in the *S* geometry. JMJD4 specifically catalyses C4-lysine hydroxylation. Adapted from Markolovic et al., 2018

Although knockout mouse models of LH1 are viable and fertile, they show abnormal collagen fibril formation compared to wild type with some LH1 null mice dying due to spontaneous haemorrhages in the thoracic or abdominal cavity (Takaluoma et al., 2007).

The LH enzymes have been used as prognostic markers in various cancers, where low expression generally correlates with better survival (Noda et al., 2012, Dong et al., 2005, Tsai et al., 2018, Wang et al., 2018). Conversely, LH2 is a known positive regulator of tumour metastasis through the formation of mature 'collagen highways', along which tumour cells travel to the vasculature in order to metastasise (Eisinger-Mathason et al., 2013, Hollern et al., 2014, Song et al., 2017, Gilkes et al., 2013, Xu et al., 2017). Therapeutically, LH2 and 65-kDa FK506-binding protein (FKBP65) are under clinical investigation because FKBP65 inhibitors could prevent cancer metastasis in the absence of LH2 (Chen et al., 2017).

1.2.4 Prolyl Hydroxylase Domain enzymes

Hypoxia inducible factor (HIF) is a transcription factor which, under hypoxic conditions, is activated and controls expression of hypoxia related genes via their HIF responsive elements (HRE) (O'Rourke et al., 1997). In normoxia (~21% O_2), HIF is hydroxylated on two residues in its oxygen dependent domain (ODD) by three 2OG oxygenases: prolyl hydroxylase domain -1, -2 and -3 (PHD1, PHD2 and PHD3, respectively) (Epstein et al., 2001) . The two hydroxylation sites serve as a docking mechanism for the von Hippel Lindau (VHL) ubiquitin E3 ligase, resulting in HIF polyubiquitination and subsequent degradation (Figure 1.7). The PHD enzymes have a relatively low affinity for oxygen, compared to other 2OG oxygenases (Yang et al., 2014). Therefore, they are sensitive to changes in environmental oxygen levels: If the

O_2 concentration drops, the PHD enzymes become less active. Subsequent loss of HIF hydroxylation results in reduced ubiquitination and increased abundance of HIF (Figure 1.7) (Schofield and Ratcliffe, 2004).

The three PHD enzymes share 42-59% sequence identity to each other and are evolutionarily conserved in *C.elegans* and *D.melanogaster* (Hirsila et al., 2003, Epstein et al., 2001). Overexpression studies show distinct localisation of PHD1 in the nucleus, PHD2 exclusively in the cytoplasm and PHD3 evenly distributed between the nucleus and the cytoplasm (Metzen et al., 2003). The significance of this differential localisation is unknown, although it has been speculated that this could be important for nuclear HIF inactivation after reoxygenation of the cellular environment (Webb et al., 2009). Interestingly, during normoxia PHD2 is the most abundant and therefore dominant isoform, whereas PHD1 and PHD3 expression are only increased upon hypoxic conditions (Webb et al., 2009). Alternative splicing of each PHD enzyme generates additional catalytically active and inactive enzymes (Hirsila et al., 2003). PHD1 has two isoforms: the well characterised 43kDa protein, and a shorter 40.3kDa form. The smaller isoform is less stable, but similar to the major isoform, is regulated by oestrogen and displays comparable hydroxylase activity (Tian et al., 2006). In contrast, the alternative PHD2 isoforms are thought to be catalytically inactive and their functions are yet to be characterised. PHD3 is alternatively spliced into two additional enzymes of 17kDa and 24kDa where only the 24kDa protein displays hydroxylase activity (Tian et al., 2006). All PHDs display varied tissue distribution: PHD1 is found mostly in the testes, brain, kidney, heart and liver; PHD2 is expressed in most tissue types; and PHD3 is found predominantly in the heart, placenta and small intestines (Cioffi et al., 2003, Cervera et al., 2006). In addition to

their function as HIF hydroxylases, the PHD enzymes are reported to display HIF-independent functions. For example, PHD1 also functions in the cell cycle as a Centrosomal Protein 192kDa (CEP192) hydroxylase, and is a regulator of NF-kβ (Moser et al., 2013, Cummins et al., 2006, Ortmann et al., 2016). Furthermore, PHD3 is a regulator of cardiomyocyte apoptosis through interaction with Bcl-2 (Liu et al., 2010b), a regulator of glycolysis during hypoxia via interaction with PKM2 (Chen et al., 2011a), and a regulator of the cell cycle and DNA damage via hydroxylation of the human biological clock protein (HCLK2) protein (Xie et al., 2012). The assignment of alternative substrates of the HIF proyl hydroxylases remains controversial however.

1.2.5 OGFOD1

The 2-OxoGlutarate and Fe(II) dependent Oxygenase Domain containing 1 protein, or OGFOD1, is a prolyl hydroxylase targeting Proline 62 of the ribosomal RPS23 subunit (Singleton et al., 2014, Loenarz et al., 2014, Katz et al., 2014). OGFOD1 is one of four 2OG oxygenases to target ribosomal proteins, including JMJD5, MINA53 and NO66 (discussed later). Similar to some other 2OG oxygenase substrates, the exact function of OGFOD1 hydroxylation is not fully understood. However, hydroxylation of RPS23 is thought to effect ribosomal 'decoding' including translation termination efficiency (Singleton et al., 2014). OGFOD1 knockdown significantly reduced growth in proliferation assays of human cells, without effecting cell death. In contrast, increased apoptosis (and autophagy) was observed in a knockout model in *D.melanogaster* (Katz et al., 2014). Furthermore, it was reported in *D.melanogaster* that knockdown of Sudestada1 (the OGFOD1 orthologue) results in defects in the unfolded protein response (UPR). However, UPR appeared unaffected in mammalian

cells, possibly owing to differences in the complexity of the stress response pathways (Katz et al., 2014, Singleton et al., 2014).

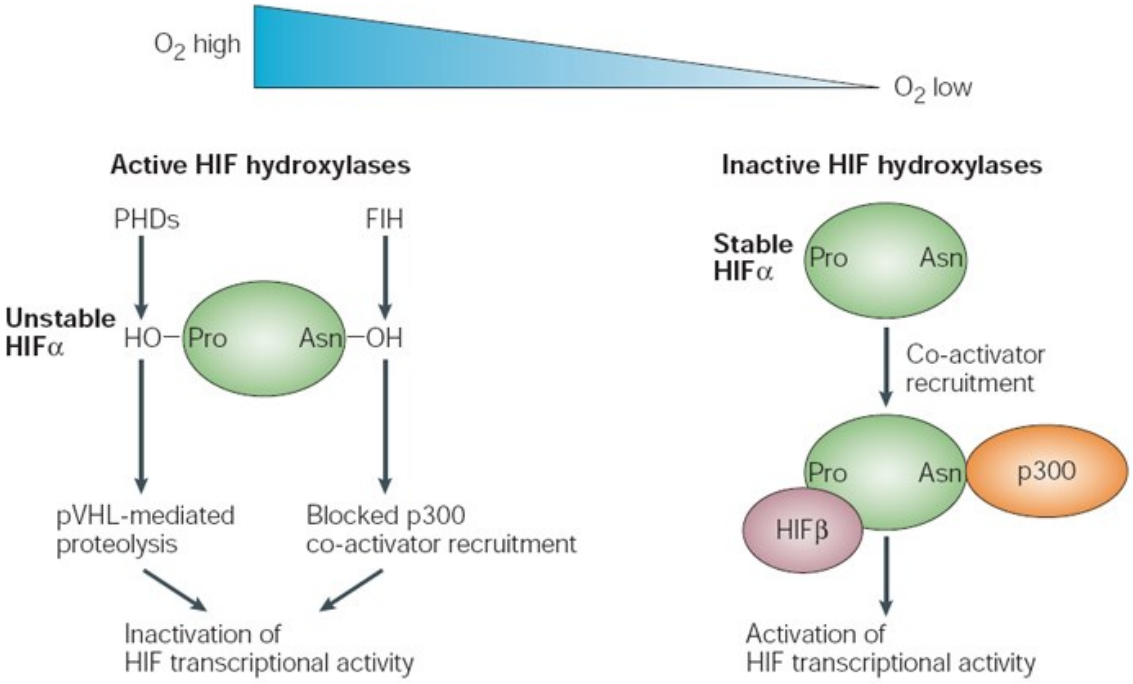

Figure 1.7 Oxygen sensing by HIF hydroxylases. In normoxia (left) the affinity of the PHDs and FIH for molecular oxygen is high and therefore HIF-α hydroxylase activity is high. In the case of PHDs, hydroxylation of HIF-α in its ODD results in docking of E3 ubiquitin ligase VHL, which promotes HIF-α degradation. In conditions of low oxygen (right), PHD activity towards HIF-α is reduced, therefore stabilising HIF-α by binding to HIF-β, which in turn promotes HIF transcriptional activation. FIH is also controlled by O_2 tension. In normoxia, FIH actively hydroxylates HIF therefore prevents association with its transcriptional co-activator, p300. During periods of low oxygen FIH activity towards HIF is reduced therefore promoting the HIF/p300 transcriptional activation. Adapted from Figure 3, (Schofield and Ratcliffe, 2004)

1.2.6 EGF repeat hydroxylases

The importance of hydroxylation in cancer was first recognised following the discovery of asparagine and aspartic acid hydroxylation by Aspartyl (asparaginyl) beta-hydroxylase (ASPH) (Dinchuk et al., 2002, Stenflo et al., 1989, Sepe et al., 2002). This type of hydroxylation is restricted to EGF repeats in 25 proteins with calcium-binding EGF modules. Although the biological role of EGF repeat hydroxylation remains unclear (Wouters et al., 2005), ASPH knockout mice display significant developmental defects. With respect to cancer, overexpression of ASPH in human pancreatic tumours is thought to promote cell proliferation, migration, invasion and colony formation (Ploumakis and Coleman, 2015, Dong et al., 2015, Dinchuk et al., 2002).

1.3 The JmjC Domain

The “Jumonji C” (JmjC) domain is a sub-class of the catalytic DSBH apparent in approximately thirty 2OG oxygenases in the histone demethylase and JmjC hydroxylase families (Figure 1.2). The name Jumonji literally translates to cruciform in Japanese. It was named so because the DSBH of JmjC enzymes structurally mimics that of the neural grooves of the Jumonji knockout mouse (Takeuchi et al., 1995). The JmjC domain hosts a characteristic barrel-like or ‘cupin’ fold originating in archaea, bacteria and eukarya (Clissold and Ponting, 2001). An additional ‘JmjN’ domain features in a small section of JmjC containing proteins and it is structurally and functionally distinct from the JmjC domain. Although little is known about the function of the JmjN domain, a recent study showed it is essential for dimerisation, and therefore activity of KDM4A and KDM4C (Levin et al., 2018). Early studies of enzymes containing a JmjC domain noted chromatin remodelling functions, which led

to the assignment of the JmjC domain as a DNA or chromatin binding domain (Clissold and Ponting, 2001). Since then however, JmjC-containing proteins have also been characterised as nucleotide hydroxylases and protein hydroxylases, highlighting that this domain is not exclusively associated with histone demethylation (Noma et al., 2010, Ploumakis and Coleman, 2015).

1.4 Histone Demethylases

Many 2OG oxygenases of the JmjC sub-family are involved in the epigenetic control of histone lysine methyl marks on chromatin, and are known as histone demethylases (Figure 1.2). Chromatin is the packaging system used to accommodate all DNA into the cell nucleus and is made up of nucleosomes. A nucleosome comprises of 147 base pairs of DNA wrapped around a histone octamer (two of each of histones H2A, H2B, H3 and H4) and stabilised by an additional histone (H1) (Turner, 2012). Epigenetic modifications occur through the work of "writers" and "erasers", where the writer is the transfer enzyme (e.g. acetyltransferases and methyltransferases), and the eraser is the removal enzyme (e.g. deacetylase and demethylases, respectively). The "reader" proteins bind to histone tail PTMs, including methylated and acetylated lysine residues, in order to recruit complexes that regulate gene transcription (Gillette and Hill, 2015). Methylation of lysine residues is a complex process involving mono- (me1), di- (me2) and tri-methyl (me3) marks that function to either repress or enhance transcription (Nebbioso et al., 2018). Each type of methyl modification has been shown to have a variety of effects on transcription, with the outcome dependent on a variety of factors including the specific lysine residue modified. For example Histone H3 lysine 4 di- and tri- methylation (H3K4me2/3) is a mark of transcriptional activation, whereas

H3K27me3 is a gene silencing mark (Horton et al., 2016, Hong et al., 2007). Furthermore, each methyl mark is specifically targeted by certain lysine demethylases (Figure 1.8) (discussed below).

Although histone demethylation catalysed by 2OG oxygenases utilises the same mechanism as previously described (Chapter 1.2), the resulting hydroxylation is highly unstable, with the hydroxymethyl product rapidly fragmenting into formaldehyde and a demethylated lysine (Figure 1.3b) (Tsukada et al., 2006, McDonough et al., 2010). There are significant structural differences between the JmjC histone demethylases and the JmjC hydroxylases. Firstly, the JmjC hydroxylases lack an essential hydrophobic region that is necessary for binding the N^6-methyl lysine. Secondly, histone demethylases contain other nucleic acid or chromatin binding domains necessary for substrate binding. Alternatively, histone arginine demethylation by 2OG oxygenases has also been described, however it has not yet been proven in cells (Walport et al., 2016). The first family of enzymes identified as histone lysine demethylases, the KDM1 family, are not 2OG oxygenases, instead these enzymes require a flavin adenine dinucleotide (FAD) as a cofactor for catalysis (Shi et al., 2004). This family is comprised of two enzymes, KDM1A and KDM1B (or LSD1 and LSD2), which catalyse the demethylation of mono- and di-methylated lysines (Burg et al., 2015). However, inclusion of these enzymes hereafter is beyond the scope of this thesis. In total there are seven families of histone lysine demethylases (KDM) six families belong to the 2OG oxygenase family (KDM2-7), and all 2OG KDMs contain a characteristic JmjC domain plus additional functional motifs, as explained below.

1.4.1 Histone Lysine Demethylase Family 2

The KDM2 family of 2OG oxygenases was the first family of JmjC histone demethylases to be described, and consists of KDM2A and KDM2B (Tsukada et al., 2006). Tsukada et al. (2006) hypothesised that the JmjC domain could function in histone lysine demethylation because the function of the JmjC domain in KDM2A and KDM2B is conserved from humans to *Saccharomyces cerevisiae*. They found that both KDM2A and KDM2B demethylate the first and second methyl marks on Histone 3 lysine 36 (H3K36me1 and H3K36me2). In addition to their JmjC domain, KDM2 proteins also contain an F-box domain, CXXC zinc finger, Plant Homeodomain zinc Finger (PHF) and three leucine rich repeats, which enable chromatin binding and localisation (Tsukada et al., 2006, Johansson et al., 2014).

1.4.2 Histone Lysine Demethylase Family 3

JmjD1A, JmjD1B, JmjD1C and Hairless (HR) make up the KDM3 family. JMJD1A, JMJD1B and JMJD1C (also known as KDM3A-C) are very similar proteins, all sharing C2HC4-zinc finger and a JmjC domain (Johansson et al., 2014). Furthermore, all three enzymes are nuclear localised, display similar tissue distribution, and share 64% amino acid similarity in their JmjC domain (Brauchle et al., 2013). KDM3A and KDM3B are the two most similar proteins sharing 84% sequence similarity in their JmjC domain (Brauchle et al., 2013). Both KDM3A and KDM3B are *bona fide* H3K9me1 and me2 demethylases (Brauchle et al., 2013). Initially, KDM3C was shown to have histone demethylase activity towards H3K9me1 and me2 (Kim et al., 2010). However, more recent attempts to reproduce this observation have been unsuccessful (Brauchle et al., 2013).

HR has a less well-conserved JmjC domain compared to the other family members, and contains a CxD/E…H Fe(II) coordination motif (Clissold and Ponting, 2001). It

has been proposed that this deviation from the canonical HxD/E…H motif may not completely abrogate demethylase activity, since cysteine also has the capacity to bind and coordinate Fe(II) (Liu et al., 2014). Therefore, HR may still hold demethylase activity towards H3K9me1 and me2, similar to that of other KDM3 family members. Further investigation may be needed to corroborate HR as a histone lysine demethylase.

1.4.3 Histone Lysine Demethylase Family 4

The KDM4 family of histone demethylases is the largest and best studied sub-family encompassing six members (KMD4A-F). High sequence homology is found between all six family members with 55% sequence identity and 81% similarity overall. KDM4E and F are the most similar of the two enzymes with 94% sequence similarity between their catalytic domains (Hillringhaus et al., 2011). Each enzyme holds a typical JmjC domain, a JmjN domain, two PHF domains and two tudor domains which impart histone reader functions (Chen et al., 2006). The predominant substrate to these enzymes is H3K9me3 and H3K36me3, and the less well known H1.4K27me3 (Berry and Janknecht, 2013). Furthermore, KDM4A-C also catalyse the demethylation of H3K36me2, albeit less effectively than H3K9 (Berry and Janknecht, 2013).

1.4.4 Histone Lysine Demethylase Family 5

The KDM5 group, also known as JARID1 enzymes, consists of four histone demethylases, JARID1A-D (or KDM5A-D). Their domain organisation homology is relatively high, including JmjC, JmjN, ARID DNA binding, and C5HC2 DNA binding domains and two or three zinc fingers (Johansson et al., 2014). Because KDM5 enzymes specifically target H3K4me2 and me3, epigenetic marks associated with transcriptional activation, they are thought to act as transcriptional repressors (Horton

et al., 2016). KDM5A has been reported as a regulator of differentiation through various targets including retinoblastoma binding protein, HOX homeotic genes, circadian rhythm, and has also been implicated in breast cancer metastasis (Christensen et al., 2007, Benevolenskaya et al., 2005, Horton et al., 2016). Although KDM5B is normally expressed in the testis and brain, over-expression of KDM5B has been observed in cancers arising in multiple tissues (Horton et al., 2016). Similar to KDM5A, KDM5B plays a role in differentiation through control of cell cycle exit and progenitor cell fate (Dey et al., 2008).

KDM5C and KDM5D are localised to the X and Y chromosomes, respectively. Interestingly, KDM5C is not silenced by X-linked chromosome inactivation and is highly associated with X-linked intellectual disability (XLID) and Huntingtin disease (Johansson et al., 2014, Horton et al., 2016). Although less is known about the fourth family member KDM5D, it has been studied in the context of disease. KDM5D inhibits metastatic invasion in prostate cancer, and has been used a marker of prognosis, whereby low expression correlates with poor survival in prostate cancer (Li et al., 2016). Collectively, evidence suggests that members of the KDM5 family may function as oncogenic drivers (Rasmussen and Helin, 2016, Horton et al., 2016) and in neuronal development disorders (Wynder et al., 2010).

1.4.5 Histone Lysine Demethylase Family 6

The KDM6 subfamily consists of three proteins: UTX (Ubiquiously Transcribed tetratricopeptide repeat X chromosome protein), UTY (Ubiquiously Transcribed tetratricopeptide repeat Y chromosome protein) and JMJD3. UTX and UTY are located on the X- and Y- chromosome, respectively. Similar to KDM5C, UTX escapes male X-chromosome inactivation (Shpargel et al., 2012). Both UTX and JMJD3 are

bona fide histone demethylases with specificity towards the gene silencing mark H3K27me3, and to a lesser extent H3K27me2 (Hong et al., 2007, Walport et al., 2014). UTX and UTY share 88% overall sequence identity and 98% similarity in their JmjC domains (Shpargel et al., 2012). Interestingly, UTY was initially thought to be inactive. However, recent structural and functional studies have indicated that UTY is an active demethylase with specificity towards H3K27me3, albeit with significantly reduced activity compared with UTX and JMJD3 (Shpargel et al., 2012, Hong et al., 2007, Walport et al., 2014). Mutation of UTY proline 1214 to isoleucine (P1214I), a residue found conserved in JMJD3 and UTX and thought to be essential for substrate binding, increased UTY KDM activity significantly. This suggested that UTY is an active 2OG oxygenase with non-histone substrates (Walport et al., 2014). Conversely, Shpargel et al. (2012) identified a role for UTX and UTY in the regulation of cardiac transcription factors independent of their KDM activity. Interestingly, UTY is potentially regulated through phosphorylation of a conserved threonine residue (Walport et al., 2014). Though the functional relevance is not yet known, it could be important for regulating enzyme-dependent or -independent functions. In disease, UTY is thought to be involved in prostate differentiation and has been associated with prostate cancer (Dutta et al., 2016, Lau and Zhang, 2000). JMJD3 is a broadly studied lysine demethylase with known roles in development, neurodegenerative disorders, the immune system, cell plasticity and cancer (Burchfield et al., 2015). With specific reference to cancer, JMJD3 is implicated in the regulation of epithelial-mesenchymal transition (EMT). Furthermore, JMJD3 is also associated with specific roles in many types of cancer including breast, lung, prostate, renal cell carcinoma, kidney, pancreatic, liver, colorectal and glioblastoma (Burchfield et al., 2015).

1.4.6 Histone Lysine Demethylase Family 7

The seventh class of KDM enzymes is formed by three enzymes with a characteristic DNA binding PHF domain in addition to their JmjC domain: KIAA1718 (KDM7A), PHF8 (KDM7B) and PHF2 (KDM7C) (Johansson et al., 2014). KDM7A is a histone lysine demethylase with dual activity towards H3K9me2 and K3K27me2, and to a lesser extent, H3K9me1 and H3K29me1 (Tsukada et al., 2010). KDM7A is highly expressed in the brain of zebrafish and mice, consistent with a role in neuronal development and differentiation (Huang et al., 2010). This is supported by evidence from chromatin immunoprecipitation (ChIP) experiments demonstrating that KDM7A is found in abundance at the transcriptional start site (TSS) of genes involved in neuronal differentiation and development (Tsukada et al., 2010, Huang et al., 2010). Similar to KDM7A, PHF8 has an unusually broad substrate specificity including H3K9me2, H3K9me1, H3K27me2 and H3K36me2 (Loenarz et al., 2010). Several lines of evidence have demonstrated a role for PHF8 during different phases of the cell cycle (Sun et al., 2015, Lim et al., 2013, Liu et al., 2010a). For example, KDM7B is thought to be phosphorylated at Serine 844 by CDK2-CycE which regulates G1/S phase transition. Phospho-S844 promotes KDM7B H3K9me2 demethylase activity at the promoter of Cyclin E, E2F2 and E2F7, positively regulating transcription of cell cycle genes (Sun et al., 2015). On the other hand, KDM7B expression is tightly controlled by the anaphase promoting complex (APC) during mitosis (Lim et al., 2013). The APC is required for progression through and exit from mitosis, as such PHF8 expression is highest at the G2/M boundary of the cell cycle (Lim et al., 2013, Castro et al., 2005). Furthermore, KDM7B interacts with proteins involved in the G2/M transition, consistent with a role in mitosis (Liu et al., 2010a, Lim et al., 2013).

PHF2 is a 2OG oxygenase that was originally thought to be enzymatically inactive despite having the required Fe(II) coordinating residues (Johansson et al., 2014, Tsukada et al., 2010). Since then it has been identified as the first 2OG oxygenase to require phosphorylation for enzymatic activity (Baba et al., 2011). Baba et al. (2011) showed that phosphorylated PHF2 catalysed the demethylation of the repressive mark, H3K9me2, to promote gene expression.

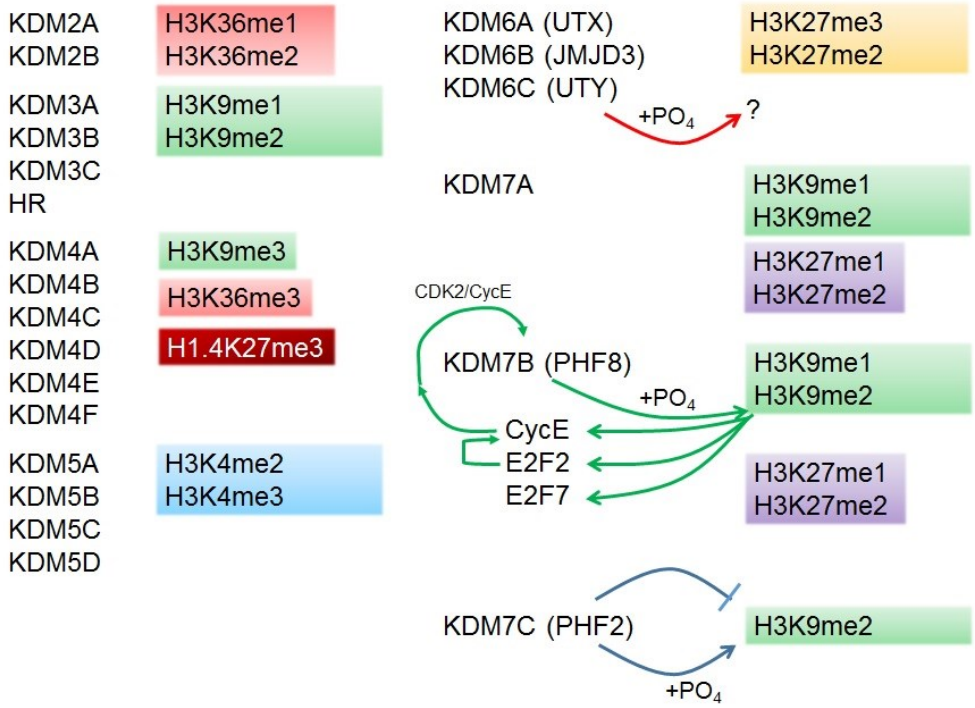

Figure 1.8 Demethylase specificity of KDM family of 2OG oxygenases. Alignment of substrate specificity of each KDM family to their histone mark including those regulated by phosphorylation. The methyl marks are colour co-ordinated to emphasise enzyme overlap. KDM6C (UTY) phosphorylation has an unknown function. PHF8 phosphorylation promotes transcription of cell cycle associated genes, CycE, E2F2 and E2F7 therefore introducing a positive feedback loop. PHF2 is inactive until phosphorylated, then it confers activity towards H3K9me2, similar to other KDM7 family members.

1.5 JmjC Only Hydroxylases

1.5.1 TYW5

TYW5 was the first RNA hydroxylase to be identified in the 2OG oxygenase family. Although it is a member of the JmjC only family and most closely related to JMJD5 and FIH (both of which are protein hydroxylases, introduced below) (Figure 1.2), it catalyses hydroxylation of phenylalanine tRNA (Noma et al., 2010, Kato et al., 2011). Phenylalanine tRNA is subjected to multiple post-transcriptional modifications at guanosine 37 (G37) to produce a unique nucleoside termed 'wybutosine'. Through a sophisticated series of reactions wybutosine (yW) becomes hydroxywybutosine (OHyW): TYW5 catalyses hydroxylation in the penultimate reaction in this cascade. Although the functional significance of OHyW is as yet unknown, position 37 of the anti-codon is known to be essential for reading frame maintenance during translation. (Kato et al., 2011, Noma et al., 2010, Sample et al., 2015).

1.5.2 FIH

Factor Inhibiting Hypoxia (FIH) is good example of how protein hydroxylation can have a major impact on cellular signalling. The best characterised function of FIH, similar to the PHD enzymes, is as a HIF regulator (Figure 1.7). FIH acts to hydroxylate an asparagine residue in the C-terminal transactivation domain (CTD) of HIF, giving rise to another layer of HIF regulation (Mahon et al., 2001, Lando et al., 2002a, Lando et al., 2002b, Hewitson et al., 2002, Freedman et al., 2002). Specifically, FIH mediated HIF hydroxylation during normoxia inhibits the association of HIF with CBP/p300 and in turn, prevents HIF transcriptional activation (Figure 1.7) (Mahon et al., 2001). During conditions of nutrient starvation and limited oxygen availability FIH-mediated HIF hydroxylation is repressed, although to a lesser extent than PHD-mediated HIF hydroxylation (Lando et al., 2002a). The CBP/p300 complex

serves as a transcriptional co-activator for many transcription factors, and in this case it promotes transcriptional activation from HIF target genes when recruited by HIF (Koivunen et al., 2004). Although hypoxia is a major regulator of FIH activity towards HIF-α, a phospho-threonine (Thr796) modification on HIF-α can also inhibit FIH-mediated HIF hydroxylation, thereby promoting the interaction with p300/CBP and driving HIF mediated transcription (Lancaster et al., 2004). Interestingly, FIH forms a dimer in cells via the C-terminal domains of each monomer: A single point mutation in the dimerisation domain of FIH was able to abolish hydroxylase activity, suggesting that oligomerisation of FIH is required for full HIF hydroxylase activity (Lancaster et al., 2004).

1.5.3 MINA53 and NO66

MINA53 (Myc induced nuclear antigen of 53kDa), otherwise known as ribosomal oxygenase 2 (RIOX2), was first published as a myc target gene in HeLa cells (Tsuneoka et al., 2002). It is a highly conserved member of the JmjC only family of 2OG oxygenases, closely related to NO66 (Nucleolar protein 66 kDa, RIOX1) (Eilbracht et al., 2004). Phylogenetic analysis has revealed that NO66 and MINA53 are two orthologues of YcfD from *E. coli*, an arginyl ribosomal hydroxylase acting on RpL16 (Ge et al., 2012). NO66 and MINA53 are localised to the nucleolus and are both ubiquitously expressed in cells. However, the catalytic functions of both enzymes have been controversial (Bundred et al., 2018). Early studies on NO66 and MINA53 were performed at a time when the JmjC domain was thought to be exclusively involved in chromatin remodelling and histone demethylase activity (Klose et al., 2006, Clissold and Ponting, 2001), and was not widely appreciated to also be a protein hydroxylase domain. This likely contributed to both enzymes being initially assigned as histone lysine demethylases (Ayoub et al., 2003, Lu et al., 2009).

These assignments were associated with reported changes in histone H3 lysine methylation levels following overexpression of each enzyme (Sinha et al., 2010, Lu et al., 2009). However, Chen et al. (2015) reported that the observed H3K9me3 regulation seen by MINA53 manipulation could be an indirect effect of MINA53-dependent regulation of KDM4A expression. More recently however, MINA53 and NO66 have been described as ribosomal histidyl hydroxylases. Consistent with previous observations that MINA53 and NO66 may participate in ribosome biogenesis, they catalyse the hydroxylation of the ribosomal subunits, RpL27a and RpL8, respectively (Eilbracht et al., 2004, Ge et al., 2012). Importantly, biochemical, mass spectrometry and crystallographic studies on MINA53 and NO66 have been unable to reproduce any enzymatic activity towards histones but have demonstrated high affinity towards their specific ribosomal substrates (Williams et al., 2014, Wang et al., 2015a, Chowdhury et al., 2014). A recent review highlights the structural, biochemical and phylogenetic data underlying MINA53 and NO66 as histidyl hydroxylases as opposed to histone lysine demethylases (Bundred et al., 2018). Interestingly, a role for MINA53 and NO66 in cancer cell invasion and migration has come to light, perhaps representing an interesting link between cell proliferation and metastasis (Yu et al., 2014, Geng et al., 2017). More work is needed to identify the function of RpL27a and RpL8 hydroxylation and whether or not MINA53 and NO66 have additional substrates and functions.

Both NO66 and MINA53 have been extensively studied with respect to health and disease (Bundred et al., 2018). In bone development, NO66 mouse models indicate direct correlations between NO66 expression and bone mass. Furthermore, NO66 plays a role in osteoblast differentiation via an interaction with the transcription factor,

Osterix (Osx) (Chen et al., 2015, Sinha et al., 2010). The exact role of NO66 in bone development is yet to be fully understood however. In cancer, NO66 has been highlighted as a marker of poor prognosis in malignant renal tumours (Pires-Luis et al., 2015) and has proposed functions in invasion and metastasis (Nishizawa et al., 2017).

MINA53 has been more extensively studied than NO66 and has been implicated in atopic asthma, Helmith expulsion, pulmonary fibrosis and cancer (Chen et al., 2011b, Pillai et al., 2014, Thakur et al., 2015, Bundred et al., 2018). Interestingly, three knockout MINA53 mouse models show varied results. One homozygous MINA53 knockout mouse was embryonically lethal (Thakur et al., 2015). On the other hand, Mori et al. (2013) and Yosef et al. (2013) knockout mice were viable, supporting context dependant roles for MINA53. Furthermore, MINA53 is another enzyme in this family with context dependent roles in cancer and has been identified as a prognostic factor in a number of tumour types (Yu et al., 2014, Geng et al., 2017, Teye et al., 2004, Tan et al., 2014, Tsuneoka et al., 2004, Fujino et al., 2018).

1.5.4 JMJD4

The only known C4 lysyl hydroxylase is another member of the JmjC only family, the newly characterised JMJD4 (Feng et al., 2014). The only identified substrate of JMJD4 thus far is 'eukaryotic release factor 1' (eRF1) (Figure 1.6), an essential protein involved in translation termination. Termination of protein synthesis occurs when the stop codon reaches the A site of the ribosome, where it is recognised ('decoded') by eRF1 (Feng et al., 2014, Dever and Green, 2012). JMJD4 hydroxylates K63 within a conserved Asn-Ile-Lys-Ser (NIKS) sequence in eRF1, a motif known to play an important role in decoding stop codons. Interestingly, JMJD4

knockdown increased the stop codon 'read-through' of ribosomes in cells, suggesting that hydroxylation of eRF1 K63 is required to promote translational termination and maintain the fidelity of protein synthesis (Feng et al., 2014). Structural analyses have led to the proposal that eRF1 K63 hydroxylation promotes translational termination by correctly orientating the K63 side chain to improve the efficiency of base discrimination at the first position of the stop codon (the invariant Uridine) (Matheisl et al., 2015). Knockout mouse models of JMJD4 appear to be viable, but knockdown of JMJD4 in NIH3T3 fibroblasts has been shown to reduce growth (Feng et al., 2014, Hu and Imbalzano, 2016, Yoo et al., 2016).

1.5.5 JMJD5

Defining the exact function of JMJD5 has been controversial: It has been described as a protein hydroxylase, a histone demethylase, and a histone tail specific protease (Del Rizzo et al., 2012, Hsia et al., 2010, Liu et al., 2017a, Liu et al., 2018a, Shen et al., 2017, Wilkins et al., 2018). Originally, JMJD5 was termed "KDM8" following a report that it was a H3K36me2 demethylase targeting the coding region of Cyclin A1, indicating a potential role in cell cycle progression (Hsia et al., 2010). On the other hand, recent studies have suggested that JMJD5 acts as a protease enzyme capable of clipping histone tails, thereby removing lysine and arginine methyl marks (Shen et al., 2017, Liu et al., 2017a, Liu et al., 2018a). The reported histone demethylase functions of JMJD5 are strongly debated since other groups have been unable to reproduce these results (Youn et al., 2012, Wilkins et al., 2018). Moreover, the crystal structure of JMJD5 has been solved and compared with *bona fide* KDM enzymes and other JmjC only hydroxylases (Del Rizzo et al., 2012): The results indicate that the catalytic domain of JMJD5 does not possess the structural features

required for KDM activity. For example, an essential methyl carbon-oxygen hydrogen bonding residue required for demethylation activity is not present in JMJD5 (Del Rizzo et al., 2012). A recent discovery found that JMJD5 is the first human protein hydroxylase to be characterised with specificity towards arginine. Wilkins et al. (2018) reported that JMJD5 is able to hydroxylate synthetic peptides derived from the 40S ribosomal protein RPS6 and a known binding partner, RCCD1 (Wilkins et al., 2018). Whether JMJD5 targets these proteins as a substrate in cells is not clear however. Although, the identity of the physiologically relevant substrates of JMJD5 may require further investigation, it is clear that this enzyme has important biological roles: Knockout mouse models of JMJD5 were embryonic lethal, consistent with an important role in development. JMJD5 may also be associated with circadian rhythm and cell cycle progression (Hsia et al., 2010, Oh and Janknecht, 2012, Youn et al., 2012, Jones et al., 2010). Similar to other 2OG oxygenases, JMJD5 has opposing tumour suppressive and oncogenic roles in cancer and it is clear from the current literature that the exact function of JMJD5 and its substrates are yet to be fully elucidated (Wu et al., 2016, Zhang et al., 2015, Suzuki et al., 2006).

1.5.7 JMJD6

Although JMJD6 is a member of the JmjC only family of 2OG oxygenases, early reports assigned it as a phosphatidylserine receptor (PSR) (Fadok et al., 2000, Chang et al., 2007, Hahn et al., 2008). The identification of the JmjC domain subsequently led to it being renamed JmjC domain containing protein 6' (JMJD6) (Cikala et al., 2004). In addition to its JmjC domain, JMJD6 also has three Nuclear Localisation Signal (NLS) sequences, a poly-serine domain (which also contributes to nuclear localisation), and an AT-hook like domain thought to be involved in RNA binding (Cikala et al., 2004, Wolf et al., 2013, Filarsky et al., 2015).

Roles for JMJD6 have been described in epigenetic remodelling (as a histone demethylase), pre-mRNA splicing (as a C5-lysyl hydroxylase), and a regulator of P-TEFb in transcription elongation (Webby et al., 2009, Liu et al., 2013). Three independent studies demonstrated that JMJD6 knockout is embryonically lethal in mice and zebrafish, demonstrating its importance in development (Bose et al., 2004, Kunisaki et al., 2004, Li et al., 2003, Hahn et al., 2008, Hong et al., 2004).

In vitro experiments identified JMJD6 as the first histone arginine demethylase (Chang et al., 2007). However, this was later challenged by evidence demonstrating that JMJD6 is a C5-lysyl hydroxylase with specific activity towards the U2 small nuclear ribonucleoprotein auxillary factor 65kDa (U2AF65) (Figure 1.6) (Webby et al., 2009). Webby et al. (2009) showed that loss of either JMJD6 or U2AF65 resulted in reduced exon inclusion events, suggesting that U2AF65 hydroxylation promotes exon inclusion in alternative splicing. Interestingly, through its interaction with U2AF65 JMJD6 knockdown impairs angiogenic sprouting: Boeckel et al. (2011) demonstrated that loss of JMJD6 results in expression of an isoform of vascular endothelial growth factor (VEGF) -receptor 1 (Flt1) which includes exon 13. This exon encodes a premature stop codon, and in turn, results in a soluble protein able to bind to VEGF and placental growth factor (PIGF), thereby inhibiting angiogenic sprouting (Boeckel et al., 2011).

JMJD6 has also been reported as a lysyl hydroxylase of histone tails following the observation that JMJD6 interacts with histone tails (Unoki et al., 2013). The exact function of histone tail hydroxylation is yet to be fully elucidated, although a role in PTM cross-talk has been proposed (Unoki et al., 2013). Alternatively, JMJD6 has also been suggested as a p53 hydroxylase: Mass spectrometry data identified a

possible interaction between the two enzymes via a single p53 hydroxylation site at K382 (Wang et al., 2014). It was proposed that hydroxylation of p53 K382 may affect its transcriptional activity. Furthermore, methylation and acetylation of p53 K382 have also been observed at this site (Reed and Quelle, 2014), again suggestive of potential PTM cross-talk (Unoki et al., 2013).

JMJD6 has been implicated in a range of diseases including, but not limited to, Huntington's, Hepatitis B, Wardenburg syndrome, diabetes and preeclampsia (Ratovitski et al., 2015, Chen et al., 2014, Wu et al., 2015, Yanagihara et al., 2017, Alahari et al., 2018). Furthermore, JMJD6 has been extensively studied in cancer. For example, reports demonstrate that JMJD6 could be used as a negative prognostic marker in breast cancer, lung adenocarcinoma, oral carcinoma, melanoma, neuroglioma, and glioblastoma (Wang et al., 2014, Lee et al., 2012, Zhang et al., 2013, Poulard et al., 2015, Aprelikova et al., 2016, Lee et al., 2016, Liu et al., 2017b, Miller et al., 2017), potentially consistent with a role as an oncogenic driver.

1.6 'Orphan' JmjC hydroxylases

1.6.1 HSPBAP1

HSPBAP1 (HSPB1 Associated Protein 1) was originally named as 'Protein Associated with Small Stress proteins' (PASS1) due to its association with heat shock protein 27 (hsp27) (Liu et al., 2000). Although there are currently no known hydroxylase targets of HSPBAP1, it retains the conserved Fe(II) binding HxD…H motif suggesting that it may function as a 2OG oxygenase with unique substrates (Jiang et al., 2001). Despite the lack of functional data, HSPBAP1 has been studied in the context of neurological disease and cancer. For example, disease specific

expression has been observed in epileptic patients, where high expression correlated with severe epilepsy (Jiang et al., 2001, Liu et al., 2000, Xi et al., 2007, Xi et al., 2009). Furthermore, HSPBAP1 is thought to interact with miR-455-3p.2, a mircoRNA associated with the progression of Alzheimer's disease, therefore presenting a role for HSPBAP1 in Alzeimer's (Kumar and Reddy, 2018). In cancer, HSPBAP1 overexpression has been observed in hepatocellular carcinoma (HCC) and prostate cancer, where high expression correlated with poor prognosis (Yang et al., 2015, Saeed et al., 2015).

1.6.2 JMJD8

JMJD8 is another uncharacterised member of the JmjC only family with disputed specificity. It is thought by some to be catalytically inactive because, similar to HR, JMJD8 does not present the usual HxD/E…H facial triad, but instead has a less common HxH…H Fe(II) binding motif (Yeo et al., 2017). In a study by Yeo et al. (2016) JMJD8 was shown to regulate TNF signalling to favour a pro-survival pathway. The authors observed that JMJD8 is responsible for regulation of NF-kB activation and notably, ubiquitination of Receptor Interacting Protein 1 (RIP1). RIP1 is a serine/threonine kinase which plays fundamental roles in apoptosis, necrosis and cell survivial (Declercq et al., 2009). Since RIP1 ubiquitination is an essential step in formation of the pro-survival tumour necrosis factor α receptor 1 (TNFR1) complex 1, Yeo and colleagues hypothesised that JMJD8 might function in TNF-induced NF-kB pro-survival signalling. Alternatively, an additional role for JMJD8 has been proposed in endothelial cells: Boeckel et al. (2016) found that JMJD8 is upregulated during mouse endothelial cell (EC) differentiation, which in turn, led them to investigate a role for JMJD8 in angiogenic sprouting. They found that knockdown of both PKM2 (a promoter of angiogenesis in ECs) and JMJD8 reduced angiogenic sprouting in ECs.

In their model, JMJD8 binds to PKM2 to modulate pyruvate synthesis and, in turn, angiogenesis. However, the mechanism by which JMJD8 regulates PKM2 is unclear. In addition, they found that although JMJD8 knockout mice are viable they show reduced number of capillaries in skeletal muscles. More recently, Yeo et al. (2017) reported that the JMJD8 protein sequence contains both a signal peptide and a transmembrane domain, and speculated a role for JMJD8 in protein folding. Finally, Khoueiry and colleagues have recently proposed a role for JMJD8 in embryonic development: They report that JMJD8 is a co-repressor of the TET1 2OG oxygenase, co-localising with TET1 at loci of genes in mouse epiblast stem cells (Khoueiry et al., 2017). They suggest that JMJD8 is capable of overriding the demethylating effects of TET1 in target genes to further fine tune embryonic development.

1.6.3 JMJD7

Prior to 2014 (when this PhD project commenced), almost nothing was known about the JmjC only enzyme, JMJD7 (Figure 1.9a). Originally, JMJD7 was identified in a 'readthrough transcript' with its neighbouring gene, phospholipase A2 beta (PLA2G4B) (Pickard et al., 1999). Readthrough transcripts are full-length or partial gene sequences from different genes that have combined to create conjoined transcripts (Prakash et al., 2010). JMJD7 forms two fusion transcripts with PLA2G4B, the gene immediately juxtaposed to JMJD7: Isoform 1 incorporates the first 233 amino acids of JMJD7 (initial 105 residues from the JmjC domain) and the entire PLA2G4B gene giving rise to a 114kDa protein (Figure 1.9b), whereas isoform 2 is missing a 115 amino acid region in the C-terminus of PLA2G4B generating a 100kDa protein product (Figure 1.9c) (Pickard et al., 1999). This readthrough transcript was originally thought to be another splice variant of PLA2α and, as such, was characterised as an active cytoplasmic calcium dependant phospholipase enzyme

(Song et al., 1999, Pickard et al., 1999). Although little is known about the structure or function of JMJD7-PLA2G4B, the C-terminal Fe(II) co-ordinating residue (H277) in the JmjC domain of JMJD7 is missing, which would likely render it inactive as a protein hydroxylase (Figure 1.9b and 1.9c). Interestingly, JMJD7-PLA2G4B expression has been associated with Head and Neck Squamous Cell Carcinoma (HNSCC), YAP1 negative Non-Small Cell Lung Cancer (NSCLC), Oesophageal cancer and Autism (Matsunami et al., 2014, Cheng et al., 2017, Ito et al., 2016, Su et al., 2016). With respect to the latter, two independent papers have reported that mutations in JMJD7 may be associated with autism and intellectual disability, although the mechanisms are unknown (Matsunami et al., 2014, de Ligt et al., 2012). Furthermore, JMJD7 was a positive hit in an siRNA screen of predicted KDMs that aimed to identifying genes involved in the invasion of squamous cancer cells (Ding et al., 2013).

Considering the potential importance of JMJD7 in disease it is an orphan JmjC only 2OG oxygenase worthy of further investigation. Specifically future studies should aim to characterise how JMJD7 activity is regulated, to explore how its function is deregulated in disease, and to identify its substrates.

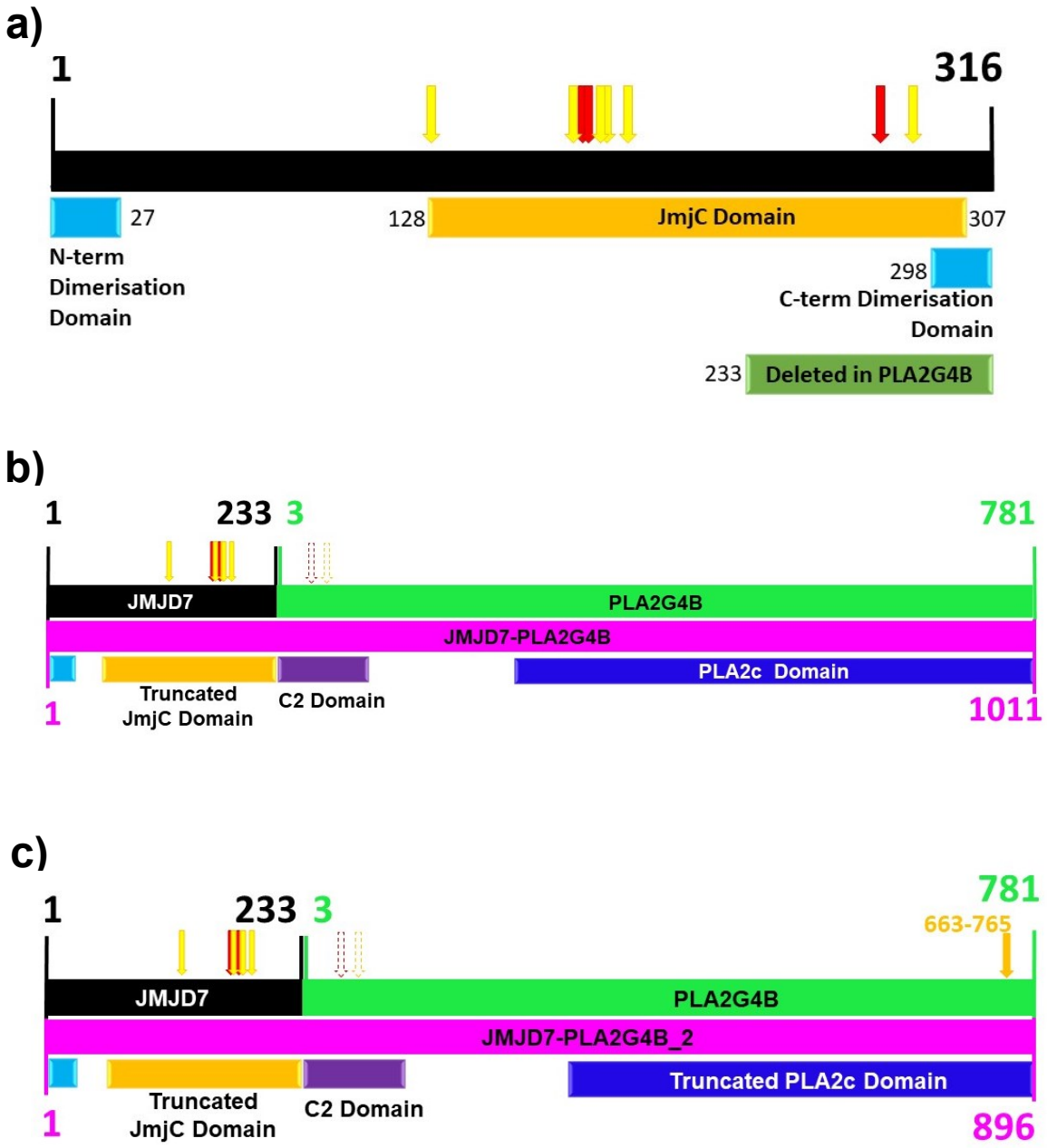

Figure 1.9. Basic Schematic of JMJD7 and JMJD7-PLA2G4B readthrough transcripts. a) JMJD7 has one functional domain (JmjC domain, yellow), two alpha helices located at the N-terminus and the C-terminus participate in JMJD7 oligomerisation (light blue). Essential co-factor binding residues are demonstrated with yellow and red arrows. The C-terminal 83 residues, shown by green bar, are deleted in the JMJD7-PLA2G4B readthrough transcripts. b) and c) JMJD7-PLA2G4B transcripts both consist of the first 233 residues of JMJD7 including a truncated JmjC domain, a C2 lipid binding domain and a PLA2c domain. Isoform 2 (c) has an additional 115 amino acids missing located at the C-terminal end of the PLA2c domain.

1.7 Aims and Objectives:

This literature review has presented an overview of post-translational modifications and 2OG oxygenases. The presence of these enzymes within multiple layers of gene expression control and their conservation throughout evolution exemplifies how they perform important cellular functions. Although the functions and substrates of some JmjC only enzymes are yet to be elucidated (e.g. JMJD8, JMJD7 and HSPBAP1), their association with disease suggests important biological roles. The objective of the work that forms the basis of this Thesis was to contribute to the characterisation of JMJD7. The work in Chapter 2 contributes to the basic biochemical and cellular characterisation of JMJD7, providing insight into its function. In Chapter 3 we explore the genetic evidence for a potential role of JMJD7 and its substrates in cancer. Finally, the work presented in Chapters 4 and 5 extends key findings from Chapter 3, to understand how JMJD7 is regulated, and what effect this has on cell biology.

Chapter 2

Initial characterisation of JMJD7, an orphan JmjC-only hydroxylase

Introduction

Currently characterised enzymes within the JmjC-only family of 2OG oxygenases are involved in fundamental cellular processes and have been implicated in disease (Ploumakis and Coleman, 2015). As outlined in the Introduction however, a number of enzymes within the JmjC-only family remain poorly- or un-characterised. Understanding the role of such JmjC proteins is of growing interest and importance.

In 2014, prior to the start of this PhD project, there were no published research articles that directly focussed on investigating the function of JMJD7. However, there were indications from large-scale genetic analyses that JMJD7 might be involved in neurological disease and mental retardation (Matsunami et al., 2014, de Ligt et al., 2012). Whether JMJD7 has a role in other diseases, including cancer, was not known, but of interest (explored in Chapter 3).

Molecular mechanisms underlying the potential role(s) of JMJD7 in neurological (and possibly other) disease are unclear, largely because the biochemical activity of JMJD7 remains elusive. JmjC-only 2OG oxygenases have generally been assigned as protein hydroxylases (Feng et al., 2014, Webby et al., 2009, Ge et al., 2012, Mahon et al., 2001), and in some cases as histone lysine and arginine demethylases (Lu et al., 2009, Chang et al., 2007, Hsia et al., 2010). However, the latter assignments have recently been challenged by detailed structural, phylogenetic, and biochemical analyses (Chowdhury et al., 2014, Williams et al., 2014, Wang et al., 2015a, Bottger et al., 2015). Therefore, the available evidence suggests that JMJD7 is likely to function as a protein hydroxylase, but the substrates of this potential activity are unknown. This Chapter describes work aimed at contributing to the basic characterisation of JMJD7, using a variety of biochemical and cell biology

approaches in cell models. The findings have contributed towards a joint second author publication in Nature Chemical Biology (Markolovic et al., 2018).

2.1 Structural analyses: JMJD7 oligomerises *in vivo.*

The biochemical activity of 2OG oxygenases can be inferred by detailed structural analyses (Markolovic et al., 2016). Therefore, our collaborators in the Schofield laboratory (Oxford) solved the crystal structure of human JMJD7 (Markolovic et al., 2018). The structure reveals many similarities with other JmjC oxygenases, including the presence of all the conserved Fe(II) co-ordinating and 2OG binding residues, consistent with it likely being an active oxygenase. Specifically, the DSBH consists of the usual eight β-strands which align to form two anti-parallel β-sheets (Figure 2.1a, orange residues). Within the DSBH are the conserved Fe(II) co-ordinating residues (H178, D180 and H277) forming an octahedral with three water molecules (Figure 2.1a, green residues) (Markolovic et al., 2018). Hydrogen bonds are formed between the C1 carboxylate of 2OG and both N184 and N289 of JMJD7. The 2OG C5 carboxylate group forms electrostatic and hydrogen bonds with K193, and further hydrogen bonding between the C5 and Y127, T175 and Y186 create a tight interaction which, in turn, results in a slow substrate turnover (Figure 2.1a, cyan residues) (Markolovic et al., 2018). JMJD7 has recently been reported as a histone demethylase (Liu et al., 2017a, Liu et al., 2018a), however, the JMJD7 structure does not have any of the residues or domains normally associated with demethylase activity and DNA or histone binding (Markolovic et al., 2018). Furthermore, mass spectra data showed that JMJD7 is unable to modify either mono-, di-, or tri-methylated H3K4, H3K9, H3K27 and H3K36 *in vitro*. Therefore, the initial structure

and biochemical analyses are more consistent with protein hydroxylases, rather than histone demethylase, activity.

Protein hydroxylases of the JmjC-only family, such as FIH, MINA, NO66 and JMJD6 are known to require dimerisation for activity. Indeed, the JMJD7 structure indicates that JMJD7 is also a dimer, but that dimerisation occurs via a unique mechanism: Hydrophobic interactions between N- and C-terminal α-helices on both monomers come together to form a dimerisation interface (Figure 2.1a). The cysteine at position 47 forms a disulphide bond between the two monomers and is thought to be important for dimer stabilisation (see purple asterix in Figure 2.1a). In contrast, other JmjC-only hydroxylases (e.g. MINA53 and FIH) dimerise via an interface formed by only C-terminal terminal α-helices (Lancaster et al., 2004, Chowdhury et al., 2014).

The oligomerisation status of a protein in a crystal, or in solution *in vitro*, does not necessarily reflect the native state *in vivo*. Therefore, we developed a cellular assay to test whether JMJD7 oligomerises in cells, based on differential epitope-tagging and immunoprecipitation (IP) (Figure 2.1b). HEK293T cells were transfected with N-terminally HA- or FLAG-tagged JMJD7 plasmids, either together or alone, followed by anti-HA or -FLAG immunoprecipitation and western blotting. If JMJD7 dimerises in cells we predicted that HA-JMJD7 would be detected in anti-FLAG IP's, and vice versa (Figure 2.1b). Indeed, Figure 2.1c shows that HA-JMJD7 bound to FLAG-JMJD7 and that FLAG-JMJD7 bound to HA-JMJD7, suggesting that JMJD7 is able to dimerise in cells. When FLAG-JMJD7 was transfected without HA-JMJD7 no signal was detected, (and vice versa), indicating that the interactions were specific.

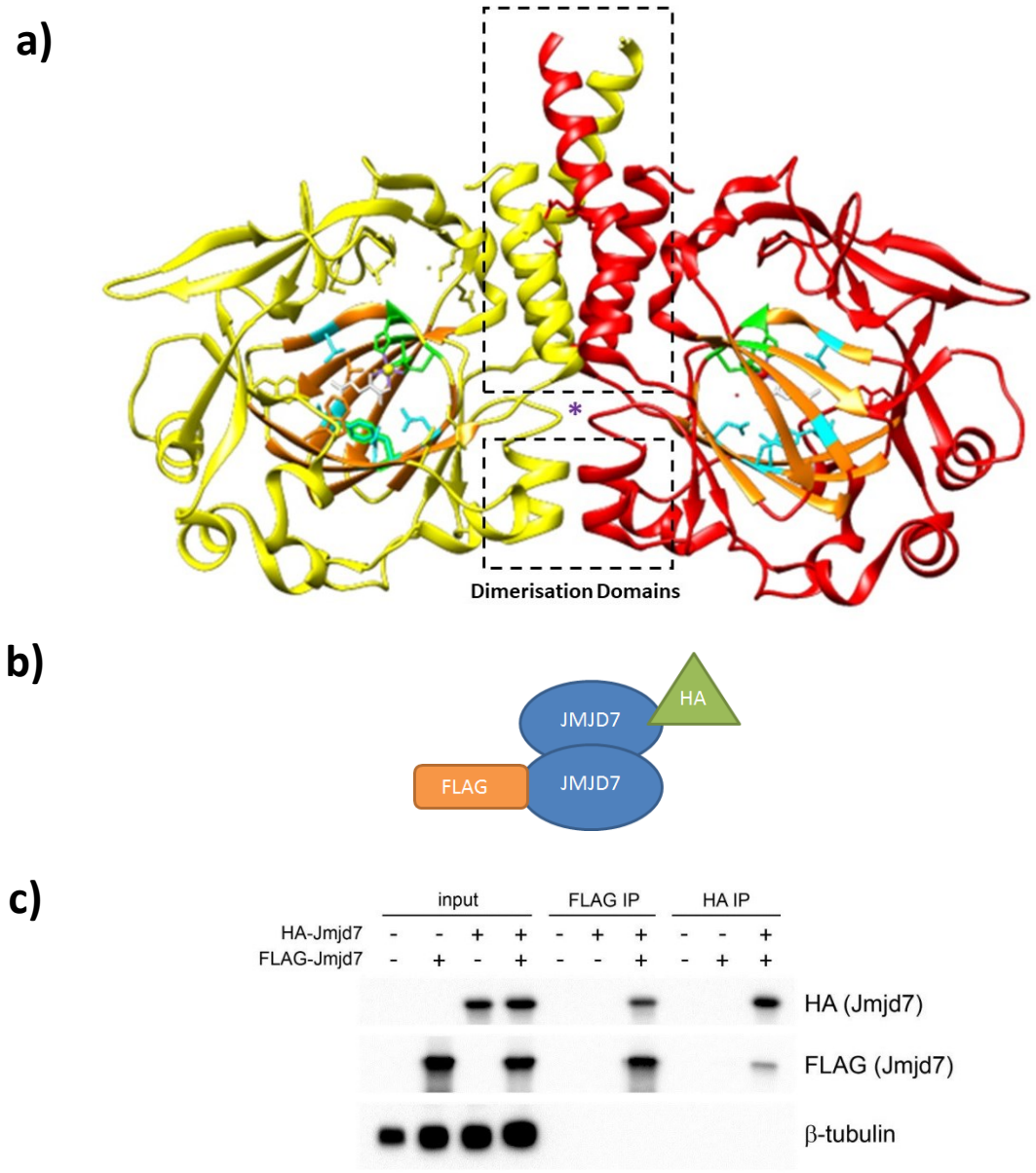

Figure 2.1 JMJD7 oligomerises *in vitro* and *in vivo* a) The crystal structure of JMJD7 modelled in Chimera (Pettersen et al., 2004). JMJD7 oligomerises in cells using a unique interaction between the N-terminal and C-terminal α-helices (α1 and α9). The DSBH is seen in orange with 2OG and Mg^{2+} in the active site. The purple asterix marks the disulphide bond between the two C47 residues, thought to be critical for oligomerisation. The essential Fe(II) co-ordinating residues are noted in green and 2OG binding residues are shown in cyan. Structure crystallised by Dr Markolovic, used from Markolovic et al., 2018, modified using Chimera: Petterson et al., 2004 b) basic illustration of the concept behind the cellular dimerisation assay. HEK293T cells were transfected with HA-JMJD7 or FLAG-JMJD7 either together or alone. Cell lysates were immunoprecipitated with either FLAG or HA epitope tag and western blotted for the reciprocal tag. c) western blot after dimerisation IP demonstrating that JMJD7 can oligomerise in cells. n=3

2.2 JMJD7 hydroxylates Developmentally Regulated GTP-binding proteins 1 and 2.

The structural analyses by our collaborators indicated conservation of critical co-factor residues required for activity (reviewed above), consistent with JMJD7 being an active hydroxylase. Therefore, to screen for potential substrates a proteomic assay was initiated by Dr Qinqin Zhuang in the Coleman laboratory. The assay uses large-scale immunoprecipitation coupled to mass spectrometry to identify proteins that specifically interact with active (WT) JMJD7, but not to an inactive JMJD7 mutant (H178A mutation causes loss of Fe(II) binding). This approach has successfully identified novel substrates for other JmjC-only protein hydroxylases (Feng et al., 2014, Dr Coleman personal communication). HEK293T cell lines were created that stably expressed WT or mutant 3XFLAG-tagged JMJD7 before treating with dimethyl-*N*-oxalyglycine (DMOG, a cell permeable 2OG competitive inhibitor used to 'lock-in' substrates). Cell extracts were subject to anti-FLAG-IP followed by mass spectrometry identification of interacting proteins (by the Advanced Mass Spectrometry service, Oxford). A comparative analysis of WT vs H178A was performed to identify candidate substrates binding in an 'activity-dependent' manner. This approach identified Developmentally Regulated GTP binding proteins 1 and 2 ('DRG1/2'), and their obligate binding partners, DRG Family Regulator Protein 1 (DFRP1) and DFRP2. Independent western blotting experiments validated the results (Figure 2.2a, provided by Dr Mathew Coleman and Dr Qinqin Zhuang). Further investigation by Dr Zhuang identified that DRG1 and DRG2 are the primary substrates, and that JMJD7 hydroxylates a conserved lysine at their N-terminus, at K22 and K21, respectively (Malkovic *et al*. 2018).

Developmentally Regulated GTP binding proteins 1 and 2

The JMJD7 hydroxylation sites reside within a conserved domain at the N-terminus of DRGs located on the 'turn' of a helix-turn-helix (HTH) (Figure 2.2b and 2.2c). Although the function of this domain in DRGs is not known, complementation experiments in yeast demonstrate it is critical for function (Francis et al., 2012). Structural analyses of yeast DRG1 demonstrated the presence of additional domains including a Ribosomal protein S5 2-like (S5D2L) domain, the GTPase catalytic domain, and a C-terminal 'TGS' domain which is thought to be essential for the interaction of DRGs with DFRPs and ribosomes (Francis et al., 2012).

Although DRG proteins are better characterised than JMJD7, their exact function is unclear, complicating attempts to rapidly elucidate the consequences of their hydroxylation. Initial work on DRG (now known as DRG1) was reported in a mouse model where, at the time, it was the only known family member (Kumar et al., 1993). However, DRG was more similar to a *C.elegans* and *S.pombe* orthologue than that in higher eukaryotes such as *D.melanogaster* and *Xenopus*, highlighting the potential for another unknown, related protein. It was not until 1998 that this second gene was cloned, resulting in the nomenclature DRG1 and DRG2 (Zhao and Aplan, 1998, Li and Trueb, 2000). DRG1 and DRG2 share 57% sequence identity and 66% similarity (Figure 2.2c). Perhaps consistent with important biological roles, high sequence conservation is seen between human, mouse, xenopus and yeast (Li and Trueb, 2000). As their name suggests, both DRGs have been associated with development (Sazuka et al., 1992, Kumar et al., 1993, Kumar et al., 1992, Schenker et al., 1994).

An added complication with respect to the DRG literature is in the nomenclature, with at least three other proteins using the same acronym: AAA-ATPase *d*iazaborine *r*esistance *g*ene *1 (DRG1*), Differentiation related gene 1/N-myc downstream regulated 1 (DRG1/NDRG1) or Dorsal Root Ganglia (DRG). As such, some papers have studied the Developmentally Regulated GTP-binding protein 1, but have accidentally reviewed literature on unrelated DRGs in discussion (Delassus et al., 2011). Any further use of "DRG" will specifically refer to the Developmentally Regulated GTP-binding protein identified as novel JMJD7 substrates.

As members of the 'Obg' branch of the broader 'TRAFAC' (**TRA**nslation **FAC**tor) subfamily of GTP-ases, DRG1 and DRG2 are thought to function in ribosome assembly and/or cellular growth (Francis et al., 2012, Li and Trueb, 2000, Morimoto et al., 2002). Endogenous RBG1 (yeast DRG1) associates with actively translating polyribosomes with Tma46 (DRG Family Regulatory Protein 1 (DFRP1)) (Wout et al., 2009, Daugeron et al., 2011, Francis et al., 2012, Ishikawa et al., 2009a). In contrast, DRG2 was reported not to associate with polysomes, but its yeast orthologue, Rbg2 and Gir2 (DFRP2), co-purified with translation-associated proteins (Daugeron et al., 2011, Ishikawa et al., 2009a, Wout et al., 2009). Interestingly, gene knockout experiments indicated that Rbg1 and Rbg2 may be functionally similar and have a role in cell proliferation (Daugeron et al., 2011). Although the exact mechanisms by which Rbg1 and Rbg2 regulate growth have not been elucidated, it seems likely their common roles in protein synthesis may be involved.

The DRG enzymes have also been implicated in other cellular pathways. For example, DRG2 overexpression in Jurkat T cells supressed growth and caused loss of cell-to-cell adhesion (Ko et al., 2004). In this study, gene expression analysis

showed that a sub-set of genes were deregulated in cells over expressing DRG2, including DUSP7, a phosphatase which acts within the MAP kinase signalling pathway (Theodosiou and Ashworth, 2002). Furthermore, in hepato-carcinoma cells, DRG2 overexpression rescued chemically induced apoptosis, possibly by inducing the expression of pro-survival genes (Song et al., 2004a, Chen et al., 2012). However, DRG2 knockdown negatively regulates expression of CDK1-CycB1 via up regulation of the CDK1-CycB1 regulatory proteins, Wee1, Myt1 and p21 (Jang et al., 2016). Alternatively, DRG2 has also been implicated in endosome formation and transferring recycling (Mani et al., 2016, Mani et al., 2017). In addition to cancer DRG2 has also been linked to bone formation and multiple schlorosis (Ko et al., 2014, Ke et al., 2013).

DRG1 and DRG2 stability is regulated by their binding partners, DFRP1 and DFRP2, respectively. It was shown that knockdown of DFRP1 resulted in loss of DRG1 protein, over expression of DFRP1 induced DRG1 protein expression and the same for DRG2 and DFRP2 (Ishikawa et al., 2009a, Ishikawa et al., 2005). Interestingly, although DFRP1 and DFRP2 are evolutionarily distinct proteins they share high sequence similarity in a single DFRP domain, a domain identified as critical for DRG binding (Ishikawa et al., 2009a, Ishikawa et al., 2005).

Overall, the lack of basic characterisation of JMJD7 and DRG/DFRP complexes (and the complex literature associated with the latter) will impede future studies aimed at understanding the function of this novel pathway in cell biology and disease. For example, it might be beneficial to know more about; (i) where DRG1/2 localise in human cells and how this compares to JMJD7, (ii) how ubiquitous JMJD7 expression is and whether this correlates with DRG1/DFRP1 and DRG2/DFRP2 expression, (iii)

whether the hydroxylation of DRGs by JMJD7 is conserved, (iv) and whether (like DRGs) JMJD7 is involved in cellular growth control.

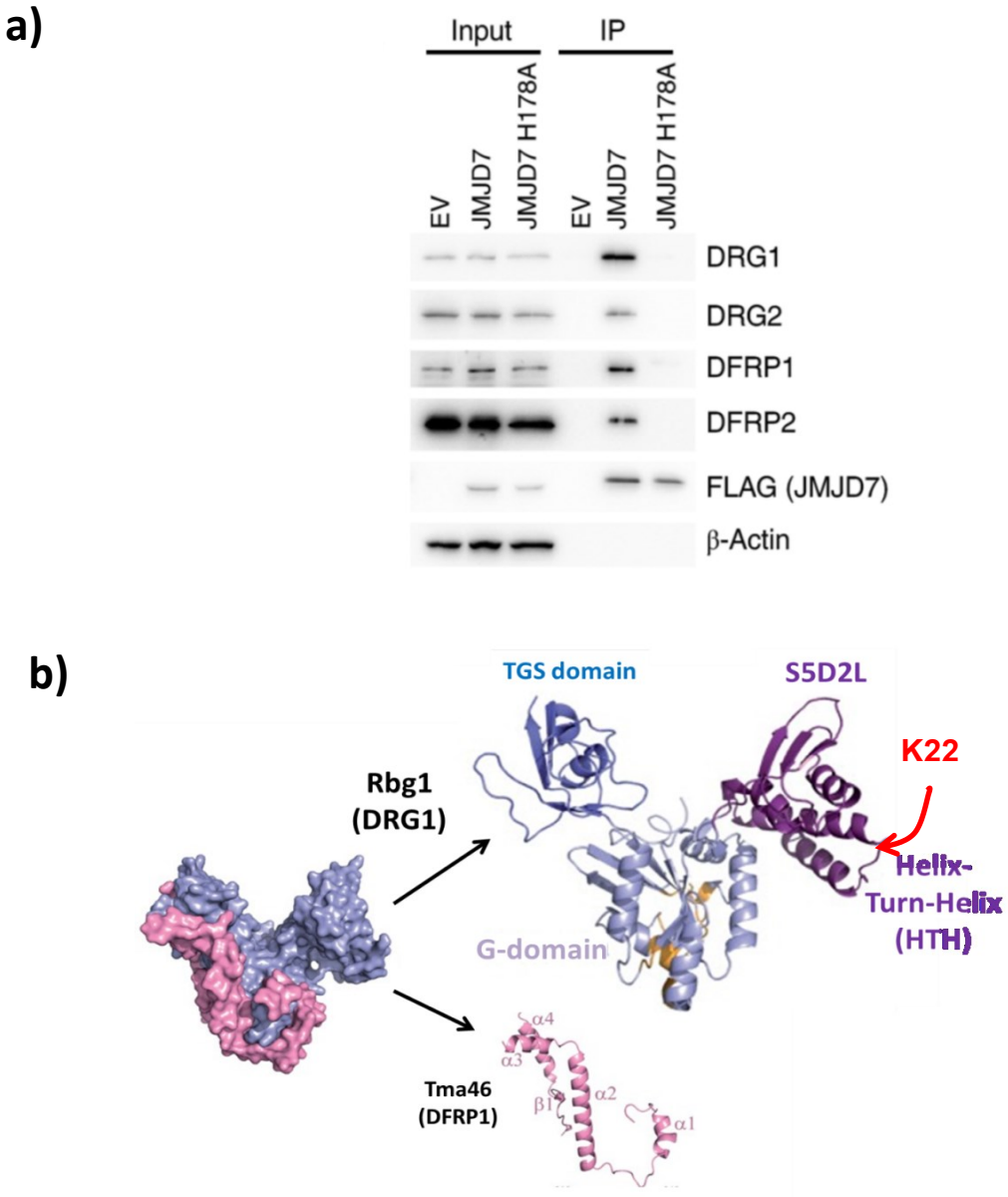

Figure 2.2 Identification of the DRGs and DFRPs as JMJD7 substrates. (a) Confirmation of DRG1, DRG2, DFRP1 and DFRP2 as hydroxylase substrates of JMJD7. HEK293T cells were transfected with JMJD7 WT and inactive JMJD7 H178A and subject to 10 hours of DMOG treatment. Cell lysates were immunoprecipitated with FLAG beads and western blotted for candidate substrates. Figure from Markolovic et al. 2018, Fig 2a, performed by Dr Zhuang. b) Crystal structure adapted from (Francis et al., 2012) representing the yeast orthologues of DRG1 and DFRP1 in complex. DRG1 is hydroxylated by JMJD7 on K22 of the HTH domain (red arrow).

c)

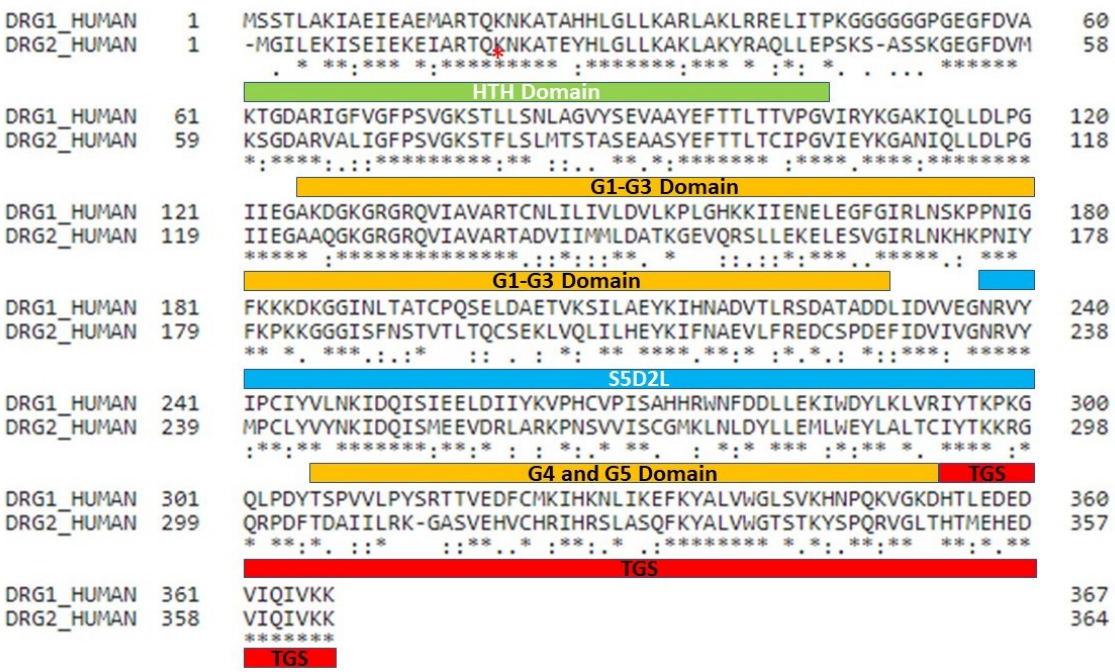

Figure 2.2 c) Protein alignment of DRGs highlighting the site of hydroxylation (K22 or K21 for DRG1 and DRG2, respectively) with a red Asterix and their conserved domains. Alignment performed by Uniprot (The Uniprot Consortium, 2017).

2.3 JMJD7 co-localises with substrates, DRG1 and DRG2.

Next, we performed exogenous and endogenous localisation studies to further characterise JMJD7, DRGs, and their interaction. First, we PCR cloned FLAG-tagged JMJD7 into pcDNA3, with pcDNA3 DRG1 and DRG2 expression vectors provided by Dr Qinqin Zhuang. HeLa cells were seeded onto a sterile glass cover slip and subject to transient transfection. 48 hours after transfection cells were fixed and permeabilised before blocking and staining for either JMJD7, DRG1 or DRG2, and 4′,6-diamidino-2-phenylindole (DAPI). Panels 3 and 5 of Figure 2.3a show that

JMJD7 co-localises with both DRG1 and DRG2 in HeLa cells, consistent with the interaction data presented above.

Although DRG1, DRG2 and JMJD7 all display their highest expression in the cytoplasm, some nuclear staining was also observed. Interestingly, nuclear staining for DRG1 was more prominent than DRG2 (Figure 2.3a, HA stain in panel 2 and 4, respectively), perhaps consistent with additional functions. Finally, neither DRG1 nor DRG2 localisation was significantly affected by co-transfection with JMJD7 (compare panels 2 vs 3 and panels 4 vs 5), suggesting that JMJD7 catalysed hydroxylation does not affect DRG sub-cellular localisation. Attempts to extend these microscopy experiments to the corresponding endogenous proteins failed because the antibodies were not suitable (data not shown).

To attempt to observe the localisation of all the endogenous pathway components we next performed biochemical fractionation using a commercially available kit. In keeping with the exogenous studies, DRG1 is equally distributed between the cytoplasm and the nucleus, and JMJD7 and DRG2 are mostly expressed in the cytoplasm with some residual nuclear expression (Figure 2.3b). Consistent with the differential DRG expression, DFRP1 is evenly distributed between the nucleus and cytoplasm, whereas DFRP2 is mostly cytoplasmic, with a small amount residing in the nucleus.

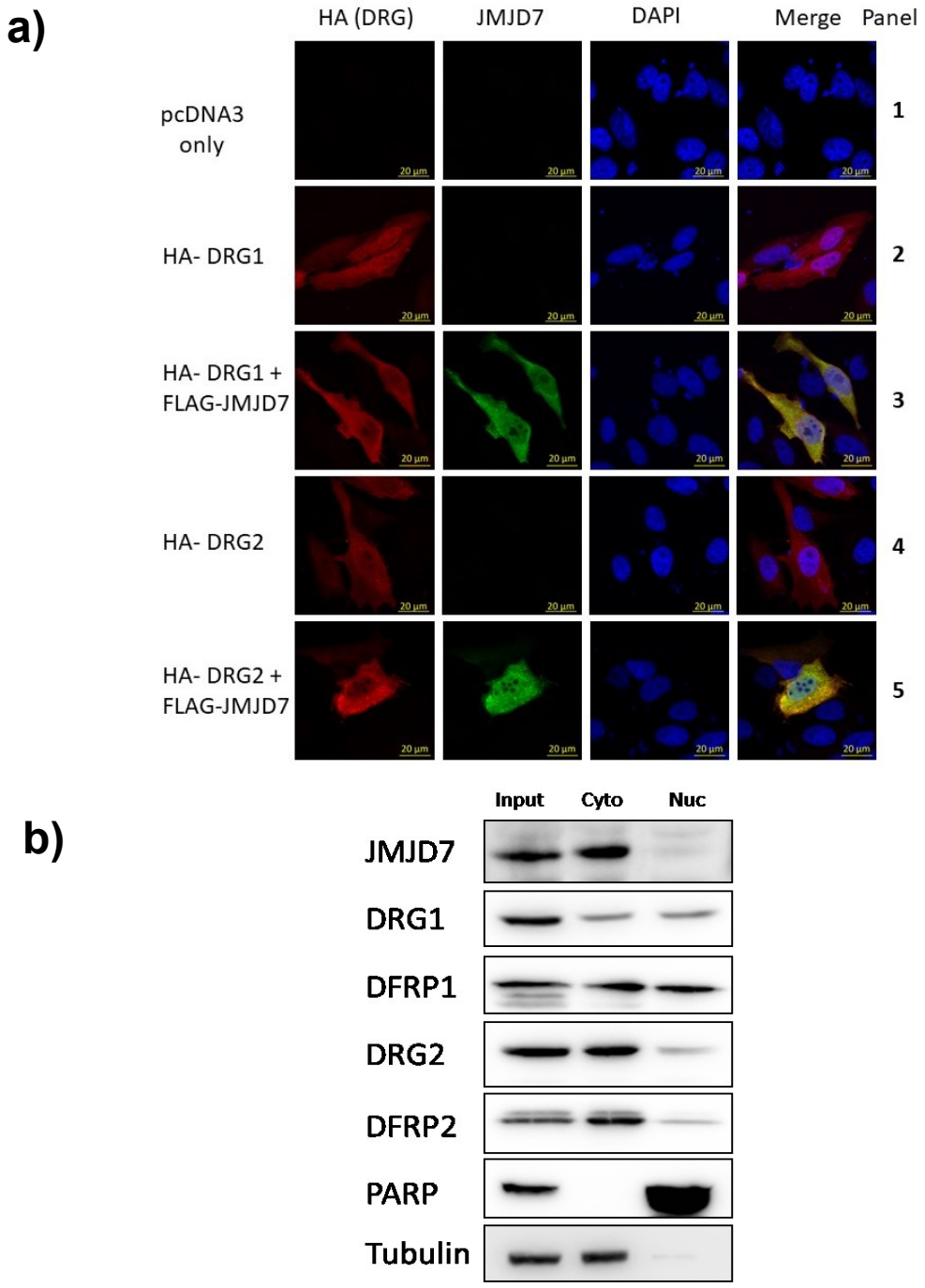

Figure 2.3 JMJD7 subcellular localisation. a) Confocal microscopy identifying co-localisation of JMJD7 with DRG1 and DRG2. HeLa cells were seeded onto glass cover slips and transfected with either DRG1 or DRG2, and with or without JMJD7. After 48 hours of over expression the cover slips were fixed stained with JMJD7 (green) and HA (Red) antibodies, DNA was stained using DAPI direct stain. n=2 b) HeLa cells whole cell extracts were subject to biochemical fractionation (NE-PER™ Nuclear and Cytoplasmic Extraction Reagents) and analysed by western blot. Showing JMJD7 co-localises with endogenous DRG1, DFRP1, DRG2 and DFRP2. n=3

2.4 JMJD7 is ubiquitously expressed

Having contributed to the validation of the JMJD7/DRG interaction we next sought to explore how widespread this novel 'pathway' might be. To test this, nine cell lines derived from different tissues were tested for endogenous pathway component expression by western blotting. HeLa cells (cervical cancer), HEK293T (embryonic kidney), AGS (gastric cancer), Caco2 (colo-rectal cancer), SKRC45 (renal cancer), A549 (lung cancer), H1299 (lung cancer), KTCL126 (kidney cancer), and SHSY5Y (paediatric neuroblastoma) cells were lysed in Radioimmunoprecipitation assay (RIPA) buffer and protein concentration normalised by Biorad Pierce assay. In Figure 2.4a, the band predicted from siRNA knockdown experiments (Figure 2.4b) to be JMJD7 is highlighted with a red arrow. The antibodies for endogenous DRG1, DRG2, DFRP1 and DFRP2 were generally significantly more specific than JMJD7 and were also previously validated in JMJD7 immunoprecipitation experiments (Figure 2.2a). The results show that JMJD7 is ubiquitously expressed throughout the cell lines tested with slightly more in the paediatric neuroblastoma cell line, SHSY5Y. Similarly, DRG2 and DFRP2 are also ubiquitously expressed. DRG1 is also present in all cell lines but is expressed most highly in HeLa (cervical cancer) and HEK293T cells (embryonic kidney) with the least expression in KTCL126 (kidney cancer) and SHSY5Y (paediatric neuroblastoma). DFRP1 is expressed in all cell lines except the gastric cancer cell line, AGS. The highest DFRP1 expression was observed in in H1299 cells (lung cancer) and HeLa cells (cervical cancer). With the exception of DFRP1, all other pathway components are expressed in all the tested cells lines indicative of ubiquitous expression and a conserved role within the cell.

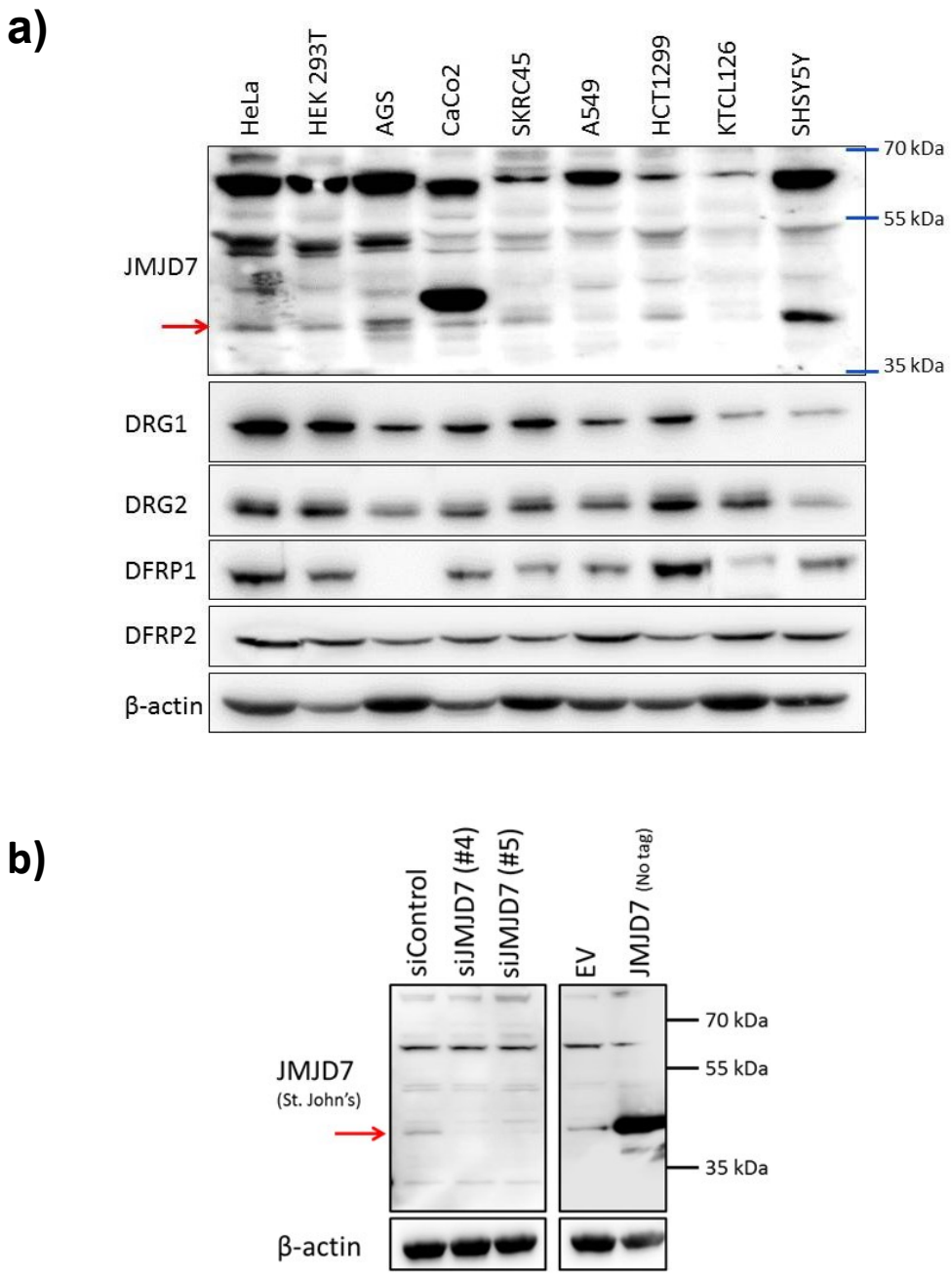

Figure 2.4 JMJD7 expression between cancer cell lines. a) Comparison of protein expression for JMJD7 and pathway components between cell lines. Nine cell lines from various tissues were lysed and protein expression analysed by western blot. SHSY5Y cells have highest JMJD7 expression. n=1 b) Assignment of the endogenous JMJD7 band in HeLa cells. western blot after siRNA knockdown of JMJD7 (siRNA from Sigma, Cat no. SASI_Hs02_00326*04*, SASI_Hs02_00326*05*) over 72 hours, and 48 hour transient transfection of untagged JMJD7. n=2

2.5 JMJD7 function is conserved throughout species

Ubiquitously expressed proteins that perform important functions are often highly conserved throughout evolution. Although DRGs are highly conserved (see above), nothing is known about the conservation of JMJD7. Therefore, the sequence alignment tool on the Uniprot database was used to align assigned JMJD7 protein sequences from human, mouse, fruit fly, bovine and zebrafish. Figure 2.5a shows high sequence homology between all the represented species. Furthermore, all the essential Fe(II)- and 2OG-binding residues are fully conserved, consistent with potential conservation of JMJD7's lysyl hydroxylase activity towards DRG1/2.

To test whether the activity-dependent binding of DRGs to JMJD7 is conserved in other species we focussed on the JMJD7 orthologue from *D.melanogaster*, as follows. The mRNA from twenty whole female *D.melanogaster* was isolated and reverse transcribed before PCR amplification of *D.melanogaster* JMJD7 (dmJMJD7) with an N-terminal FLAG tag and cloning into pcDNA3. The dmJMJD7 and human JMJD7 were transiently transfected into HEK293T cells, and allowed to express for 48 hours before treating with DMOG for 16 hours. Cells were lysed for protein before anti-FLAG-immunoprecipitation and immunoblot for FLAG (JMJD7's) and endogenous human DRGs. As seen in Figure 2.5b, dmJMJD7 was able to confer DMOG-dependent binding to DRG1 and DRG2, consistent with a hydroxylase/substrate interaction. This degree of functional conservation could suggest an important role for JMJD7 and DRG hydroxylation within the cell.

In light of the data above with dmJMJD7, we sought to explore the potential importance of JMJD7 in *D.melanogaster* through collaboration with the group of Pablo Wappner (Buenos Aires, Argentina) who use the fruit fly as a working model to

study the function of 2OG oxygenases. To this end, *D.melanogaster* were purchased which hosted either RNAi targeting control or endogenous *dmJMJD7* ('CG10133') in the posterior wing compartment. Images were taken on a DP71 digital camera connected to an Olympus MVX10 steromicroscope and were analysed using ImageJ. Wing size was calculated by measuring the distance between three standardised regions of the wing. Interestingly, Figure 2.5c shows that after JMJD7 knockdown the wing increased in size (Figure provided by M Katz). This phenotype is likely explained by an increase in cell size, rather than an increase in cell number (Figure 2.5d). These results indicate that JMJD7 is involved in cell growth control in *D.melanogaster* and would therefore be an interesting target for loss-of-function models in human cells.

a)

```
JMJD7_HUMAN   MAEAALEAVRSELREFPAAARELCVPLAVPYLDKPPTPLHFYRDWVCPNRPCIIRNALQH
JMJD7_MOUSE   MAEAALEAVRRALQEFPAAARDLNVPRVVPYLDEPPSPLCFYRDWVCPNRPCIIRNALQH
Q9VU77_DROME  -----MSEVERALDVLLQEAEELCIGSSVVELDRIPTALEFCREFYSKNQPVVIRKAL-N
F1MEH3_BOVIN  MAEAALDAVRRELREFPVAARELSVPLAVPYLDEPPSPLHFYRDWVCPNRPCIIRNALQH
F1R3W9_DANRE  -----MDEVKECLRDFPKEARELYLNDAVPYLDEPLSPLQFYRDWIGPNKPCIIRNAFND

JMJD7_HUMAN   WPALQKWSLPYFRATVGSTEVSVAVTPDGYADAVR----GDRFMMPAERRLPLSFVLDVL
JMJD7_MOUSE   WPALQKWSLSYLRATVGSTEVSVAVTPDGYADAVR----GDRFVMPAERRLPISHVLDVL
Q9VU77_DROME  WPAIGKWTPKYLIEALGDRSVDVAITPNGYADGLATQNGQEYFVLPLETKMKLSEVVRRL
F1MEH3_BOVIN  WPALRKWSLPYLRATVGSTEVSVAVTPDGYADAVR----GDRFVMPAERRLPLSHVLDVL
F1R3W9_DANRE  WPALSKWNPTYLREKVGSKVISVAVTPNGFADAVN----GNRFVMPEERQMSFSSLLDIV

JMJD7_HUMAN   EGRAQHPGVLYVQKQCSNLPSELPQLLPDLE-SHVPWASEALGKMPDAVNFWLGEAAAVT
JMJD7_MOUSE   EGRAQHPGVLYVQKQCSNLPTELPQLLSDIE-SHVPWASESLGKMPDAVNFWLGDASAVT
Q9VU77_DROME  DDP--TGAVHYIQKQNSNLSVDLPELAADLRVSDLDFAQQSFNKPPDAVNFWLGDERAVT
F1MEH3_BOVIN  EGRAQHPGVLYVQKQCSNLPTELPQLLPDVE-PHVPWASEALGKMPDAVNFWLGEAAAVT
F1R3W9_DANRE  EGKIKSSAVFYVQKQCSNLMEEIPELTGDVQ-THIPWMSEALGKLPDAVNFWLGEESAVT

JMJD7_HUMAN   SLHKDHYENLYCVVSGEKHFLFHPPSDRPFIPYELYTPATYQLTEEGTFKVVD----EEA
JMJD7_MOUSE   SLHKDHYENLYCVVSGEKHFLLHPPSDRPFIPYNLYTPATYQLTEEGTFRVVD----EEA
Q9VU77_DROME  SMHKDPYENVYCVISGHKDFVLIPPHQLSCVPRGIYPTGVYKTSDSGQFYIEPLRDEEGS
F1MEH3_BOVIN  SLHKDHYENLYCVVSGEKHFLLHPPSDRPFIPYELYTQATYQLTEEGSFRMVD----EEA
F1R3W9_DANRE  SMHKDHYENLYCVISGQKEFVLLPPTDRPFIPYELYQPATYRQKDDGTFEIVD----EEN

JMJD7_HUMAN   MEKVPWIPLDPLAPDLARYPSYSQAQALRCTVRAGEMLYLPALWFHHVQQSQGCIAVNFW
JMJD7_MOUSE   MEKVPWIPLDPLAPDLTQYPSYSQAQALHCTVRAGEMLYLPALWFHHVQQSHGCIAVNFW
Q9VU77_DROME  DQFTEWVSVDPLSPDLAKYPEYARAKPLKVRVHAGDILYLPNYWFHHVSQSHKCIAVNFW
F1MEH3_BOVIN  MEKVPWIPLDPLAPDLARYPSYCQAQALRCTVRAGEMLYLPALWFHHVQQSHGCIAVNFW
F1R3W9_DANRE  SPKVPWIPLDPLKPDFERFPSYRHAKALHCTVKAGEMLYLPSLWFHHVRQSHGCIAVNFW

JMJD7_HUMAN   YDMEYDLKYSYFQLLDSLTKASGLD
JMJD7_MOUSE   YDMEYDLKYSYFQLMDTLTRATGLD
Q9VU77_DROME  YDLDYDSRYCYYRMLEQMTSARSG-
F1MEH3_BOVIN  YDMEYDLKYSYFQLLDSLTKVSGLN
F1R3W9_DANRE  YDMEYDIKYNYFQLVEALTNAVGSL
```

b)

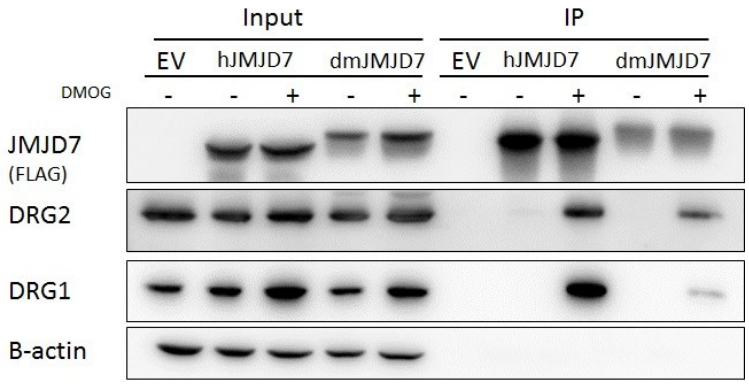

Figure 2.5 JMJD7 is highly conserved in eukaryotes. a) JMJD7 sequence alignment between human, mouse, fruitfly, cow and zebrafish highlighting the essential Fe(II) binding residues (red arrows) and the 2-OG binding residues (green arrows), all of which are conserved. Sequences obtained and analysed using Uniprot (The Uniprot Consortium, 2017) b) D.*melanogaster* JMJD7 binds to human DRG1 and DRG2 in a DMOG-dependent manner. HEK293T cells were transfected with either human or D.*melanogaster* JMJD7 and treated with DMOG or vehicle for 15 hours. Cell lysates were subject to anti-FLAG immunoprecipitation before western blot. n=4

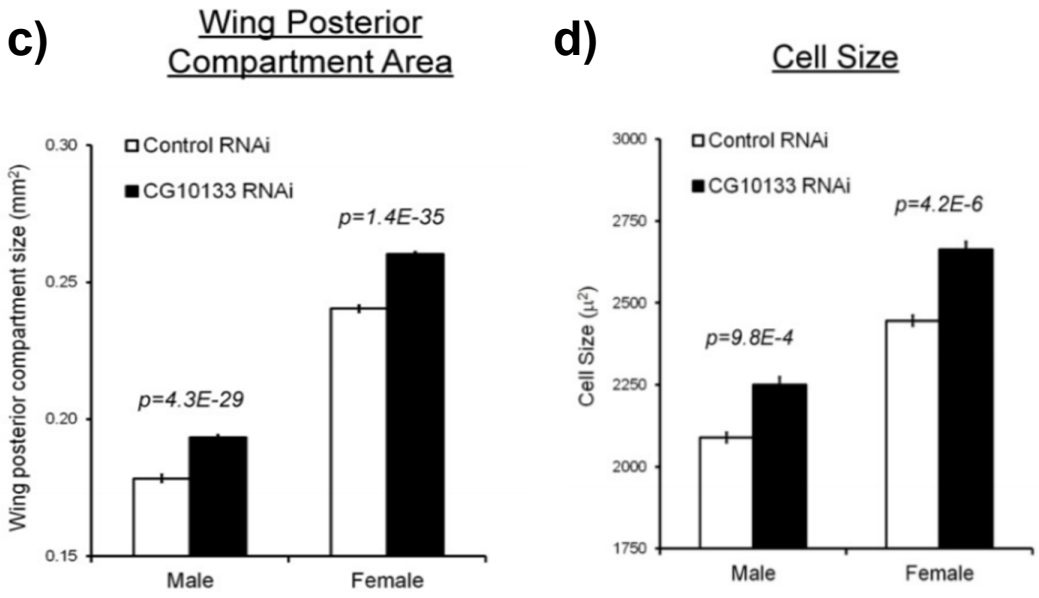

Figure 2.5 c) *D.melanogaster* containing siJMJD7 (CG10133) or siControl were analysed for posterior wing compartment size. siJMJD7 cells shows larger wings than control flies, concluding that this is a result of larger cell size d) Quantification of cell size was achieved by counting the number of wing hairs per square mm. Error bars represent standard error of the mean. Six wings used in each individual experiment. Figures c) and d) performed by M.Katz.

2.6 Developing a JMJD7 shRNA loss of function model

Loss of function models in the fruit fly model indicate that JMJD7 may be important for growth control. To test this observation in human cells, three commercial short hairpin RNA (shRNA) vectors targeting JMJD7 were purchased from Transomics. These pZIP-TRE3G lentiviral vectors confer puromycin resistance and express doxycycline-inducible shRNAs in combination with GFP (Figure 2.6a). Figure 2.6b maps the shRNAs to the JMJD7 gene sequence. JMJD7 shRNA#1 targets a similar region to shRNA#2 with only a two base pair difference, at a position that is also present in the read-through transcript, JMJD7-PLA2G4B. The third shRNA targets a sequence towards the C-terminus that is only present in JMJD7 and not in JMJD7-PLA2G4B.

All shRNA sequences were initially tested in the gastric cancer cell line, AGS. After lentiviral infection and puromycin selection cells were tested using a doxycycline titration over 48 hours. Before lysis, cells were imaged on an EVOS microscope to capture GFP expression (Figure 2.6b). As seen in Figure 2.6c treatment with as little as 0.05µg/ml of doxycycline was sufficient to induce almost maximal GFP from most of the shRNA vectors. After imaging the cells were lysed, JMJD7 protein was detected using a specific antibody (St. John's Laboratory) and western blotting (Figure 2.6d). Consistent with Figure 2.6c, Figure 2.6d shows significant loss of JMJD7 protein expression with as little as 0.05µg/ml doxycycline.

a)

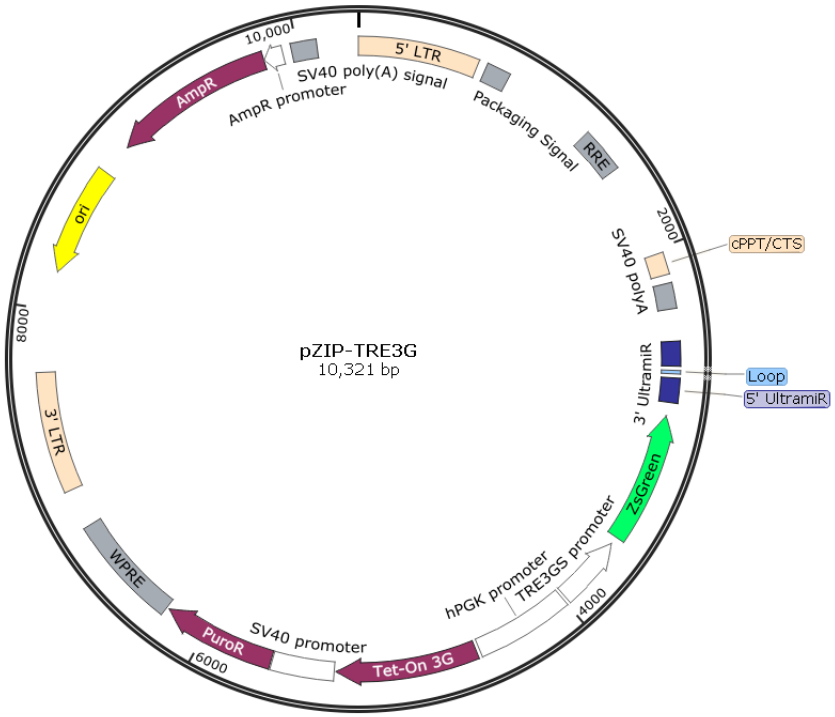

b)

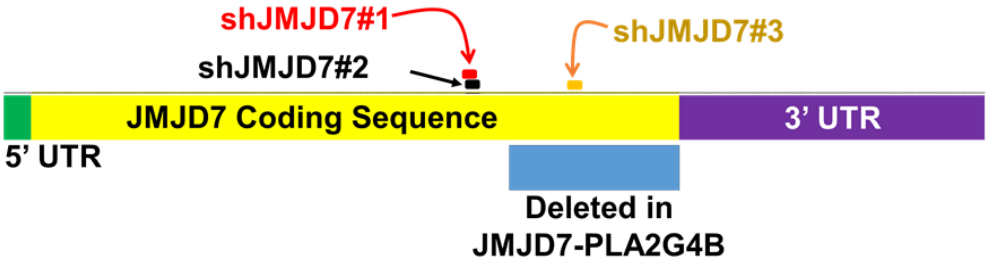

Figure 2.6 Validation of shRNA viral infection into AGS cells. a) Vector map of pZIP-TRE3G showing puromycin resistance cassette, tet-on/off sequence and GFP at the 3' of UltramiR shRNA sequence (Image from TransOMIC). b) Schematic diagram of JMJD7 gene sequence mapping the location of each shRNA on to the sequence. Two shRNA target the region of JMJD7 which is incorporated into the read-through transcript, PLA2G4B-JMJD7 (shJMJD7#1 and shJMJD7#2), the third (shJMJD7#3), targets the C-terminal region which is only present in JMJD7.

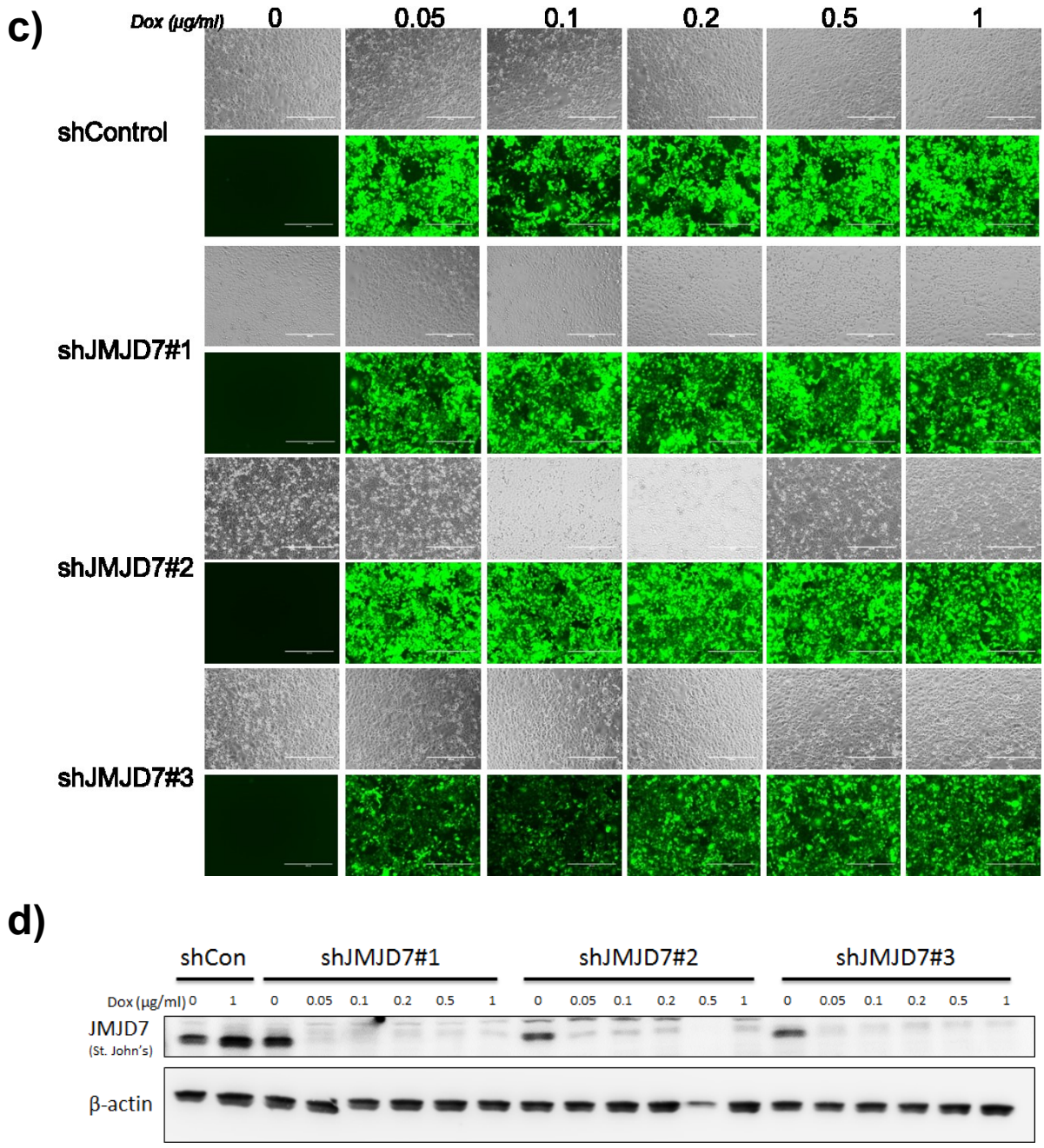

Figure 2.6 c) GFP images of AGS cells after lentivirus infection with pZIP-TRE3G shRNAs. Each cell line was treated with increasing doses of doxycycline for 48 hours, imaged on EVOS microscope before cell lysis and analysed by western blot dox (µg/ml) n=2 (d). GFP and JMJD7 knockdown is present in all cell lines with as little as 0.05µg/ml doxycycline (c) and (d). n=2

To test if the efficiency of knockdown changed with treatment time, the same cells were seeded and subject to a doxycycline timecourse using a standard dose of 1 µg/ml. As with doxycycline titration, images were taken on the EVOS microscope to capture GFP expression prior to lysis. Figure 2.7a shows the GFP images after doxycycline treatment of 0hr, 24hr, 48hr and 72hr. As expected, little or no leaky GFP expression was observed without doxycycline. GFP expression was visible after 24 hours of doxycycline and by 48-72 hours the induction had plateaued in all cell lines (Figure 2.7a). Similarly, western blotting of the respective proteins samples indicated that JMJD7 knockdown looks to plateau at 48-72 hours for shRNA1-3, with no loss of JMJD7 in control cells, as expected (Figure 2.7b). Surprisingly, in Figure 2.7b, endogenous JMJD7 levels appear to be reduced in the 0 µg/ml samples despite no detectable GFP being present in Figure 2.7a, probably due to “leaky” shRNA expression. Leaky expression in doxycycline inducible systems is often seen because fetal bovine serum (FBS) supplemented in cell culture media contains residual tetracycline levels. Taken together, we have identified three effective JMJD7 shRNAs that act in a dose- and time-dependent manner, thus validating their use for investigating the role of JMJD7 in growth.

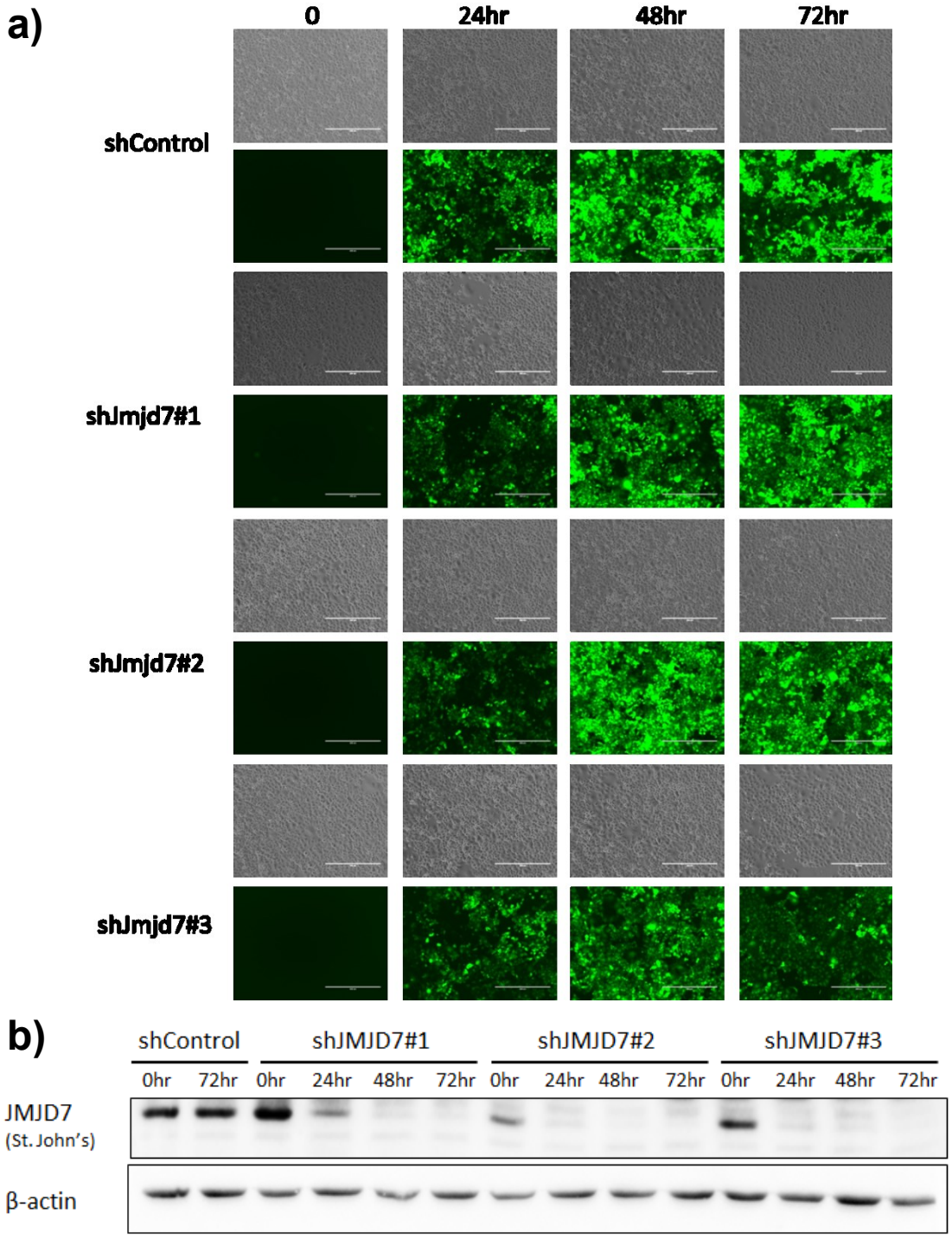

Figure 2.7 Validation of shRNA Viral Infection into AGS Cells. a) Doxycycline time course (1µg/ml, 0-72 hours) showing GFP expression of JMJD7 after just 24 hours but peaking at around 48-72 hours. AGS cells were seeded into plates, treated with 1µg/ml doxycycline for 0-72 hours, and imaged on EVOS microscope before lysis, n=2. Cells were lysed and analysed by western blot (b). western blot shows JMJD7 knockdown after 24 hours of doxycycline induction that peaks at 48-72 hours. n=2

2.7 Loss of JMJD7 results in delayed proliferation in AGS cells

To begin to directly investigate the role of JMJD7 in the growth of human cells, the AGS shRNA model described above was tested in an (3-(4,5-dimethylthiazol-2-yl)-5-(3-carboxymethoxyphenyl)-2-(4-sulfophenyl)-2H-tetrazolium) (MTS) cell proliferation assay. The MTS assay is used to measure the rate of cellular proliferation of viable cells. The principle behind the assay begins with the reduction of the MTS tetrazolium by metabolically active cells to create a formazan dye which can be measured by colourimetric assay at absorbance of 490nm. Each cell line (shControl and shJMJD7#1-3) was treated with doxycycline for an extended period (120 hours) to maximise the possibility of capturing potential consequences of reduced DRG hydroxylation. Cells were then reseeded for an MTS assay in the presence of doxycycline. The remaining cells were lysed for protein and used for western blot validation of knockdown (Figure 2.8a). Figure 2.8b shows the MTS cell proliferation curve of each cell line: Whereas the control cells demonstrate a classical exponential growth curve (blue line) all three JMJD7 shRNA cell lines show delayed growth. Strikingly, shJMJD7#3 cells grew significantly slower than shJMJD7#1 and shJMJD7#2 (Figure 2.8c): This could be due to shJMJD7#1/2 knocking down the JMJD7-PLA2G4B transcript, whereas shJMJD7#3 only targets JMJD7. Alternatively, subtle differences in the knockdown efficiencies of these shRNA sequences could explain the difference observed. Finally, we cannot rule out the contribution of off-target knockdown contributing to the differences in growth kinetics observed.

Overall however, the data presented are consistent with JMJD7 *positively* regulating cell growth in human cells, which may be at odds with the data obtained in the fruit fly model.

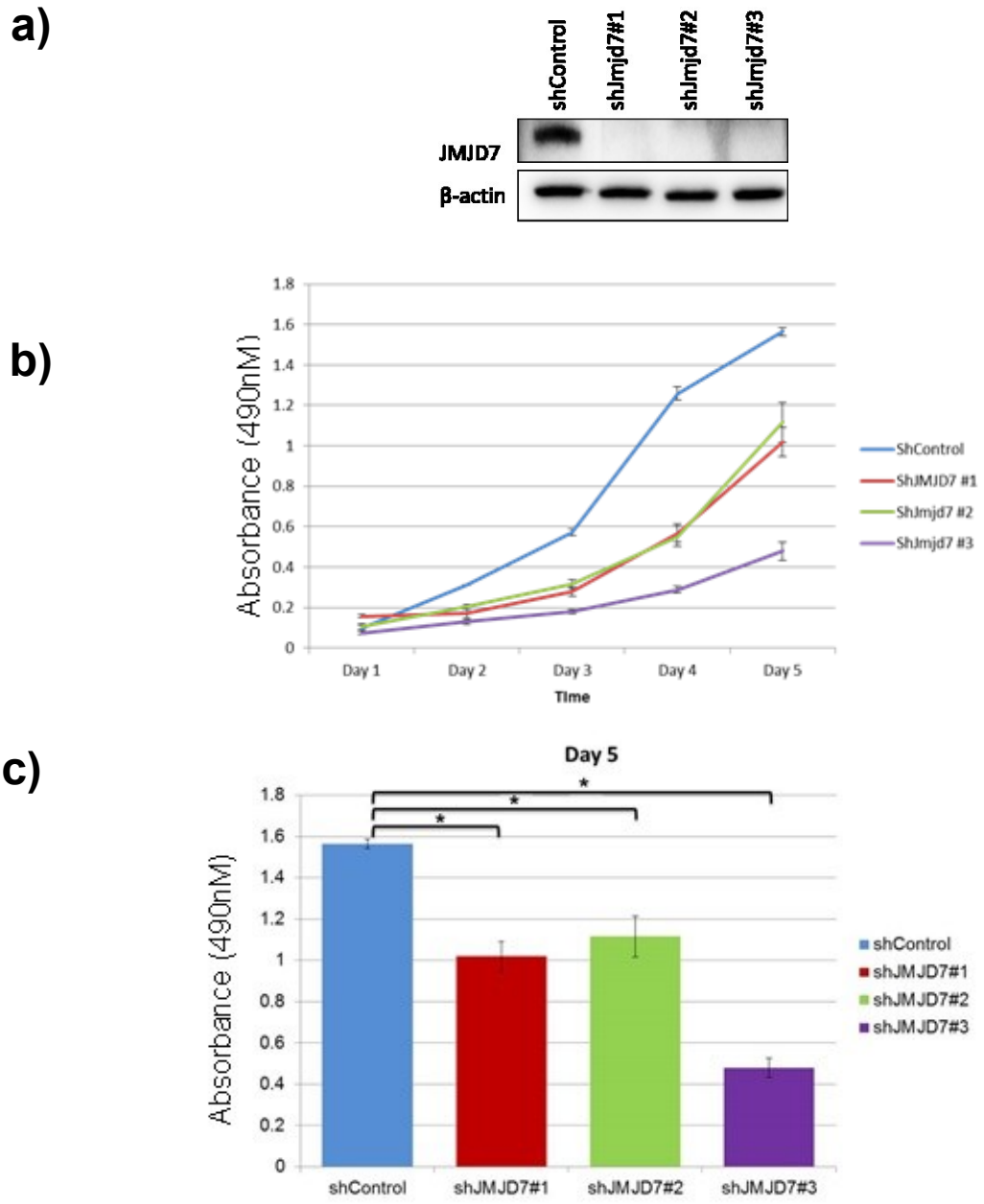

Figure 2.8 JMJD7 shRNA knockdown delays growth in AGS cells. Doxycycline inducible shRNA targeting JMJD7 was infected into AGS cells and tested for metabolic activity by MTS assay. The shJMJD7 AGS cells were seeded into 10cm plates, once settled the cells were treated with 1μg/ml doxycycline. 120 hours after first treatment the cells were trypsinised and either a) lysed for protein expression by western blot, or b) reseeded for MTS assay in the presence of 1μg/ml doxycycline and observed over 5 days. b) JMJD7 knockdown causes a significant growth defect in AGS cells. c) histogram representing day 5 of MTS assay highlighting significant growth defects of all JMJD7 shRNA compared to control. shJMJD7#1, $p < 0.05$, shJMJD7#2, $p < 0.05$, shJMJD7#3, $p < 0.05$. Full ANOVA tables in Appendix 1. n=5

2.8 Loss of JMJD7 results in delayed proliferation in HeLa cells

Considering the potential conflict between the fruit fly phenotype and the AGS model data presented above, we tested the role of JMJD7 in the growth of two additional human cell lines, starting with the widely used cervical cancer cell line, HeLa. Because of the highly similar targeting sequence and AGS cell phenotype of shJMJD7#1 and #2, only shJMJD7#2 and #3 were used to create lentivirally-infected puromycin resistant HeLa cells. Control shRNA and shJMJD7#2/3 cell lines were doxycycline treated for 120 hours then trypsinised and reseeded in the presence of doxycycline for MTS assay. The remaining cells were lysed for western blot analysis of knockdown (Figure 2.9a). Similar to the previous experiment in AGS cells, knockdown of JMJD7 caused delayed growth in HeLa cells and shJMJD7#2 was less effective than shJMJD7#3 (Figure 2.9b, 2.9c). These data would indicate that the dominant role of JMJD7 in human cell growth may be positive (at least with respect to proliferation), and not restricted to a single cell type.

.

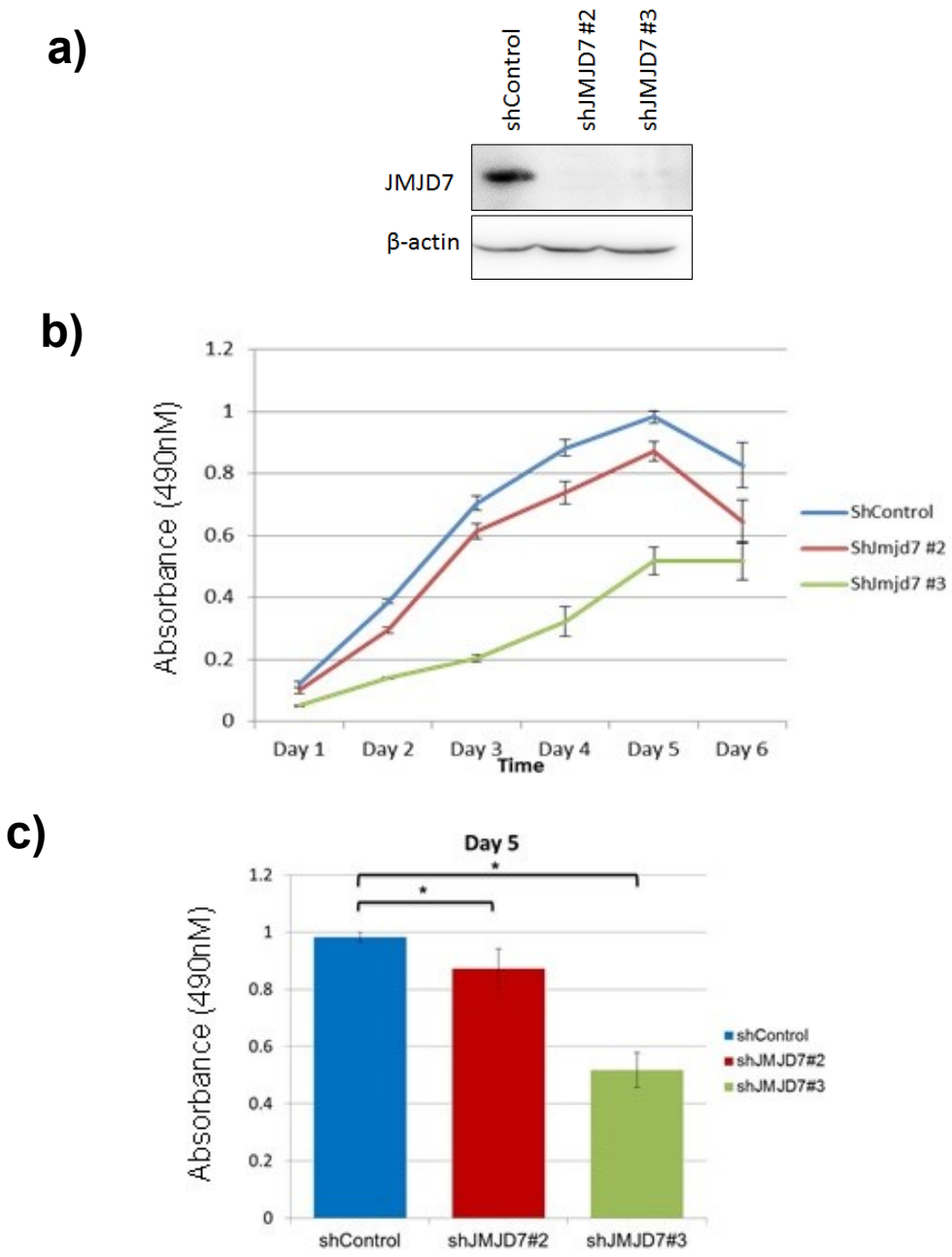

Figure 2.9 JMJD7 shRNA knockdown delays growth in HeLa cells. Doxycycline inducible shRNA targeting JMJD7 was infected into HeLa cells to test for metabolic activity using MTS assay. Infected cells were seeded into 10cm plates and treated with 1µg/ml doxycycline for 120 hours. After initial treatment cells were trypsinised and a) lysed for protein and analysed via western blot, or b) reseeded in the presence of 1µg/ml doxycycline for MTS assay over 5 days. (b) JMJD7 knockdown causes a significant growth defect in HeLa cells while in exponential growth phase. c) histogram representing day 5 of MTS assay highlighting significant growth defects of all JMJD7 shRNA compared to control., shJMJD7#2, $p < 0.05$, shJMJD7#3, $p < 0.05$. Full ANOVA tables in Appendix 1. n=3

2.9 Loss of JMJD7 results in delayed proliferation in HEK 293T cells

To continue exploring if JMJD7 regulates growth similarly in multiple cell lines, we next tested the shRNA-mediated JMJD7 mRNA knockdown in another widely used cell line, HEK293T cells. The same three shRNA sequences were infected into HEK293T cells (shControl, shJMJD7#2 and shJMJD7#3), subjected to 120 hours of doxycycline treatment, and then reseeded for MTS cell proliferation assay in the presence of doxycycline. The remaining cells were lysed for protein, and analysed by western blot for endogenous JMJD7 to validate knockdown (Figure 2.10a). As predicted, knockdown of JMJD7 also delayed growth of HEK293T cells compared to control cells. However, unlike what was previously observed in AGS and HeLa cells (Figure 2.8 and 2.9), there was little difference between the effect of shJMJD7#2 and shJMJD7#3 (Figure 2.10b). Taken together, we have shown that JMJD7 is essential for cell growth control in a variety of cancer and non-cancer cell lines of different tissue types, suggesting that this is likely to be a common function of JMJD7 in human cells.

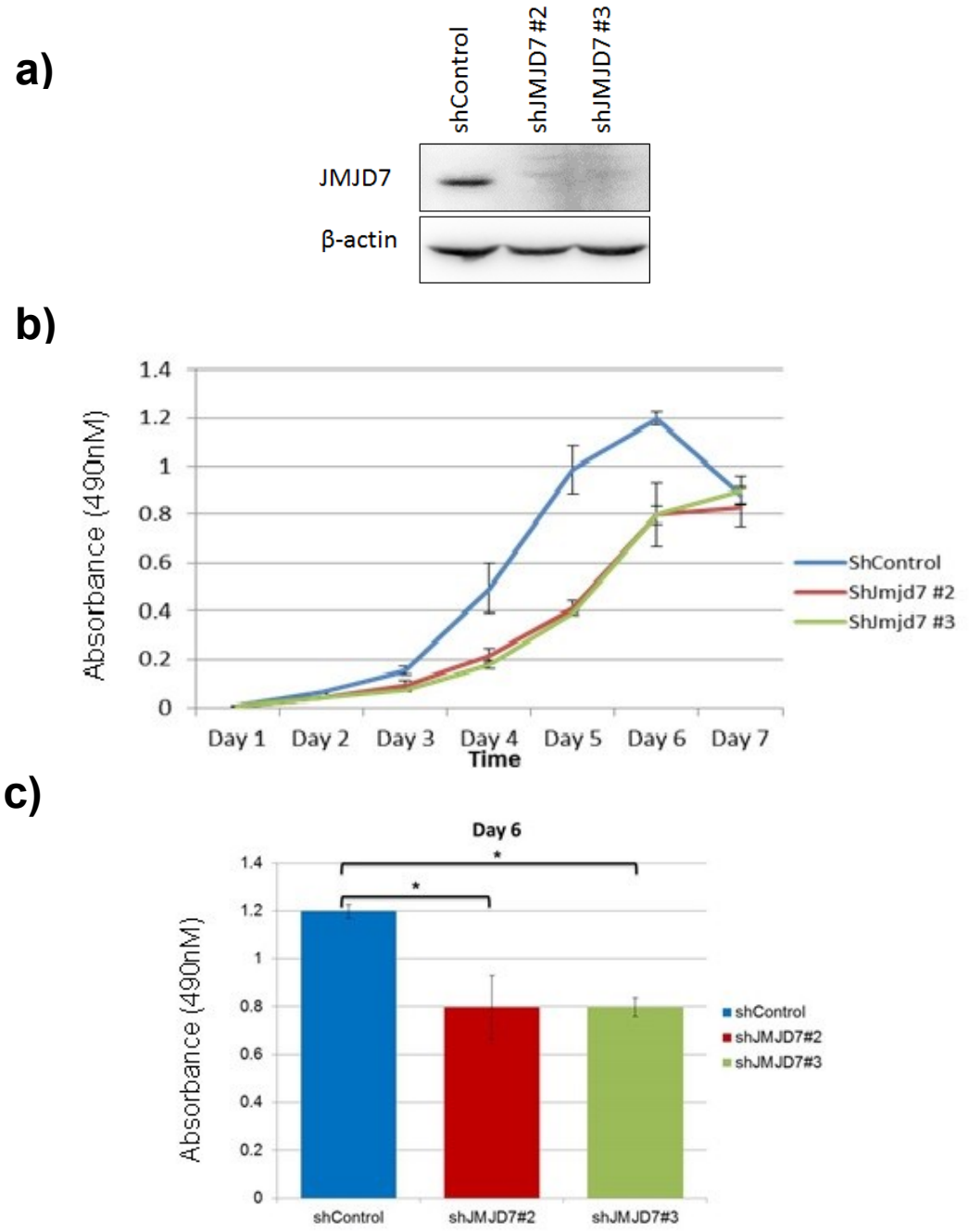

Figure 2.10 JMJD7 shRNA knockdown delays growth in HEK293T cells. Doxycycline inducible shRNA lentivirus targeting JMJD7 were infected into HEK293T cells and metabolic activity was used as an indicator of proliferation using MTS assay. HEK293T cells were seeded into 10cm plates and treated with 1µg/ml doxycycline for 120 hours. After initial treatment, cells were trypsinised and a) lysed for protein expression analysis via western blot or b) reseeded in the presence of doxycycline for analysis by MTS assay over 5 days. (b) JMJD7 knockdown causes a significant growth defect in HEK293T cells while in exponential growth phase (day 3-6) c) histogram representing day 5 of MTS assay highlighting significant growth defects of all JMJD7 shRNA compared to control. shJMJD7#2, $p < 0.05$, shJMJD7#3, $p < 0.05$. Full ANOVA tables in Appendix 1. n=3

Discussion

Within the series of experiments presented in this Chapter we have begun to characterise the enzyme, JMJD7. The JmjC only family of enzymes are involved in fundamental cellular processes, therefore, uncharacterised member JMJD7 was of interest. Structural analysis was consistent with JMJD7 being a protein hydroxylase with closest similarities to FIH and JMJD5 (Markolovic et al., 2018) (Figure 2.1a). Mass spectrometry identified DRG1 and DRG2 as candidate substrates which was confirmed by co-immunoprecipitation (Figure 2.2a). Consistent with this, localisation studies of exogenous and endogenous proteins confirmed co-localisation (Figure 2.3a and 2.3b). Sequence alignment between species (Figure 2.5a), and co-immunoprecipitation of dmJMJD7 and hJMJD7 demonstrated that JMJD7 may be evolutionarily important (Figure 2.5b). Finally, loss-of-function studies identified that JMJD7 may be playing a negative role in cell size in lower eukaryotes and a positive role in cell proliferation in higher eukaryotes.

The function of DRG1 and DRG2 hydroxylation is yet to be fully elucidated. The hydroxylation sites, K22 and K21 on DRG1 and DRG2, respectively, are located on the apex of the ‘turn’ on the Helix-Turn-Helix (HTH) domain. The HTH domain is part of a region on DRG1 that is protruding from the main body of the protein with an unknown function. Yeast studies have suggested that the HTH domain is essential for stability but not for interaction with Tma46 (DFRP1), or association with polysomes. Possible effects of hydroxylation were explored using RNAi interference targeting JMJD7, JMJD7 overexpression, and DRG hydroxylation site mutants, K22A for DRG1 and K21A for DRG2 by Dr Qinqin Zhuang (Markolovic et al., 2018). DRG1 and DRG2 stability was tested but was not significantly affected using JMJD7 WT

and H178A overexpression or DMOG treatment. Moreover, mutation of K22 (DRG1) and K21 (DRG2) to alanine did not affect either their ability to bind to their respective DFRP, or their GTPase activity. Similarities to the JMJD4 catalysed hydroxylation of K63 on eRF1 and previous studies linking DRGs with RNA binding prompted investigation into RNA binding (Feng et al., 2014, Ishikawa et al., 2003). As predicted, DRG2 hydroxylation site mutant and JMJD7 knockdown negatively regulated DRG2 affinity to RNA binding columns. This is further supported by immunofluorescence which localised significant proportions of DRG1, DRG2 and JMJD7 to the cytoplasm, consistent with polysome or RNA association (Figure 2.5a) (Markolovic et al., 2018, Feng et al., 2014).

Cellular growth assays following JMJD7 shRNA in multiple cell lines indicated that JMJD7 is required to support cell proliferation (Figure 2.8, 2.9 and 2.10). Whether this phenotype is due to reduced DRG hydroxylation is not yet clear, but could be consistent with studies implicating DRG1 and DRG2 in cellular proliferation. Yeast RNAi experiments highlighted that Rbg1 (DRG1) and Rbg2 (DRG2) may be functionally similar and that, when depleted together alongside Ski2-like helicase 1 (slh1) (mutant *Δrbg1 Δrbg2 Δslh1)*, it can have profound effects on proliferation (Daugeron et al., 2011). Interestingly, both DRG1 and DRG2 have been implicated in cell cycle control. In human cells, DRG1 is reported to be critical for normal mitosis transitioning (Lu et al., 2016, Schellhaus et al., 2017). Furthermore, DRG2 over expression in human cells causes growth suppression, probably through deregulation of downstream signalling pathways, e.g. MAP kinase signalling (Ko et al., 2004). Alternatively, knockdown of DRG2 in human cell lines is thought to cause cell cycle arrest at G2/M (Jang et al., 2016).

The observable differences in growth defects between shJMJD7#2 and shJMJD#3 are particularly interesting. Indeed, one simple answer is that this is a result of differences in knockdown efficiency between the two shRNA sequences. Alternatively, this could be due to the respective sequences targeting different JMJD7 transcripts. The shJMJD7#1 and shJMJD7#2 target regions on JMJD7 which are also present in the JMJD7-PLA2G4B readthrough transcript, whereas shJMJD7#3 targets the 3' end of the JMJD7 coding sequence which is not present in this readthrough. Early reports on JMJD7-PLA2G4B prove it can function as an active cytoplasmic calcium dependant phospholipase and evidence in cancer cells suggest it might be important for growth (Pickard 1999, Song 1999, Chang 2017). To explore this further, future experiments should include mRNA analysis by qPCR to quantify the level of JMJD7 knockdown compared to control. Furthermore, a rescue system which reconstituted PLA2G4B and JMJD7-PLA2G4B expression in shJMJD7#2 and shJMJD7#3 depleted cells would be essential to identify the cause of these differences in growth.

The roles of JMJD7 and DRG1/2 in supporting the growth of human cell lines could be related to their potential deregulation in human diseases and syndromes. As outlined above, JMJD7 mutations have been described in both autism and intellectual disability. Although the relevant pathways acting downstream of JMJD7 in cognitive behaviour disorders are not yet known, DRG1 and DRG2 may be good candidates as both have independently been associated with autism. The DRG2 gene is located on Chromosome 17 at 17p11.2 and elevated mRNA expression levels of DRG2 were described in a patient with 17p11.2 duplication syndrome. In

addition to other behavioural and dysmorphic characteristics the patient was diagnosed with autism spectrum disorder (ASD) (Nakamine et al., 2008). Interestingly, *deletion* of 17p11.2 also results in a developmental disorder associated with intellectual disability, termed Smith-Magensis Syndrome (SMS) (Koyama et al., 1996) (OMIM: 182290). Although this chromosomal region encompasses many other genes, it is possible that altered gene dosage of DRG2 could contribute to the associated phenotypes. Consistent with DRG1s high expression during embryonic development (Kumar et al., 1993, Ishikawa et al., 2003, Sazuka et al., 1992), genetic alterations in DRG1 have also been associated with autism: Polymorphisms in the DRG1 gene were highlighted as a risk factor for patients with autism (de Krom et al., 2009). Moreover, a homozygous DRG1 mutation (G54X) was identified as a candidate gene in intellectual disability (Al-Nabhani et al., 2018). Similarly, DFRP1 is associated with a developmental syndrome known as “2q.32 deletion syndrome”, although the exact risk factors of this disease are not yet known (Van Buggenhout et al., 2005).

How JMJD7, DRG1 and DRG2 are involved in autism and intellectual disability is unknown, but could be explained by a collective role within a novel signalling pathway.

Currently, our data suggests that JMJD7 and its substrates, DRG1 and DRG2, may be involved in growth and have a role in disease. In light of this, further studies on this pathway in other pathological conditions would be warranted. Specifically, diseases where cellular proliferation is primary to its progression would be of interest. For example, one of the major hallmarks of cancer is deregulated cell proliferation and genetic mutations in proteins that control proliferation play central roles in

oncogenesis (Hanahan and Weinberg, 2011). In the next Chapter we investigate whether JMJD7 is associated with cancer.

Chapter 3

Exploring the potential for deregulation of the JMJD7 pathway in Cancer

Introduction

In the previous Chapter we presented data suggesting that JMJD7 loss-of-function causes delayed growth of human cell lines. Normal growth control is critical for tissue and organismal 'homeostasis' and is commonly deregulated in human disease (Rue and Martinez Arias, 2015). Whether the role of JMJD7 in cell growth might be relevant to human pathology, and whether JMJD7 is deregulated in diseases associated with altered growth control is not currently known. Interestingly however, evidence is emerging that might support these possibilities, particularly in the context of neurological disorders. As outlined previously, independent studies have associated point mutations in both JMJD7 and DRG1, and deregulated expression of DRG2, with autism and intellectual disability (Matsunami et al., 2014, Nakamine et al., 2008, Koyama et al., 1996, de Krom et al., 2009, de Ligt et al., 2012, Bi et al., 2002). Together with our preliminary growth data on JMJD7, this may indicate that the JMJD7 'pathway' may regulate cell growth and/or other cellular processes involved in development. Whether the JMJD7 pathway is regulated in other pathological conditions associated with altered growth control is of interest. Since the Coleman laboratory focusses on tumour cell biology and specifically the role of protein hydroxylation in tumourigenesis, we were particularly interested in exploring whether the JMJD7 pathway is altered in cancer. Precedents for this possibility include a growing appreciation of the role of 2OG oxygenases in tumourigenesis (Ploumakis and Coleman, 2015), and the fact that altered growth control is considered a hallmark of cancer (Hanahan and Weinberg, 2011). Furthermore, initial reports implicate DRGs in tumour biology: For example, DRG1 is involved in mitotic spindle formation and DRG2 enhances resistance to chemotherapeutic drugs (Chen

et al., 2012, Lu et al., 2016). Indeed, many genes involved in mitogen-activated signal transduction pathways and in cell cycle control are altered and deregulate in cancer (Dhillon et al., 2007).

Cancer-associated genes are often deregulated by multiple independent mechanisms including epigenetic silencing, transcriptional over-expression, gene amplification/deletion ('copy number alteration'), altered mRNA splicing, and missense mutation (Sharma et al., 2010, Delgado and Leon, 2006, Albertson, 2006, Singh and Eyras, 2017, Garnis et al., 2004). In some cases, these alterations directly 'drive' tumourigenesis and can be associated with effects on patient prognosis. Here, we describe work aimed at identifying whether genetic evidence exists to support a role for the JMJD7 pathway in cancer, through the interrogation of publically available tumour DNA sequencing and patient prognosis databases.

3.1 JMJD7 and pathway components as markers of prognosis in gastric cancer

To begin to explore potential associations between JMJD7 pathway components and cancer we interrogated 'KM Plotter' (Gyorffy et al., 2010), online software that plots Kaplan Meier graphs (i.e. estimated patient survival over time) for patients whose tumours express a given gene mRNA at either 'low' or 'high' levels (based on meta-analysis of microarray data). Thus, this approach has the potential to identify correlations between gene expression changes and cancer patient prognosis. KM Plotter was therefore used to generate Kaplan-Meier graphs for high and low mRNA expression of JMJD7, DRG1, DFRP1, DRG2 and DFRP2. Because of the emerging role of JMJD7-related protein hydroxylases in gastrointestinal cancers (Dr Mathew Coleman, personal communication), we chose to focus our analysis on gastric cancer in the first instance. Interestingly, we observed a statistically significant

(p=1.8e-05) interaction between low mRNA expression of JMJD7 and poor patient prognosis (Figure 3.1a). Likewise, we observed that low mRNA expression levels of DRG1 (Figure 3.1b; p=6.5e-05) and DFRP1 (Figure 3.1c; p=3.9e-07) associated with worse patient prognosis. Conversely, analysis of DRG2 demonstrated the opposite trend, that *high* DRG2 mRNA levels correlated with worse patient prognosis (Figure 3.1d; p=1.2e-12). Finally, unlike DRG1/DFRP1, there was a discourse between DRG2 and DFRP2, with low DFRP2 mRNA expression correlated with worse patient prognosis (Figure 3.1e; p=5e-04). Overall however, this preliminary analysis would support a tumour suppressor role for the JMJD7/DRG1/DFRP1 pathway in gastric cancer. The potential role of the DRG2/DFRP2 arm of the pathway is less clear but might be consistent with a more oncogenic role of DRG2, which might suggest that DRG1 and DRG2 have alternative biological functions and/or opposing roles in cancer. Given these findings we sought to explore whether other evidence exists to support a role for JMJD7 and pathway components in cancer.

a)

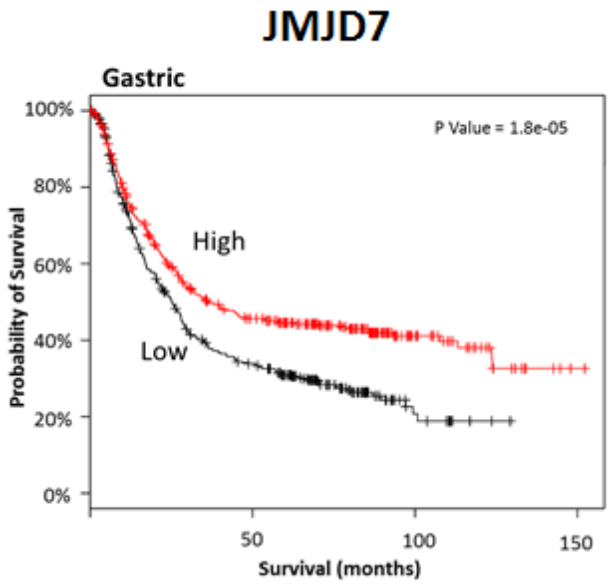

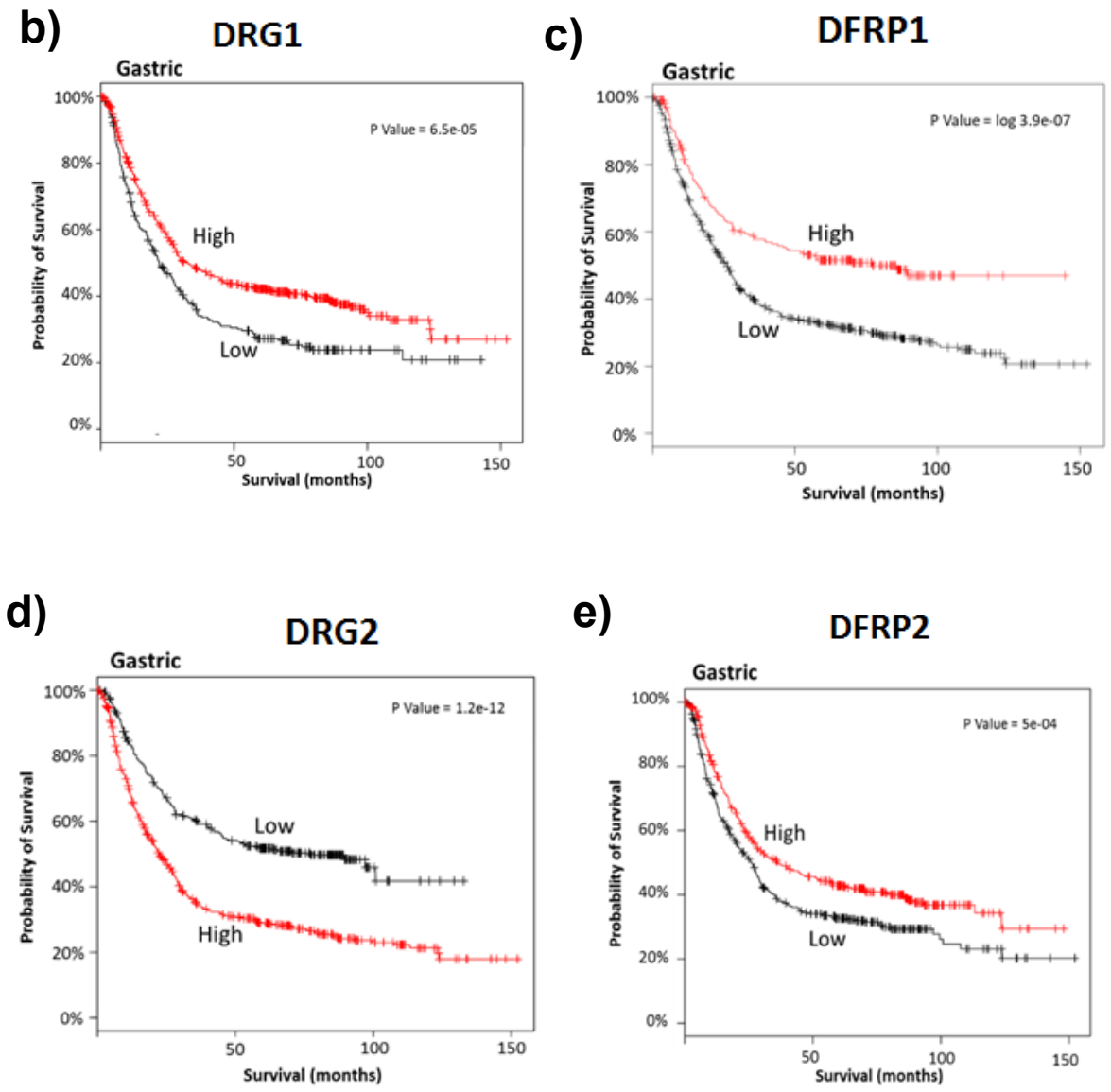

Figure 3.1 Altered mRNA expression of JMJD7 and pathway components is associated with altered prognosis of gastric cancer patients. Kaplan Meier Survival data illustrating the correlation between mRNA expression and patient prognosis in Gastric cancer. (a-c) High JMJD7, DRG1 and DRG2 expression correlated with better survival in gastric cancer with p values of 1.8-e0.5, 6.5e05 and 3.9e-07, respectively, supporting a role in a tumour suppressor pathway. DRG2 survival data shows that in gastric cancer, low expression correlated with better prognosis, p=1.2e-12 (d), Similar to JMJD7, DRG1 and DFRP1, high DFRP2 expression correlated with better survival (p=5e-04). Data obtained from public database: KMPlotter (Gyorffy et al., 2010). Microarray probes used: 222256_s_at (JMJD7), 202810_at (DRG1), 201595_s_at (DFRP1), 203268_s_at (DRG2), 203268_s_at (DFRP2).

3.2 Genetic alteration of JMJD7 and pathway components in cancer

We next sought to determine the spectrum of genetic alterations in JMJD7 pathway components across different cancers. cBioPortal is an online large scale cancer genomics database that allows users to visualise publically available tumour sequencing data sets (Cerami et al., 2012, Gao et al., 2013). Using their respective gene names, we searched cBioPortal for JMJD7 and pathway components (DRG1, DRG2, DFRP1 (ZC3H15) and DFRP2 (RWDD1)) and presented output data as frequency of alteration (deletion, amplification and missense mutation) against tumour sequencing study (Figure 3.2). Interestingly, we observed a general trend towards deletion (blue bars) of the JMJD7 gene in a variety of tumour types with a frequency of approximately 2-8% (Figure 3.2a), with the highest frequency deleted tumours including Diffuse Large B-Cell Lymphoma (DLBCL), Neuro-endocrine Prostate Cancer (NEPC), Prostate cancer, and Mesothelioma. This would be consistent with a potential tumour suppressor role for JMJD7, and might be in line with the patient survival data presented above (Figure 3.1a). In addition to gene deletion, we observed gene amplification (red bars) in two studies, and low levels of missense mutation (green). Potential trends in the types of genetic alteration of DRG1 and DFRP1 were less clear than for JMJD7 (Figure 3.2b and 3.2c, respectively). In both cases we observed total alteration frequencies of 2-8%, consisting of amplifications, deletions, and missense mutations in similar proportions (although slightly biased towards amplifications for DFRP1). Overall however, we observed reduced frequency of DRG1/DFRP1 gene deletion compared to JMJD7, but an increased frequency of missense mutation and gene amplification. Interestingly, the tumour type with only deletion and missense mutation of DRG1 (i.e.

no gene amplification) was Prostate, which was also observed in the most frequently deleted JMJD7 tumours (Prostate and NEPC). Tumours with the highest proportion of DFRP1 deletion/missense mutations included gastrointestinal cancers of the oesophagus and stomach, which is of interest with respect to the association between reduced JMJD7, DRG1 and DFRP1 mRNA expression and the survival of gastric cancer patients (Figure 3.1a, 3.1b and 3.1c, respectively).

Similar to DRG1/DFRP1, potential trends in the types of genetic alteration of DRG2 and DFRP2 were less clear than for JMJD7 (Figure 3.2d and 3.2e, respectively). Interestingly, the most frequently altered tumour type for DRG2 and DFRP2 was Breast cancer, with 12% and 15% gene amplification, respectively. Gastrointestinal cancers with altered DRG2/DFRP2 included Pancreas (2% DRG and 4% DFRP2 deletion) and oesophagus (2% DFRP2 deletion). Tumour types with the most frequent DFRP2 deletion included DLBCL and Prostate, similar to JMJD7.

Overall, the cBioPortal analyses provide reasonable evidence to suggest that JMJD7 is deleted in some cancers, potentially consistent with tumour suppressor activity. Although there may be some overlap of alteration and cancer types between JMJD7 and other components of the pathway, the landscape of alterations for DRG1/DFRP1 and DRG2/DFRP2 is much more heterogenous than JMJD7.

To gain further insight into potential genetic alteration of the JMJD7 pathway, we focussed in more detail on missense mutations. The rationale for this was that even rare mutations can be functionally important in cancer (so called ‘mini-drivers’) (Castro-Giner et al., 2015), and the pattern of mutations can infer functional importance. For example, mutations that are recurrent (i.e. identical mutations in

multiple patients) or clustered (i.e. enriched in a given sequence/domain) indicate potential selection and possible functional consequence (Miller et al., 2015). To gather all the publically available cancer missense mutation data we collated information from cBioportal, COSMIC, and COSMIC Cell Lines (Figure 3.3) (Cerami et al., 2012, Gao et al., 2013, Forbes et al., 2017).

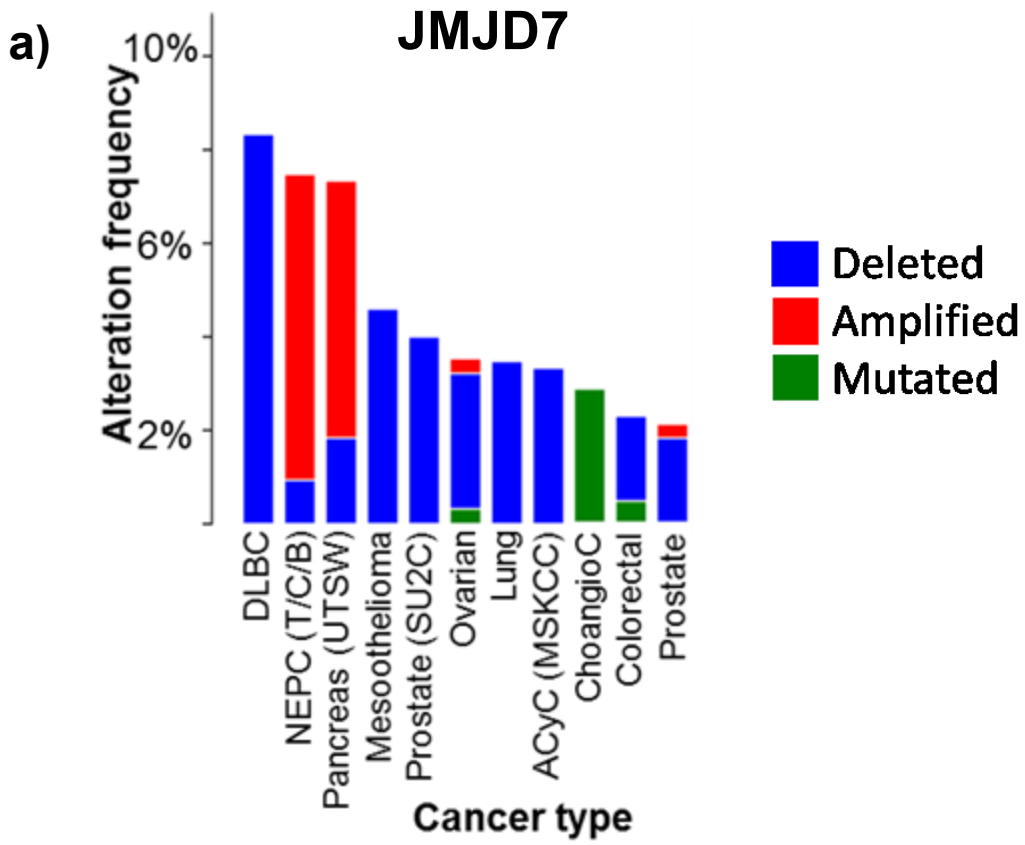

Figure 3.2 Genetic alterations of JMJD7 and pathway genes across cancers. Online database, cBioPortal, was interrogated for alteration frequency data for each gene within the JMJD7 pathway. a) Bar chart representing the alteration frequency of JMJD7. Shows that it is mutated up to 8% in Diffuse Large B-Cell Lymphoma patients (DLBCL). Graphs modified from Gao et al., 2013 and Cerami et al., 2012. AcyC, Adenoid Cystic Carcinoma; Unless otherwise stated, the data was collected from the TCGA database. MSKCC, Memora Sloan Kettering Cancer Centre; UTSW, University of Texas Southwestern Medical Centre; SU2C, Stand up to Cancer; T/C/B, Trento, Cornel, Broad. The top 9 cancers with highest JMJD7 alteration frequency shown.

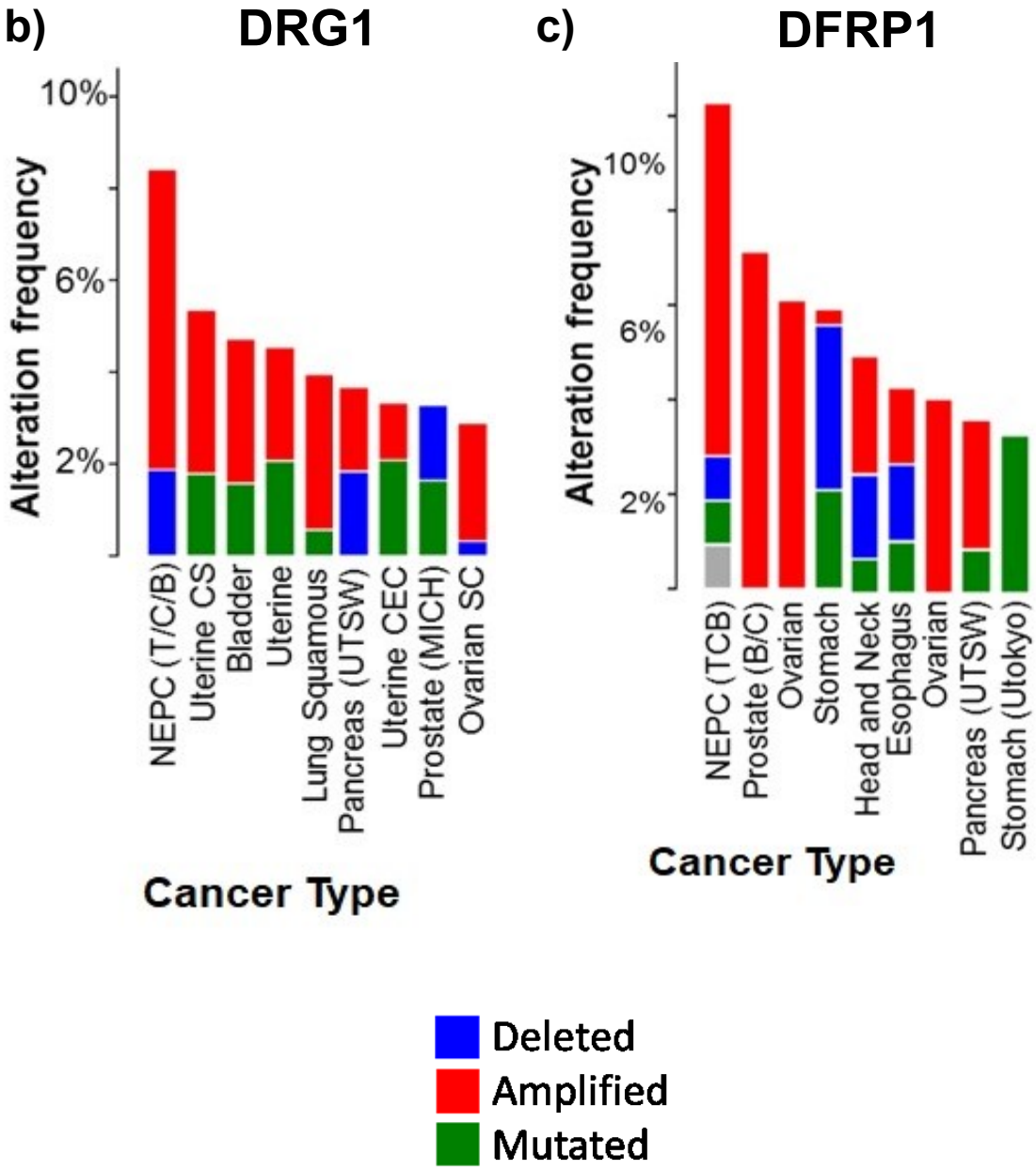

Figure 3.2 (b) DRG1 bar chart shows it is most frequently mutated in Neuroendocrine prostate cancer (NEPC) (up to 8%). (c) DFRP1 is also mutated in up to 10% of NEPC. Graphs modified from Gao et al., 2013 and Cerami et al., 2012. CS, Carcinosarcoma; Uterine CEC, Corpus Endometrial Carcinoma; Unless otherwise stated, the data was collected from the TCGA database. UTSW, University of Texas Southwestern Medical Centre; T/C/B, Trento, Cornel, Broad; MICH, Michigan; B/C, Broad, Cornell; UTokyo, University of Tokyo. The top 9 cancers with highest alteration frequency shown.

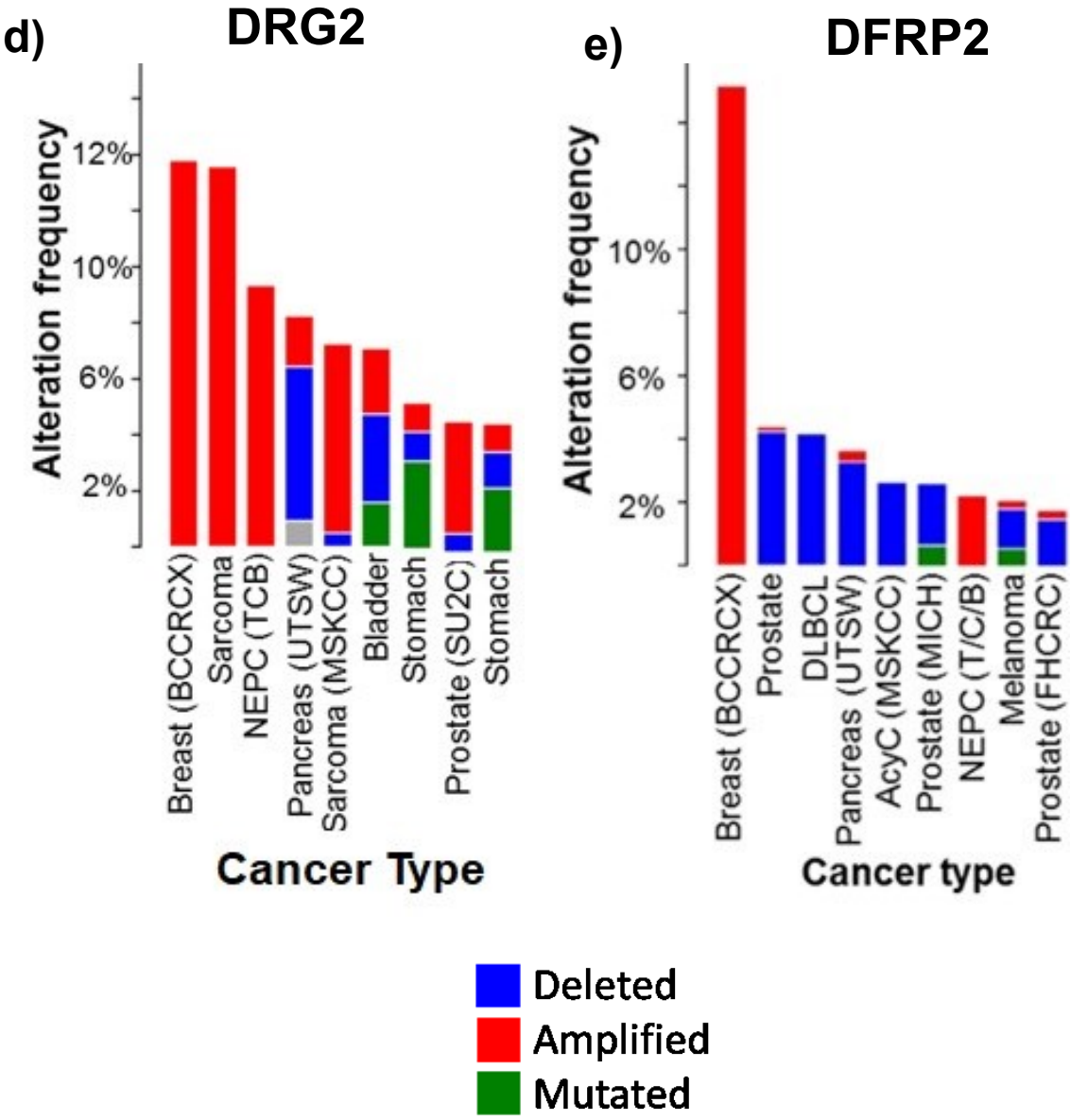

Figure 3.2 (d) DRG2 is most frequently mutated in Breast cancer and sarcomas. e) DFRP2 is mutated up to 12% in Breast cancer. Graphs modified from Gao et al., 2013 and Cerami et al., 2012. AcyC, Adenoid Cystic Carcinoma; NEPC, Neuroendocrine Prostate Cancer; Unless otherwise stated, the data was collected from the TCGA database. MSKCC, Memora; Sloan Kettering Cancer Centre; UTSW, University of Texas Southwestern Medical Centre; SU2C, Stand up to Cancer; T/C/B, Trento, Cornel, Broad; MIC, Michigan; DFCF, Dana-Farber Cancer Institute; B/C, Broad, Cornell; BCCRC, Breast Cancer Research Centre; FHCRC, Fred Hutchinson Cancer Research Centre. The top 9 cancers with highest JMJD7 alteration frequency shown.

3.3 Cancer missense mutations in JMJD7 and pathway components

Collated missense mutations were graphically represented by overlaying on the primary protein sequence of JMJD7 and pathway components, in order to highlight recurrence and clustering in relation to known catalytic and functional domains (Figure 3.3). Silent, missense and nonsense mutations were distinguished with blue, red and green arrows, respectively, and in-frame deletions were represented by pink arrows. Silent mutations were included because there is a growing appreciation that these alterations can actually be functional in some cases due to effects of splice sites (Supek et al., 2014). Figure 3.3a shows the mutation profile of JMJD7 which, although only modestly mutated, shows multiple 'hot-spots' including V28-R43, P62-T75, G96-F111, R260-A273 and Q280-A312. These hot-spots are located in the N-terminal half of the protein, the JmjC catalytic domain, and the C-terminal helices that contribute to the dimerisation domain. In addition, there are ten residues which are mutated in more than one patient tumour. Of potential importance, the most recurrent of these mutations, R264W (identified in cholangiocarcinoma, uterine cancer and glioma), is located within one of the previously identified hot-spots in the JmjC catalytic domain (R260-A273) and has been identified as damaging in two independent *in silico* damage prediction tests (see Table 3.1 for full list). Interestingly, another uterine cancer mutant in this hot-spot, R260C (yellow arrow), is identical to a mutation associated with autism (Matsunami et al., 2014) (for comparison, we have also highlighted another mutation reported to be associated with intellectual disability (M160V, yellow arrow)). Interestingly, we observed a Y127C mutation in a Burkitt's Lymphoma cell line (EB2): Y127 is a known catalytic residue involved in binding to

the essential co-factor 2OG (Markolovic et al., 2018) and was also predicted to be damaging by both prediction software used (Table 3.1).

Overall, the pattern of JMJD7 missense mutations, their position in known catalytic residues and domains, and the overlap with a mutation in an independent disorder, would suggest that these cancer mutations have some functional consequence.

We next explored the mutational landscape of DRG1, DFRP1, DRG2 and DFRP2. DRG1 missense mutations were distributed throughout the protein (Figure 3.3b), although slightly enriched within the GTPase domains (G1 to G3). Hotspots included A60-V75, I113T-E123K and L152-I161V in the N-terminal GTPase domain, N178-A202 (in the S5D2L insert), and K213-V234 (also in the S5D2L insert). Although we observed patches of mutations at either end of the HTH domain, we did not (yet) observe any cancer mutations in the JMJD7 hydroxylation site (K22, orange asterix). However, we did observe 7 sites of recurrent non-synonymous (i.e. not silent) mutation that generally fell within the previously highlighted hotspots, which may be consistent with potential functional consequences of these mutations.

DFRP1 is also only modestly mutated but contains five potential mutation hotspots and ten sites of recurrent mutation (Figure 3.3c). Notably, one of these recurrent mutation sites (R298C/H) has been identified in four independent tumours (colorectal, skin, and lung cancers). Furthermore, this recurrent site is located in a potential hotspot (R292-D325) that is located within the DRG1-binding domain. Interestingly, the DRG1-binding domain includes another potential cancer mutation hot-spot (T251-E271), suggesting that altered DRG1/DFRP1 interaction could perhaps be one functional consequence of cancer mutations in these genes.

Figure 3.3c shows cancer mutations plotted onto the DRG2 protein sequence. DRG2 is modestly mutated and displays only three potential hot-spots (M58-S72, F94-V103, H137-W336). One of these hot-spots (M58-S72) is adjacent to a residue (S76) whose equivalent in yeast was recently identified as critical for DRG2 function and DFRP2 association (Ishikawa et al., 2013). Furthermore, a non-conservative mutation at the residue next to S76 (T77K) might also be predicted to be damaging. Unlike DRG1, we did observe at least one mutation (E24K) within the DRG2 HTH domain in close proximity to the JMJD7 hydroxylation site (K21). It would be interesting to test whether this mutation can effect JMJD7 catalysed hydroxylation. Overall however, the number of recurrent non-synonymous missense mutations in DRG2 was lower than DRG1. Similarly, the DFRP2 mutation profile (Figure 3.3d) shows a relatively low frequency of mutation, only one potential hotspot (L75-S81) and only three non-synonymous recurrent mutations. Together, these preliminary observations might suggest that cancer mutations in JMJD7 and the DRG1/DFRP1 complex may be more likely to be functionally relevant than those in the DRG2/DFRP2 complex, although further work is required. Taken together, the data thus far are consistent with JMJD7 having potential tumour suppressor activity, possibly mediated by one or both DRG substrates.

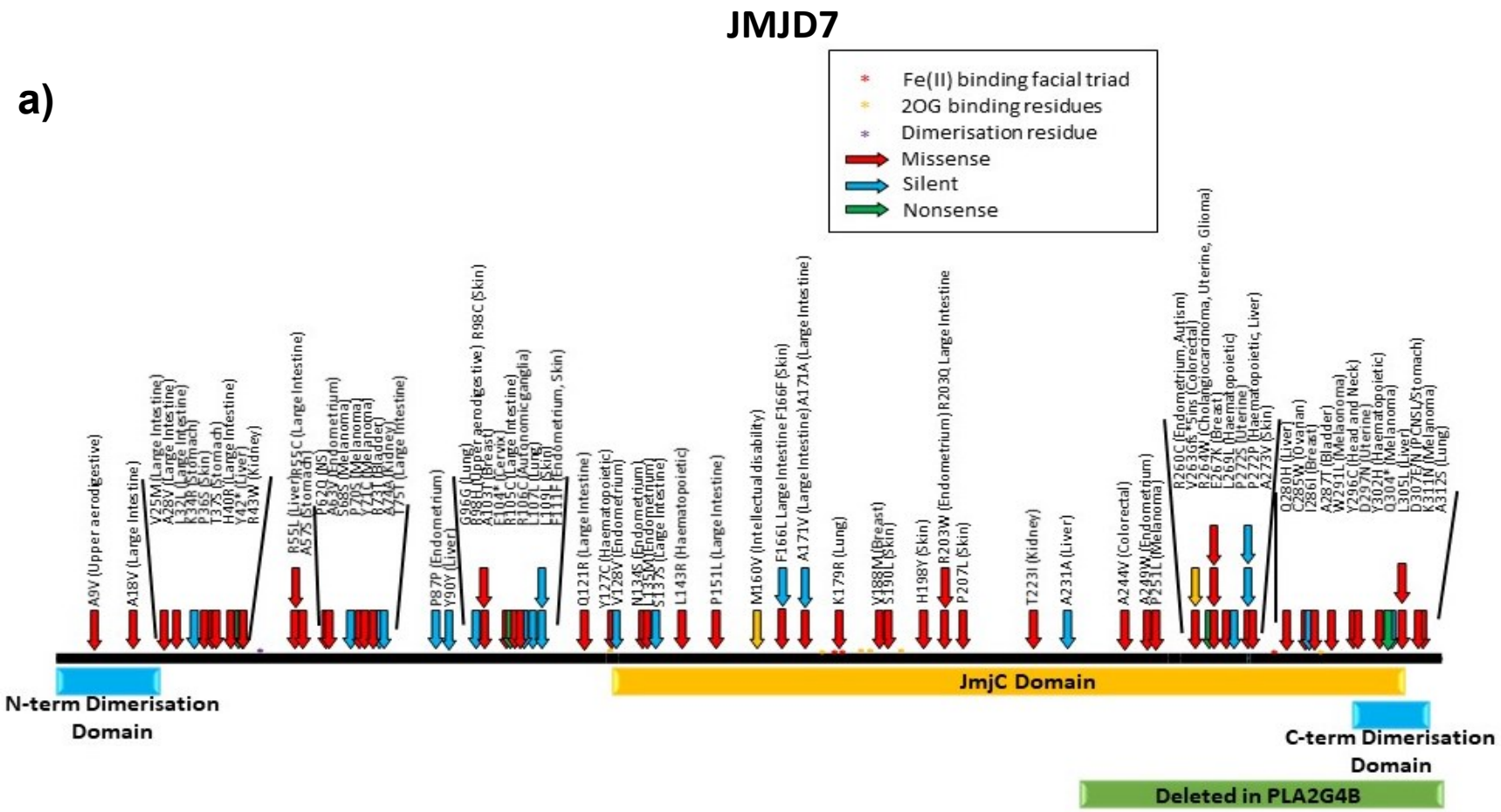

Figure 3.3 JMJD7 and pathway components are mutated in cancer. Visual representation of cancer mutations collated from cBioPortal, COSMIC and COSMIC Cell Lines Project databases (Forbes et al., 2017, Cerami et al., 2012, Gao et al., 2013) for JMJD7, DRG1, DFRP1, DRG2 and DFRP2. a) JMJD7 shows five striking hot spots between residues V28-R43, P62-T75, G96-F111, R260-A273 and Q280-A312. Blue, red, and green arrows indicate silent, missense and non-sense mutations, respectively. The purple, red and yellow Asterixs represent residues important for dimerisation, 2OG binding and Fe(II) co-ordination, respectively.

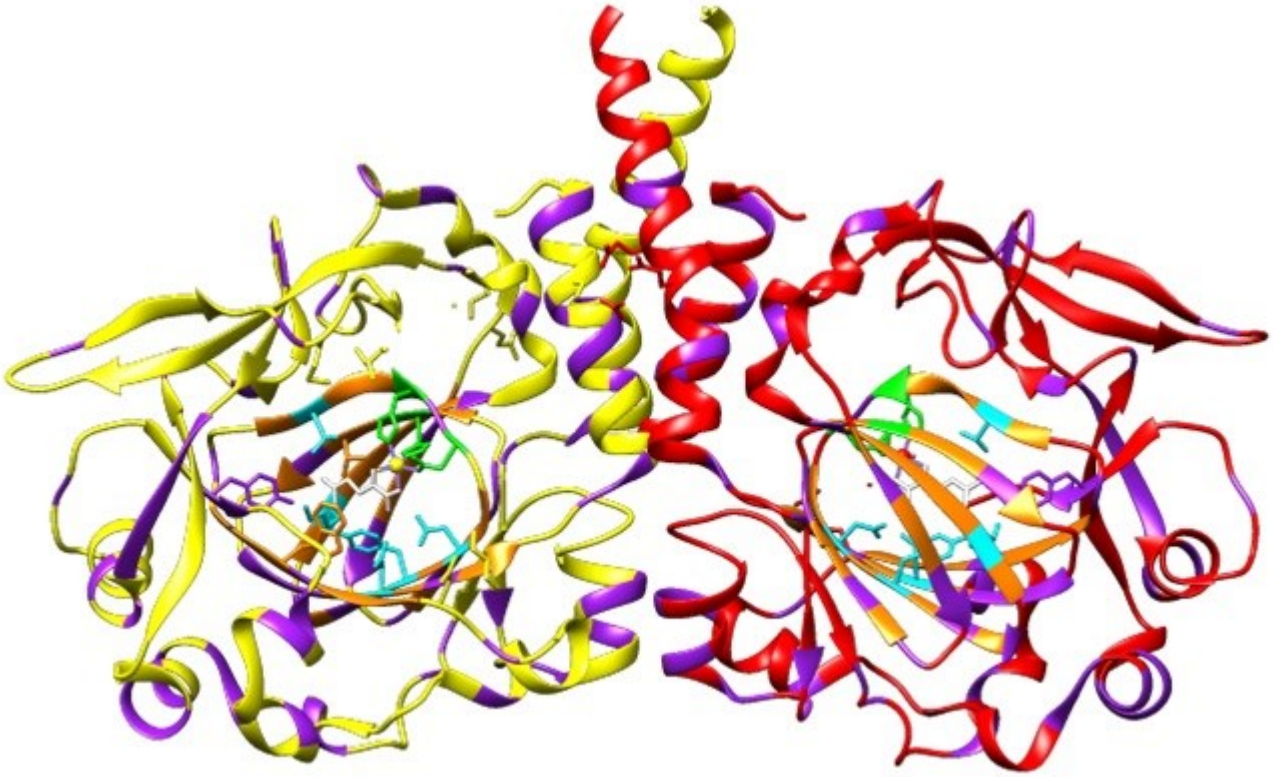

Figure 3.3 JMJD7 and pathway components are mutated in cancer. Visual representation of cancer mutations collated from cBioPortal, COSMIC and COSMIC Cell Lines Project databases (Forbes et al., 2017, Cerami et al., 2012, Gao et al., 2013) for JMJD7 dimeric crystal structure (PDB: 5NFN), DRG1, DFRP1, DRG2 and DFRP2. a,i) shows JMJD7 cancer mutations mapped on to the dimer crystal structure (shown in purple). DSBH shown in orange, green residues are Fe(II) coordinating, cyan represents 2OG binding residues.

Table 3. 1 *JMJD7 Missense Mutation Damage Prediction*

Mutation	SIFT Prediction	PolyPhen-2 Prediction	Mutation	SIFT Prediction	PolyPhen-2 Prediction
V9A	Tolerant	Damaging	L135M	Damaging	Damaging
A18V	Tolerant	Tolerant	L143R	Possibly Damaging	Tolerant
V25M	Possibly Damaging	Tolerant	P151L	Tolerant	Tolerant
A28D	**Tolerant**	**Tolerant**	W152R	Damaging	Damaging
K34R	**Tolerant**	**Tolerant**	M160V	Tolerant	Tolerant
P36S	**Tolerant**	**Tolerant**	F166L	Damaging	Damaging
T37S	**Tolerant**	**Tolerant**	A171V	Damaging	Tolerant
H40R	**Tolerant**	**Tolerant**	K179R	Damaging	Damaging
R43W	**Damaging**	**Damaging**	V188M	Damaging	Damaging
R55C	Damaging	Damaging	S190L	Damaging	Damaging
R55L	Damaging	Damaging	H198Y	Damaging	Tolerant
A57S	Damaging	Damaging	R203Q	Damaging	Tolerant
P62Q	**Damaging**	**Damaging**	R203W	Damaging	Damaging
A63V	**Damaging**	**Damaging**	P207L	Damaging	Damaging
P70S	**Tolerant**	**Tolerant**	T223I	Tolerant	Tolerant
Y71C	**Damaging**	**Damaging**	A244V	Possibly Damaging	Tolerant
R73T	**Damaging**	**Tolerant**	R249W	Damaging	Damaging
R98C	**Damaging**	**Tolerant**	R249Q	Tolerant	Tolerant
R98H	**Tolerant**	**Tolerant**	P251L	Damaging	Damaging
A103T	**Possibly Damaging**	**Tolerant**	**R260C**	**Tolerant**	**Damaging**
R105C	**Damaging**	**Damaging**	**R264W**	**Damaging**	**Damaging**
R106C	**Damaging**	**Tolerant**	**E267K**	**Possibly Damaging**	**Damaging**
Q121R	Tolerant	Tolerant	**P272S**	**Damaging**	**Damaging**
Y127C	Damaging	Damaging	**A273V**	**Possibly Damaging**	**Damaging**

Mutation	SIFT Prediction	PolyPhen-2 Prediction	Mutation	SIFT Prediction	PolyPhen-2 Prediction
Q281R	Damaging	Damaging	D297N	Damaging	Damaging
C285W	Damaging	Damaging	Y302H	Damaging	Damaging
A287T	Damaging	Damaging	D307E	Tolerant	Tolerant
W291L	Damaging	Damaging	D307N	Damaging	Damaging
Y296C	Damaging	Damaging	K311N	Tolerant	Tolerant
			A312S	Tolerant	Tolerant

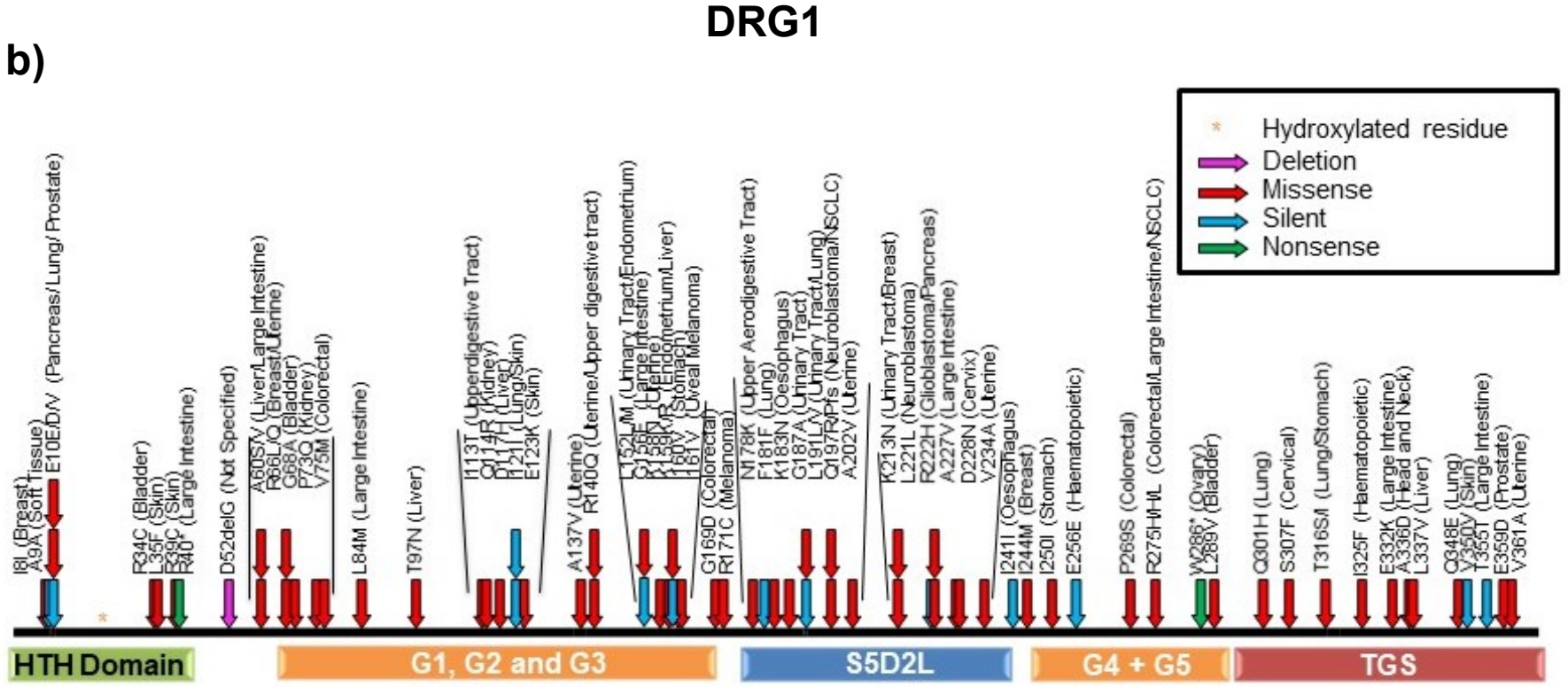

Figure 3.3 JMJD7 and pathway components are mutated in cancer. Visual representation of cancer mutations collated from cBioPortal, COSMIC and COSMIC Cell Lines Project databases (Forbes et al., 2017, Cerami et al., 2012, Gao et al., 2013) for JMJD7, DRG1, DFRP1, DRG2 and DFRP2. b) DRG1 mutations are generally evenly spread with five potential mutational hotspots including, A60-V75, I113-E123, L152-I161, N178-A202, K213-V234. Blue, red, green and pink arrows indicate silent, missense, non-sense and deletion mutations, respectively. The yellow Asterix represents K22, the site of hydroxylation by JMJD7.

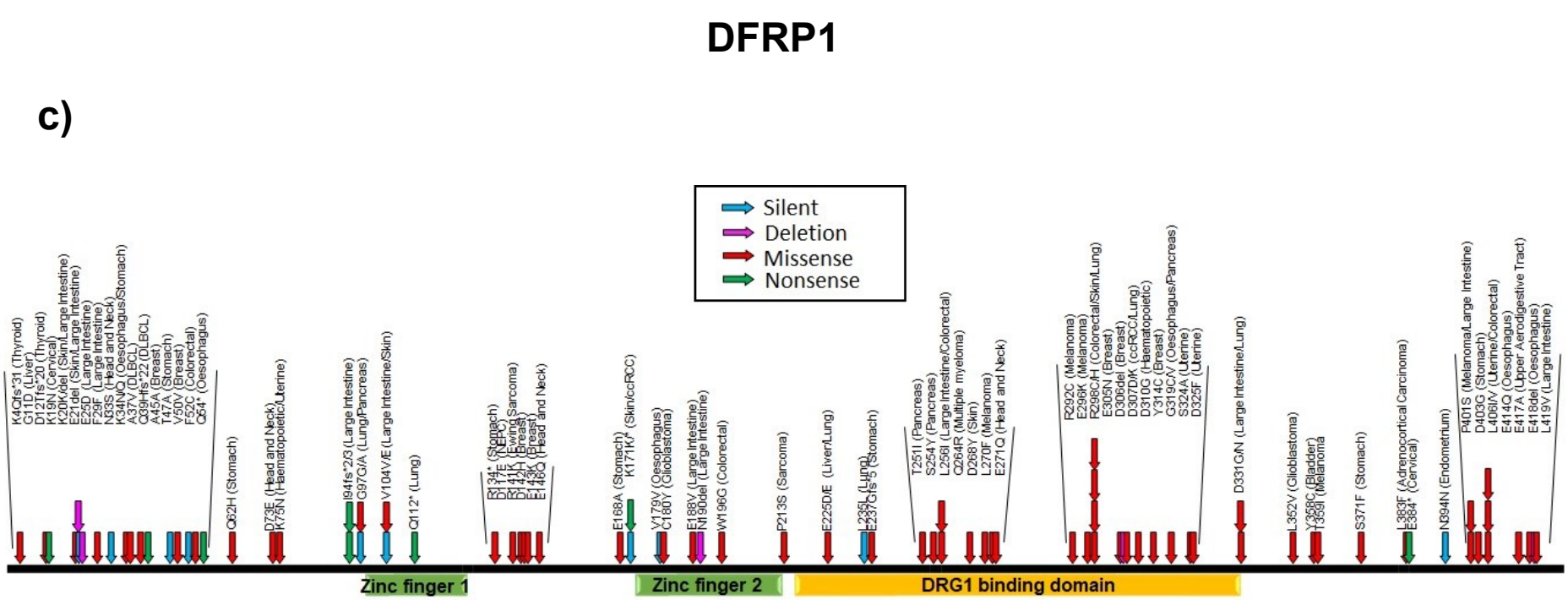

Figure 3.3 JMJD7 and pathway components are mutated in cancer. Visual representation of cancer mutations collated from cBioPortal, COSMIC and COSMIC Cell Lines Project databases (Forbes et al., 2017, Cerami et al., 2012, Gao et al., 2013) for JMJD7, DRG1, DFRP1, DRG2 and DFRP2. c) DFRP1 is modestly mutated with one significantly recurrent mutation at R298 located within the fourth hotspot (R292-D325). Other hotspots include are located at K4-Q54, R134-E146, T251-E271 and P401-L419. Blue, red, green and pink arrows indicate silent, missense, non-sense and deletion mutations, respectively.

DRG2

d)

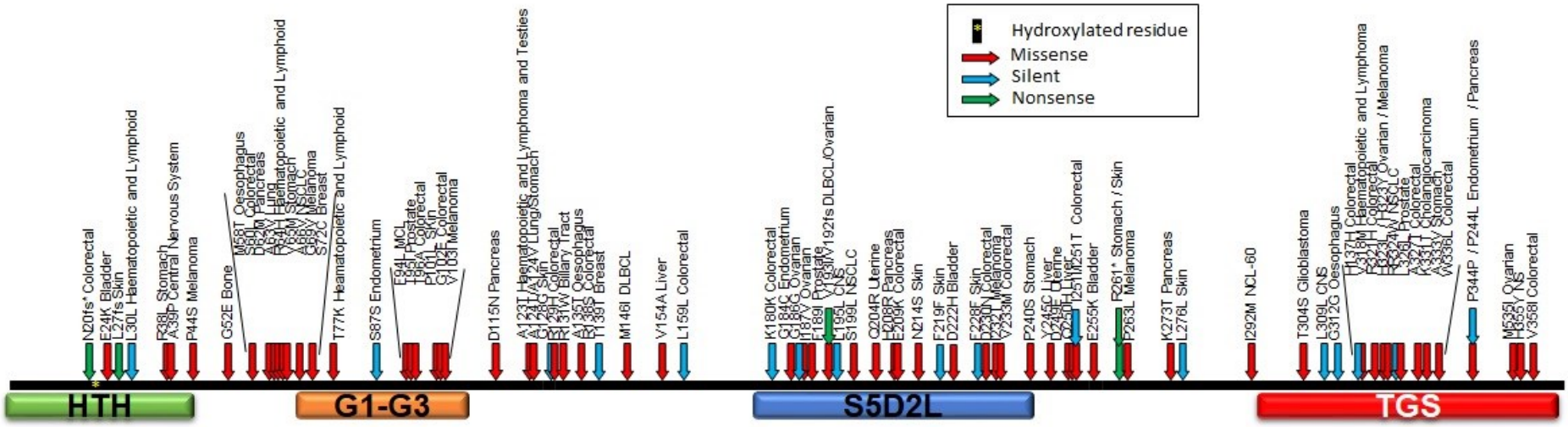

Figure 3.3 JMJD7 and pathway components are mutated in cancer. Visual representation of cancer mutations collated from cBioPortal, COSMIC and COSMIC Cell Lines Project databases (Forbes et al., 2017, Cerami et al., 2012, Gao et al., 2013) for JMJD7, DRG1, DFRP1, DRG2 and DFRP2. d) DRG2 has three significant hotspots between residues M58-S72, F94-V103 and H317-W336. Blue, red, and green arrows indicate silent, missense and non-sense mutations, respectively. The yellow Asterix represents K21, the site of hydroxylation by JMJD7.

e)

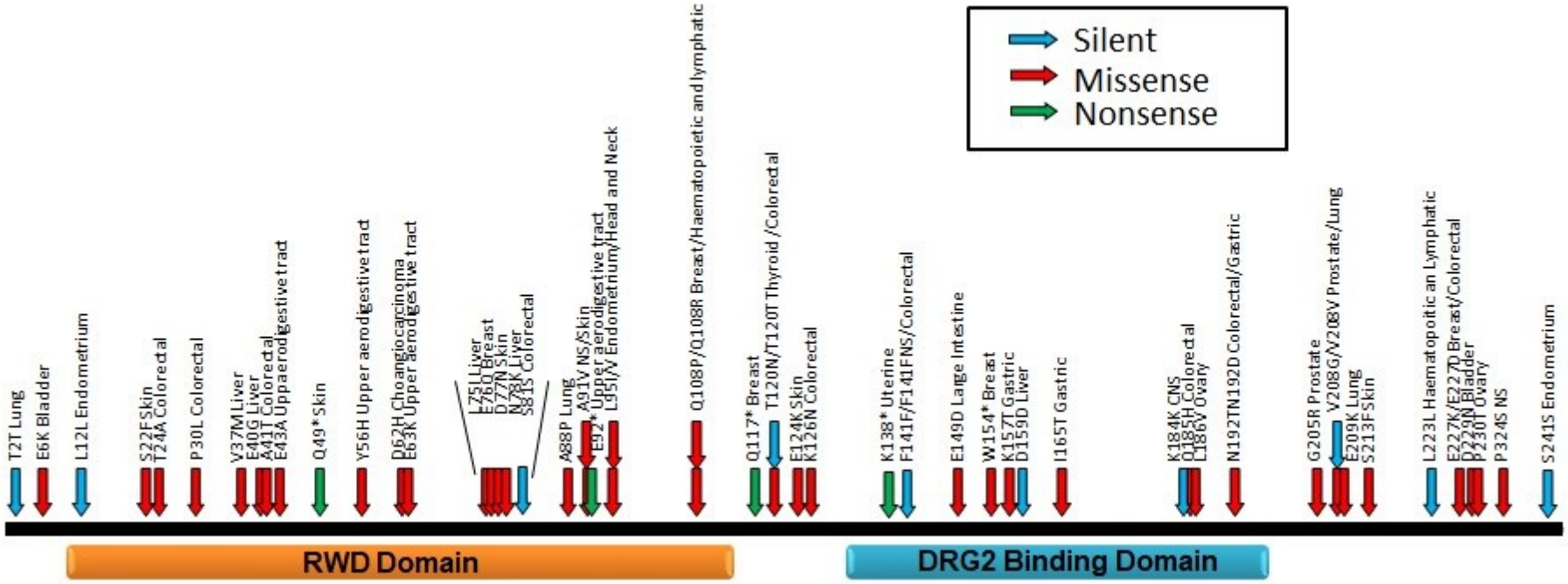

Figure 3.3 JMJD7 and pathway components are mutated in cancer. Visual representation of cancer mutations collated from cBioPortal, COSMIC and COSMIC Cell Lines Project databases (Forbes et al., 2017, Cerami et al., 2012, Gao et al., 2013) for JMJD7, DRG1, DFRP1, DRG2 and DFRP2. e) DFRP2 mutations are generally evenly spread with one hotspot located between residues L75-S81. Blue, red, and green arrows indicate silent, missense and non-sense mutations, respectively.

3.4 Effect of cancer mutations on JMJD7 expression and substrate binding

Point mutations can have varying effects on a protein, including little or no consequence (so called 'passenger' mutations), positive effects (gain-of-function) or negative effects (loss-of-function) (Stratton et al., 2009, Wang et al., 2006). In general, activating mutations in oncogenes tend to be restricted to a limited number of positions and substitutions (e.g. K-Ras G12V, B-RAF V600E), whereas inactivating mutations in tumour suppressor genes are more variable (i.e. non-conservative missense mutations, nonsense and frameshift mutations) and located throughout the gene. Overall, the genetic data presented above is more consistent therefore with cancer mutations of the JMJD7 pathway being inactivating as opposed to gain-of-function. Although bioinformatic software has been developed to predict whether disease mutations are damaging (Adzhubei et al., 2010), definitive proof is only possible from functional experiments in cells. Therefore, in order to explore the potential consequences of JMJD7 pathway cancer mutations we first cloned a panel of fifteen JMJD7 cancer mutants by site-directed mutagenesis (mutants were selected in 2014 when the available tumour sequencing data was more limited). The position of the cloned mutants within the dimeric structure of JMJD7 is represented by dark blue ribbons (Figure 3.4a) (adapted from PDB: 5NFN).

Cancer mutations can be inactivating by multiple different mechanisms, including altered splicing, destabilisation of the protein, loss of enzyme activity, altered protein:protein interactions (including substrates), and incorrect sub-cellular localisation, to name a few. We first tested whether JMJD7 cancer mutations effected protein expression by transient transfection. We tested 15 of the cancer mutants, including R260C, which was also mutated in an autistic individual. For completeness

therefore, we also included M160V, which was mutated in an individual with intellectual disability. The corresponding WT and variant expression vectors were transfected into HEK293T cells for 48 hours (Figure 3.4b). To control for potential technical differences, including transfection efficiency, we co-expressed a small amount of a related protein hydroxylase, MINA53. Although 10 cancer mutants expressed normally, 6 mutants were expressed at dramatically lower levels than wildtype JMJD7, despite normal expression of MINA53 (Figure 3.4b). These 6 unstable cancer mutants all reside within one of two previously identified mutation hot-spots (P62-T75 and R260-A273), and include the most recurrent JMJD7 cancer mutation, R264W. Interestingly, an 'experimental' JMJD7 mutant (H178A, iron-binding mutant) with validated loss of activity (Markolovic et al., 2018) was also poorly expressed, raising the possibility that (i) JMJD7 expression might be linked in some way to its enzyme activity, and (ii) reduced expression of JMJD7 cancer mutants could potentially reflect reduced enzyme activity. Overall, this expression trial suggests that one mechanism of JMJD7 loss-of-function in cancer is *via* missense mutation and reduced enzyme expression.

Of the JMJD7 cancer mutants that expressed normally we also wished to test their substrate binding efficiency and activity. In the absence of a rapid and cost-effective method for screening the activity of JMJD7 variants, we initially employed a co-IP strategy in the presence or absence of the hydroxylase inhibitor DMOG to monitor activity-dependent binding (as in Figure 2.2a). Wildtype JMJD7, seven cancer mutants, and the M160V intellectual disability variant, were transfected into HEK293T cells for 36 hours before treatment with vehicle or DMOG followed by cell lysis and anti-FLAG IP (Figure 3.4c). All the mutants expressed normally, as expected. The

DMOG-dependent capture of DRG1 and DRG2 was comparable between JMJD7 and all the mutants, which may be consistent with no major effects on enzymatic activity. However, a modest reduction in DRG1/2 binding to some of the JMJD7 variants was apparent in the absence of DMOG. Further work is required to determine if this is a meaningful reduction and whether it reflects a subtle reduction in DRG-binding affinity and/or JMJD7 activity. Alternatively, if functionally relevant, these mutations might be deregulating JMJD7 via different mechanisms such as altered interactions, subcellular localisation and regulatory PTMs, which also deserve further investigation in the future.

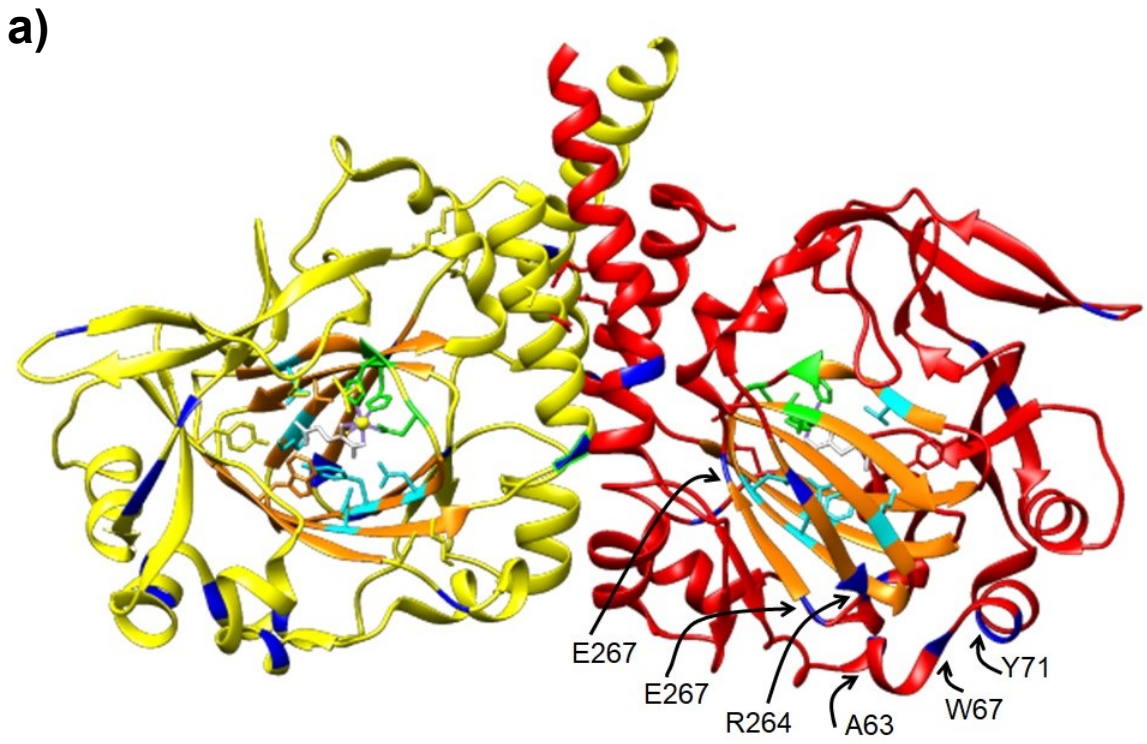

Figure 3.4 JMJD7 cancer mutations effect expression but not substrate binding. (a) dimeric JMJD7 crystal structure adapted from Figure 1a, Markolovic et al., 2018 (PDB: 5NFN). Fe(II) coordinating residues shown in green, 2OG binding residues seen in cyan. Shows the location of the sixteen cancer mutants (blue) known to be mutated in cancer or intellectual disability. Location of destabilising mutations (A63, W67, Y71, R264, E267, P272) highlighted with black arrows.

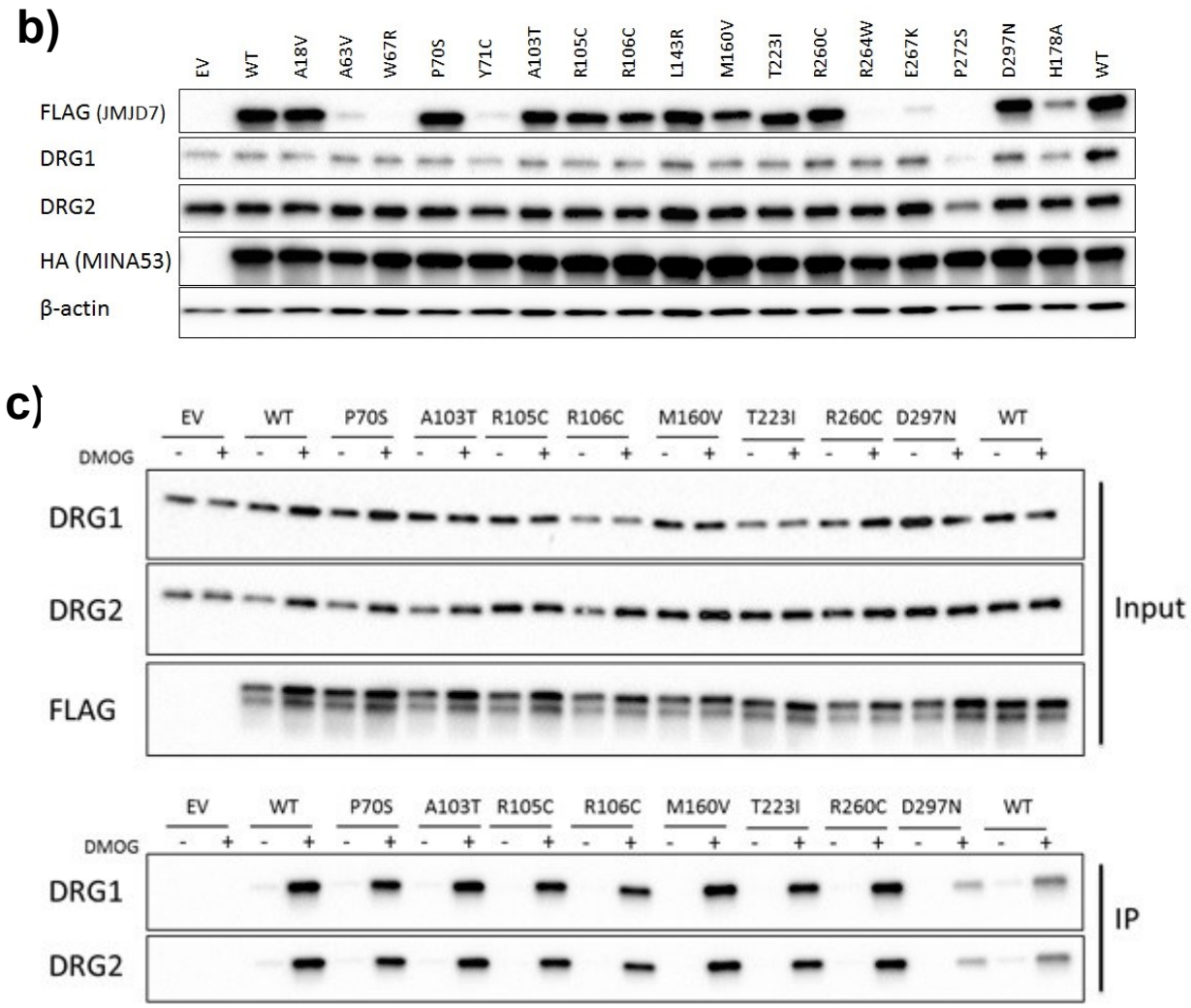

Figure 3.4 (b) Western blot of FLAG-JMJD7 and endogenous DRGs highlighting the differential expression of JMJD7 WT and cancer mutants after transient transfection into HEK293T cells. Also includes an iron binding mutant (H178A) as an inactive negative control. Six out of the fifteen cancer mutants and the iron binding mutant effect stability. The remaining stable mutants were tested for substrate binding in HEK293T cells. After 36 hours of over expression cells were treated with or without DMOG for 15 hours following lysis and FLAG-IP. n=2 c) shows western blot of FLAG-JMJD7 and endogenous DRG1 and DRG2. None of the tested mutants affected binding of either DRG1 or DRG2. n=2

Discussion

Within this Chapter we have begun to collate evidence supporting a role for the JMJD7 pathway in cancer, including correlations between gene expression and patient prognosis, genetic alterations identified in tumour sequencing studies, and functional experiments in cell models.

At the beginning of this study there was no scientific literature that focussed on a role for JMJD7 in cancer. Our Kaplan-Meier analyses was the first indication that JMJD7 and DRG1/DFRP1 may be functioning in a novel tumour suppressor pathway in gastric cancer (Figure 3.1a, 3.1b and 3.1c). Whether a similar trend is observed in other cancer types is not yet clear, although preliminary analyses in Breast cancer suggest a more complex pattern of associations (data not shown). The evidence for a potentially meaningful role in gastrointestinal cancers also included the observation of gene deletions for JMJD7 in colorectal cancer, and DFRP1 in stomach and oesophageal cancers. Potentially consistent with this, we previously observed loss of DFRP1 protein expression in AGS cells (Figure 2.4a, Chapter 2), a cell line derived from a patient with gastric adenocarcinoma. Whether loss of DFRP1 in AGS cells contributes to the tumourigenic phenotype of these cells is unclear, but may be worth further investigation. Interestingly, the DFRP1 gene is located on chromosome 2q32.1, a region known to be deleted in oesophageal, lung, gastric, prostate, and breast cancers, and in a developmental disorder known as “2q32 deletion syndrome” (Ferreira et al., 2012). Interestingly, patients with this syndrome present with various symptoms including intellectual disability (Van Buggenhout et al., 2005), which is of interest with respect to the documented mutations in JMJD7 and DRGs in related disorders. Although it is unclear how loss of DFRP1 function might support

tumorigenesis and altered neuronal development, knockout experiments in yeast have proven that DFRP1 is required for the recruitment of the DRG1/DFRP1 complex to polysomes (Francis et al., 2012). Furthermore, the DFRP1/DRG1 interaction is known to be critical for normal DRG1 protein stability and expression (Ishikawa et al., 2005). Interestingly, we observed potentially damaging mutations enriched within the DRG1 binding domain of DFRP1 (Figure 3.3c), and mutations within the TGS domain of DRG1 (and a nonsense mutation that precedes it) (Figure 3.3b). Complementation studies in yeast have demonstrated that the TGS domain mediates the binding of DRG1 to DFRP1 and the localisation of DRG1 to polysomes (Francis et al., 2012). Therefore, it is possible that the DRG1-DFRP1 interaction is a target for deregulation in some cancers. Overall, our preliminary bioinformatics analyses of clinical and genetic data support a potential tumour suppressor role for JMJD7 and possibly downstream signalling through DRG1/DFRP1. Potential biological explanations for this are explored in the Final Discussion in Chapter 6.

Our observations supporting a potential tumour suppressor role for the JMJD7 pathway may be at odds with the limited literature on its components, and the data presented at the end of Chapter 2 suggesting that JMJD7 supports cell growth (Figures 2.8, 2.9 and 2.10). Our growth data would be more consistent with JMJD7 being a tumour 'driver', in potential agreement with data from an siRNA screen demonstrating that loss of JMJD7 supressed invasion of squamous cell carcinomas (Ding et al., 2013). Furthermore, a recent study showed a reduction in colony formation in JMJD7 shRNA knockdown cells (Liu et al., 2017). Other evidence supporting a potential driver role in some contexts might include our observation that the JMJD7 gene is amplified in NEPC and pancreatic cancer (as opposed to the

majority of other cancers where it was predominantly deleted). Likewise, in addition to the other types of genetic alterations discussed, we also observed some gene amplification for DRG1, DFRP1 and DRG2 (Figure 3.1b, 3.1c and 3.1d, respectively). Interestingly, DFRP2 has been identified as a potential prognostic marker for melanoma, where high expression correlated with poor survival (Vuong et al., 2014). The apparent discourse between these various observations could simply reflect context-dependence, either in terms of mutational mechanisms or biological roles. However, it is also possible that the apparent complexity could be a reflection of the biology of this pathway, which remains poorly characterised, and which will be discussed further in Chapter 6.

Our cancer analyses of the JMJD7 pathway were supported by comprehensively collating all the available missense mutations from across three sequencing databases (cBioPortal, COSMIC and COSMIC Cell Lines). Although our mutational analyses was up to date as of 2018, this will need to be regularly updated since these databases are constantly evolving as sequencing costs fall and the number of datasets continues to increase. Overall, our analyses indicated that the JMJD7 pathway is relatively infrequently mutated in cancer, but the mutations that were observed may be consistent with potential loss of function and tumour suppressor activity, particularly for JMJD7, DRG1 and DFRP1. Specifically, we noted the presence of mutation hotspots and recurrent mutations found in multiple independent tumours, including those in known catalytic residues and functional domains (Figure 3.3). We partially validated these analyses by cloning a panel of JMJD7 cancer mutations and demonstrating that 6 out of 15 dramatically reduced JMJD7 protein expression. This would suggest that at least one functional consequence of

cancer missense mutation might be to prevent JMJD7 protein expression, analogous of course to the consequence of JMJD7 gene deletion observed in Figure 3.2a. Further functional studies are required to explore the functional consequences of other JMJD7 mutations (ideally on an update 'library' of mutants). Assays could include monitoring effects on dimerisation (as in Figure 2.1c), substrate binding (as in Figure 3.4c), and activity. Indeed, it would also be of interest to undertake functional studies on DRG1/DFRP1 cancer mutants, particularly DRG1/DFRP1, as outlined above. Using hotspots and recurrent mutations as a guide for selecting relevant mutations to test would likely be beneficial. As outlined above, clustering and recurrence of cancer mutations can be indicative of a selective pressure to maintain such alterations. As such, these mutational patterns can imply the presence of novel functional domains, particularly in poorly characterised proteins such as those in the JMJD7 pathway. Therefore, it is also of interest whether the mutation patterns we have collated here might indicate the presence, for example, of protein interaction domains, novel regulatory sites (including other PTMs), or sub-cellular targeting sequences.

Chapter 4

Investigating the role of phosphorylation in regulating the biological function of JMJD7

Introduction

In the previous Chapters we demonstrated that JMJD7 is necessary for cellular growth control and that it may be a cancer-associated gene. Growth regulating and cancer-associated proteins are often themselves dynamically regulated (Duronio and Xiong, 2013). However, nothing is currently known about the molecular mechanisms by which JMJD7 and pathway components might be regulated, or how potential regulation might contribute towards JMJD7's role in growth control. The activity of enzymes can be regulated by multiple, often overlapping mechanisms, including gene expression changes (e.g. epigenetic and transcriptional regulation), altered translation and post-translational regulation (Gibcus and Dekker, 2012, Corbett, 2018, Van Der Kelen et al., 2009, Dhillon et al., 2007). Post-translational modifications (PTMs) are a major level at which the activity and function of enzymes and other proteins is regulated (Lothrop et al., 2013). For example, tumour suppressors such as p53 and BRCA1 are heavily modified by a variety of PTMs and each event is essential for its role in a specific pathway (Taira and Yoshida, 2012, Henderson, 2012). Understanding whether JMJD7 is post-translationally modified, and how this might affect its function, activity, and its role in growth control is therefore of interest.

Interestingly, there is precedent for other 2OG oxygenases being regulated by PTMs, particularly phosphorylation. As outlined in Chapter 1, PHD1 has recently been shown to defer substrate specificity under normoxic conditions to hydroxylate CEP192 after phosphorylation by CDK1 (Ortmann et al., 2016). Furthermore, the histone demethylase KDM7C (PHF2) phosphorylation by Protein Kinase A (PKA) promotes complex formation and, in turn, KDM7C histone demethylase activity (Baba

et al., 2011). As a previously uncharacterised enzyme, JMJD7 is yet to be investigated with respect to PTM, specifically phosphorylation. Here we describe work which identifies a unique phosphorylation site at the N-terminus of JMJD7, our efforts to develop cell models for studying its role in regulating JMJD7 function, and data suggesting this PTM may be required for JMJD7's role in supporting cell growth.

4.1 JMJD7 is phosphorylated on a conserved N-terminal threonine residue

In Chapter 3 we identified several cancer mutation 'hot-spots' in the JMJD7 gene sequence (Figure 3.3e). Mutational hot-spots are often found at locations within a gene that encode parts of the corresponding protein that are functionally important. Therefore, in order to attempt to identify novel JMJD7 regulatory domains we interrogated various online databases and interpreted the results in light of our cancer mutation data presented in Chapter 3. We first tested for the presence of a signal peptide, a short amino acid sequence found at the N-terminus of a protein which enables transport of proteins across a membrane, out of the cytoplasm and into the Endoplasmic Reticulum (ER) (Izard and Kendall, 1994). To test for the presence of a signal peptide on JMJD7 online tool "SignalP4.1" (Nielsen, 2017) was used. As expected, from localisation data in Chapter 2, the results suggested that JMJD7 does not contain a signal peptide. Similarly, analysis by "SeqNLS" (Lin et al., 2012), which tests for nuclear localisation sequences (NLS), also suggested an absence of classicial NLS sequences in JMJD7. In contrast, Nuclear Export Signals (NES) were analysed using the database "NetNES1.1" (la Cour et al., 2004) which suggested that JMJD7 residues Leu109-Leu113, may contain an NES. However, there are no missense mutations within this sequence, suggesting that nuclear localisation may not be a frequent mechanism of altered JMJD7 regulation in cancer.

With respect to PTM, the JMJD7 protein sequence was analysed by PhosphoSitePlus (Hornbeck et al., 2015), which despite the suggestion by its name, collates several MS-identified PTMs including phosphorylation, acetylation, methylation, and ubiquitylation. Interestingly, the N-terminus of JMJD7 hosts a potential site of phosphorylation (Figure 4.1a) identified 12 times in MS studies (Figure 4.1b). Importantly, the residue in question is threonine 37 (T37), which is located in the middle of a cancer mutation hot-spot (Figure 4.1a; T37 is highlighted by a yellow arrow and labelled as “T37” in Figure 4.1b). Perhaps consistent with a potential role of T37 phosphorylation in cancer, all 12 MS identifications were made in cancer samples and cell lines, including breast, gastric and lung cancer.

To explore the potential for JMJD7 T37 phosphorylation in more detail, we first turned to the available crystal structure. T37 is located close to the interface of the JMJD7 dimer and is solvent exposed (seen in yellow in Figure 4.1c) indicating that it could be accessible for a kinase. We postulated that if T37 phosphorylation was functionally important then the T37 residue and surrounding sequence might be evolutionarily conserved. Therefore, we next assessed sequence conservation in this area by bioinformatic alignment of multiple eukaryotic sequences. Potentially consistent with an important role in JMJD7 function, we observed that this N-terminal region of JMJD7 was highly conserved, including the target phosphorylated residue at positon 37 (Figure 4.1d, conservation at position 37 was between Threonine and Serine, which can also support phosphorylation, at least in other contexts). Finally, we directly tested for evidence of JMJD7 T37 phosphorylation in our own database of overexpressed FLAG-JMJD7 MS analyses. Consistent with the findings of others (as collated by PhosphoSitePlus), we observed tryptic JMJD7 peptides with an +80

dalton shift on T37, consistent with the addition of a phosphate group, thus confirming that JMJD7 is phosphorylated in cells (Figure 4.1e). How phosphorylation might regulate JMJD7 function is unknown, but is the subject of the remainder of this Chapter.

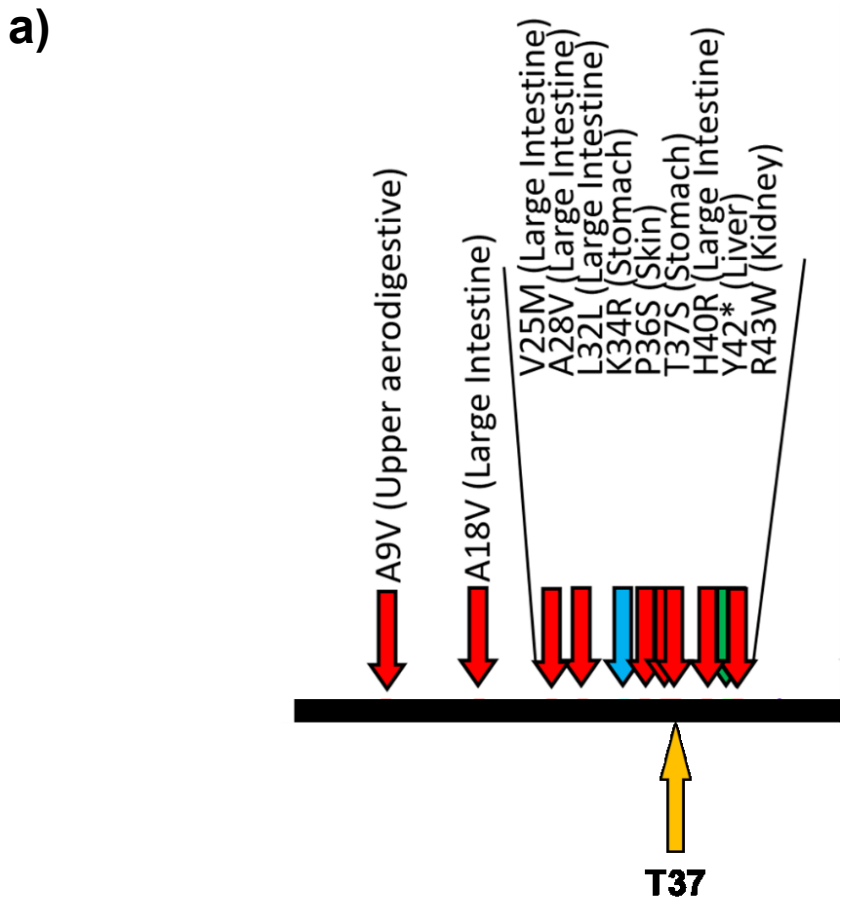

Figure 4.1 JMJD7 is phosphorylated on a conserved threonine residue. a) N-terminal JMJD7 cancer hot-spot (V25-R43) (adapted from Figure 3.3e) showing the site of phosphorylation as identified by online database, PhosphositePlus. The black line covers the N-terminal residues, M1-C51. Yellow arrow highlights position of T37.

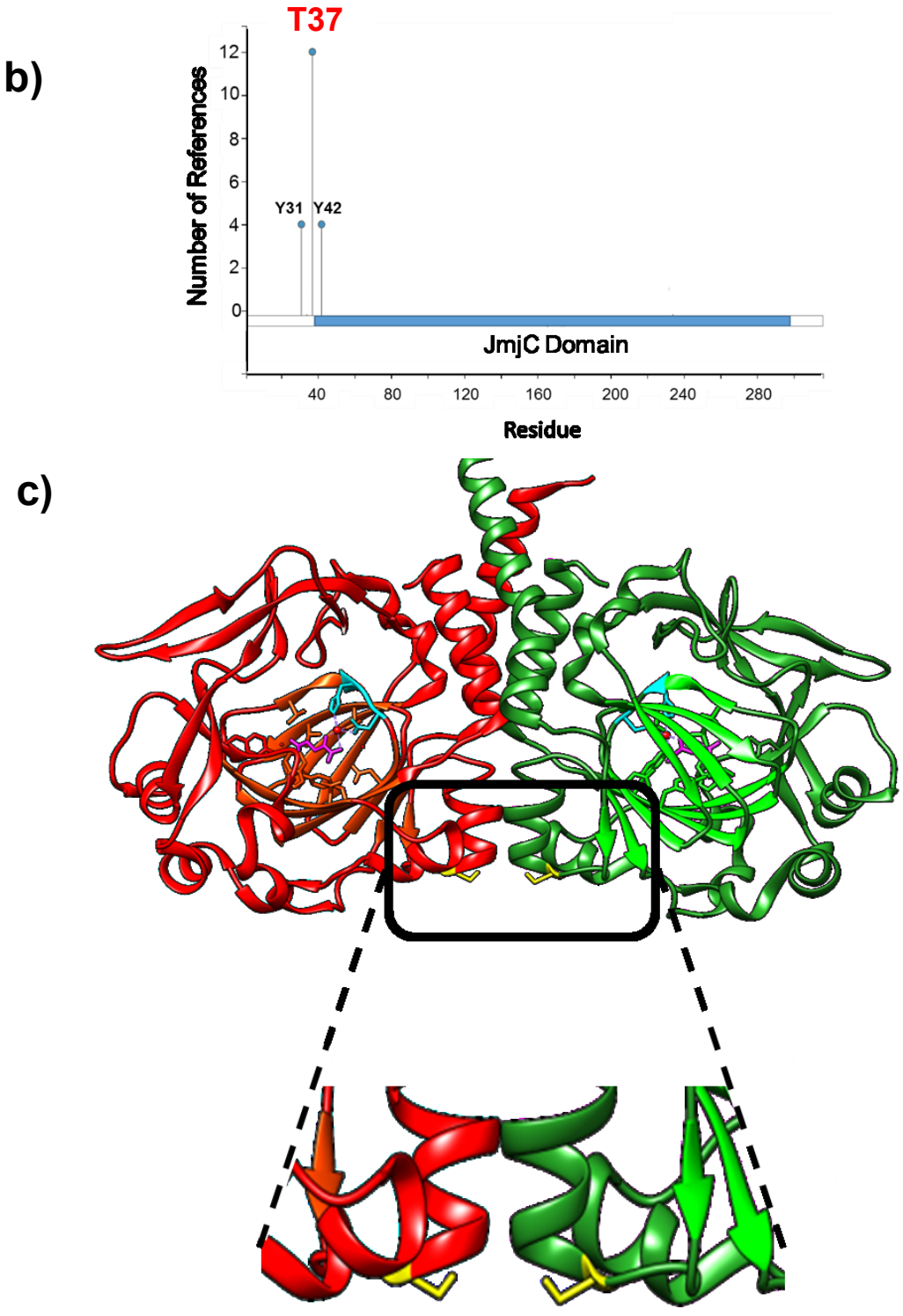

Figure 4.1 (b) Three sites of phosphorylation have been documented in PhosphositePlus (Y31, T37 and Y42), however, only T37 has been identified in multiple studies with high confidence (PhosphositePlus, personal communication) (Hornbeck et al., 2015). c) close up of the JMJD7 crystal structure highlighting that Threonine 37 (yellow) is close to the interface of the dimer and solvent exposed.

d)

e)

#	b	b-H2O	b-NH3	b (2+)	Seq	y	y-H2O	y-NH3	y (2+)	#
1	130.050	112.040	113.023	65.525	E					22
2	243.133	225.124	226.117	122.067	L	2576.313	2558.303	2559.286	1288.657	21
3	403.161	385.152	386.155	202.083	C(+57.02)	2463.229	2445.219	2446.202	1232.115	20
4	502.227	484.216	485.244	251.617	V	2303.199	2285.188	2286.172	1152.099	19
5	599.301	581.276	582.259	300.143	P	2204.130	2186.120	2187.103	1102.565	18
6	712.357	694.360	695.343	356.685	L	2107.078	2089.067	2090.051	1054.039	17
7	783.401	765.397	766.380	392.178	A	1993.993	1975.983	1976.966	997.497	16
8	882.476	864.465	865.449	441.738	V	1922.956	1904.946	1905.929	961.978	15
9	979.529	961.518	962.502	490.234	P	1823.888	1805.877	1806.861	912.449	14
10	1142.592	1124.581	1125.565	571.796	Y	1726.835	1708.825	1709.808	863.918	13
11	1255.672	1237.659	1238.649	628.350	L	1563.758	1545.761	1546.745	782.386	12
12	1370.703	1352.693	1353.676	685.852	D	1450.688	1432.677	1433.661	725.844	11
13	1498.798	1480.787	1481.771	749.899	K	1335.661	1317.650	1318.634	668.317	10
14	1595.851	1577.840	1578.824	798.425	P	1207.562	1189.555	1190.539	604.283	9
15	1692.903	1674.893	1675.876	846.952	P	1110.513	1092.503	1093.486	555.757	8
16	1873.917	1855.907	1856.891	937.459	T(+79.97)	1013.460	995.450	996.433	507.230	7
17	1970.970	1952.960	1953.943	985.985	P	832.440	814.436	815.426	416.723	6
18	2084.054	2066.044	2067.027	1042.527	L	735.394	717.383	718.367	368.197	5
19	2221.113	2203.103	2204.086	1111.057	H	622.304	604.299	605.283	311.655	4
20	2368.182	2350.171	2351.155	1184.591	F	485.244	467.240	468.224	243.133	3
21	2531.245	2513.234	2514.218	1266.122	Y	338.179	320.172	321.155	169.591	2
22					R	175.118	157.108	158.092	88.059	1

Figure 4.1 (d) sequence alignment of JMJD7 region spanning T37 showing conservation between species between serine and threonine. e) HEK293T cells were transfected with FLAG-JMJD7, lysed for protein and immunopreciptated with Sigma M2 FLAG beads overnight. The JMJD7 eluent was subject to analysis by mass spectrometry (MS/MS). This table shows a peptide species with mass shift of +79.97 Da at T37, consistent with the addition of a phosphate group. The +57.02 shift on C24 is an alkylated residue (C_4H_9), a process which inhibits the reformation of disulphide bonds. Each column represents the different ions detected. When ionised, the peptide can form different ions (loss or addition of NH_3 or H_2O).

4.2 T37 phosphorylation does not significantly affect JMJD7 localisation, dimerisation, or substrate binding

Having validated that JMJD7 T37 is phosphorylated in cells, we wanted to investigate how this might regulate the biochemical characteristics and biological functions of JMJD7, particularly those characterised in Chapter 2. To approach this in the absence of knowing the identity of the JMJD7 T37 kinase (which is explored in Chapter 5) we aimed to use molecular biology to mutate the phosphorylation site. Using site directed mutagenesis, we created an unphosphorylatable JMJD7 mutant, T37A, and a phospho-mimetic mutant, T37E (which mimics the negative charge of the phosphate group).

We first aimed to use the T37 phospho-mutants to explore whether phosphorylation might regulate JMJD7 localisation, for the following reasons. In Chapter 2 we identified that JMJD7 is localised in multiple sub-cellular compartments (Figure 2.3a and 2.3b), raising the possibility that distribution between these is actively regulated. Indeed, the cytoplasmic/nuclear distribution of other proteins is dynamically regulated by PTMs such as phosphorylation (e.g. FOXO proteins) (Van Der Heide et al., 2004). Therefore, HA-tagged JMJD7 WT and mutants were transfected into HeLa cells on glass cover slips for 48 hours before fixing. HA primary antibody and Alexaflour 555 secondary antibody were used to stain for the over expressed JMJD7 and variants. As seen in Figure 4.2a, there was no significant difference between the staining pattern of JMJD7 WT, T37A or T37E suggesting that phosphorylation may not play a major role in the sub-cellular distribution of JMJD7.

The site of phosphorylation is found at the bottom of helix ‘α1’, one of the α-helices involved in dimerisation (Figure 3.1a) (Markolovic et al., 2018). Therefore we tested

whether T37 mutation regulates JMJD7 dimerisation using the assay described previously (see Figures 2.1b and 2.1c) (Markolovic et al., 2018). As seen in Figure 4.2b there was no significant difference between the dimerisation of FLAG-JMJD7 WT, T37A or T37E, suggesting that T37 phosphorylation does not significantly regulate JMJD7 oligomerisation.

Phosphorylation is an established mechanism of regulating enzyme activity (Ardito et al., 2017). As outlined above, the phosphorylation site is proximal to the dimerisation domain. The dimerisation domain is required for the activity of some JmjC-only hydroxylases because of its role in providing an interface for substrate binding (Lancaster et al., 2004, Chowdhury et al., 2014). Therefore, we next aimed to test for a role of T37 phosphorylation in regulating JMJD7 enzyme activity. Initially, as a surrogate for activity, we analysed the ability of the T37A and T37E mutants to interact with the known JMJD7 substrate complexes, DRG1/DFRP1 and DRG2/DFRP2. HEK293T cells were infected with lentivirus containing a pTIPZ plasmid (pTRIPZ derivative with the RFP cassette removed) that conditionally expresses FLAG-JMJD7 WT or T37A. Stable puromycin-selected cells were seeded and left to grow for 36 hours before DMOG treatment for 15 hours prior to lysis. Whole protein extract was subject to anti-FLAG-IP overnight followed by elution by boiling in Laemmli buffer and western blot analysis. Figure 4.2c indicates no major difference between the interaction of DRG1, DFRP1, DGR2 or DFRP2 to WT or T37A JMJD7. Although a slight reduction in DRG2/DFRP2 binding can be seen to WT versus T37A JMJD7, this could be explained by an artefact of variation in endogenous expression levels (see “Input”). Interestingly, we did observe a subtle increase in DRG1 binding to T37A versus WT JMJD7, under conditions in which the

Input levels were actually slightly decreased (compare lanes 3 and 6). Overall however, we did not observe any large differences in substrate complex binding between WT and T37A JMJD7 that was reproducible between experimental repeats.

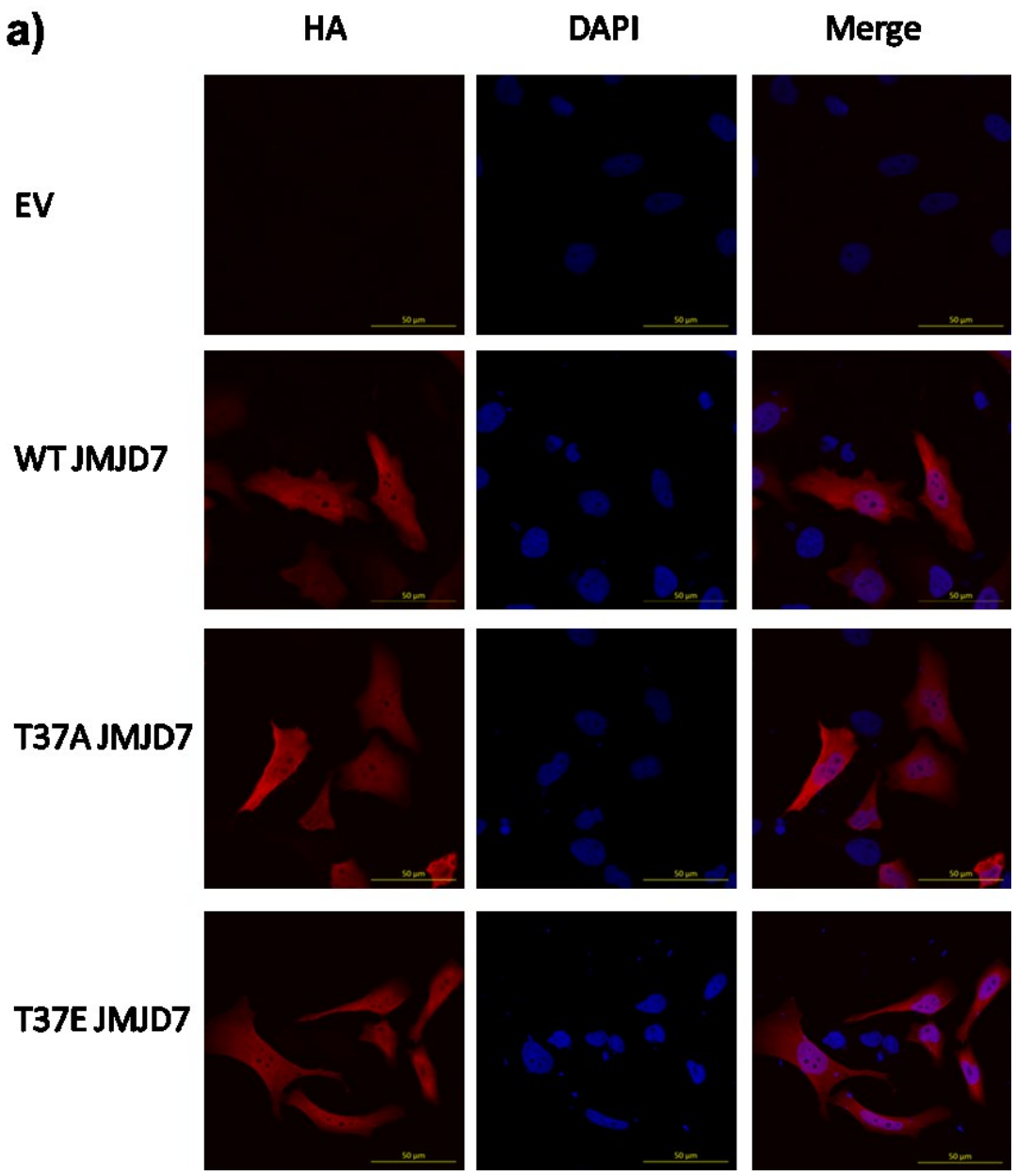

Figure 4.2 JMJD7 phosphorylation site mutants do not significantly affect localisation, dimerisation or substrate binding. a) HeLa cells were seeded on to glass cover slips and transfected with HA-JMJD7 WT or mutants for 48 hours prior to fixing. Over expressed JMJD7 was stained with anti-HA antibody (BioLegend) and Alexaflour 555 (Thermo). Images were taken on a LSM880 confocal microscope. Mutation of T37 to phospho-mutant or mimetic does not affect JMJD7 localisation in HeLa cells. n=3

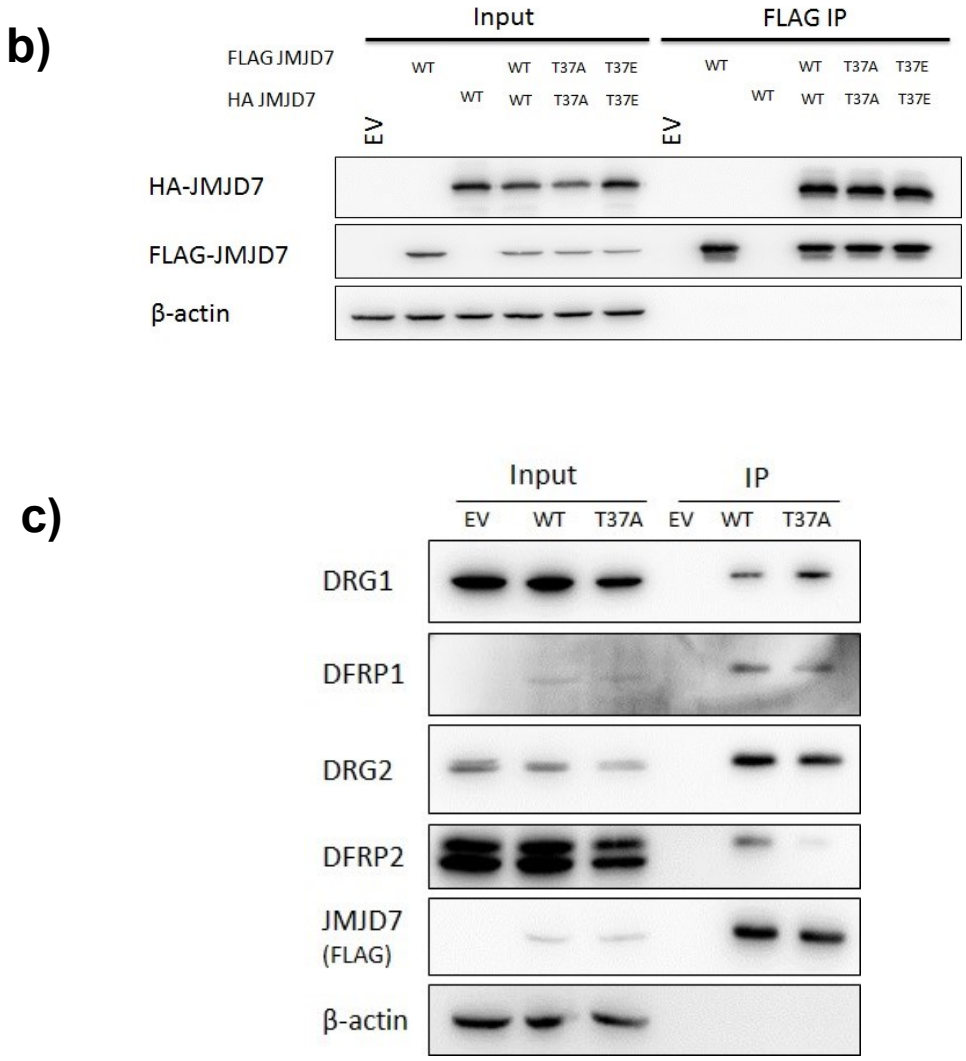

Figure 4.2 b) JMJD7 WT or mutants tagged with either a FLAG- or HA-epitope tag were transfected into HEK293T cells and over expressed for 48 hours. Cells were lysed for proteins and immunoprecipitated over night with FLAG. Bound proteins were boiled off the beads using Laemmli buffer and analysed by western blot. JMJD7 T37 phosphorylation does not affect its ability to dimerise. n=2 c) HEK293T cells with doxycycline inducible pTIPZ vectors containing FLAG-JMJD7 WT or T37A were seeded and allowed to grow using “leaky” JMJD7 expression. 15 hours before lysis, DMOG was added to cells. Lysates were FLAG-immunoprecipitated overnight, eluted by boiling and analysed for the presence of pathway components by western blot. Mutation of T37 to alanine does not significantly effect JMJD7 binding to its substrates, DRG1 and DRG2, or their binding partners, DFRP1 and DFRP2, respectively. n=3

4.3 JMJD7 T37 phosphorylation does not affect DRG2 hydroxylation

Since substrate binding does not always reflect enzyme activity and substrate modification it remains possible that T37 phosphorylation regulates the intrinsic hydroxylase activity of JMJD7. Therefore, we next sought to explore this directly by measuring the hydroxylation status of DRG1 and DRG2 using mass spectrometry. We chose to use HEK293T as a model because endogenous DRG1 and DRG2 hydroxylation levels had previously been measured in these cells (Markolovic et al., 2018): Dr Qinqin Zhuang demonstrated that DRG1/2 hydroxylation at K22/K21 (respectively) was incomplete, and that it could respond to JMJD7 knockdown and overexpression. We rationalised therefore that this might be a good context in which to observe potential increases or decreases in JMJD7 activity. Using the HEK293T pTIPZ-JMJD7 cells described above, four 15cm plates of HEK293T cells with leaky WT or T37A JMJD7 expression (Figure 4.3a) were seeded, and lysed when confluent. Cell lysates were incubated with sepharose beads and anti-DRG1 (8µg) or -DRG2 (4µg) primary antibodies (ProteinTech) overnight. Beads were washed and proteins were eluted by boiling and electrophoresis on a 12% SDS polyacrylamide gel before coomassie staining overnight (Figure 4.3b). Figure 4.3b shows that proteins corresponding to the anticipated sizes of endogenous DRG1 (yellow arrow), DFRP1 (red arrow), DRG2 (orange arrow) and DFRP2 (purple arrow) were present in the pulldown. The DRG1 and DRG2 bands were excised from the gel and sent for trypsin digest and MS analyses (MSMS sequencing and hydroxylation assignment) at the Advanced Oxford Proteomics Facility. Unfortunately, however, the MS analyses of the DRG1 samples failed to identify the relevant K22-containing tryptic peptides, possibly due to insufficient sample abundance (data not shown). In

contrast, MS analyses of the DRG2 samples reproducibly identified the tryptic peptides containing unmodified and hydroxylated K21, as observed previously (Markolovic et al., 2018). MS analyses of JMJD7-mediated hydroxylation is complicated relative to other lysyl hydroxylases (e.g. JMJD4 or JMJD6) because the modification is at the C3 carbon of the side chain (i.e. nearer to the 'backbone') (see Figure 1.7) and partially inhibits the action of trypsin (Markolovic et al., 2018). The result is that as the activity of JMJD7 changes, and the DRG hydroxylation level is altered, the pattern of tryptic peptides for MS analysis changes. This makes it difficult to make the type of quantitative measurements between samples used for other projects (Feng et al., 2014). Rather, we previously published a qualitative approach that monitors the shift between the abundance of hydroxylated and unhydroxylated tryptic DRG peptides within a sample (Markolovic et al., 2018). Using this approach we detected a range of hydroxylated and unmodified K21-containing peptides in the DRG2 samples analysed (Figure 4.3c), where the abundance of hydroxylated peptides make up around 25-30% of the K22-containing peptides species detected. In Figure 4.3c the various hydroxylated DRG2 K21-containing peptides are shown in various shades of red and pink, while the various unhydroxylated K21-containing peptides are shown in multiple shades of blue. As expected, the overall abundance of DRG2 K21-containing peptides that were hydroxylated was significantly increased upon JMJD7 over expression (compare EV to WT). However, this remained unchanged with the overexpressed phospho-mutant (compare WT to T37A). Overall, this would suggest that T37 phosphorylation does not significantly affect JMJD7 activity, at least with respect to DRG2.

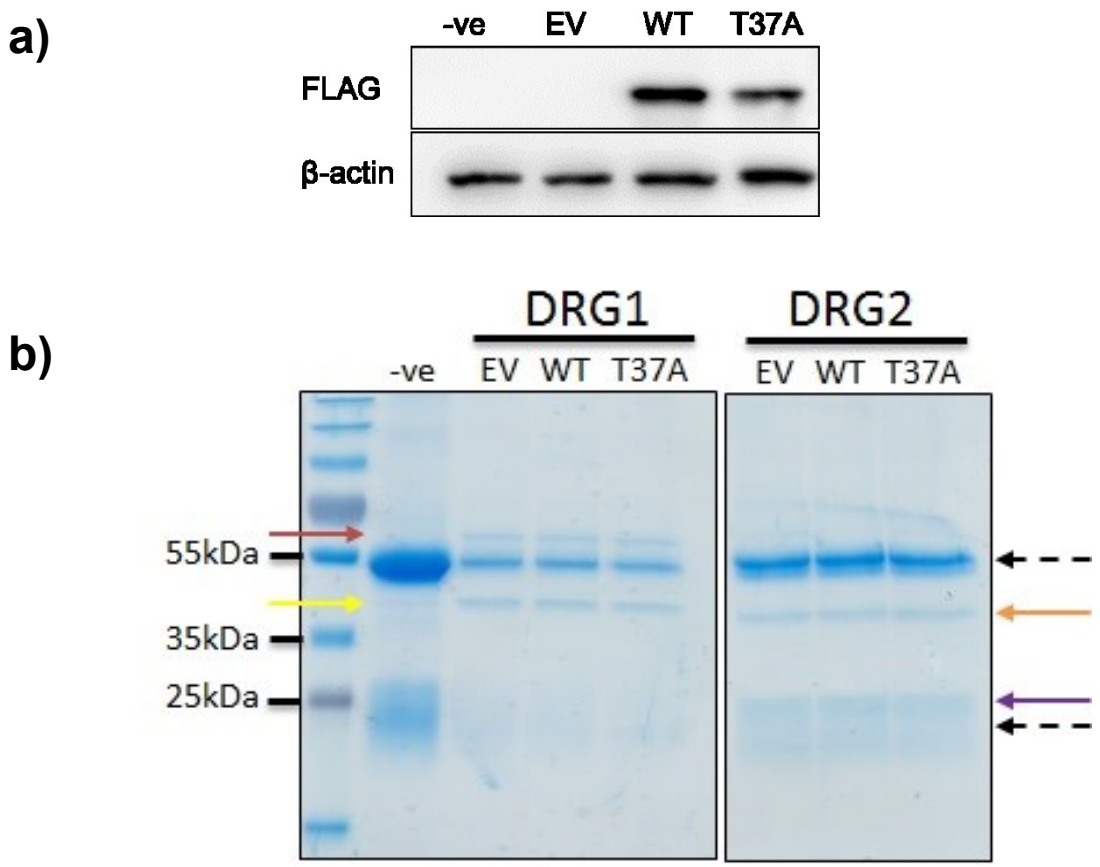

Figure 4.3 A JMJD7 T37 phosphorylation site mutant does not alter activity towards DRG2 K21. HEK293T cells containing a lentiviral inducible pTIPZ with or without JMJD7 WT or T37A were seeded into four 15cm plates and left to grow for 4 days, until confluent. Cells were lysed for protein and subject to endogenous DRG2 and DRG1 IP overnight. The following day the beads were isolated and washed before elution by FLAG peptide competition. a) shows western blot of the pre-IP input samples confirming the presence of FLAG JMJD7. b) shows the coomassie gel that was used to visualise the immunoprecipitated DRG1 and DRG2 which were excised from the gels and sent for in-gel trypsin digest mass spectrometry. The yellow and orange arrows indicate the DRG1 and DRG2 bands, respectively, that were sent for analysis. Red arrow shows the presence of DFRP1 and Purple arrow shows DFRP2. Heavy chain and light chain antibodies were also present in the samples and are shown by the black dashed arrows. Parental HEK293T cells used as negative control (-ve), EV (empty vector) indicates cells with pTIPZ alone.

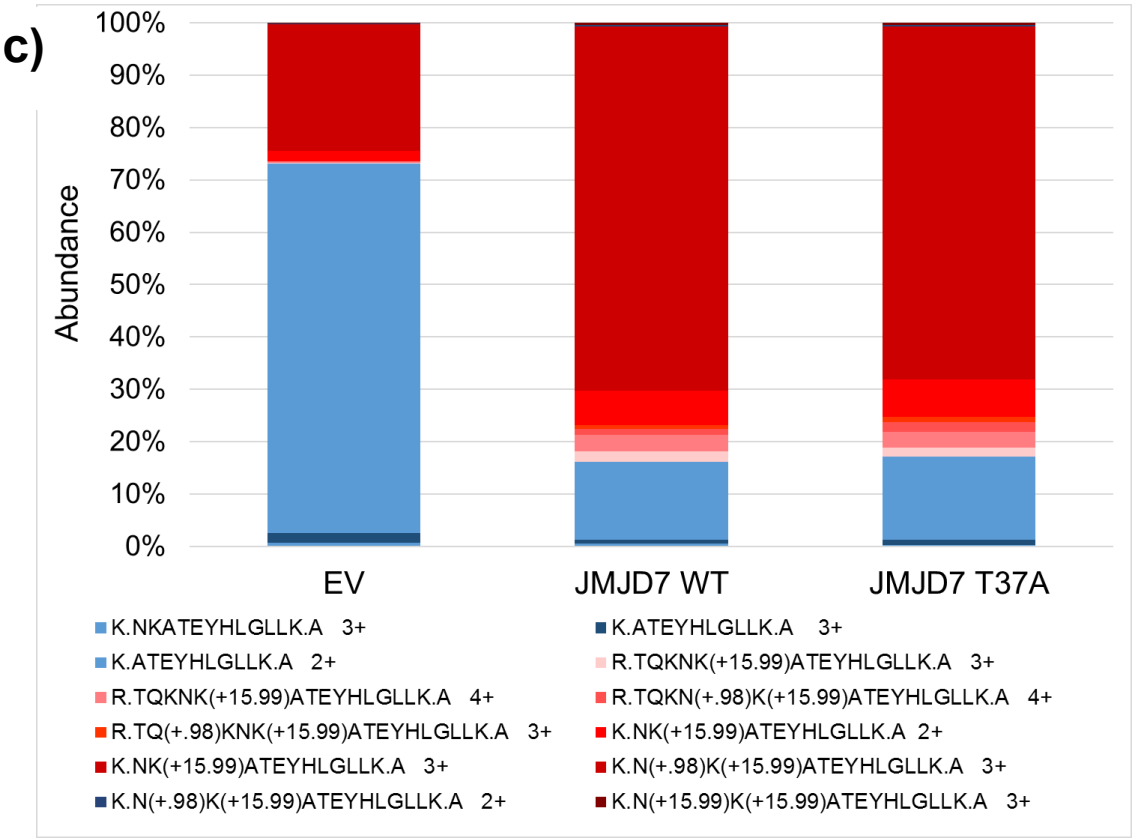

Figure 4.3 c) bar chart demonstrating the relative abundance (expressed as a % of the total abundance of K21-containing peptides in each sample) of the various hydroxylated vs unhydroxylated K21-containing peptides. Hydroxylated DRG2 is seen in various shades of red/pink and unhydroxylated is seen with various shades of blue. When JMJD7 was over expressed in cells, DRG2 hydroxylation (+15.99Da) is significantly increased (compared to EV), as expected, but this remains unchanged between WT and T37A JMJD7. n=1

4.4 JMJD7 WT and T37E, but not T37A, are able to partially rescue JMJD7 knockdown phenotype

In the work presented above we did not observe any significant effects of a non-phosphorylatable T37 mutant on functions that might be considered biochemically 'proximal' to JMJD7. Therefore, we considered testing a more 'distal' phenotype, such as the role of T37 phosphorylation in JMJD7-mediated growth control (Chapter 2). To do so it was first necessary to develop a cell model in which it was possible to restore JMJD7 (WT or T37A mutant) expression in a loss-of-function model such as the shRNA knockdown system validated in Chapter 2 (Figure 2.9). We generated 'shRNA-resistant' WT, T37A and T37E JMJD7 cDNA's by cloning four silent mutations within the relevant JMJD7 cDNA sequence targeted by shRNA#3 (see Figure 2.6b). These cDNAs were then cloned into the lentiviral vector pIPZ (a derivative of pGIPZ, with the GFP cassette removed, for constitutive expression of JMJD7) and termed pIPZ-shRes_FLAG.-JMJD7WT, -T37A and -T37E (collectively termed 'pIPZ-shRes_J7'). The pIPZ-shRes_J7 vectors and an 'empty' pIPZ (EV) were used to generate lentiviral supernatants (see Methods) for infection of HEK293T cells. Subsequently, a second lentiviral infection delivered the doxycycline-inducible pZIP-JMJD7 shRNA#3 vector into pIPZ-shRes_J7 cells (and termed 'shJ7#3_pIPZ-shRes_J7'). Given that both of the infected vectors contained a puromycin selection cassette, the shRNA positive cells were selected for using Fluorescence Assisted Cell Sorting (FACS). The top 15% of GFP expressing cells were sorted and kept for further experiments (data not shown).

We tested whether JMJD7 T37 mutation effects the role of JMJD7 in cell growth as follows. Two 10cm plates of each shJ7#3_pIPZ-shRes –EV, -WT, -T37A and –T37E cell line were seeded. After 1 day, one plate of each cell line was either treated or

untreated with doxycycline to induce shRNA and cause knockdown of JMJD7. After 120 hours the cells were reseeded in the presence or absence of doxycycline to measure cell proliferation using an MTS assay (as in Chapter 2, Figure 2.9b) over 5 days. Parallel samples were lysed for either protein or RNA. Western blot analyses of protein lysates harvested on Day 0 (day of reseeding for MTS) shows the presence of JMJD7 both with and without doxycycline (Figure 4.4a), thus confirming the shRNA-resistance of the exogenous cDNA. Unfortunately, we were unable to test for endogenous JMJD7 protein knockdown in pIPZ-shRes_J7 cells by anti-JMJD7 western blot because the chemiluminescence signal from the exogenous FLAG-JMJD7 overexpression confounded that of the endogenous protein (data not shown). Therefore, to accurately measure the amount of endogenous JMJD7 knockdown in this context we turned to qPCR analysis. Two SYBR green qPCR primers were designed to target the 3' untranslated region (UTR) of JMJD7 (which is absent in the exogenous cDNA, and in the PLA2G4B-JMJD7 readthrough transcript).

Using this approach, we determined that doxycycline treatment induced approximately 50% knockdown of endogenous JMJD7 mRNA (Figure 4.4b) and similar results were obtained at day 5 (Figure 4.4d). Under these conditions of partial JMJD7 knockdown, our MTS analyses (Figure 4.4c) confirmed delayed growth of EV cells compared to the same cells in the absence of doxycycline. Importantly, and consistent with an 'on-target' effect of shRNA#3, reconstitution with FLAG-JMJD7 WT partially restored the growth defect induced by JMJD7 knockdown (Figure 4.4e and 4.4f). Furthermore, reconstitution with FLAG-JMJD7 T37E restored growth to a similar extent to FLAG-JMJD7 WT. Interestingly, however, reconstitution with FLAG-JMJD7 T37A was completely unable to rescue the shRNA knockdown

phenotype (Figure 4.4c and 4.4d). Overall, these preliminary results suggested that JMJD7-mediated growth control may require T37 phosphorylation. However, there were some limitations in the experimental validation that suggested the system may require further optimisation (discussed and explored below).

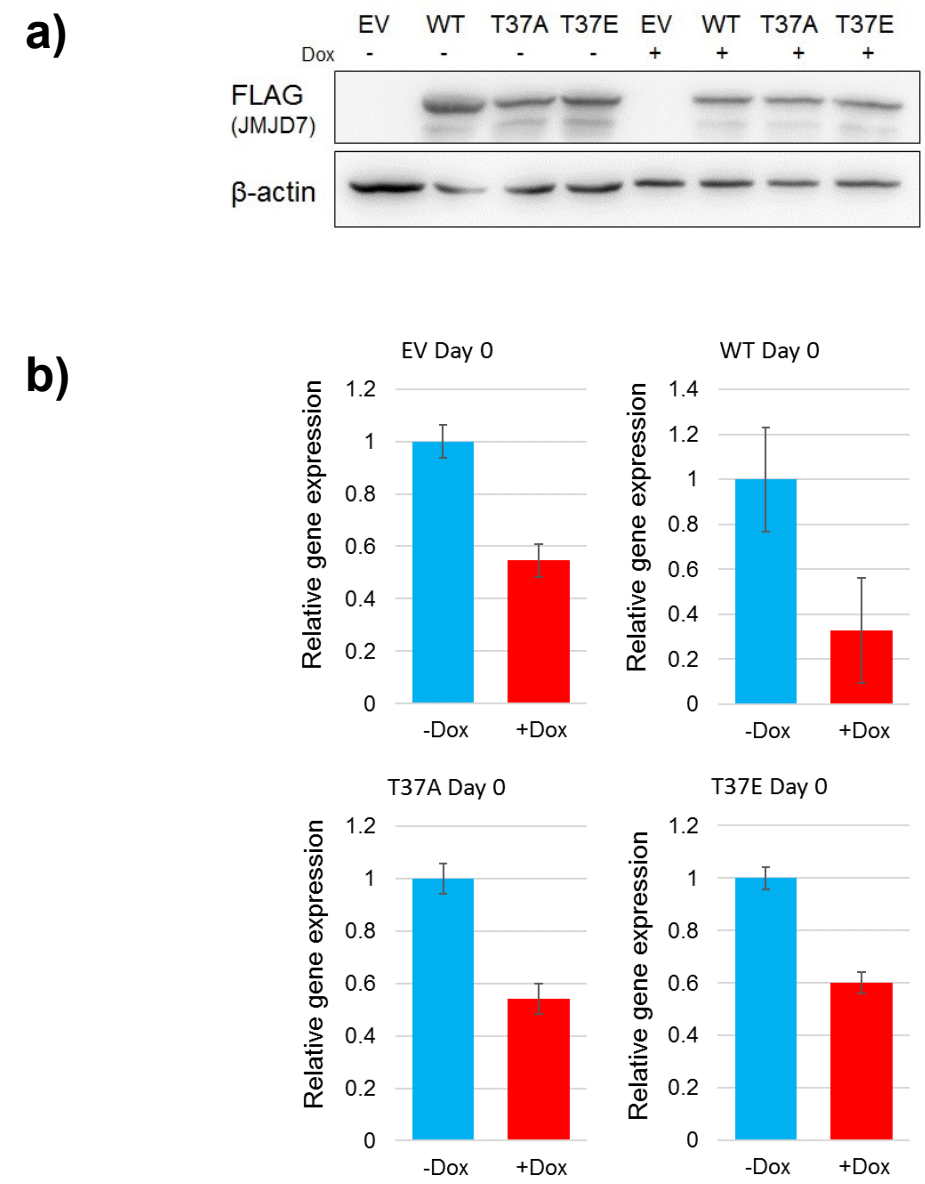

Figure 4.4 Re-expression of JMJD7 WT, but not T37A, can partially rescue the JMJD7 shRNA knockdown phenotype. HEK293T cells lentivirally infected with control pIPZ (EV) or pIPZ-shRes_J7-WT, -T37A or –T37E and JMJD7 shRN#3 (shJ7#3_pIPZ-shRes -WT, -T37A or –T37E) followed by GFP FACS sorting to generate a homogenous pool of JMJD7-shRNA#3 cells. Two plates for each cell line were seeded and one from each was subject to 1µg/ml of doxycycline treatment for 120 hours before reseeding for MTS cell proliferation assay. a) shows the western blot of JMJD7 in the treated and untreated cells at the day of reseeding indicating shRNA resistant JMJD7 expression. b) shows SYBR Green qPCR validation of endogenous JMJD7 knockdown in all of the doxycycline-treated cell lines.

c)

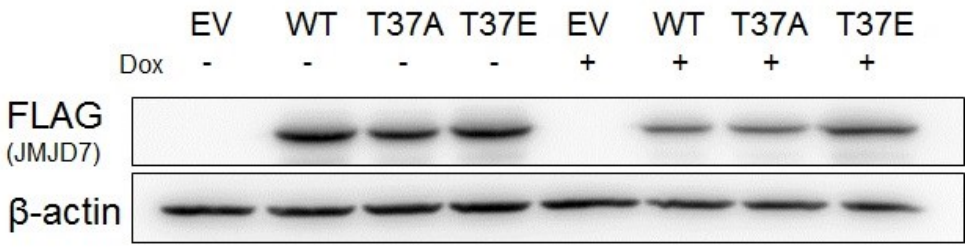

d)

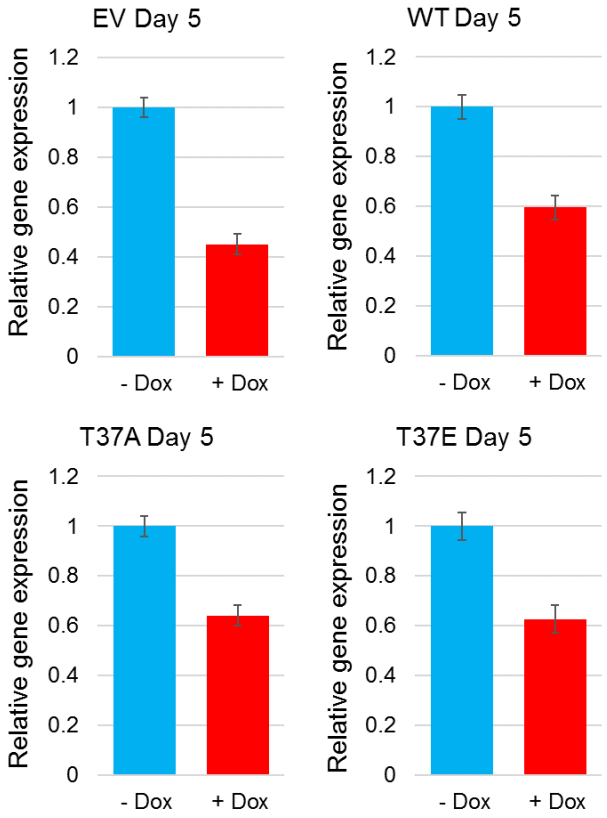

Figure 4.4 (c) Western blot shows reduced exogenous JMJD7 in the +dox cells compared to the –dox cells at day 5 after seeding. d) SYBR Green qPCR analysis shows endogenous JMJD7 knockdown is still present on the 5th day of the MTS assay, albeit to a lesser extent than day 0.

e)

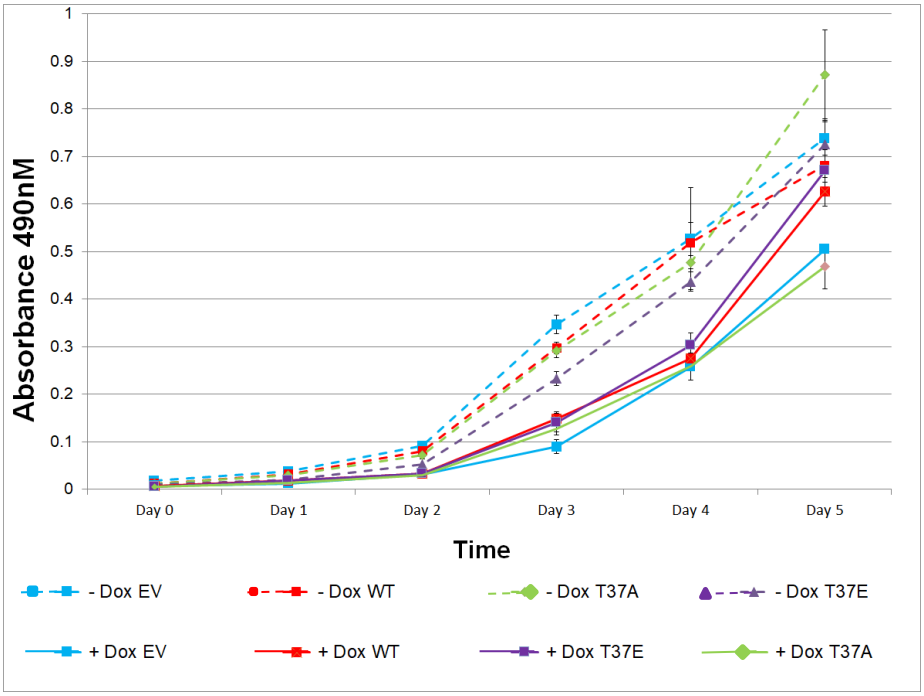

f)

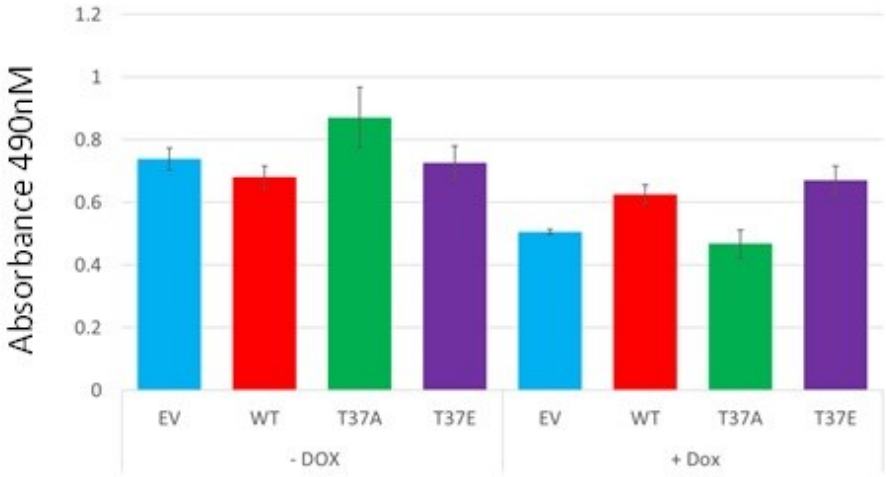

Figure 4.4 e) shows MTS cell proliferation curve. Re-expression of JMJD7 WT and T37E is able to partially rescue the JMJD7 knockdown phenotype. The histogram in f) represents the absorbance values of all cell lines at day 5, again highlighting the partial rescue phenotype shown in JMJD7-WT and –T37E cell lines with endogenous JMJD7 knockdown. n=3

4.5 Troubleshooting the shRNA resistant JMJD7 'rescue' cell model

The work presented in Figure 4.4 suggested a potential role for T37 in JMJD7-mediated growth control. However, the results were poorly reproducible (data not shown) and were not strongly conclusive (i.e. inefficient knockdown and incomplete phenotype 'rescue'), partly because of some apparent limitations in how well the system performed, which we discuss below.

The knockdown phenotype shown by the EV samples did not represent the expected level of growth delay compared to previous observations (Figures 2.7b, 2.8b and 2.9b), perhaps consistent with poor knockdown efficiency (Figure 4.4b and 4.4d). We considered several hypotheses to account for the inefficient knockdown. For example, we considered whether ineffective doxycycline treatment could be responsible, although fresh doxycycline aliquots were used for each new experiment. Selection against the shRNA vector was considered a likely explanation given that the pIPZ plasmid was also puromycin resistant.

The reduced expression with the reconstituted JMJD7 suggested that this aspect of the model might also be a problem. One explanation for the reduced expression might be that our exogenous JMJD7 may not be fully shRNA resistant. However, two silent mutations are probably sufficient to ensure siRNA resistance (Jiang and Price (2004) and our constructs have four silent mutations in the sequence targeted by shRNA#3 and are expressed (Figure 4.4a and 4.4c). An alternative explanation might be that the JMJD7 expression vector is selected against during the course of the growth assay, which is potentially possible because it has the same antibiotic resistance cassette as the pIPZ vector (as discussed above).

An additional problem was the incomplete rescue observed in Figure 4.4e, where reconstituted JMJD7 was unable to fully restore normal growth to JMJD7 knockdown cells. One possibility was that some of the growth delay previously observed was due to off-target effects of the shRNA used. However, similar results were seen using multiple shRNA sequences (Figures 2.7, 2.8 and 2.9) and alternative knockdown approaches (see below, Figure 4.8). An alternative explanation could be that the FLAG-tag could be interfering with JMJD7 function in some way. However, data from both this thesis (Figure 4.3c) and Dr Zhuang (Markolovic et al. (2018) suggest that a FLAG-tagged JMJD7 is able to hydroxylate DRG1 and DRG2. Specifically, Markolovic et al. (2018) reported that FLAG-JMJD7 over expression in HEK293T cells can drive the hydroxylation of DRG1 and DRG2 from 20 to 98% and 7 to 63%, respectively. Therefore, although possible, impaired activity of JMJD7 due to epitope tagging appears unlikely to fully account for incomplete phenotype rescue. Finally, incomplete rescue could potentially be explained by the knockdown and reconstitution occurring in distinct or partially over-lapping populations within the culture, as a result of sub-optimal antibiotic selection (again, both vectors were puromycin resistant).

Overall, several of the limitations discussed above could perhaps be explained by a technical limitation of the system which meant that both lentiviral vectors could not simultaneously be maintained in the target cells. This could result in a heterogeneous population of cells, that although all puromycin resistant, express either pIPZ FLAG-JMJD7, pZIP shRNA, or both. To test this, we first investigated whether FLAG-JMJD7 was uniformly expressed in the each of the shJ7#3_pIPZ-shRes -WT, -T37A or –T37E cell lines derived above. Initially, we

aimed to measure FLAG-JMJD7 expression in cells in the absence of endogenous JMJD7 knockdown (i.e. in the absence of doxycycline): Figure 4.5a shows confocal microscopy after shJ7#3_pIPZ-shRes -WT, -T37A and –T37E cells were seeded onto cover slips, fixed and stained. The pink arrows show regions of cells which do not appear to have any FLAG-JMJD7 expressed when compared to the presence of DAPI, confirming that these cell lines do not homogenously express the reconstituted FLAG-JMJD7 vectors. Next, we explored this in the context of endogenous JMJD7 knockdown following doxycycline-mediated expression of shRNA#3: Figure 4.5b shows confocal microscopy after shJ7#3_pIPZ-shRes -WT, -T37A and –T37E cells were seeded onto cover slips, treated with doxycycline for 120 hours, fixed and stained. Again, purple arrows indicate cell 'colonies' where FLAG-JMJD7 appears not to be expressed. Furthermore, white arrows highlight cell colonies which appear not to express GFP and which are unlikely therefore to express shJMJD7#3. Taken together, these imaging analyses would suggest that the 'rescue' model presented in Figure 4.4 was sub-optimal, partly due to the inability to maintain the selection of both lentiviral constructs in every cell.

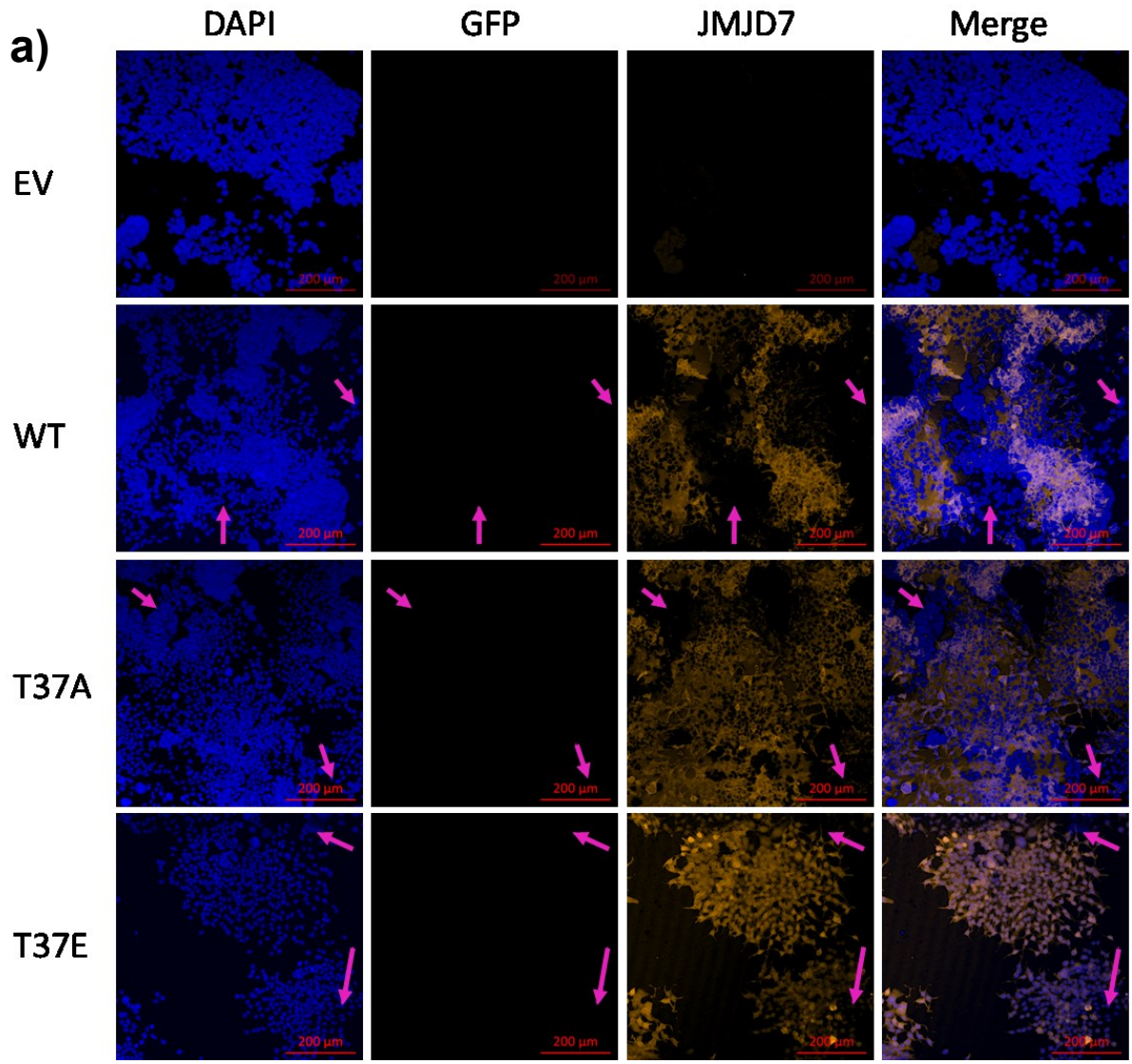
a)
DAPI
GFP
JMJD7
Merge
EV
WT
T37A
T37E
200 µm

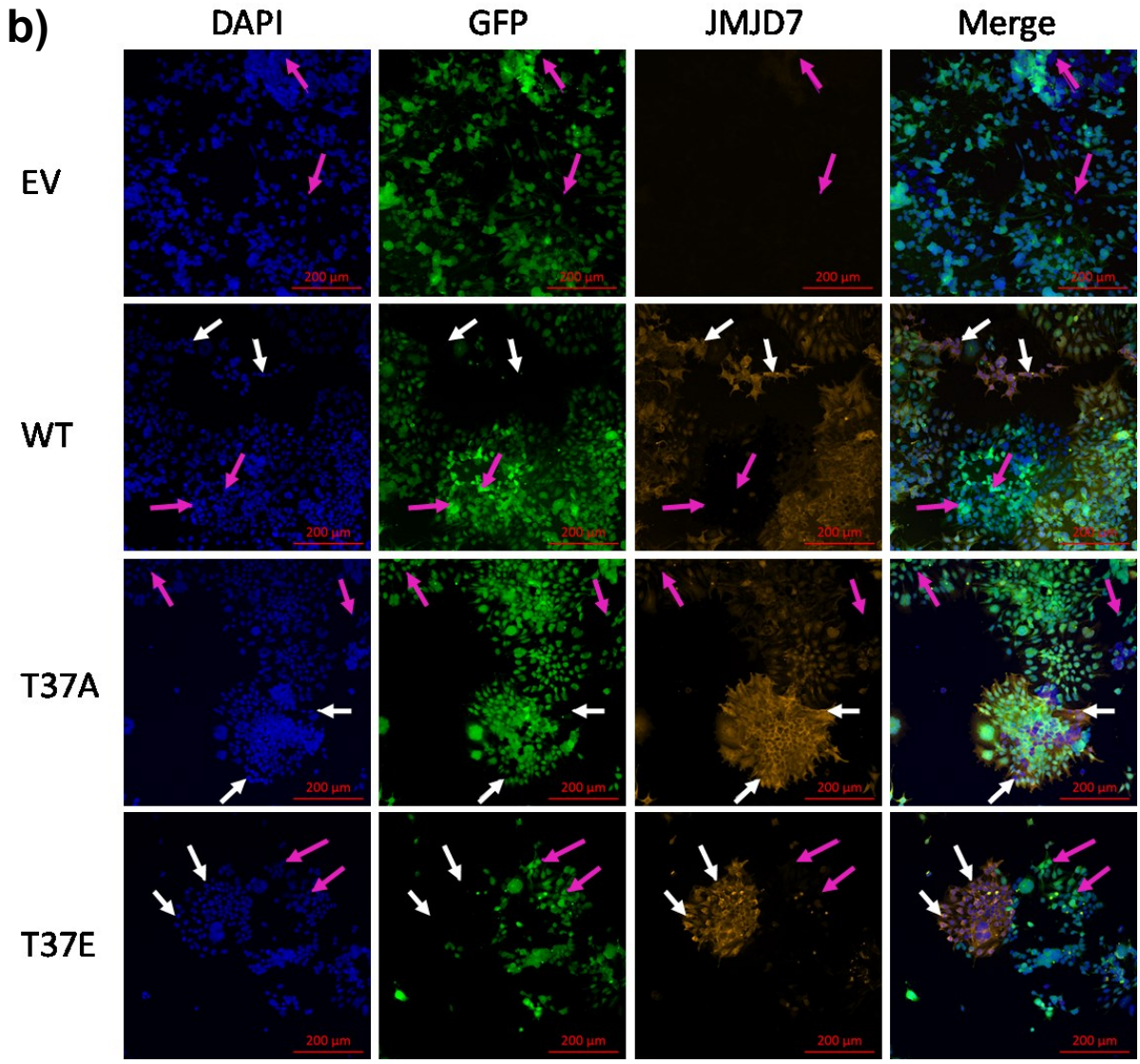

Figure 4.5 Confocal microscopy of shJ7#3_pIPZ-shRes -WT, -T37A and –T37E cells with and without doxycycline indicates heterogeneous populations. The previously described HEK293T sh#3_pIPZ-shRes_J7-WT, -T37A or –T37E were tested for the presence of JMJD7 shRNA #3 and over expressed JMJD7 in the absence (a) or presence (b) of 1µg/ml of doxycycline. In both a) an observed loss of exogenous JMJD7 is seen in all cell lines, and in b) a more striking loss of over expressed JMJD7 and the induced JMJD7 shRNA #3. Pink arrows highlight cells which are not expressing shJMJD7, white arrows indicate cells without FLAG-JMJD7 over expression. n=1

4.6 Further attempts to development a JMJD7 rescue model: FLAG-tagged JMJD7 WT and T37E, but not T37A, are able to partially rescue the JMJD7 knockdown growth phenotype

To attempt to eliminate the issues identified above with sub-optimal co-selection of expression vectors, the FLAG-JMJD7 cDNA sequences were re-cloned into a retroviral plasmid, pWZL, which contains a hygromycin selection cassette. HEK293T cells were infected with retrovirus encoding either pWZL-shRes_FLAG.JMJD7 (pWZL-J7) -WT, -T37A, –T37E, or an empty pWZL control (EV), and subjected to antibiotic selection with hygromycin. Subsequently, hygromycin-resistant cell lines were infected with lentivirus encoding either shControl or shJMJD7#3 (shCon_pWZL-J7 or shJ7_pWZL-J7). Following puromycin selection, hygromycin/puromycin-resistant cell lines were seeded into 10cm plates and treated with doxycycline for 120 hours before reseeding for MTS cell proliferation assay in the presence of doxycycline, as described above. The remaining cells were lysed for either protein for analysis of the presence of FLAG-JMJD7 by western blot (Figure 4.6a), or lysed for RNA and analysed for the presence of JMJD7 endogenous knockdown by SYBR green qPCR (Figure 4.6b). Western blot data shows that although JMJD7 is more equally expressed in these samples than Figure 4.4a, there may be a slight reduction of FLAG-JMJD7 in shJMJD7#3 compared to control. Similar to the previous model, qPCR of endogenous JMJD7 cDNA indicated relatively poor knockdown efficiency (Figure 4.6). That being said, MTS growth curves were more in line with what we might expect (Figure 4.6c), considering previous observations in Figure 2.9. We previously observed that JMJD7 knockdown cells grew approximately one third less than control cells on day 6. Here, in Figure 4.6c and 4.6d we can see that JMJD7 knockdown cells grow at approximately half the rate

of control knockdown cells by day 5, which is a marked improvement on that seen from Figure 4.4e. However, consistent with previous observations, WT JMJD7 was only able to partially rescue the knockdown phenotype. Importantly however, T37E rescued the phenotype to the same extent as WT, but T37A unable to rescue to the same extent, showing a growth delay equivalent to EV cells. Although more repeats would need to be conducted to prove statistical significance, this data indicates that the phospho-mutant, T37A, was unable to rescue the growth defect, as observed previously.

Although some of the apparent limitations in the shRNA/FLAG-JMJD7 ‘rescue’ model appear to persist despite engineering new FLAG-JMJD7 expression vectors with alternative antibiotic selection, the growth results appear to be consistent. Overall, the data presented above support that a mutation that blocks JMJD7 T37A phosphorylation is unable to alleviate the growth defects caused by JMJD7 knockdown. However, considering our concerns around the performance of these cell models we still sought to obtain further evidence using an alternative approach.

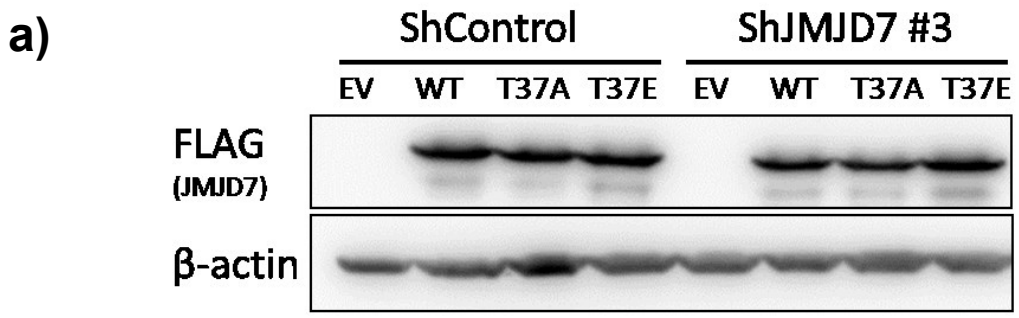

Figure 4.6 JMJD7 WT and T37E, but not EV or T37A, is able to partially rescue the growth phenotype of JMJD7 knockdown. HEK293T cells were retrovirally infected with pWZL plasmid either alone (EV) or with shRes_FLAG.J7-WT, -T37A or –T37E, followed by lentiviral infection of JMJD7 shRNA#3 or control shRNA into each. One 10cm plate of each cell line was seeded and doxycycline treated (1μg/ml) for 120 hours prior to reseeding for MTS cell proliferation assay in the presence of doxycycline. After seeding for MTS assay, the remaining cells were analysed by western blot (a) or qPCR (b). a) shows the presence of FLAG-JMJD7 in these cells on the day of reseeding.

b)

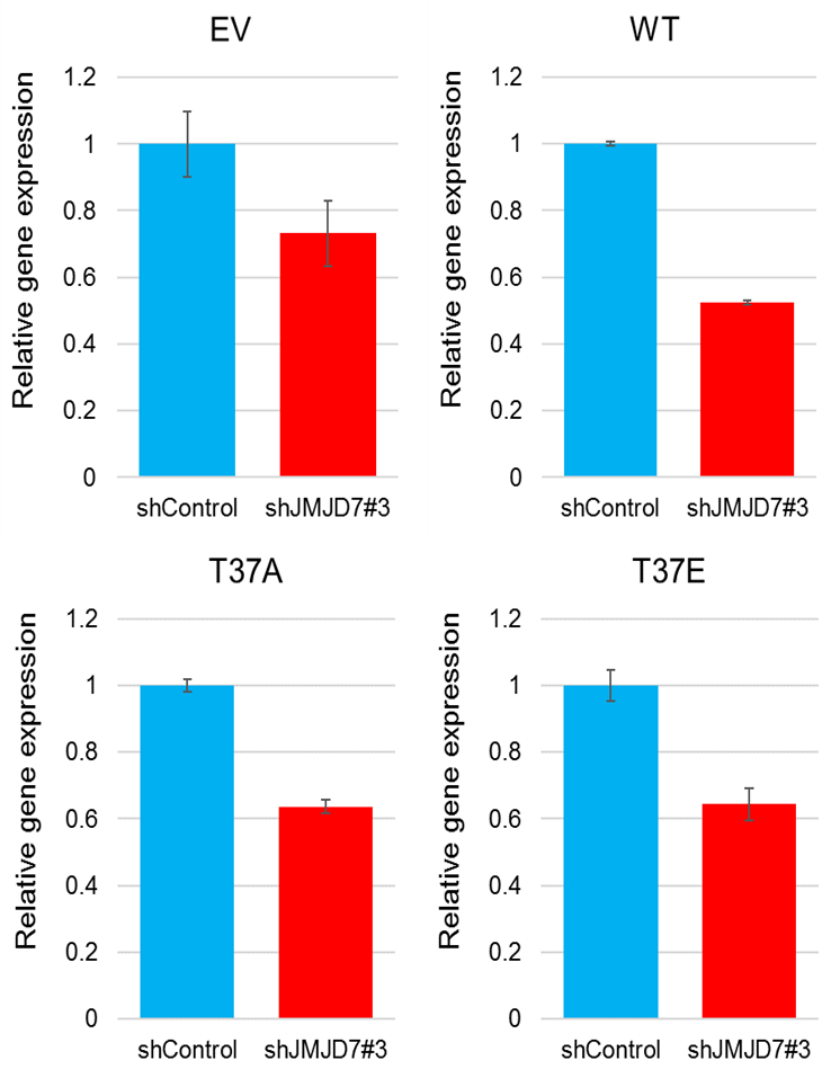

Figure 4.6 b) HEK293T cells were retrovirally infected with pWZL plasmid either alone or with shRes_FLAG.J7-WT, -T37A or –T37E, followed by lentiviral infection of JMJD7 shRNA#3 or control shRNA into each. One 10cm plate of each cell line was seeded and doxycycline treated for 120 hours prior to reseeding for MTS cell proliferation assay in the presence of doxycycline. After seeding for MTS assay, the remaining cells were analysed by western blot or qPCR. b) qPCR results confirming endogenous JMJD7 knockdown in the shRNA containing cell lines.

c)

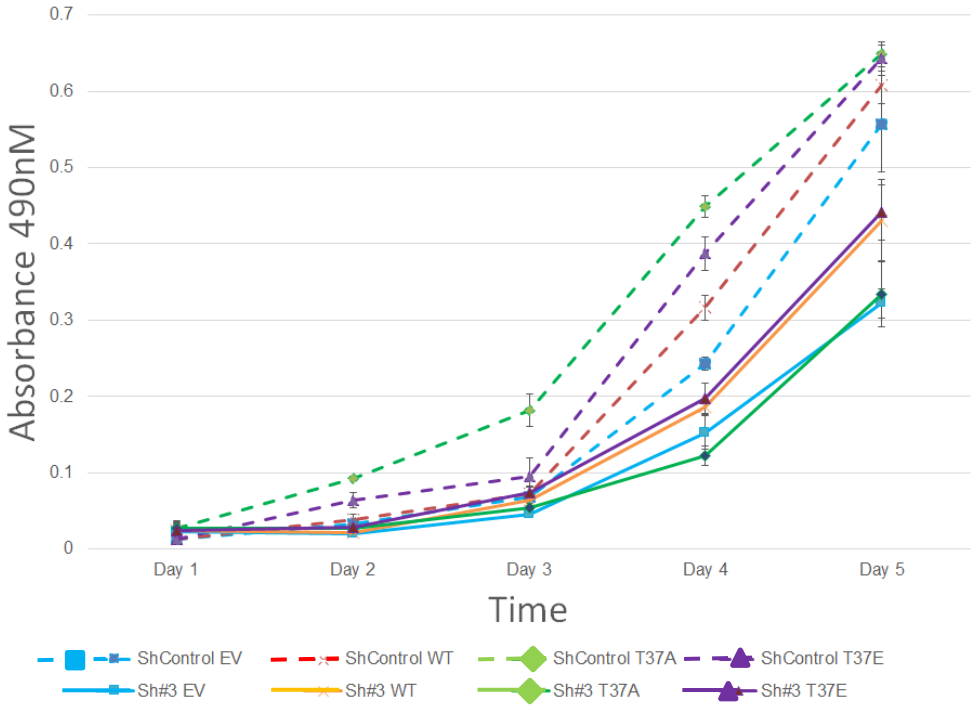

d)

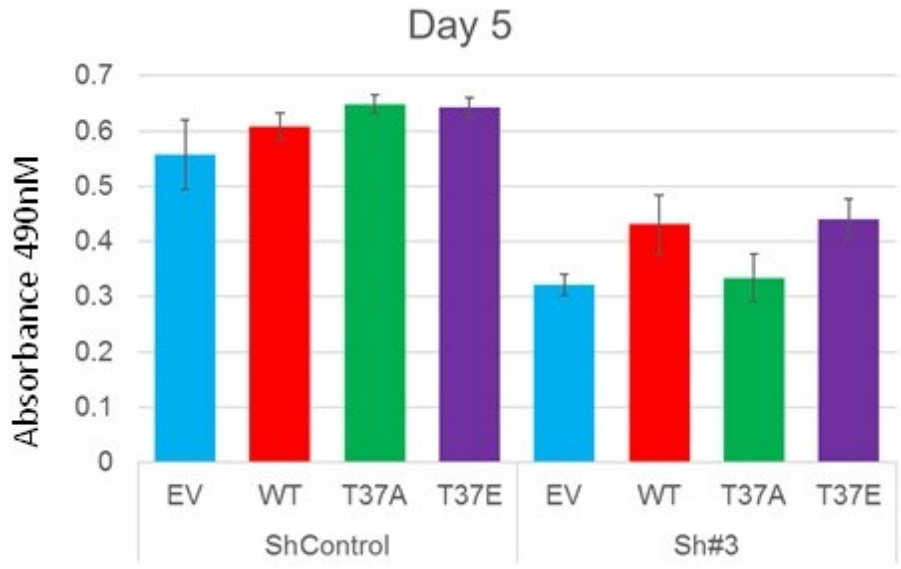

Figure 4.6 c) and d) shows MTS cell proliferation curve over 5 days. Dashed lines represent shControl cells and solid lines are shJMJD7#3 cell lines. Control knockdown does not affect cell growth, whereas JMJD7 knockdown without re-expression grew significantly slower, similar to JMJD7-T37A cells. Cells rescued with WT or T37E were able to partially rescue the JMJD7 knockdown phenotype. n=2

4.7 JMJD7 T37A mutation inhibits normal growth control by JMJD7

To continue to explore if T37 phosphorylation is necessary for JMJD7's function in growth, we developed an independent 'rescue' model based on JMJD7 loss-of-function using an siRNA sequence that targets the 3'UTR of the endogenous mRNA (validated by Dr Zhuang). HEK293T pTIPZ-JMJD7 cells were subject to two rounds of control or JMJD7 siRNA Lipofectamine™ transfection over a period of 120 hours prior to reseeding for MTS proliferation assay. Figure 4.7a shows western blot validation of knockdown of endogenous JMJD7 and confirmation of the presence of over-expressed FLAG-JMJD7. Analysis of endogenous JMJD7 mRNA expression was not necessary in this case due to successful confirmation of protein knockdown by western blot. Interestingly, under the conditions of this model we observed very efficient knockdown of endogenous JMJD7 protein, and equal expression of the reconstituted FLAG-JMJD7 cDNAs in both control and JMJD7 siRNA samples. Consistent with the shRNA data above, JMJD7 siRNA caused a slight growth delay (as expected) that was completely restored by re-expression of WT but not T37A JMJD7. The histogram in Figure 4.7c displays the MTS values at Day 6 only, clearly demonstrating that WT FLAG-JMJD7 expression rescued the delayed growth phenotype observed in JMJD7 siRNA-treated T37A and EV cells to growth levels observed with control siRNA treatment.

Overall, the results presented in the 'rescue' cell models presented above clearly demonstrate a consistent effect of T37A mutation on JMJD7-mediated cell growth control. Considering the fact that the T37E mutation behaves as WT JMJD7 in these models, we propose that these effects are consistent with a role of JMJD7 T37 phosphorylation rather than mutation *per se*.

a)

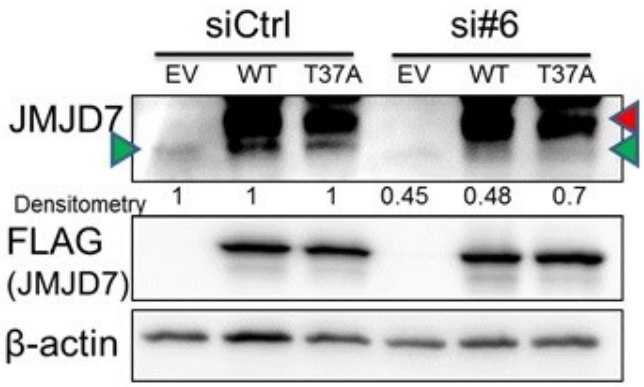

b)

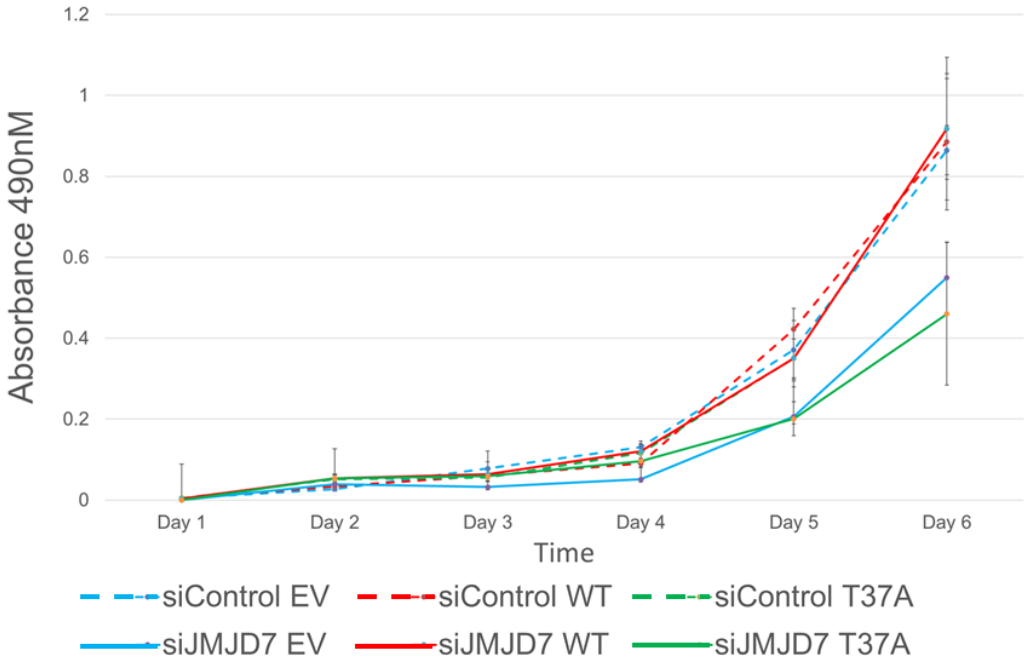

Figure 4.7 Re-expression of JMJD7 WT, but not T37A, can rescue the reduced growth phenotype observed following JMJD7 siRNA knockdown. HEK293T cells with lentiviral pTIPZ alone (EV) or with JMJD7 WT or T37A were subject to treatment with JMJD7 (Dharmacon, Cat No: J-187551-06) or control (SIGMA, Cat No: SIC001) siRNA for 120 hours. Knockdown cells were analysed for growth against control via MTS assay. a) cells were lysed for protein and analysed by western blot for protein expression. Green arrows show endogenous JMJD7, Red arrows indicate over-expressed FLAG-JMJD7. Densitometry of endogenous JMJD7 was calculated as a relative ratio of expression to control. b) MTS cell proliferations assay after knockdown shows that EV and JMJD7 T37A were unable to rescue the knockdown phenotype, whereas WT JMJD7 was able to.

c)

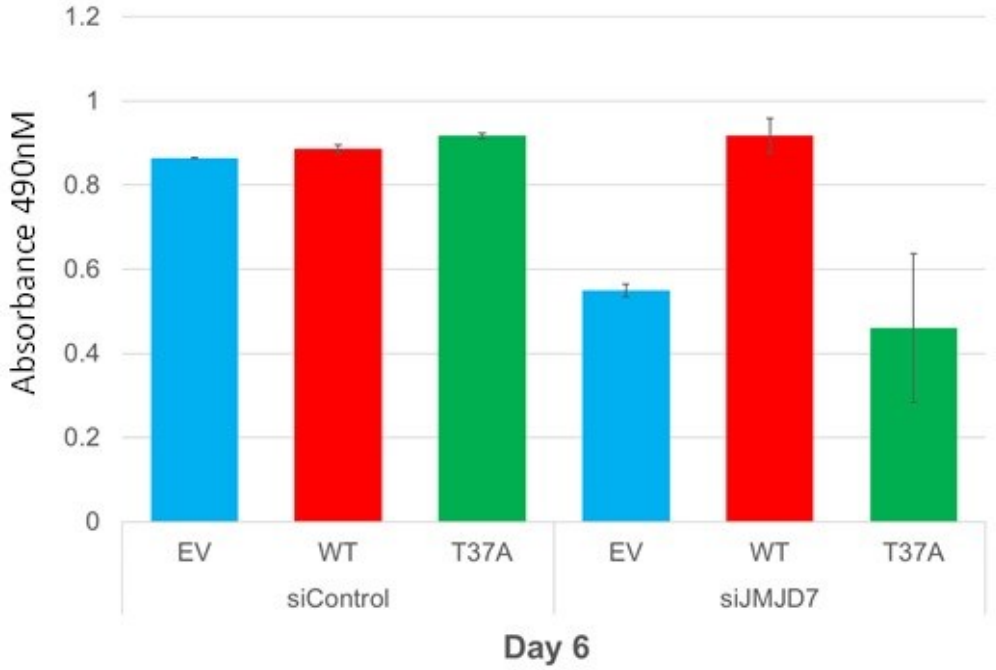

Figure 4.7. C) histogram representing absorbance values of all cell lines on day 6. The control cells are around 0.85-0.95, whereas only the JMJD7 WT sample presents within the range of absorbance values in the knockdown group. The EV and T37A were significantly less. n=2

Discussion

Here in this Chapter we have confirmed using MS that JMJD7 is phosphorylated at a highly conserved residue at the N-terminus proximal to the dimerisation interface. We show, using blocking mutants and a predicted phospho-mimetic mutant, that phosphorylation is unlikely to significantly alter JMJD7 localisation, dimerisation, substrate binding, or activity. However, we do show that T37 phosphorylation may positively contribute to the role of JMJD7 in cell proliferation identified in Chapter 2.

Although further work is required to identify the kinase responsible, and the exact functional consequences of phosphorylation, the work described in this Chapter is of interest because there is almost nothing known about regulation of 2OG oxygenases by PTMs, or whether they act in signalling pathways. Recently, Ortmann et al. (2016) found that the HIF hydroxylase PHD1 is phosphorylated on S130 by CDK2, CDK4 and CDK6. Phosphorylation of PHD1 did not affect the overall hydroxylase activity of PHD1 *in vitro* but was found to reduce HIF1α hydroxylation and promote Cep192 inhibitory hydroxylation during the cell cycle. Furthermore, PHD2 has also been highlighted as a target for regulation by phosphorylation (Di Conza et al., 2017). Alternatively, phosphorylation is used as an 'on/off' switch on the lysine demethylase, PHF2: Baba et al. (2011) showed that PKA mediated phosphorylation of S1056 on PHF2 promotes the formation of PHF2/ARID5B complex. In turn, ARID5B binds to DNA and supports PHF2 demethylase activity.

In all the cases mentioned above 2OG oxygenase phosphorylation is thought to play a regulatory role. However, MS of purified endogenous DRG2 did not highlight any significant increase or decrease in hydroxylation in cells that expressed a T37A JMJD7 mutant. Although this might indicate that T37 phosphorylation does not

regulate JMJD7 activity towards DRG2, or that phosphorylation of JMJD7 may be redirecting substrate specificity between DRGs and alternative substrates (similar to the function of CDK1 mediated PHD1 phosphorylation (Ortmann et al., 2016)), further work is required to address the limitations in the experiment presented. Firstly, although endogenous DRG1 was successfully purified and identified by MS (data not shown), the abundance was insufficient to successfully quantify the relevant peptides covering the JMJD7 hydroxylation site. This leaves open the question of whether T37 phosphorylation might function to switch the specificity of JMJD7 between its two substrates. Interestingly, we did observe a slight increase in DRG1 binding to the JMJD7 T37A mutant (in the context of reduced DRG1 levels in the 'input', this effect may even be underestimated). Secondly, comparing the blocking T37A mutant to wildtype JMJD7 may only be relevant if the wildtype enzyme is significantly phosphorylated. Further work should focus on developing a quantitative MS assay of measuring the stoichiometric levels of JMJD7 phosphorylation, and methods to manipulate (or mimic, e.g. T37E) its levels.

In the absence of identifying the molecular function of JMJD7 phosphorylation, we turned to asking whether it regulated the function of 'gross' phenotypes, particularly growth control. We showed in Chapter 2 that shRNA depletion of endogenous JMJD7 delayed cellular proliferation. Therefore, we tested whether T37 mutants were able to alter growth after endogenous JMJD7 knockdown. To do so we first attempted to develop a cDNA 'rescue' system in the shRNA model presented in Chapter 2. The initial rescue models highlighted some technical limitations: confocal microscopy of these cells in the presence and absence of doxycycline identified a heterogenous population, likely due to inappropriate antibiotic selection. Overall

however, the shRNA rescue work indicated that JMJD7 T37 phosphorylation is likely having a positive impact on JMJD7's role in growth control, which was further confirmed using an siRNA model. The mechanism of how JMJD7 phosphorylation may be involved in growth is still to be elucidated and would be interesting to investigate further. Considering the critical role of DRGs in protein synthesis, development and cell growth (Daugeron et al., 2011, Francis et al., 2012, Kumar et al., 1993, Wei et al., 2004), exploring if JMJD7 phosphorylation participates in the role of DRG1 and DRG2 in these processes would also be of interest.

The experiments presented here have highlighted a potential discourse between the positive role of T37 phosphorylation in growth and lack of function in dimerisation, localisation and activity. Importantly, this might indicate an activity-independent function of JMJD7, which is entirely possible. However, considering that thus far the only known function of JmjC-only 2OG oxygenases is as protein hydroxylases (consistent with them lacking other obvious functional domains), other explanations are also worth considering. In particular, further work is required to determine the effect of T37 phosphorylation on DRG1 hydroxylation, and whether DRG1 and/or DRG2 are involved downstream of JMJD7 in growth control.

Although there are many outstanding questions from the work presented, we felt that the observation that T37 mutation significantly impaired JMJD7 function (in growth) was sufficient to warrant further studies. In particular, we felt that understanding the role of JMJD7 phosphorylation would be supported by identifying the kinase responsible. Work related to this is presented in the Chapter that follows.

Chapter 5

Characterisation of the JMJD7 T37 Kinase

Introduction

In the previous Chapter we presented data supporting that JMJD7 is phosphorylated on an N-terminal threonine residue that is highly conserved and which resides within a cancer mutation hot-spot identified in Chapter 2. We went on to explore the function of T37 phosphorylation and identified a potential role in JMJD7-mediated cell growth control. These studies focussed on the use of T37 mutants rather than manipulating kinase activity because the identity of JMJD7 T37 kinase was not known.

Identification of the JMJD7 T37 kinase would be informative for three main reasons. Firstly, it would allow modulation of kinase activity (e.g. inhibitors) to regulate the phosphorylation state of JMJD7 without the use of mutants. Secondly, it might help uncover novel JMJD7 functions in unexpected cellular processes. For example, ATM is serine/threonine kinase that is an important regulator of the DNA damage response, and novel ATM substrates have subsequently been implicated in the cellular response to DNA damage (Bensimon et al., 2011, Cheng and Chen, 2010, Gatei et al., 2000, Kennedy and D'Andrea, 2005). Thirdly, identification of the JMJD7 T37 kinase could identify signalling pathways that couple an unexpected cellular process to JMJD7/DRG pathways. An analogy would be substrates of the cyclin-dependent kinases (CDKs), which are cell cycle-associated kinases essential for proper transition between cell cycle phases (Malumbres, 2014): The phosphorylation of CDK substrates has been shown to couple cell cycle phases to the regulation of diverse cellular processes including autophagy, senescence, transcription and translation (Rubinsztein, 2010, Mullers et al., 2017, Albert et al., 2014, Kanakkanthara et al., 2016) .

Here in this Chapter we develop an anti-phospho-T37 antibody and use it to characterise JMJD7 T37 kinase activity.

5.1 Generation and validation of an anti-phospho-T37 specific antibody

To facilitate the characterisation of JMJD7 T37 phosphorylation we commissioned the production of a phospho-specific antibody by a commercial company (Abgent). The rabbit polyclonal antibody was raised against a phospho-T37 peptide corresponding to the sequence NH_2-CLDKPP[pThr]PLHFYRD–$CONH_2$. To begin to test the purified antibody we first used it in western blots to detected over-expressed JMJD7 WT and T37A. The previously described HEK293T cells with doxycycline inducible pTIPZ JMJD7 were grown for 2 days, lysed for protein and immunoprecipitated with anti-FLAG antibody overnight. FLAG beads were washed and protein was eluted by boiling in Laemmli buffer followed by western blot analysis. The newly generated phospho-specific antibody (phT37) specifically recognised a band at the correct size for FLAG-tagged JMJD7, and only in cells over-expressing JMJD7 (Figure 5.1a). Consistent with this species being JMJD7, the signal was increased following enrichment of JMJD7 by anti-FLAG IP. Importantly, the signal was completely blocked by T37A mutation, suggesting that the antigen recognised corresponds to the peptide sequence immunised. However, these initial results do not prove the specificity of the antibody to phosphorylated versus unphosphorylated T37.

To test whether this new reagent was indeed a phospho-specific JMJD7 T37 antibody we developed a peptide competition assay (Figure 5.1b). The method involved western blotting cell lysates from the EV and JMJD7 WT samples, as follows. Three identical membranes were probed using the newly generated

anti-phT37 antibody. The first membrane was incubated with anti-phT37 antibody in TBST-BSA solution as normal, with no additional peptide. The second membrane was incubated with the anti-phT37 antibody solution but with the phosphorylated JMJD7 T37 peptide used to generate the antibody. The third membrane was incubated with the anti-phT37 antibody solution, but with the unphosphorylated peptide. If the phT37 antibody was specific, the “free” phosphorylated peptide incubated with the second western blot should be able to compete with the phosphorylated JMJD7 on the membrane for binding to the anti-phT37 antibody, therefore leaving the membrane blank. On the other hand, the third membrane with the unphosphorylated peptide should be unable to compete for binding to the phospho-specific antibody, and would display similar reactivity to the no peptide control. Reassuringly, we observed that the membrane incubated with the unphosphorylated peptide displayed similar antibody reactivity to the no peptide control. Importantly, no signal was detected on the membrane incubated with the phosphorylated peptide (Figure 5.1c). Taken together, these results suggest that the anti-phT37 antibody specifically recognises JMJD7 when phosphorylated at T37.

Because our future investigation of JMJD7 phosphorylation will likely involve the use of different N-terminally epitope tagged constructs, and the phosphorylation site in question is in the proximity of these tags, we next tested whether epitope tagging affected JMJD7 phosphorylation. Plasmids encoding JMJD7 with or without a HA- or FLAG-tag were transfected into HEK293T cells for 48 hours prior to lysis and analysis by western blot. Figure 5.1d shows no difference between the phosphorylation status of untagged, HA- or FLAG-tagged JMJD7.

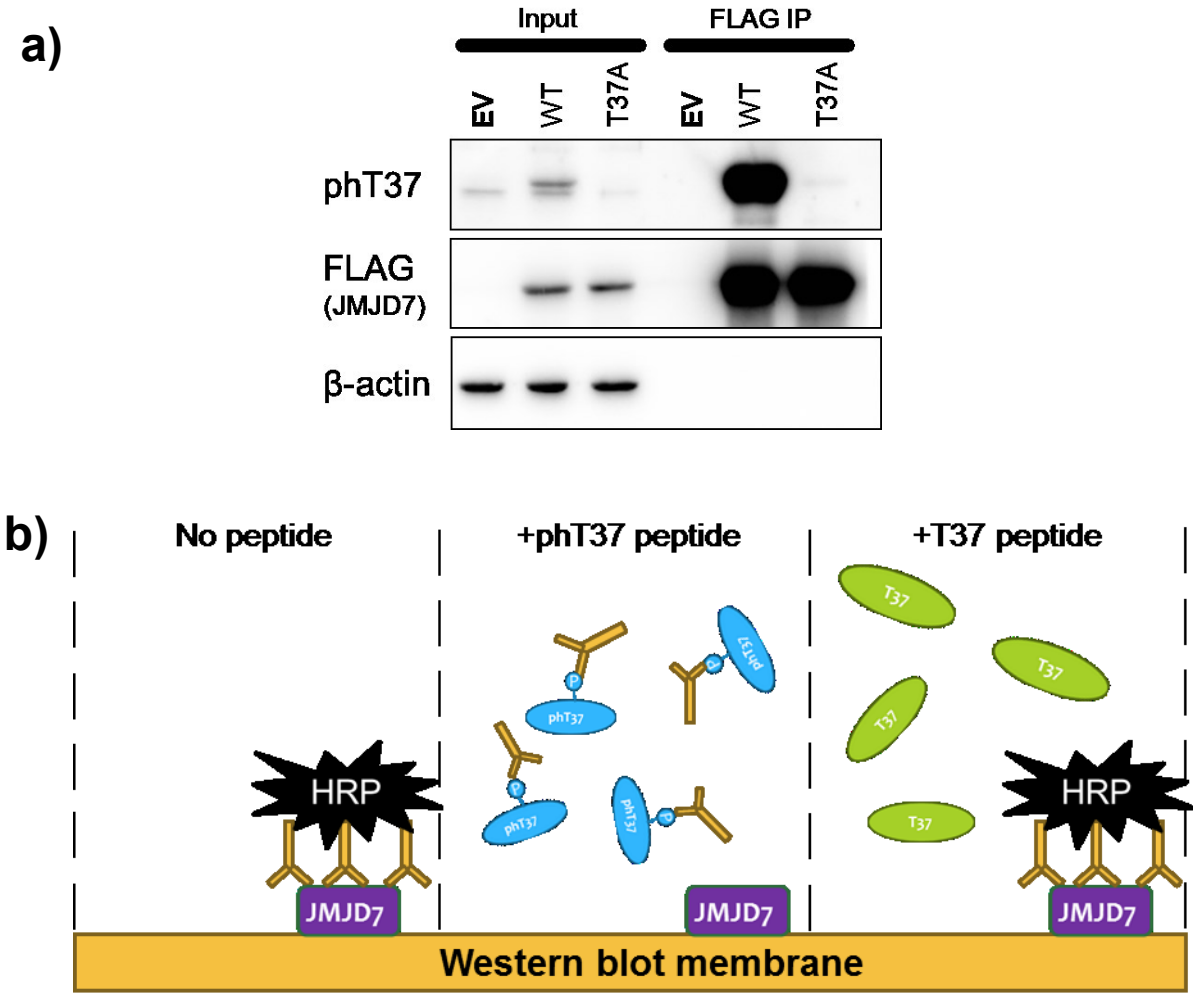

Figure 5.1 Validation of an antibody specific to phospho-T37 JMJD7. A customised polyclonal phospho-specific antibody (phT37) was generated against the sequence NH_2-CLDKPP[pThr]PLHFYRD-$CONH_2$ by Abgent. a) The phT37 antibody was tested against the phospho-mutant, T37A. HEK293T cells were transfected with JMJD7 WT or T37A, after two days cells were lysed and analysed by western blot. phT37 antibody binds to WT but not the T37A mutant. n=3. b) A peptide competition assay was developed to test the antibody specificity towards phosphorylated T37. In brief, HEK293T cells with over expressed pcDNA3 alone or FLAG JMJD7 were immunoprecipitated using anti-FLAG and analysed by western blot using phT37 antibody. Three membranes were incubated with the phT37 antibody and either no peptide (left), a phosphorylated JMJD7 peptide (middle), or an unphosphorylated peptide (right).

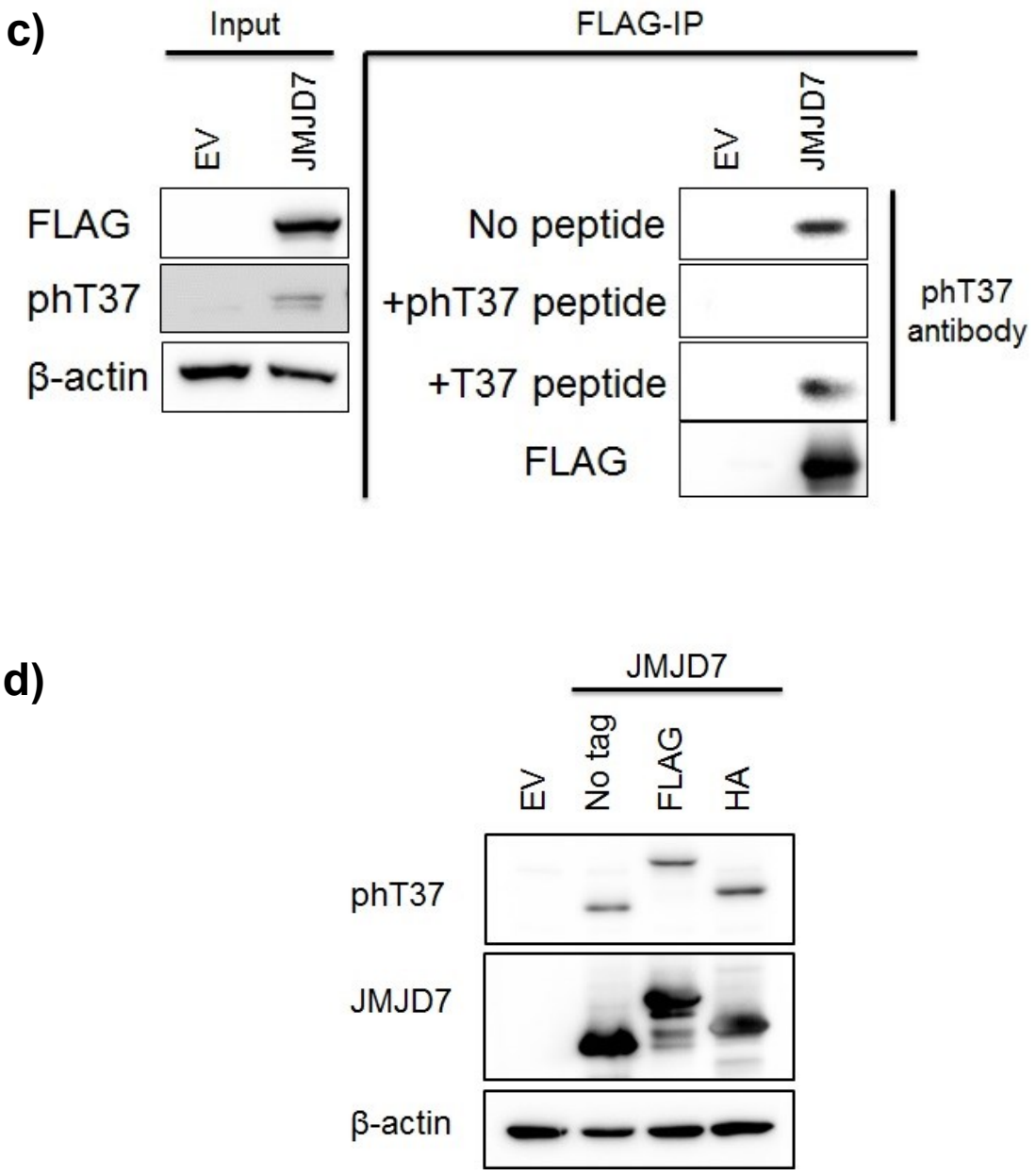

Figure 5.1 c) shows that after incubation with the phosphorylated peptide the anti-phT37 antibody was competed away from the phT37 JMJD7 on the membrane, but was not after incubation without a peptide or with the unphosphorylated peptide, confirming the specificity of the antibody. n=3. d) HEK293T cells were transiently transfected with JMJD7 with no tag, with a FLAG tag, or a HA tag, allowed to express for 48 hours before lysing for protein and analysing by western blot. JMJD7 phosphorylation is not affected by different epitope tags. n=2.

e)

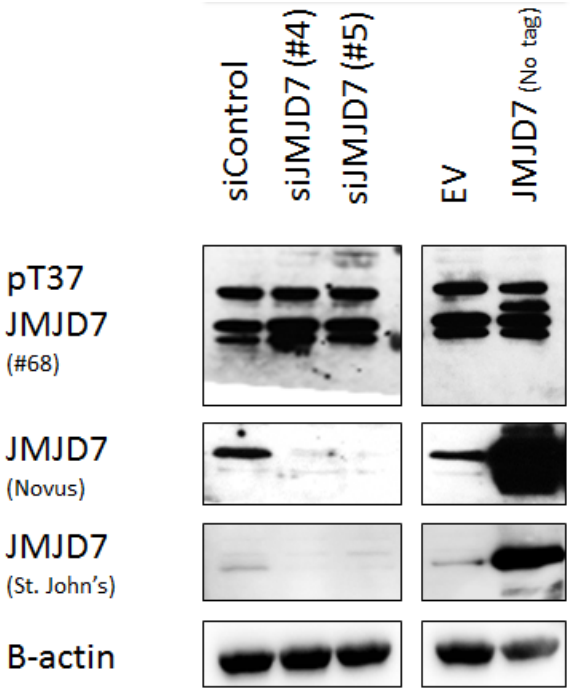

f)

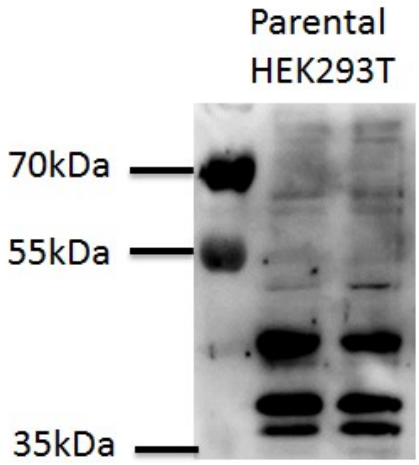

Figure 5.1 e) HeLa cells were subject to transfection with either siRNA (left) or untagged-JMJD7 pcDNA3 plasmid (right). (Left) JMJD7 Novus and St. John's antibody confirmed knockdown of the endogenous JMJD7 whereas no change was seen using the phT37 antibody. (Right) Over expression of JMJD7 confirmed using all antibodies. phT37 is therefore suitable for use with overexpressed JMJD7. (siRNA from Sigma, Cat no. SASI_Hs02_00326*04*, SASI_Hs02_00326*05*). f) phT37 western blot of parental HEK293T protein lysate.

5.2 JMJD7 phosphorylation can be regulated by mitogens

Having developed and validated a reagent for the detection of phT37 JMJD7 we sought to perform some basic characterisation of this modification in cells. Since many phosphorylation events are stimulated by stress signals or environmental stimuli, we tested whether we could manipulate JMJD7 phosphorylation by various cell stresses and treatments. Firstly, we tested to see if cell confluence could moderate JMJD7 phT37. Leaky expressing HEK293T pTIPZ FLAG-JMJD7 cells were seeded into a 6 well plate at three different seeding densities. After 2 days the cells were lysed for protein and FLAG-immunoprecipitated overnight. Western blot analysis (Figure 5.2a) showed that phT37 levels did not significantly change compared to total JMJD7.

An important physiological stimulus and pathological condition involves reduced availability of oxygen, often termed ‘hypoxia’. As introduced in Chapter 1, oxygen is a co-factor of 2OG oxygenases and interestingly, the expression level of some 2OG oxygenases is regulated by hypoxia (Pollard et al, 2008). Therefore, we considered that graded hypoxia might be a relevant stimulus in which to monitor JMJD7 phosphorylation. HEK293T cells with ‘leaky’ pTIPZ FLAG-JMJD7 were incubated at 21%, 1%, or 0.3% oxygen for 48 hours prior to lysis and immunoprecipitation. FLAG JMJD7 was eluted by boiling in Laemmli buffer and analysed by western blot. Figure 5.2b shows that, total JMJD7 levels are reduced with decreasing oxygen tensions, and that JMJD7 T37 phosphorylation changes in line with it suggesting that hypoxia is not a significant regulator of JMJD7 phosphorylation, at least under the conditions tested.

The cellular response to DNA damage is regulated at multiple levels by phosphorylation (Gatei et al., 2000, Sharma et al., 2012, Cheng and Chen, 2010, Bensimon et al., 2011), and some 2OG oxygenases have been implicated in the DNA damage response (Kafer et al., 2016, Falnes et al., 2002, Amendola et al., 2017, Khoury-Haddad et al., 2015). Since a proportion of JMJD7 is nuclear-localised (Chapter 2), and JMJD7 may be altered in cancer (Chapter 3), a hallmark of which is genome instability (Hanahan and Weinberg, 2011), we sought to test whether DNA damage can regulate JMJD7 phosphorylation. As a pilot experiment we first tested whether a widely used DNA damaging agent, etoposide, regulates JMJD7 T37 phosphorylation. Etoposide is a cancer therapeutic that acts upon DNA topoisomerase II to induce DNA double strand breaks (Montecucco et al., 2015). HEK293T pTIPZ JMJD7 cells were seeded for 3 days and used with leaky expression. On the third day, the cells were treated with or without etoposide for 6 hours prior to lysis. Cell lysates were subject to FLAG immunoprecipitation and eluted by boiling in Laemmli buffer before western blot. Figure 5.2c shows that etoposide treatment did not affect JMJD7 total protein or T37 phosphorylation levels.

Mitogens are powerful stimuli of cell signal transduction pathways, which commonly centre around kinases and are important regulators of cell growth and division. In Chapter 2, we implicated JMJD7 in normal growth control using an shRNA loss-of-function model. Therefore, we next tested whether JMJD7 phosphorylation is regulated by mitogens, as follows. Initially, HEK293T pTIPZ FLAG-JMJD7 cells were seeded in the standard concentration of serum (10% v/v). After 48 hours, the growth media on one plate was replaced with 0.2% v/v FCS growth media. After a further 24 hours all plates were lysed for protein followed by immunopreciptiation, elution by

boiling in Laemmli buffer, and analysed by western blot. Figure 5.2d shows that after 24 hours of 0.2% serum, phT37 JMJD7 levels are significantly reduced compared to total JMJD7. This suggests that JMJD7 phosphorylation is dependent on mitogens.

Mitogens stimulate quiescent cells to enter the cell cycle in order to replicate their genome and undergo mitosis and cell division. We hypothesised therefore that the observed mitogen stimulation of JMJD7 T37 phosphorylation could be associated with cell cycle progression, which we explore further below. Beforehand, we provide a brief overview of the cell cycle and its associated kinases.

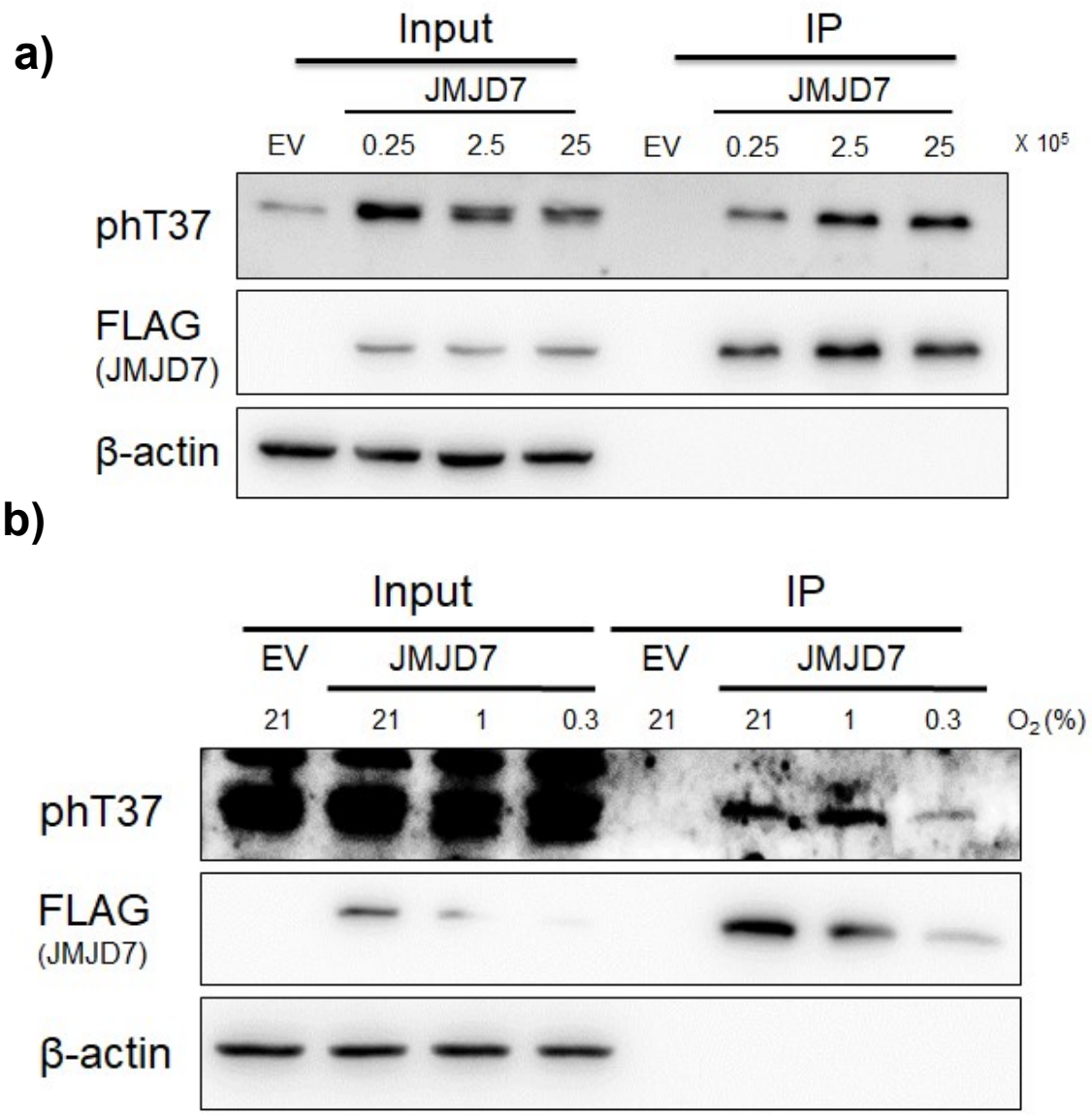

Figure 5.2 Regulation of JMJD7 T37 phosphorylation by cellular stimuli. HEK293T pTIPZ FLAG-JMJD7 cells were subject to various cell stresses. a) Western blot after immunoprecipitation of cells that were seeded at three different confluences (increasing by a factor of 10). Confluence did not affect JMJD7 phosphorylation. n=2. b) Western blot after immunoprecipitation of cells which were subject to treatment with oxygen tensions at 21%, 1% and 0.3% for 48 hours. Oxygen tension did not affect JMJD7 phosphorylation. n=1.

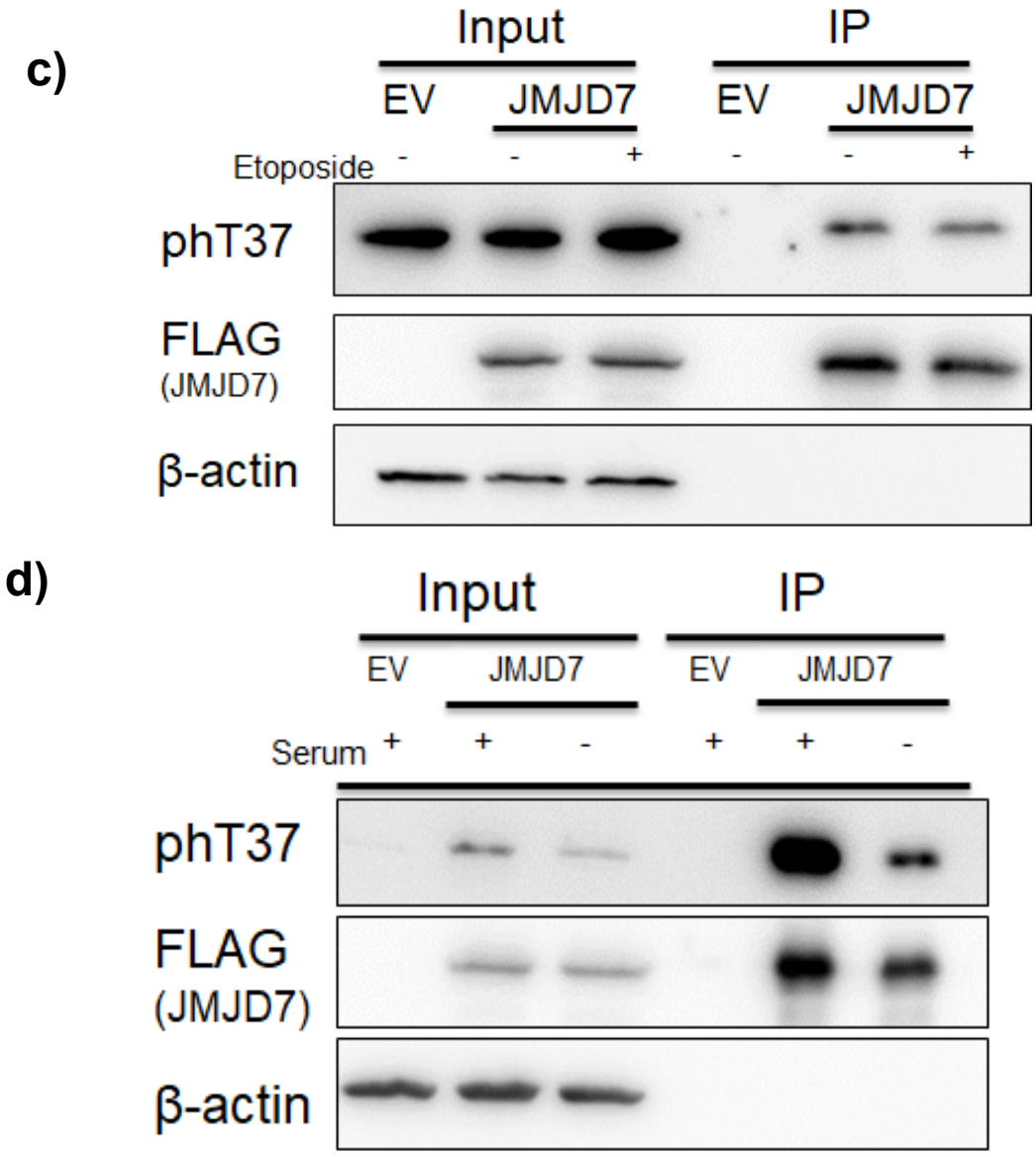

Figure 5.2 Regulation of JMJD7 T37 phosphorylation by cellular stimuli. HEK293T pTIPZ FLAG-JMJD7 cells were subject to various cell stresses. c) Western blot after immunoprecipitation of cells which were subject to treatment with or without 10μM etoposide for 6 hours. Etoposide treatment did not regulate JMJD7 T37 phosphorylation. n=2. d) Western blot after immunoprecipitation of cells treated with 10% (+ serum) or 0.2% (- serum) v/v FCS for 24 hours. Cells grown in reduced serum show significantly less JMJD7 T37 phosphorylation. n=2.

5.3 The Cell Cycle

One full cell cycle requires four stages to be sequentially transitioned; Gap 1 (G1), Synthesis (S), Gap 2 (G2) and Mitosis (M) (Figure 5.3a). The onset of G1 is generally controlled by extra-cellular signals and mitogens. For example, cells that become contact inhibited upon confluence will not re-enter G1 after division (Duronio and Xiong, 2013). During G1 CDK4 and CDK6 are activated via upregulation of Cyclin D. Active CDK/CyclinD complexes enable the release of E2F transcription factors from Retinoblastoma protein (Rb), therefore preparing the cell for S-phase (Kato et al., 1993). During S-phase the genome is replicated and DNA repackaged around histones ready to pass on to daughter cells (Duronio and Xiong, 2013). Once DNA synthesis is complete, the cell transitions into the G2 phase which is associated with increased protein synthesis and cell growth (Diril et al., 2012). Together, these three phases, G1, S and G2 are known as Interphase. The final phase of the cell cycle is Mitosis, during which the nuclear envelope breaks down and chromatids divide (Gavet and Pines, 2010). Cell cycle transitions are typically controlled by CDKs and their activating cyclins (Figure 5.3). Specifically, CDK4 and CDK6 control G1, CDK2 is most active during S-phase and G2, whereas CDK1 is famously the regulator of the G2/M transition and progression through mitosis (Malumbres, 2014).

a)

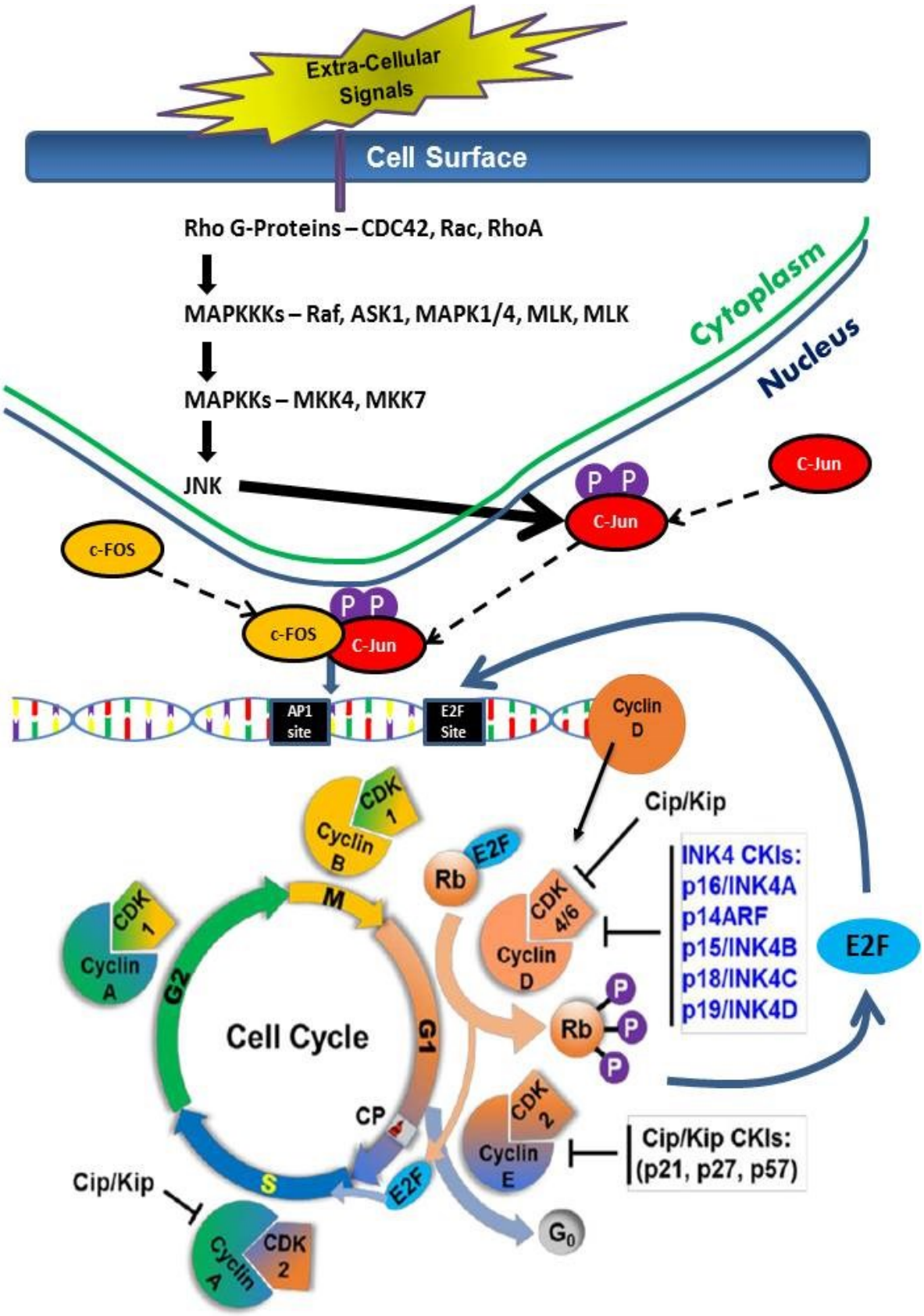
Extra-Cellular Signals
Cell Surface
Rho G-Proteins – CDC42, Rac, RhoA
MAPKKKs – Raf, ASK1, MAPK1/4, MLK, MLK
MAPKKs – MKK4, MKK7
JNK
Cytoplasm
Nucleus
C-Jun
P P
C-Jun
c-FOS
P P
c-FOS
C-Jun
AP1 site
E2F Site
Cyclin D
Cip/Kip
INK4 CKIs:
p16/INK4A
p14ARF
p15/INK4B
p18/INK4C
p19/INK4D
E2F
CDK 4/6
Cyclin D
Rb
P
P
P
CDK 1
Cyclin B
E2F
Rb
M
G2
Cell Cycle
G1
CDK 1
Cyclin A
CP
S
E2F
CDK 2
Cyclin E
Cip/Kip CKIs:
(p21, p27, p57)
Cip/Kip
Cyclin A
CDK 2
G0

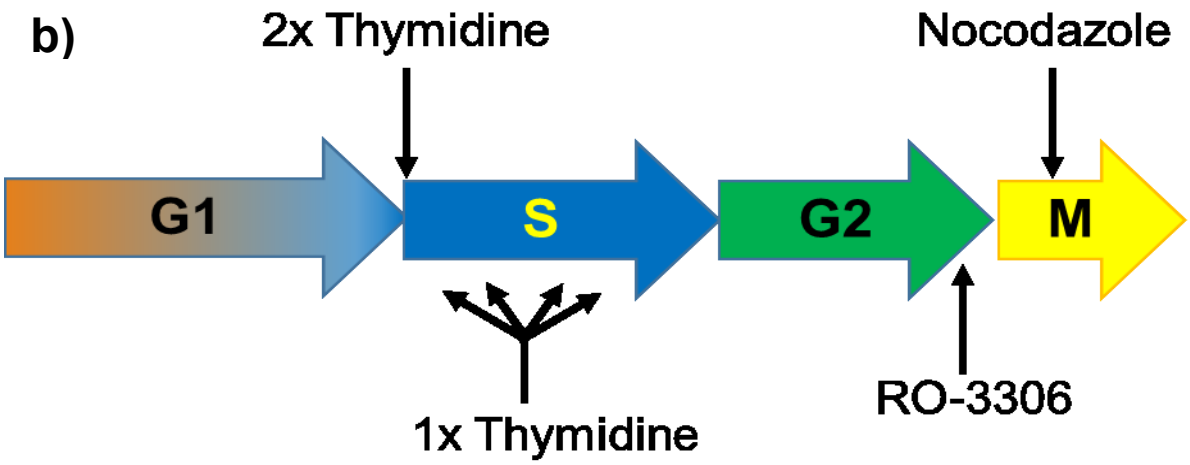

Figure 5.3 Schematic diagram of the major CDK/Cyclin complex involved in cell cycle transitioning. a) The transition into the cell cycle is initiated by extra-cellular signals. Rho G-proteins are stimulated by receptor signalling on the cell membrane, in turn they activate downstream MAPKKKs which promotes phosphorylation and activation of the MAPKKs, MKK4 and MKK7. Upon activation of the MAP Kinase, c-Jun N-terminal Kinase (JNK), by MAPKKs JNK translocates to the nucleus and subsequently phosphorylates the AP1 transcription factor, c-Jun. c-Jun forms a heterodimeric complex with c-FOS and localises to an AP1 consensus sequence on the promoter of Cyclin D for basal expression . Translated Cyclin D associates with and activates its respective CDK (CDK4 or CDK6). The CDK/CycD kinase complex promotes the inhibitory phosphorylation of Retinoblastoma protein (Rb), thereby releasing E2F transcription factors from Rb-mediated inactivation. E2F transcription factors promote the upregulation of Cyclin D in a positive feedback mechanism, CDK2-associated E-type cyclins to fully inactivate Rb and thereby promote the transcription of genes involved in G1/S transition and DNA synthesis. During S-phase CDK2/CycA phosphorylates a multitude of proteins involved in transcription and translation. Once DNA has been fully replicated S/G2 transition is initiated. The CDK1/CycA complex ensures re-replication does not take place, and with the help of CDK2/CycA prepares the cell for mitosis. CDK1/CycB is the major regulator of the G2/M boundary and progression through mitosis. Figure modified from Figure 1, (Lutful Kabir et al., 2015). b) Highlights where thymidine, RO-3306 and nocodazole act in the cell cycle.

5.4 JMJD7 phosphorylation is increased during S-phase of the cell cycle.

To test potential cell cycle dependent regulation of JMJD7 phosphorylation we first aimed to synchronise cells in S-phase of the cell cycle. Thymidine is a thymine analogue which acts as a G1/S phase synchronisation tool by inhibiting DNA synthesis. A single use of thymidine will block the cell population throughout all stages of S-phase. Therefore, to generate an entirely G1/S synchronous population the cells need to be released back into the cell cycle after the first S-phase block to then allowed to transition out of S-phase before treatment for a second time to ensure G1/S synchronisation (Figure 5.3) (Ma and Poon, 2011). Leaky expressing HEK293T pTIPZ FLAG-JMJD7 cells were seeded into 15cm plates, and the following day treated with thymidine. After 18 hours the cells were washed thoroughly and incubated in fresh media before another thymidine treatment (16 hours). After the second thymidine treatment the cells were washed in PBS again and released back into the cell cycle by incubation with fresh media. Cell cycle profiling was performed using Fluorescence Assisted Cell Sorting (FACS): DNA content was measured by Propidium Iodide (PI) staining cells and quantified using a Cyan B Flow Cytometer, with data analysed using Summit 4.3 software. One plate was lysed for protein and FACS every hour over 9 hours. Since thymidine blocks DNA replication, and FACS analysis of the cell cycle using PI works by staining total DNA content, cells in early S-phase that are analysed using this method may be observed as G1, due to having not started DNA replication. This likely explains the increased proportion of G1 cells at 0 hours of release, relative to untreated (asynchronous) cells (Figure 5.4a). As expected, cells appeared not to be immediately released from the thymidine-block, taking up to 3 hours before the proportion of S and G2/M cells begins to increase. By

hour 5 the majority of the cells are in S-phase, and by 9 hours after release the majority of cells have transitioned through G2 and mitosis into G1. Having validated a successful synchronisation and release in this model, we moved on to analysing phT37 JMJD7 levels in the corresponding cell lysates: Figure 5.4b shows a representative western blot. Interestingly, a significant spike in phT37 JMJD7 levels are observed at 4-5 hours after release, time points that correspond to when the maximum number of cells were in S-phase. As the cells transition out of S-phase, T37 phosphorylation is reduced (hours 6-7). Interestingly, T37 phosphorylation levels seem to modestly increase again after 8-9 hours of release, which may be consistent with entry or passage through G2 or mitosis. The other pathway components were also analysed by western blot however, with the exception of DRG2 there was no significant change in their expression. Interestingly, DRG2 expression increase correlated with JMJD7 phT37 4-5 hours. Overall, the data suggest that JMJD7 T37 phosphorylation is cell cycle regulated, and that JMJD7 kinase activity peaks at least once, in S-phase, with a possible second wave of activity later in the cell cycle.

To take a closer look at the potential regulation of JMJD7 phosphorylation during the G2/M transition we next used an established G2/M synchronisation protocol.

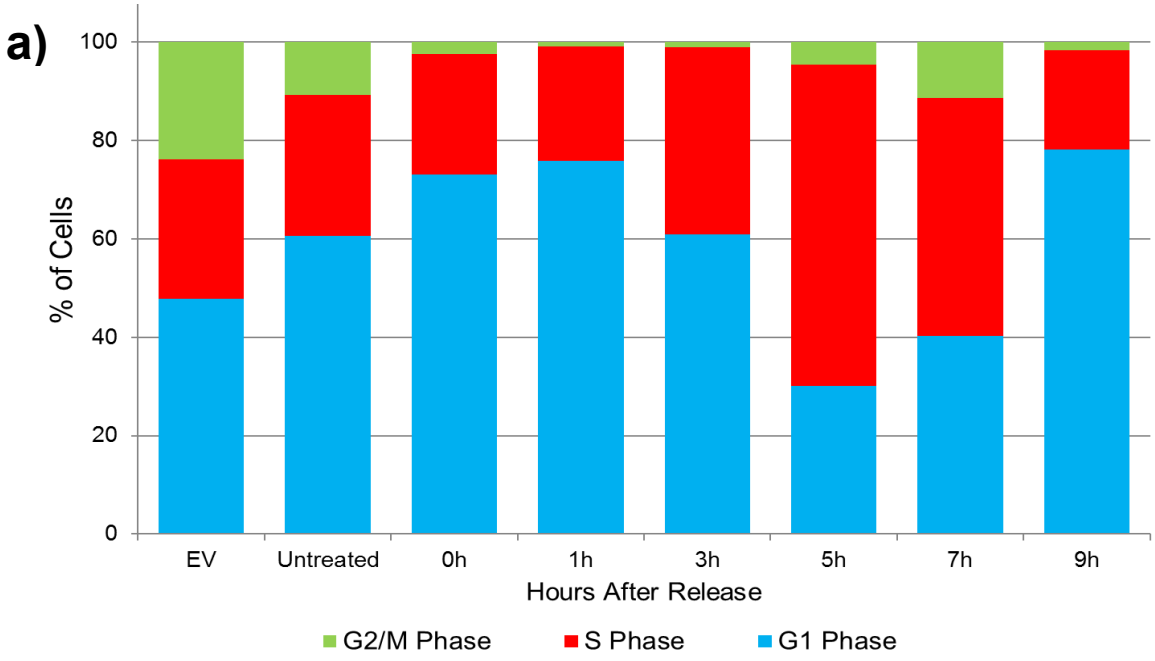

Figure 5.4 Double thymidine block indicates JMJD7 phosphorylation may be regulated during S-phase. HEK293T pTIPZ JMJD7 cells were subject to 2.5 mM thymidine treatment for 18 hours, release in fresh media followed by another thymidine block (2.5mM) for 16 hours. After second thymidine treatment cells were washed thoroughly and released into fresh DMEM. Protein and FACS samples were taken at 0 hours and every hour for 9 hours. a) FACS data shows thymidine block was successful.

b)

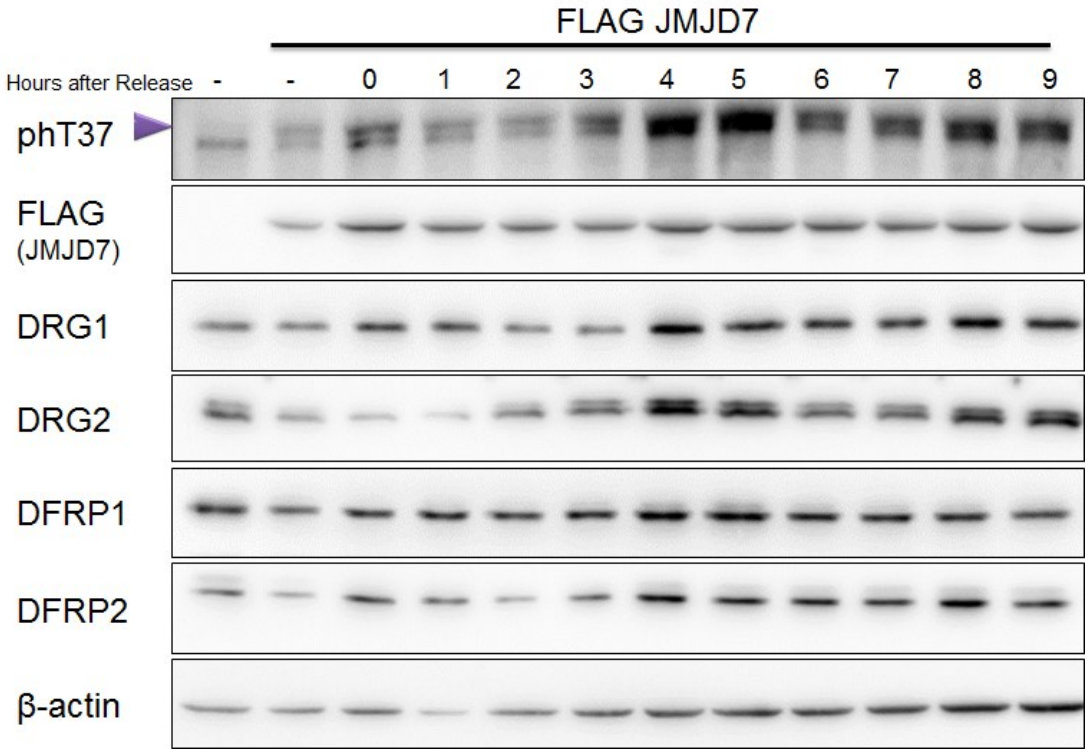

Figure 5.4 b) representative western blots suggest that JMJD7 phosphorylation may be upregulated during mid to late S-phase (Upper band, shown with purple arrow). Note that a non-specific band is seen at a similar molecular weight to the FLAG-JMJD7 band and which is regulated similarly (see lane 1). Therefore, we cannot rule out that this signal might contribute to the regulation assigned to FLAG-JMJD7. Given that this phospho-specific antibody recognises another protein that is regulated similarly it is possible that it may be phosphorylated by the same kinase. JMJD7 siRNA knockdown indicated that this non-specific band was not endogenous JMJD7 (data not shown). Other blots of pathway components, DRG1, DFRP1 and DRFRP2 did not show any significant change in protein expression over the course of the experiment. Expression of DRG2, however, correlated with the observed increase in phT37 at 4-5 hours and 9 hours. n=2.

5.5 JMJD7 phosphorylation may be regulated during G2/M-phases of the cell cycle

RO-3306 is a useful tool for blocking cells at the G2/M boundary as it inhibits CDK1 activity, which is required for the transition from G2 into mitosis (Vassilev, 2006). In order to efficiently synchronise cells in G2/M using RO-3306, cells are often first synchronised in S-phase using thymidine. Therefore, HEK293T pTIPZ FLAG-JMJD7 cells were seeded into 15cm plates and grown for 2 days prior to treatment with thymidine for 18 hours. Following thymidine treatment, cells were 'released' in fresh media for 3 hours before treating with RO-3306 for 16 hours. Cell cycle analysis by FACS indicated that, under the conditions used here, this RO-3306 synchronisation experiment actually appeared to block cells in late S-phase (Figure 5.5a). Thirty minutes after release the majority of cells were in G2/M and succinctly transitioned into G1 over the remaining time points. Figure 5.5b presents western blot analyses of the corresponding cell lysates. A clear reduction in JMJD7 T37 phosphorylation is seen at 0 minutes of release (i.e. during RO-3306 treatment), which is gradually restored within 45 minutes post-release, corresponding to late S- into G2/M-phases of the cell cycle. Based on the FACS analyses, the reduction in JMJD7 T37 phosphorylation at 0 hours of RO-3306 release may correlate with the reduced phosphorylation observed in the double thymidine block at 6-7 hours (Figure 5.4b), suggesting that JMJD7 phosphorylation oscillates during S-phase and G2/M. As seen in Figure 5.5b, no significant difference was observed in the protein expression of DRG1, DFRP1, DRG2 and DFRP2.

a)

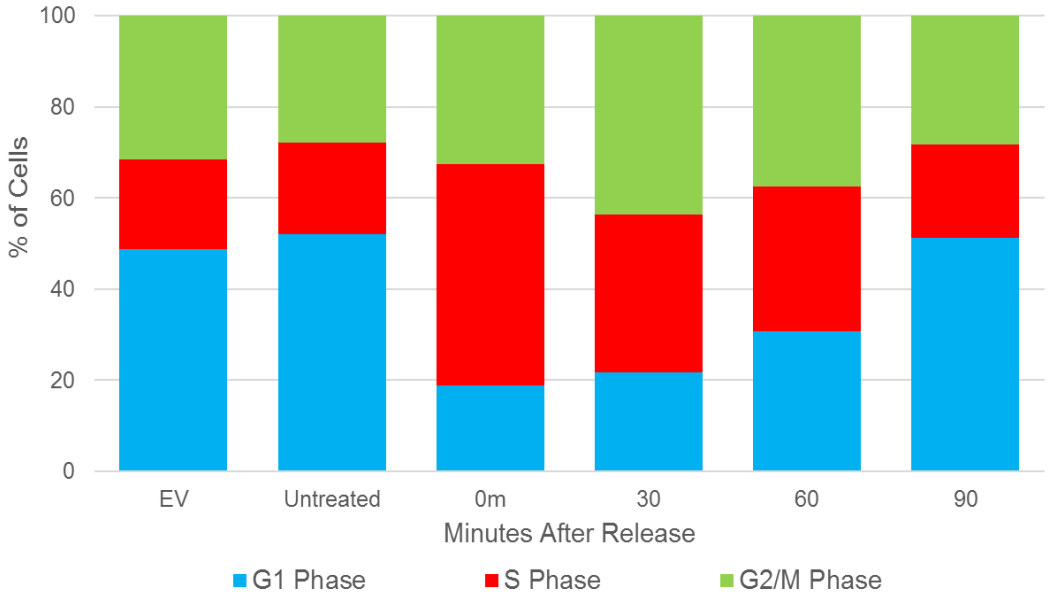

Figure 5.5 RO-3306 synchronisation indicates JMJD7 phosphorylation may be regulated during G2/M. HEK293T pTIPZ JMJD7 cells were subject to 2.5 mM thymidine treatment for 18 hours, release in fresh media followed by block with 6μM RO-3306 for 16 hours. After RO-3306 treatment cells were washed thoroughly and released into fresh DMEM. Protein and FACS samples were taken at 0 minutes and 15 minutes for 90 minutes. a) FACS data shows RO-3306 block was successful at pausing cells at late S – G2/M phase.

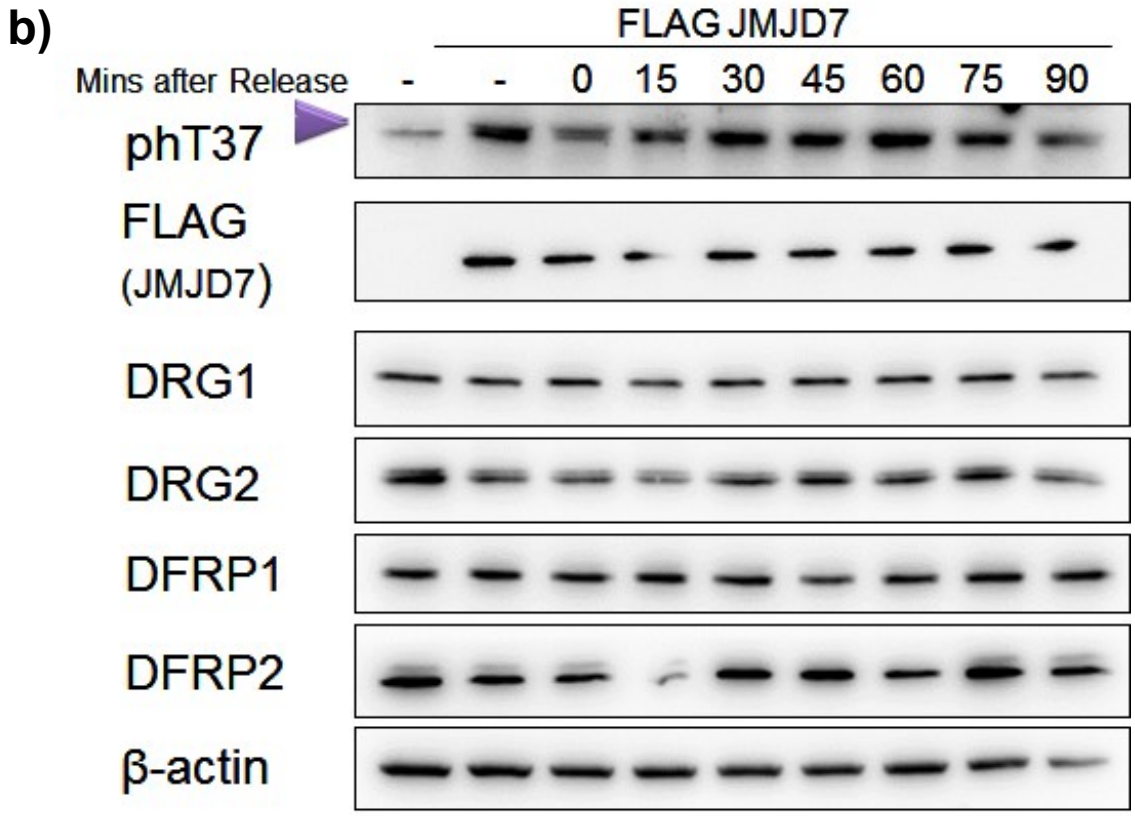

Figure 5.5. b) Representative western blots suggest that JMJD7 phosphorylation may be downregulated at late S-phase, or early G2/M, and induced during the G2/M transition. No difference observed in the expression of DRG1, DFRP1, DRG2 or DFRP2. n=2.

5.6 JMJD7 phosphorylation may be regulated during mitosis.

To explore the potential regulation of JMJD7 T37 phosphorylation during G2/M phases in more detail, we synchronised and released cells from mitosis using an independent protocol based on treatment with nocodazole. Nocodazole is an inhibitor of mitotic spindle formation and therefore effectively pauses cells in early metaphase. However, it has been shown that if cells are left with nocodazole for long periods of time they are able to break through the M phase pause and continue cycling. To avoid keeping the cell population in nocodazole for too long an initial thymidine treatment was performed before nocodazole blocking. Leaky expressing HEK293T pTIPZ FLAG-JMJD7 cells were seeded into 15cm plates and after 2 days the cells were treated with thymidine for 18 hours. Cells were then washed and incubated in fresh media for 3 hours before treatment with nocodazole. After 12 hours the cells were released into fresh DMEM and samples were taken every hour for 8 hours to observe the cells in metaphase and G1 phase of the cell cycle. Cell cycle stages were confirmed by staining ethanol fixed cells with PI. As seen in Figure 5.6a, blockage of cells in mitosis was very effective. Unfortunately, however, the subsequent transition through G1 was slower than expected, suggesting either incomplete nocodazole wash-out, a delay in recovery, or perhaps other factors such as cell stress.

Interestingly however, we did observe a marked increase in signal with the JMJD7 phT37 antibody in cells treated with nocodazole, which was rapidly reversed (within 2 hours) following release (Figure 5.6b). This increase in JMJD7 T37 phosphorylation corresponds to G2/M according to the FACS data, which could be consistent with the increases in JMJD7 kinase activity observed in Figures 5.4 and 5.5. However, due to

our inability to completely resolve phT37 FLAG-JMJD7 from the background band present in the control (EV) cells in this experiment, we cannot rule out that increase in anti-phT37 reactivity observed at 0-1 hours is a result of increase phosphorylation of the background band as opposed to JMJD7. Figure 5.6b also shows the protein expression of the pathway components throughout G1 phase. Interestingly, while DRG1, DFRP1 and DRG2 did not significantly change, DFRP2 protein expression gradually decreased from 2 hours after release and as the cell progressed through G1, with a slight increase at 8 hours. Perhaps indicative of upregulation of DFRP2 at G1/S phase.

Overall, the data presented in this section are consistent with JMJD7 T37 phosphorylation being catalysed by a cell cycle regulated kinase (or kinases), with activities that potentially peak in S- and G2/M-phases. However, the identity of these kinase(s) remains unclear.

a)

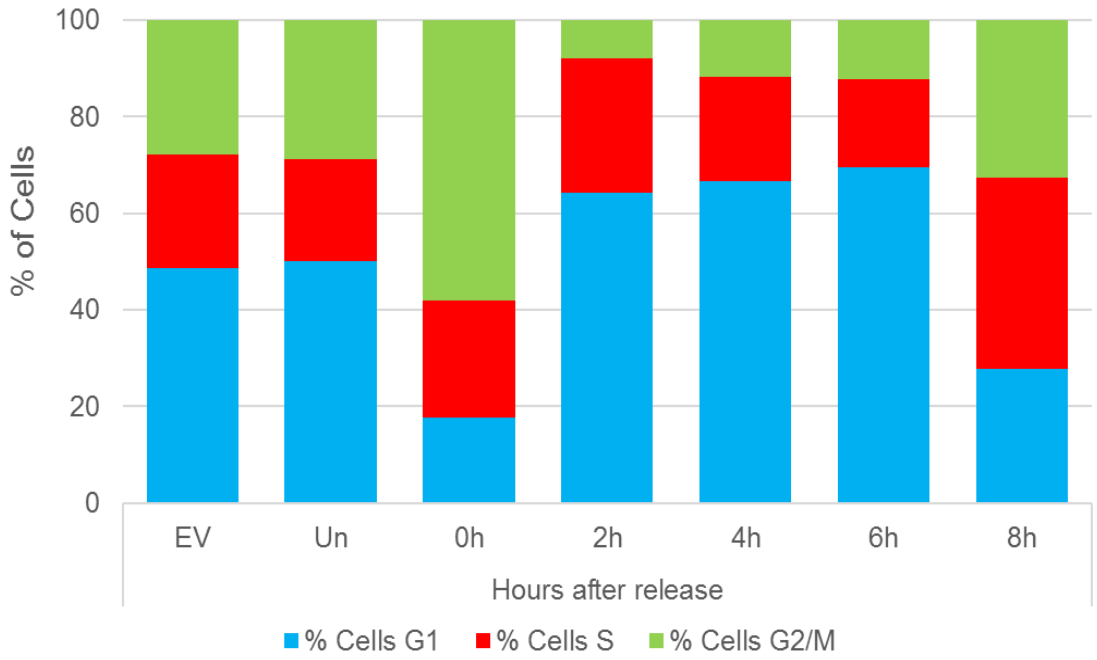

Figure 5.6 Nocodazole block confirms that JMJD7 phosphorylation may also be regulated during G2/M. HEK293T pTIPZ FLAG-JMJD7 cells were subject to 2.5mM thymidine treatment for 18 hours, release in fresh media followed by block with nocodazole for 12 hours. After (100ng/ml) nocodazole treatment cells were washed thoroughly and released into fresh DMEM. Protein and FACS samples were taken at 0 hours and every hour for 8 hours. a) FACS data shows cells were paused at G2/M and the observed “ball-like” structures from the microscope indicate a successful mitotic pause, but possibly slow release from spindle assembly stress after release.

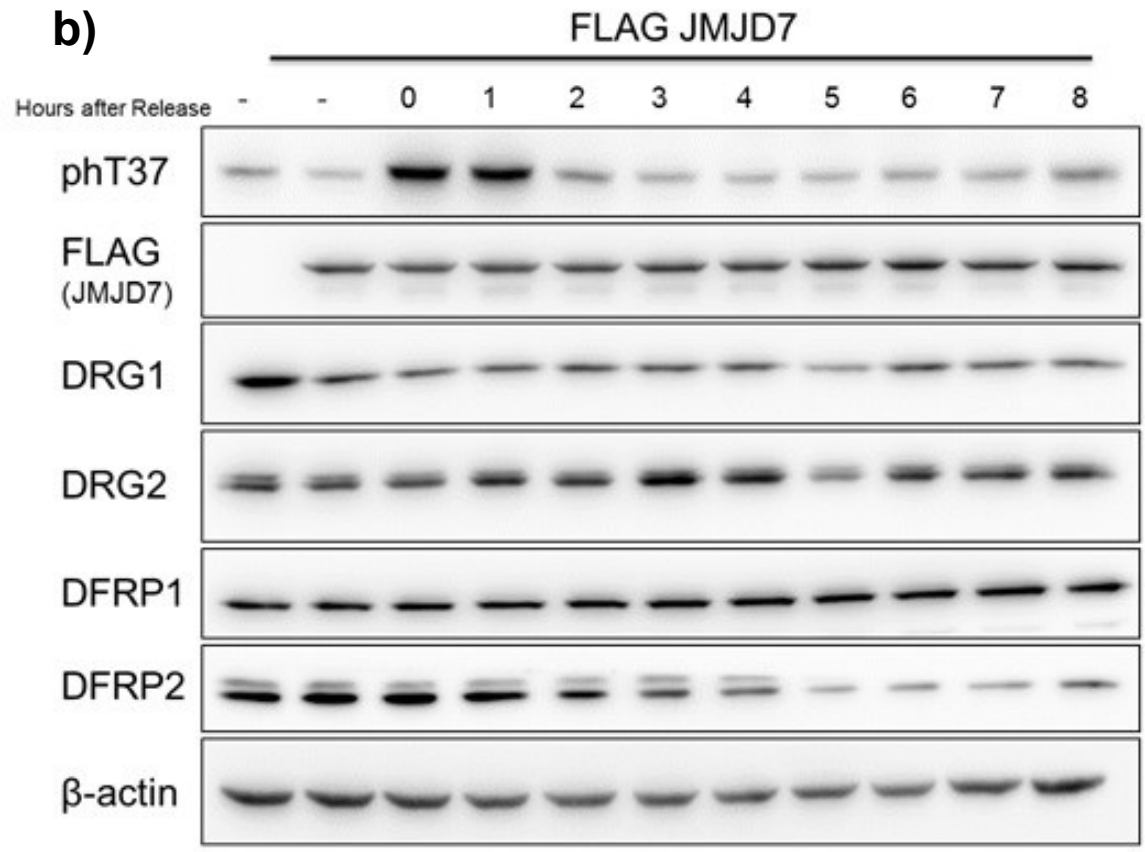

Figure 5.6 b) representative western blots suggest that JMJD7 phosphorylation may be upregulated during mitosis (hour 0-1) but not during G1. DRG1, DFRP1 and DRG2 showed not significant change. DFRP2 blots indicate reduced protein expression throughout G1 and possible increase at 8 hours, correlating with the least number of cells in G1. n=1.

5.7 JMJD7 can be phosphorylated by CMGC kinases *in vitro*.

Having undertaken some preliminary characterisation of the JMJD7 T37 kinase activity we next aimed to directly investigate the identity of the kinase(s) involved. Unfortunately however, the identification of the physiologically relevant kinase for a given phosphorylated substrate protein, such as JMJD7, is a notoriously difficult biological problem. Although chemical biology and proteomics approaches have been developed that can efficiently identify the substrates of a known kinase (Muller et al., 2016, Xue and Tao, 2013, Dephoure et al., 2005), approaches addressing the reverse biological problem are not readily available. To try and address this problem in the context of JMJD7, we proposed a combined approach involving bioinformatics, *in vitro* peptide screening, kinase inhibitor analyses, and cellular proteomic screens.

First, the kinase responsible for JMJD7 T37 phosphorylation was predicted based on known kinase recognition motifs (Figure 5.7a) (www.phosphonet.ca). Interestingly, several mitogen and cell cycle relevant kinases were identified within the list of top hits, including members of the Mitogen-Activated Protein Kinase (MAPK), Cyclin Dependent Kinase –Like (CDKL) kinase and Cyclin Dependent Kinase (CDK) families.

Next we commissioned an unbiased *in vitro* kinase screen (performed by ProQinase, Germany) in which 245 kinases were incubated with a 20mer peptide spanning the T37 phosphorylation site using a radioactive assay (Figure 5.7b, full data in Appendix ii). Interestingly, the top ranking kinases included members of the DYRK, MAPK, CDK or LIM family of kinases, all of which are members of the wider branch of CMGC kinases (CDK, MAPK, glycogen synthase kinases (GSK), CDKL). The identification of CMGC kinases appears to be largely consistent with the Phosphonet

bioinformatics analysis above. There are a total of 62 CMGC kinases, the largest and most well studied families being the CDK and the MAPK families (Varjosalo 2013). In general, CMGC kinases are responsible for cell signalling, cell-cycle regulation, cell communication and growth, perhaps consistent with the data in Chapter 4, and that presented above (Ardito et al., 2017, Varjosalo et al., 2013).

a)

Human Kinase Short Name	Human UniProt. ID
ERK1	P27361
JNK1 (MAPK8)	P45983
JNK3 (MAPK10)	P53779
ERK2 (MAPK1)	P28482
p38a MAPK (MAPK14)	Q16539
JNK2 (MAPK9)	P45984
CDKL4 (AA626859)	Q5MAI5
CDK3	Q00526
CDK2	P24941
p38b MAPK (MAPK11)	Q15759
CDK1 (CDC2)	P06493

b)

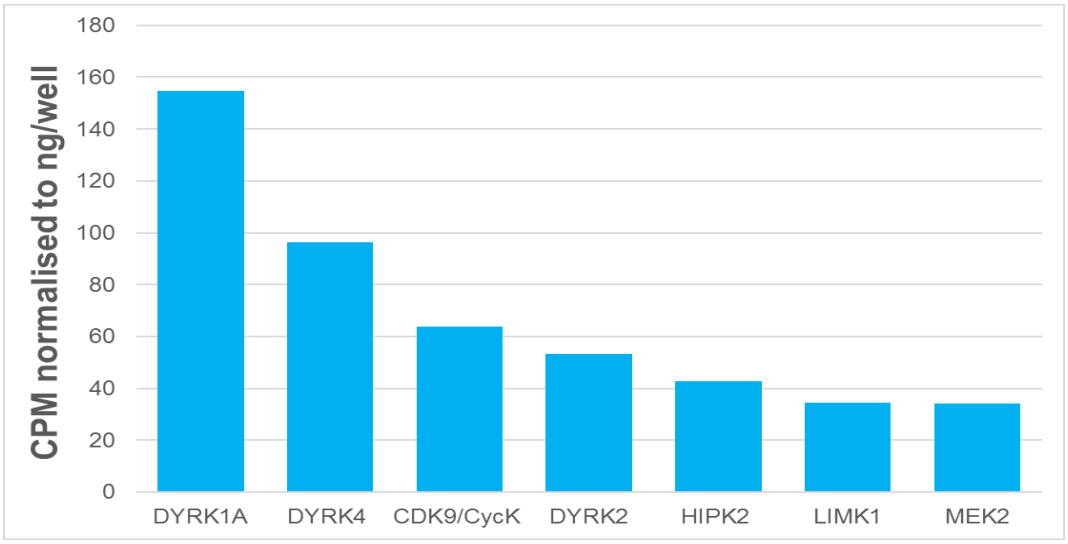

Figure 5.7. JMJD7 T37 may be the target of a CMGC kinase. a) JMJD7 kinase prediction: The Phosphonet database was searched with the JMJD7 T37 site (www.phosphonet.ca). Among the top hits were families from the CMGC group of kinases. b) A 20mer peptide spanning the T37 phosphorylation site was sent to ProQinase, to be screened against 245 recombinant kinases *in vitro*. The top hits were all members from the DYRK, MAPK, CDK and LIM family of kinases. Measured in Counts Per Million (CPM) and corrected to amount of kinase in the reaction. n=1.

5.8 Regulation of JMJD7 T37 phosphorylation by CDK inhibitors

Having identified a sub-family of kinases with potential to support JMJD7 T37 kinase activity *in vitro*, we sought to use this information to help identify the JMJD7 kinase *in vivo*. We collated a panel of small molecule inhibitors with specificity towards the kinases (and closely related enzymes) identified in Figure 5.7 (see Table 5.1 for inhibitor specificities), and used these to treat cells and monitor JMJD7 T37 phosphorylation. HEK293T and HeLa cells were transfected with FLAG-JMJD7 and allowed to express for either 24 or 48 hours before treatment with the indicated inhibitors. Treatment at two different time points post-transfection was tested in order to take into account any potential effects of cell confluence (in light of the data presented above). After 15 hours of treatment with the inhibitors the cells were lysed for protein and analysed by western blot. Densitometry was calculated by correcting for FLAG expression, where 1 is the equivalent to the average of the two DMSO controls. HEK293T and HeLa cells treated after 48 hours of JMJD7 over expression showed most significant reduction in T37 phosphorylation using the inhibitors Flavopiridol, Harmine and INDY, which target either DYRKs or CDKs (Figure 5.8a and 5.8b). Similarly, the most significant reduction in HeLa cells treated after 24 hours of over expression was observed with the same three inhibitors (Figure 5.8c). On the other hand, only Flavopiridol was effective at inhibiting phosphorylation after 24 hours of JMJD7 over expression in HEK293T cells (Figure 5.8d). Overall therefore, the most consistent inhibitor of JMJD7 T37 phosphorylation in cells was Flavopiridol, potentially indicating that JMJD7 T37 phosphorylation is CDK-dependent. Interestingly, there is evidence suggesting that Harmine is not completely specific for DYRKs, and can also inhibit CDK1 and CDK2 (Song et al., 2004b). Taken

together, these inhibitor experiments suggest a role for CDK activity in supporting JMJD7 T37 phosphorylation. Considering this preliminary assignment, we next provide a more detailed overview of cell cycle control by CDKs, prior to presenting more detailed analyses of the role of CDKs in JMJD7 T37 phosphorylation.

Cell Cycle Control by CDKs

The CDK family consists of 20 members that can generally be sub-divided into two functional groups, those involved in cell cycle control and those involved in transcription control.

Cell cycle associated CDKs are thought to have evolved from CDK1, otherwise known as CDC2, the master regulator of the cell cycle (Doree and Hunt, 2002). Cell cycle control by CDK enzymes involves four main enzymes – CDK1, CDK2, CDK4 and CDK6 (Figure 5.3a). CDK4 and CDK6 are the major regulators of G1, and transit through G1 towards S-phase. In the case of all CDKs, their activity and substrate specificity is dictated by their association with specific proteins called 'cyclins' (Cyc) (Higashi et al., 1995). CDK4- and CDK6-associated cyclins, cyclin D1-3, are upregulated by extra-cellular signalling pathways at the initiation of G1 which, in turn, promotes CDK4 and CDK6 activity (Duronio and Xiong, 2013). Progression through G1 is driven by the gradual inactivating phosphorylation of retinoblastoma protein (RB1) catalysed by CDK4 (Kato et al., 1993). Complete RB1 inactivation by CDK2/CycE releases E2F transcription factors to promote the transcription of genes involved in S-phase progression (Dyson, 1998). During S-phase the CDK2/CycE and CDK2/CycA2 kinase complexes phosphorylate multiple targets to promote chromatin duplication and protein synthesis. CDK2/CycA2 activity is increased again during mid-G2 phase which in turn promotes CDK1/CycB1 activity (De Boer et al., 2008).

Cyclin A2 is also able to bind to CDK1, and this complex (among other functions) stops cells re-replicating their DNA in G2 (Diril et al., 2012). Preparation for mitosis, including cytoskeletal reorganisation, are predominantly controlled by CDK2 complexes, and progression through Mitosis is predominantly regulated by CDK1/CycB1 (Diril et al., 2012, Malumbres and Barbacid, 2001). Another cell cycle associated protein, CDK3, associates with CycC to promote G1 progression after G0 (Ren and Rollins, 2004).

Table 5. 1 The kinase inhibitors used to characterise JMJD7 kinase activity.

Inhibitor	**Conc**	**Target family**	**Reference**
Alisertib	2.4nM	Aurora Kinase A (Non-CMGC negative control)	(Qi and Zhang, 2015)
BMS-5	2μM	Lim Kinase	(Park et al., 2014)
Flavopiridol	200nM	Cyclin Dependant Kinases (CDKs)	(Liu et al., 2011)
Harmine	10μM	Dual-Specificity Tyrosine Regulated Kinases (DYRKs)	(Ogawa et al., 2010)
INDY	10μM	Dual-Specificity Tyrosine Regulated Kinases	(Ogawa et al., 2010)
TBID	20μM	Homeodomain-Interacting Protein Kinase 2	(Cozza et al., 2014)
Trametinib	0.4μM	Mitogen Activated Protein Kinases (MAPK)	(Flaherty et al., 2012)

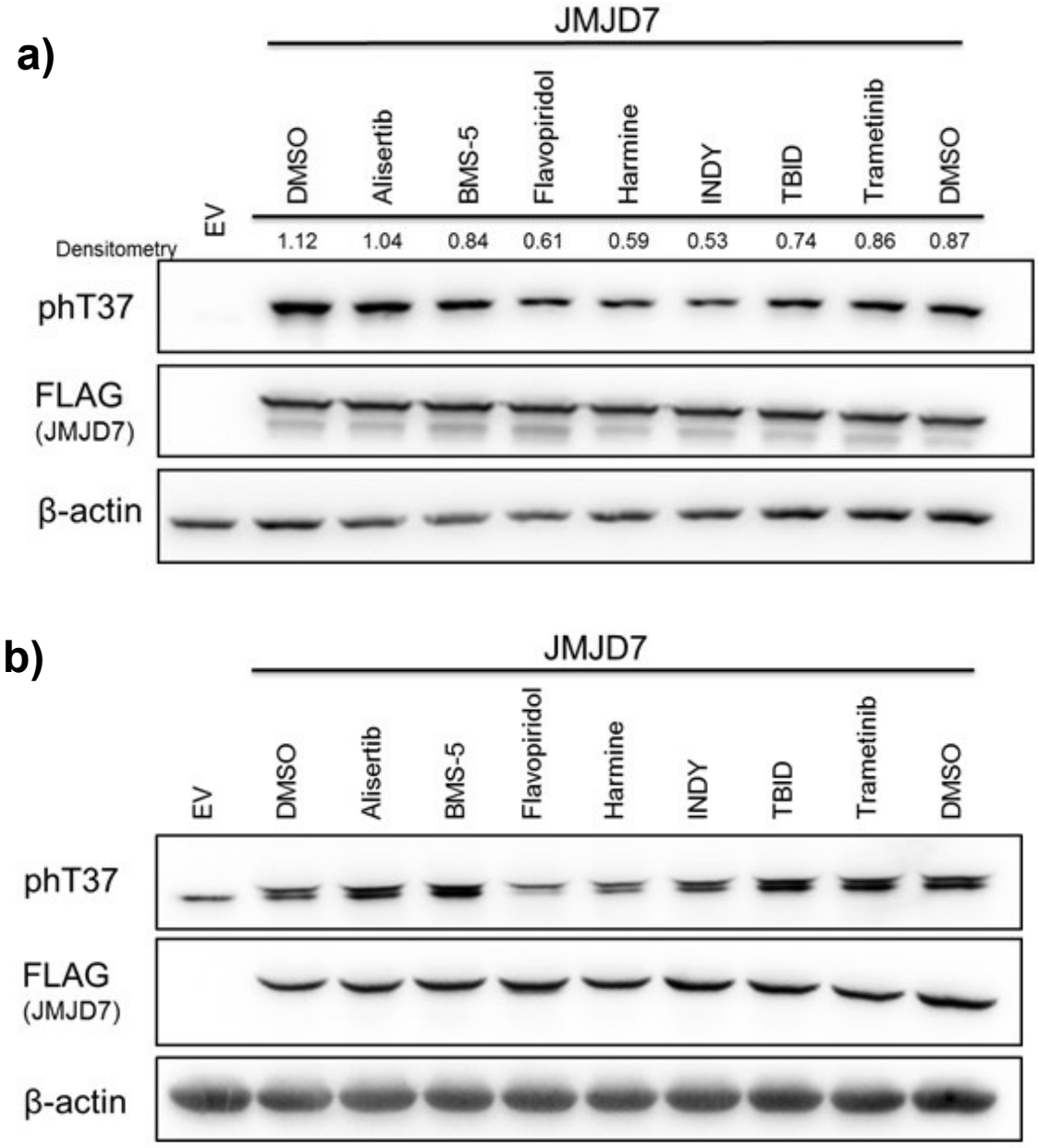

Figure 5.8. JMJD7 phosphorylation can be consistently inhibited by Flavopiridol. HEK293T and HeLa cells were transfected with FLAG-JMJD7 and treated with inhibitors that target members of the DYRK, LIMK, CDK and MAPK family. Western blots of a) HEK293T and b) HeLa cells treated with drugs after 48 hours of JMJD7 over expression. Flavopiridol and Harmine consistently reduce JMJD7 T37 phosphorylation. Phosphorylated JMJD7 expression ratios were calculated by correcting for FLAG. 1 represents the relative difference between FLAG and phT37 averaged from the two DMSO controls. n=3.

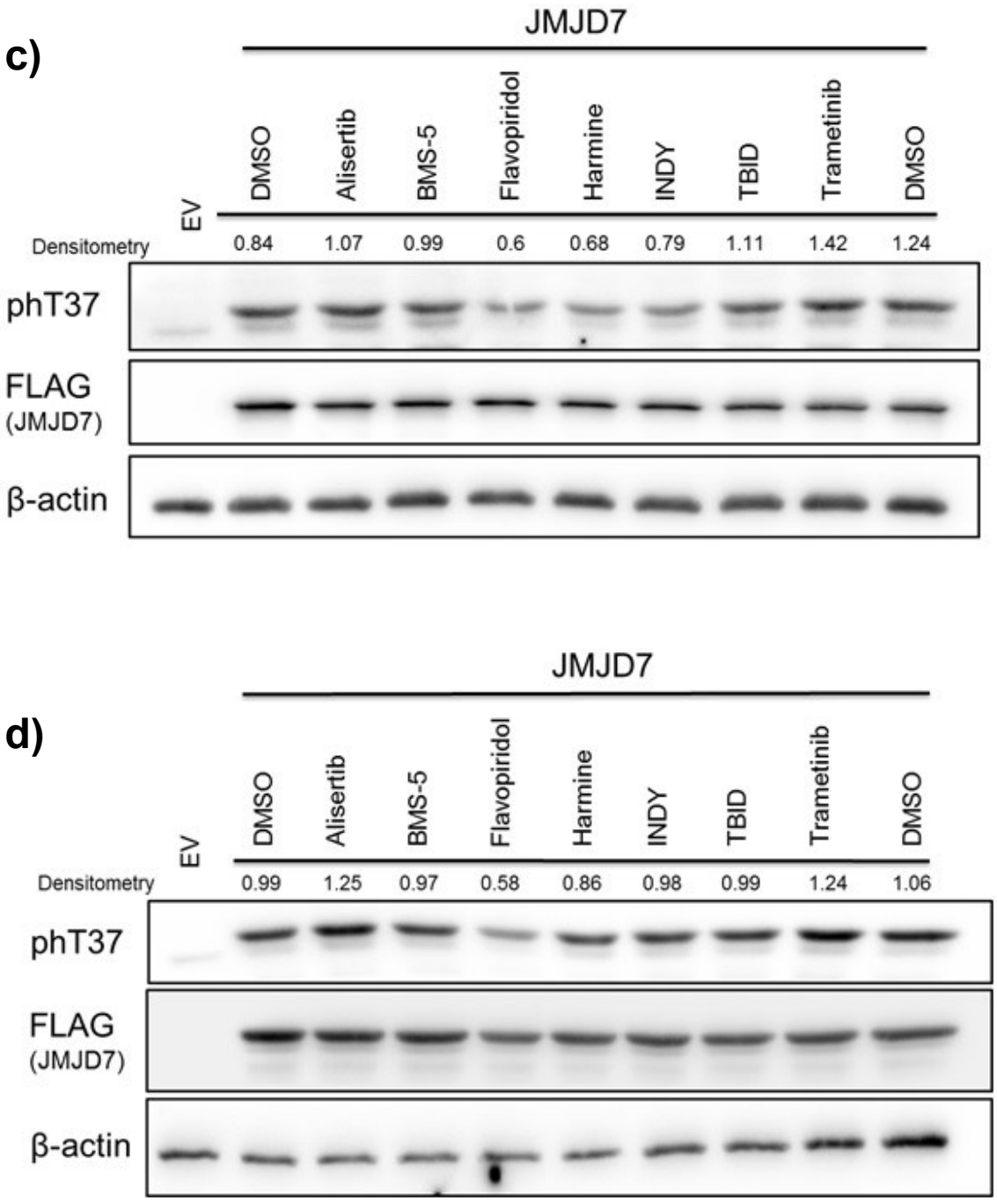

Figure 5.8. Western blot of cells treated with drugs after 24 hours of JMJD7 over expression in HEK293T (c) and HeLa (d) cells. Flavopiridol significantly and consistently inhibits JMJD7 T37 phosphorylation. Densitometry was analysed using the Evolution Capture software. Phosphorylated JMJD7 expression ratios were calculated by correcting for FLAG. 1 represents the relative difference between FLAG and phT37 averaged from the two DMSO controls. n=3.

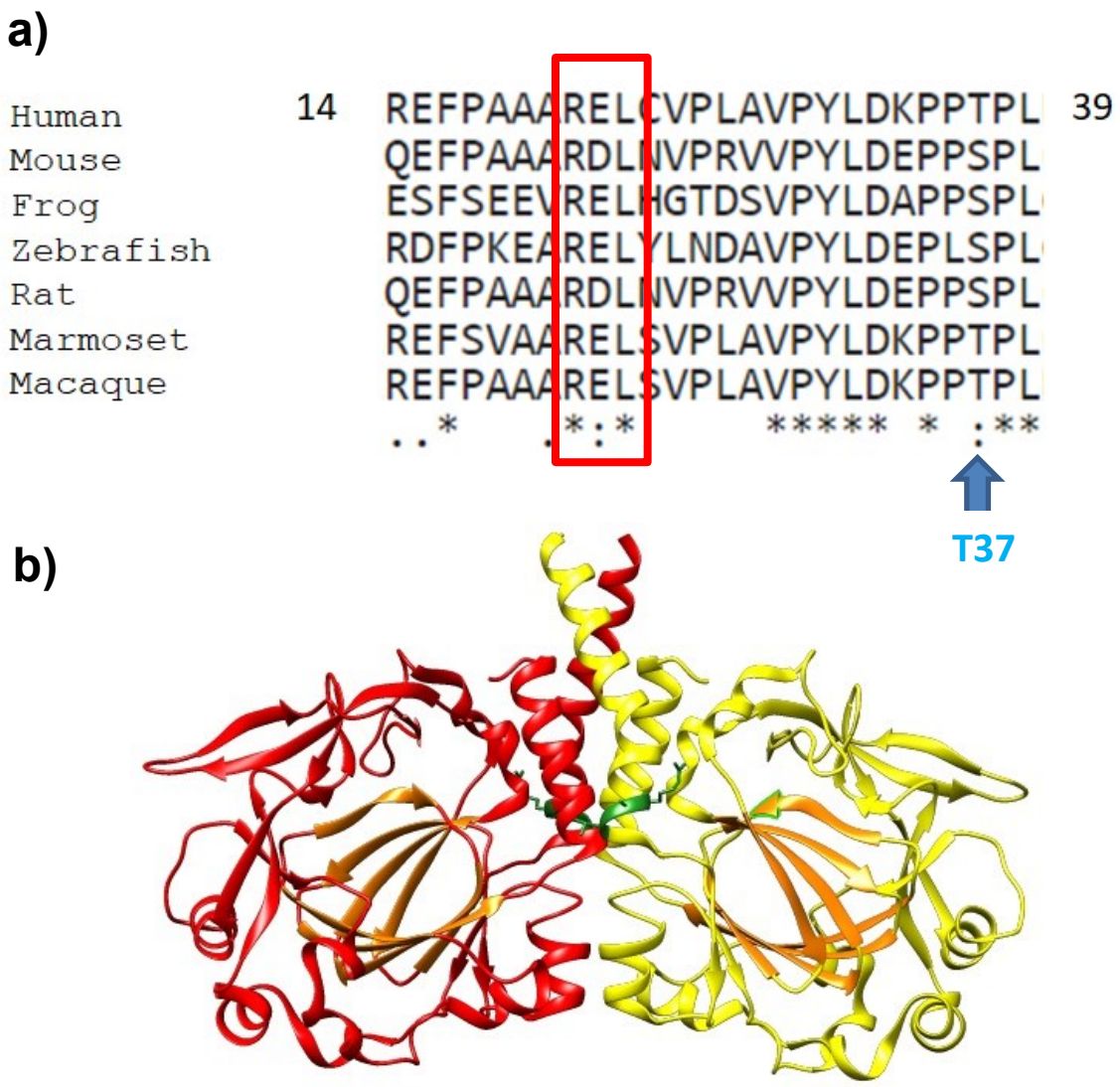

Figure 5.9. JMJD7 contains a conserved RxL cyclin binding motif. a) sequence alignment of this motif demonstrates that both the arginine and the Leucine are evolutionarily conserved. **b**) Structural analysis of JMJD7 shows that the signature cyclin binding RxL motif (green) protrudes from the surface of the dimer and is solvent exposed. JMJD7 modelled on Chimera (Pettersen et al., 2004)

5.9 The N-terminus of JMJD7 contains a conserved motif with similarity to known cyclin binding sites.

We postulated that if JMJD7 were a direct target of one or more CDKs, it might contain a cyclin binding site, analogous to other CDK substrates (Wohlschlegel et al., 2001). Cell cycle associated cyclins (CycD1-3, CycA, CycB and CycE) bind to an "RxL" (or Cy) motif in their CDK targets, located approximately 12-18 residues either C- or N-terminal from the site of phosphorylation (Malumbres, 2014, Takeda et al., 2001, Chen et al., 1996, Ferrero et al., 2011). The cyclin binding site facilitates binding to a hydrophobic patch on the associated cyclin (Archambault et al., 2005). Interestingly, JMJD7 residues 21 to 23 contain an RxL motif 14 residues N-terminal to T37 (Figure 5.9a). Figure 5.9b shows the JMJD7 crystal structure of JMJD7, highlighting in yellow that the RxL motif is located in the N-terminal dimerisation domain, is solvent exposed, and potentially therefore available for cyclin binding. Importantly, sequence alignment between higher eukaryotes (Figure 5.9a) shows that the RxL motif is evolutionarily conserved. Taken together, this supports a role for cell cycle associated cyclins in JMJD7 T37 phosphorylation.

5.10 CDK1/2 specific inhibitors, RO-3306 and SNS032, are able to reduce JMJD7 phosphorylation in HEK293T and HeLa cells.

To continue to investigate the kinase responsible for JMJD7 T37 phosphorylation a series of inhibitors targeting specific members of the CDK family were tested in cells using the same approach as previously presented (see Table 5.2). Densitometry was calculated by correcting for FLAG expression, where 1 is the equivalent to the average of the two DMSO controls. As expected, Flavopiridol inhibited JMJD7 phosphorylation in both cell lines and at both time points (Figures 5.10). Interestingly, RO-3306 and SNS032, which target CDK2 or CDK1 and CDK2, respectively, were the most effective inhibitors of JMJD7 T37 phosphorylation in HEK293T (Figure 5.10a) and HeLa (Figure 5.10b) cells when treated 48 hours after JMJD7 transfection. Figure 5.10c and 5.10d show western blots of HEK293T and HeLa cells treated 24 hours after JMJD7 transfection, respectively. As anticipated, Flavopiridol, RO-3306 and SNS032 were again able to reduce JMJD7 T37 phosphorylation in both cell lines, consistent with Figure 5.10a and 5.10b.

Table 5. 2 The CDK specific inhibitors used to identify JMJD7 kinase.

Inhibitor	Conc.	Target family	Reference
BMS265246	5μM	CDK1 and CDK2	(Misra et al., 2004)
Flavopiridol	200nM	Pan inhibitor (positive control)	(Liu et al., 2011)
LDC000067	10μM	CDK9	(Albert et al., 2014)
PD 0332991	250nM	CDK4 and CDK6	(Finn et al., 2009)
RO-3306	5μM	CDK1 and CDK2	(Vassilev et al., 2006)
SNS032	5μM	CDK2	(Misra et al., 2004)

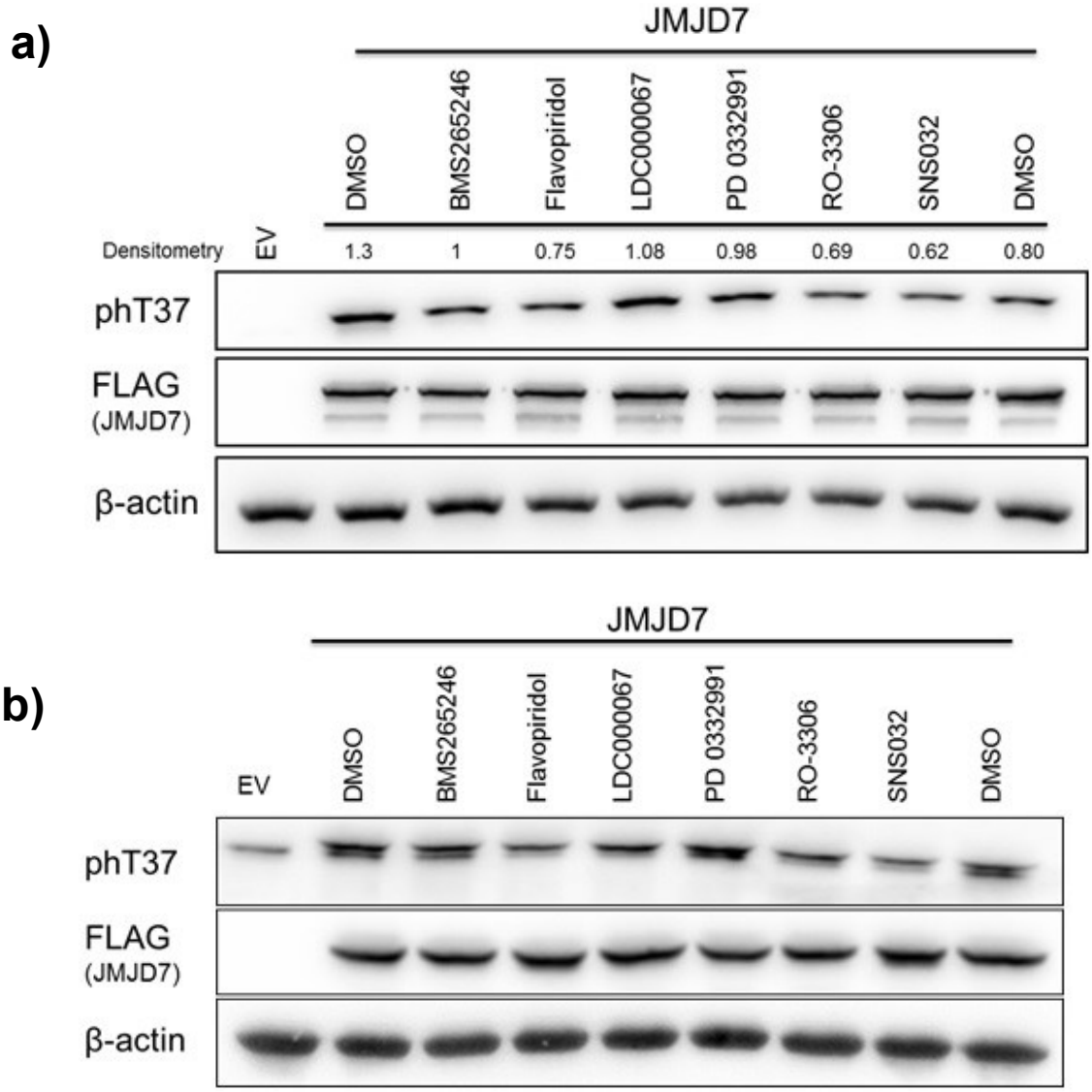

Figure 5.10. JMJD7 phosphorylation is consistently inhibited by CDK1 and CDK2 inhibitors, RO-3306 and SNS032. HEK293T and HeLa cells were transfected with FLAG-JMJD7 and treated with inhibitors that target members of the CDK family of kinases. Western blots of a) HEK293T and b) HeLa cells treated with drugs after 48 hours of JMJD7 over expression. Flavopiridol, RO-3306 and SNS032 consistently reduce JMJD7 T37 phosphorylation. Densitometry was analysed using the Evolution Capture software. Phosphorylated JMJD7 expression ratios were calculated by correcting for FLAG. 1 represents the relative difference between FLAG and phT37 averaged from the two DMSO controls. n=2.

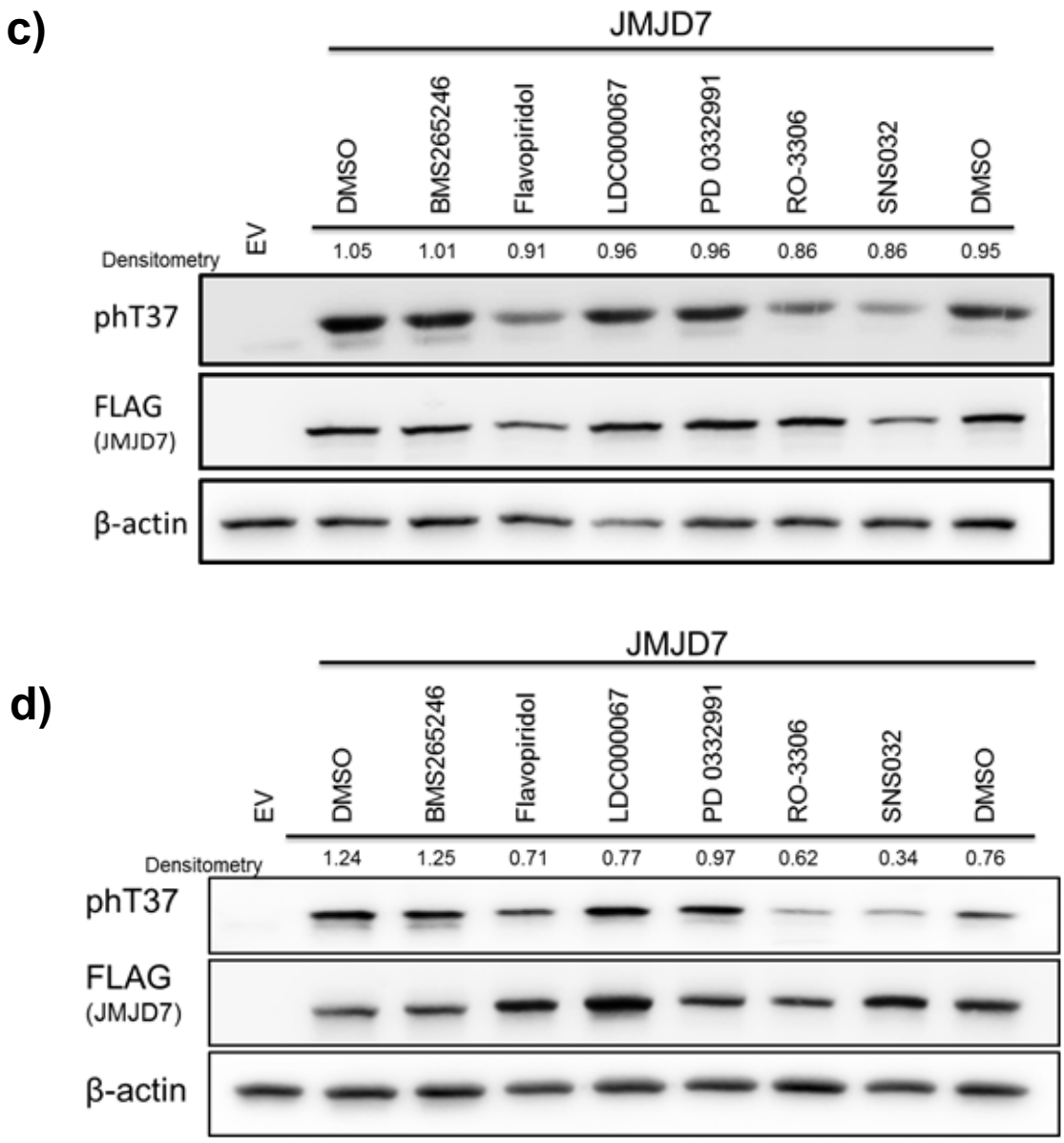

Figure 5.10. Western blot of cells treated with drugs after 24 hours of JMJD7 over expression in HEK293T (c) and HeLa (d) cells. Flavopiridol, RO-3306 and SNS032 significantly and consistently inhibit JMJD7 T37 phosphorylation. Densitometry was analysed using the Evolution Capture software. Phosphorylated JMJD7 expression ratios were calculated by correcting for FLAG. 1 represents the relative difference between FLAG and phT37 averaged from the two DMSO controls. n=2.

5.11 The inhibition of RO-3306 is specific and reversible.

Although the kinase inhibitor experiments presented above are consistent with the possibility that CDK1/2 (or related kinases) target JMJD7 T37, the relatively long treatment times also raise the possibility that reduced phosphorylation is due to indirect effects (Vassilev, 2006). We reasoned that a kinase inhibitor that rapidly reduced JMJD7 T37 phosphorylation was more likely acting directly on the kinase responsible. We tested this hypothesis using RO-3306, which is reported to be a specific and reversible CDK1 inhibitor that can also target CDK2 (albeit with 10-fold less efficacy *in vitro*) (Vassilev, 2006, Vassilev et al., 2006). Inhibition of substrate phosphorylation using RO-3306 has been demonstrated in as little as 2-4 hours (Yang et al., 2013, Marceaux et al., 2018). Therefore, to check whether JMJD7 T37 phosphorylation could be inhibited after shorter treatment times with RO-3306, a time course experiment was performed. HEK293T cells transfected with JMJD7 for 36 hours before treated with RO-3306 over a timecourse of 2-15 hours. The western blot seen in Figure 5.11a shows that after 2 hours with drug JMJD7 phosphorylation was decreased, and this continued to reduce over the 15 hour timecourse, suggesting a specific and rapid response to RO-3306 treatments. These time points were further refined in a 1-4 hour timecourse. HEK293T cells were transfected with FLAG-JMJD7 for 48 hours prior to treatment with RO-3306. Figure 5.11b shows that JMJD7 phosphorylation can be reduced at all time points. However, the 4 hour time point was less effective, suggesting a possible issue with this treatment. Taken together, Figure 5.11a and 511b show that the effect of RO-3306 is likely a direct inhibition of RO-3306 with CDK1 and/or CDK2, rather than an indirect effect of pausing of the cell cycle. Further evidence for a direct effect, would be if phosphorylation was very

rapidly restored after reversing kinase inhibition. Initial evidence supporting this possibility was observed in Figure 5.5b where thymidine/RO-3306 block and release showed JMJD7 T37 phosphorylation was inhibited with RO-3306 treatment and restored after release. To test the recovery of JMJD7 T37 phosphorylation without potentially confounding effects of thymidine treatment, we performed an “RO-3306 only” block and release experiment. JMJD7 was over-expressed in HEK293T cells for 36 hours before RO-3306 treatment for 16 hours and subsequent washout with PBS and incubation with fresh media. Samples were taken at 0 hours and then every 15 minutes for 2 hours. Figure 5.11c confirms that JMJD7 T37 phosphorylation was inhibited after incubation with RO-3306, and could be rapidly restored by replacing with fresh media. Interestingly, full phosphorylation was restored after just 45 minutes in fresh medium, perhaps consistent with JMJD7 phosphorylation being catalysed by a kinase sensitive to RO-3306.

a)

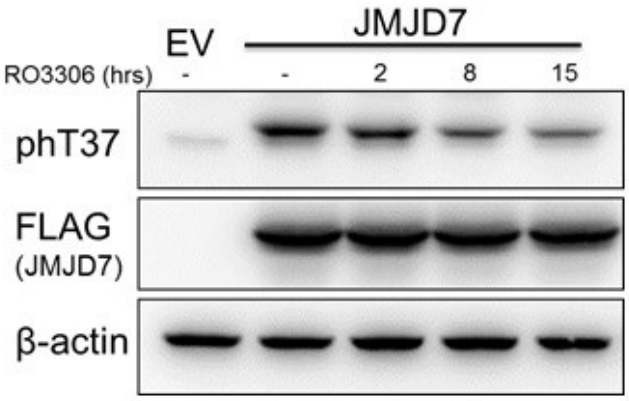

b)

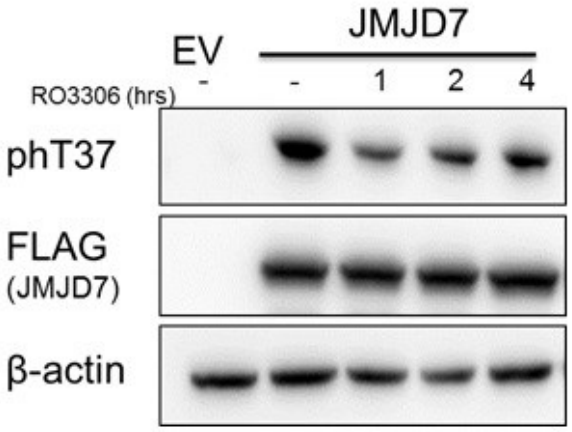

Figure 5.11. RO-3306-mediated inhibition of JMJD7 phosphorylation is rapid and reversible. a) Western blot after HEK293T cells were transfected with JMJD7 and grown for 36 hours before treatment of RO3306 over a 15-hour time course. Western blots show JMJD7 phosphorylation is inhibited by RO-3306 after 2 hours. n=2. b) Western blot after HEK293T cells were transfected with JMJD7 and grown for 36 hours before first treatment of RO3306 for a 2-hour time course. JMJD7 T37 phosphorylation is inhibited after 1 hour of treatment with RO-3306, suggesting the inhibition is a direct result of RO3306 activity. n=2.

c)

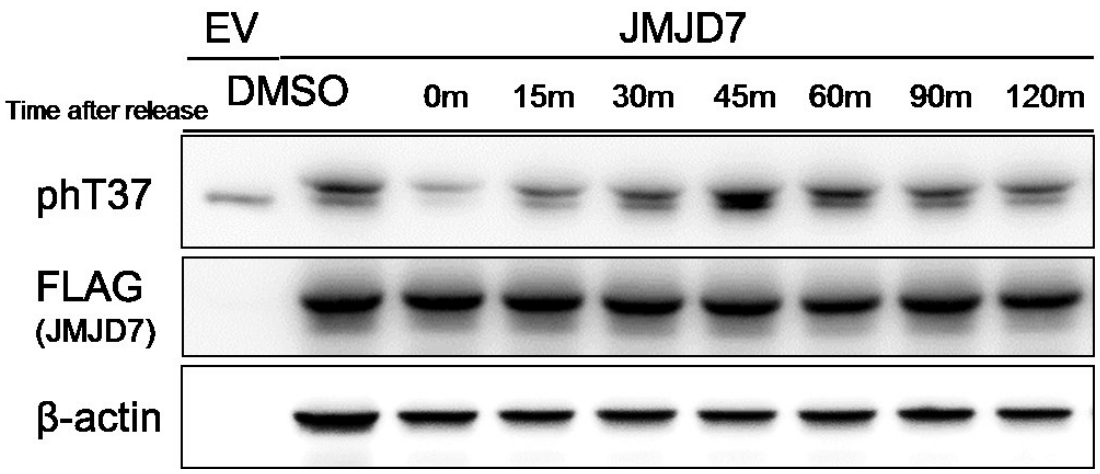

Figure 5.11. c) HEK293T cells were transfected with JMJD7 and grown for 36 hours before treatment with RO3306. After 16 hours the cells were released back into fresh media and samples taken every 15 minutes for 120 minutes. Western blot shows that phosphorylation is significantly reduced, as expected, but is readily reinstated within 45 minutes of release. n=2.

5.12 An unbiased proteomic screen to identify kinases interacting with JMJD7 in an RO3306-dependent manner

Strategies for unbiased identification of novel protein:protein interactions include large-scale purification of epitope-tagged 'bait' proteins followed by MS-based protein sequencing of interactomes (Abu-Farha et al., 2008). Such proteomic approaches can be applied to a wide variety of experimental questions, including the identification of stimulus-induced protein:protein interactions. Having taken a largely 'candidate' approach to the identification of the JMJD7 kinase thus far, (i.e. cell cycle analyses and kinase inhibitors) we considered the project would benefit from an unbiased approach. The Coleman lab regularly apply MS proteomics to successfully identify novel protein complexes and enzyme:substrate interactions (Markolovic et al., 2018, Feng et al., 2014). Therefore, we designed a proteomic approach based around our observations on the dynamic regulation of T37 phosphorylation by RO-3306 treatment and release, to attempt to identify relevant kinases interacting with JMJD7. Figure 5.12a illustrates the concept behind the experimental design. Essentially, Figure 5.12a (i) represents a cell population treated with RO-3306. Echalier et al. (2012) have reported that conformational changes occur when some ATP competitors bind to CDK2. Comparison of the crystal structure of CDK2 bound to either RO-3306 or ATP found changes occur in the substrate binding domain of CDK2 which may inhibit substrate binding and therefore, JMJD7 is seen unphosphorylated. After release, in Figure 5.12a (ii), RO-3306 is removed from the media and, in turn, kinase conformation returns to an ATP-bound active state. As such, the kinase is able to bind and phosphorylate its substrates, including JMJD7 T37. Since JMJD7 phosphorylation is rapidly restored shortly after release from RO-3306 treatment, we reasoned that maximal kinase-substrate interaction would

occur in the lead up to this, and that this event might be detectable by MS proteomics (Figure 5.12a (iii)). To test this hypothesis, parental HEK293T cells were seeded into 15cm plates and the following day FLAG-JMJD7 was transfected and allowed to over express for 36 hours before treating with RO-3306. After 16 hours with drug, cells were washed with PBS, released back into fresh media and samples were taken every 15 minutes. The cell lysates were FLAG-immunoprecipitated for 4 hours and bound proteins were competed from the beads into solution using FLAG peptide. Figure 5.12b shows the western blot of the release over 30 minutes demonstrating an increase in phosphorylation 30 minutes after release, as expected (although, to a lesser extent than that seen in Figure 5.11c). The resulting IP eluants were sent for MS analysis to identify proteins specifically bound to JMJD7. Controls included an IP sample with no JMJD7 expressed (EV) and a solvent control for RO-3306 treatment (DMSO) (Figure 5.12b). The resulting MS data was first filtered for proteins only bound to JMJD7 (and not in the EV sample). Importantly, successful purification of JMJD7 complexes was validated by the presence of DRG2, which was only detected in the control DMSO sample. Although DRG1 was readily detected in the JMJD7 pulldowns, it was also detected in the EV sample (albeit at reduced levels). Having confirmed the specificity of the IP, we filtered the JMJD7 interactome data to identify kinases, and specifically, kinases that, according to the MRC inhibitor database (http://www.kinase-screen.mrc.ac.uk), can be inhibited by RO-3306. Figure 5.12c shows that the kinases that met all these criteria were CDK2 and Aurora Kinase B (AurkB) (Also see Appendix iii).

Importantly, CDK2 was identified as a candidate JMJD7 kinase through the bioinformatics and inhibitor approaches above. As discussed, CDK2 activity is

highest throughout S-phase and G2 (Hu et al., 2001). However, AurkB is also cell cycle regulated, with activity mainly restricted to mitosis, where it regulates spindle assembly (Giet and Glover, 2001). The upregulation of JMJD7 T37 phosphorylation in S, G2 and Mitosis might perhaps be more consistent with the identification of CDK2 as a candidate, rather than AukB. Furthermore, CDK2 is more potently inhibited by RO-3306 *in vitro (*Figure 5.12c).

To independently test the proteomic results and to explore the RO-3306-dependent interaction of JMJD7 with CDK2, the block and release experiment was repeated exactly as described above and eluants analysed by western blot. This preliminary analysis confirmed increased binding of CDK2 to JMJD7 after treatment with RO-3306 (Figure 5.12d). Overall, these data indicate that JMJD7 interacts with CDK2 in cells, and that this interaction increases after release from RO-3306 treatment in parallel with increased T37 phosphorylation. Next we sought to develop an *in vitro* JMJD7 kinase assay to test the ability of CDK2 and other kinases to phosphorylate JMJD7 T37.

a)

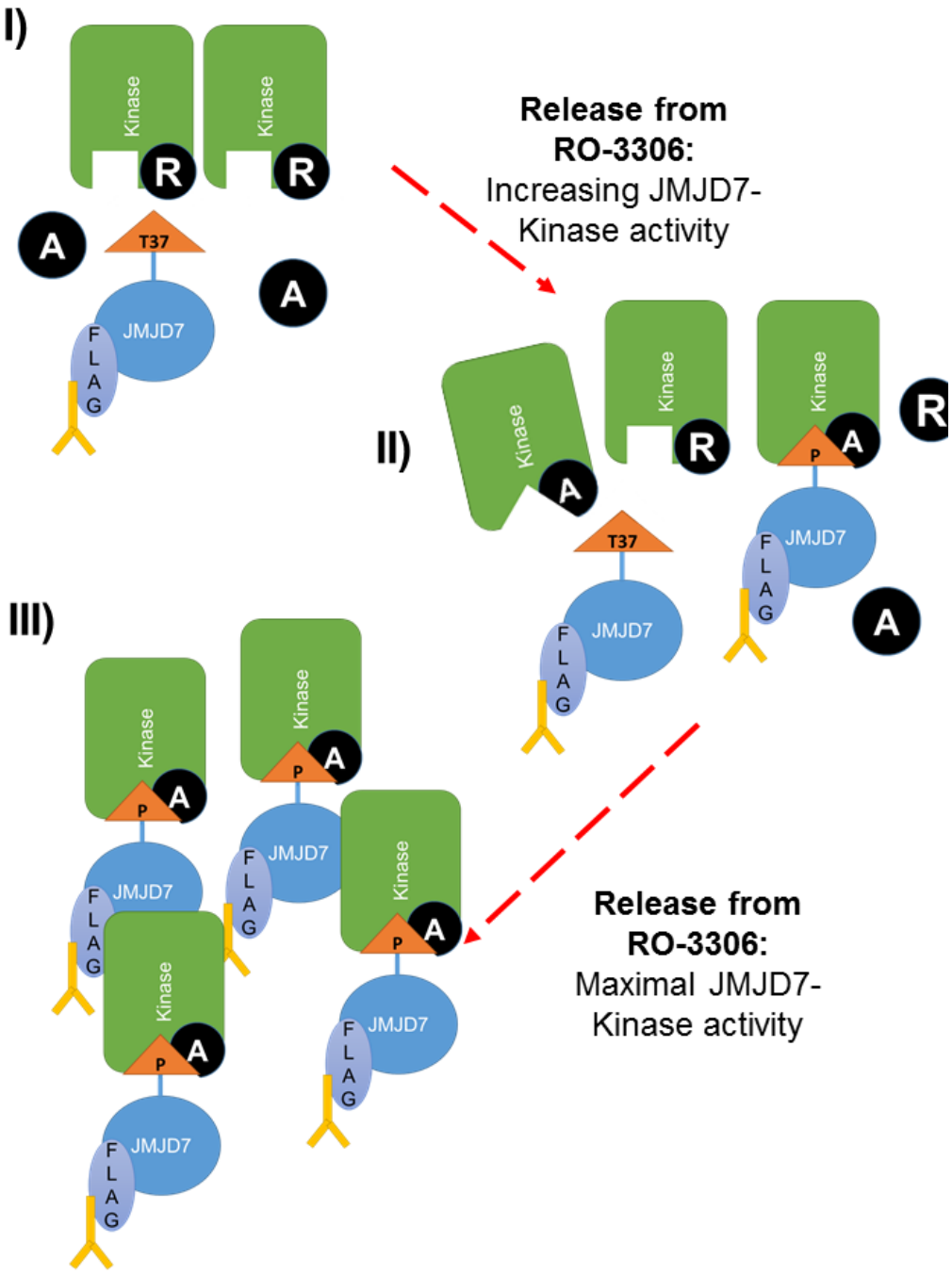
I)
Kinase
Kinase
R
R
A
T37
A
JMJD7
FLAG
Release from
RO-3306:
Increasing JMJD7-
Kinase activity
II)
Kinase
Kinase
R
R
A
P
A
T37
JMJD7
FLAG
JMJD7
A
III)
Kinase
P
A
Kinase
P
A
JMJD7
FLAG
JMJD7
FLAG
Kinase
P
A
Kinase
P
A
JMJD7
FLAG
JMJD7
FLAG
Release from
RO-3306:
Maximal JMJD7-
Kinase activity

b)

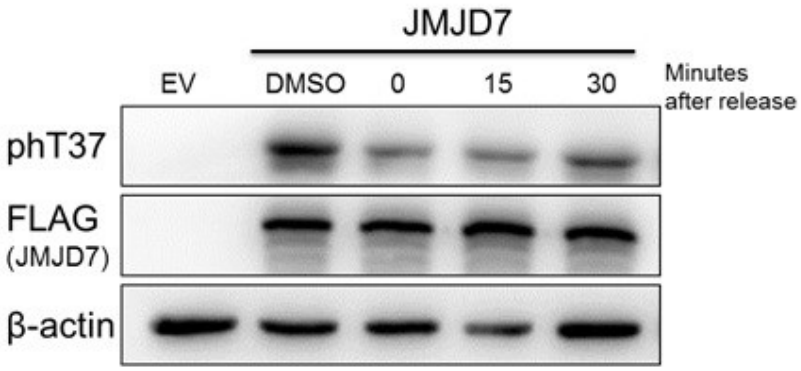

Figure 5.12. Identification of RO-3306 sensitive kinases whose interaction with JMJD7 increases following release from RO-3306 treatment. a) cartoon illustration demonstrating the concept behind the kinase capture experiment. In brief, after 15 hours of RO-3306 (shown by "R" in figure) exposure, activity of the T37 kinase is inhibited. Crystalographic studies of CDK2 in complex with RO-3306 or ATP have shown that the binding of RO-3306 alters the substrate binding domain enough to block substrate binding (Echalier et al., 2012). After release into fresh media RO-3306 is released from the kinase, replaced with ATP (seen as "A" in figure) and returns to being in an active conformation. In turn, the kinase activity upon JMJD7 is increased over time, and therefore JMJD7 phosphorylation is also increased. IP of FLAG-JMJD7 during this time may capture the T37 kinase. b) the kinase capture experiment in practice. HEK293T cells were transfected with FLAG-JMJD7 over 36 hours. After RO-3306 treatment for 16 hours cells were lysed for protein and immunoprecipitated before sending for MS. Western blot shows reduction of JMJD7 T37 phosphorylation after RO3306 incubation and gradual increase in kinase activity over 30 minutes, as expected.

c)

	emPAI					
Kinase	DMSO	0h	15m		% Kinase activity with 10uM of RO-3306	% Kinase activity with 1uM of RO-3306
Isoform 2 of Cyclin-dependent kinase 2	0.6	0.87	0.6		5	21
Aurora kinase B	0.18	0.95	0.43		13	49

d)

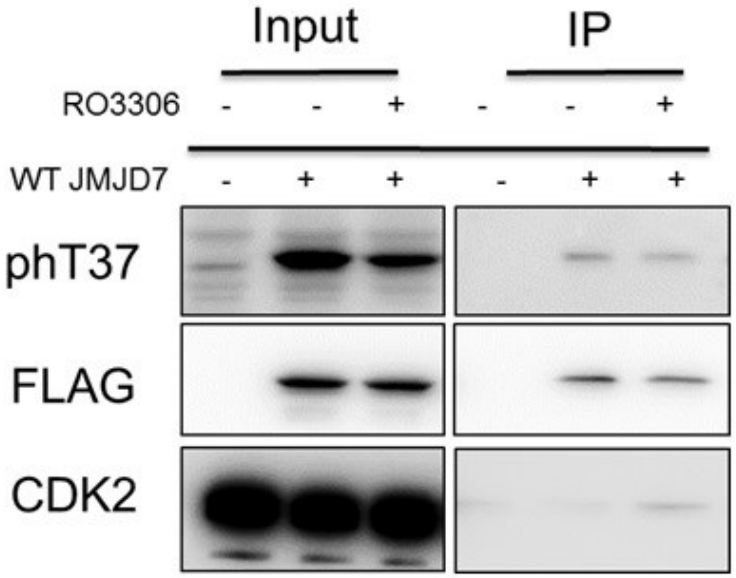

Figure 5.12. c) Results of MS analyses after filtering data for kinases specifically bound to JMJD7 which can be inhibited by RO-3306 (according to MRC kinase inhibitor database). Exponentially Modified Protein Abundance Index (emPAI) is a measure of protein abundance in large scale proteomic studies (Ishihama et al., 2005). n=1. d) Western blot validation of MS data. Protocol was repeated exactly as (b) except IP samples were analysed by western blot and tested for the presence of CDK2. CDK2 was found bound to JMJD7 upon RO-3306 release. n=1.

5.13 CDK1 and CDK2 can phosphorylate JMJD7 T37 *in vitro*.

In light of the combined bioinformatics, inhibitor, and proteomics results presented above we aimed to test whether CDK2 can support the phosphorylation of JMJD7 T37 by developing an *in vitro* JMJD7 kinase assay. This assay is based on the use of commercially available purified kinases (in complex with cyclins in the case of CDKs) and recombinant JMJD7 (Figure 5.13a; kindly provided by our collaborator Dr S. Markolovic, Oxford). We considered it worthwhile to compare CDK2 to other candidate CDKs identified previously, including CDK1 and AurkB. Since CDK2 was commercially available in multiple different cyclin complexes (CDK2/CycA1, CDK2/CycA2, CDK2/CycE, CDK2/CycO) and cyclins are important determinants of CDK substrate specificity (Lee et al., 2007), we also included these different forms of CDK2 in our experimental design. Figure 5.13b shows a 12% polyacrylamide SDS gel stained with coomassie blue to highlight the different Cyclin/CDK combinations. The recombinant JMJD7 protein shown in Figure 5.13a was incubated in 'kinase assay buffer' (see Methods) with and without the kinases in the presence or absence of phosphatase inhibitor ('Halt', to address the potential for contaminating phosphatases carried over from insect cell purifications) for 10 minutes at 30˚C. Figure 5.13c shows the western blot and validation coomassie gel after the kinase assay. As expected, we did not detect any JMJD7 T37 phosphorylation in samples not treated with kinase (lane 1). Importantly, treatment with CDK2/CycO or AurkB did not induce any detectable T37 phosphorylation (lanes 6 and 7, respectively) (despite being confirmed as active by Thermo quality control), highlighting the specificity of the assay, and suggesting that these kinase complexes are unlikely to be physiologically relevant JMJD7 kinases. In contrast, CDK1/CycB1, CDK2/CycA1,

CDK2/CycA2, and CDK2/CycE all catalysed detectable JMJD7 T37 phosphorylation. Interestingly, the most effective kinase combinations inducing JMJD7 T37 phosphorylation were CDK2/CycA2, followed by CDK1/CycB1. Although we cannot rule out these differences being explained by intrinsic differences in the specific kinase activities of the complexes tested, the results could be consistent with relatively strict requirements for specific CDK/cyclin combinations. Perhaps consistent with the cell cycle analyses (Figure 5.4b, 5.5b and 5.6b), CDK2/CycA2 is an S-phase associated kinase complex and CDK1/CycB1 is essential for mitosis and proper division of cells.

Having further implicated CDK1/2 as JMJD7 T37 kinases we wanted to compare the JMJD7 T37 phosphorylation 'motif' to that of known CDK substrates. Using the "substrate" option on PhosphositePlus (Hornbeck et al., 2015), the substrate recognition logos of CDK1 and CDK2 were aligned with the JMJD7 sequence. As expected, the CDK1 and CDK2 minimum recognition motif [S/T]-P is consistent between the sequence logo and JMJD7 (Figure 5.13d). Higashi et al. (1995) published a CDK recognition sequence P-X-[S/T]-P-X-B-X-X, where B is any basic residue, which may be consistent with the histidine found at H40 (T37+3) on JMJD7. Other studies have since identified modified versions of this sequence: P-X-[S/T]-P-X-Y-Y-Y, where Y is either K or R; or P-X-[S/T]-P-X-Z-Z-Z, where at least one residue in the Z position must be either K or R (Higashi et al., 1995, Stevenson-Lindert et al., 2003, Suzuki et al., 2015). We next dissected the CDK1 and CDK2 substrate information on PhosphositePlus to investigate whether the H40 could be sufficient to support the basic residue requirements of a CDK-substrate interaction. Figure 3.13e shows the alignment of the known substrates of CDK1 and CDK2 in which a Histidine

is found at +3 position but no arginine or lysine in the proceeding 5 residues from the point of phosphorylation. Interestingly, *bona fide* CDK1/CycB substrate, SIRT1, displays a very similar sequence to that found on JMJD7 (Sasaki et al., 2008). Together, the results presented in this Chapter suggest that specific CDK1/2/Cyclin complexes may be involved in directly targeting JMJD7 T37 phosphorylation in cells.

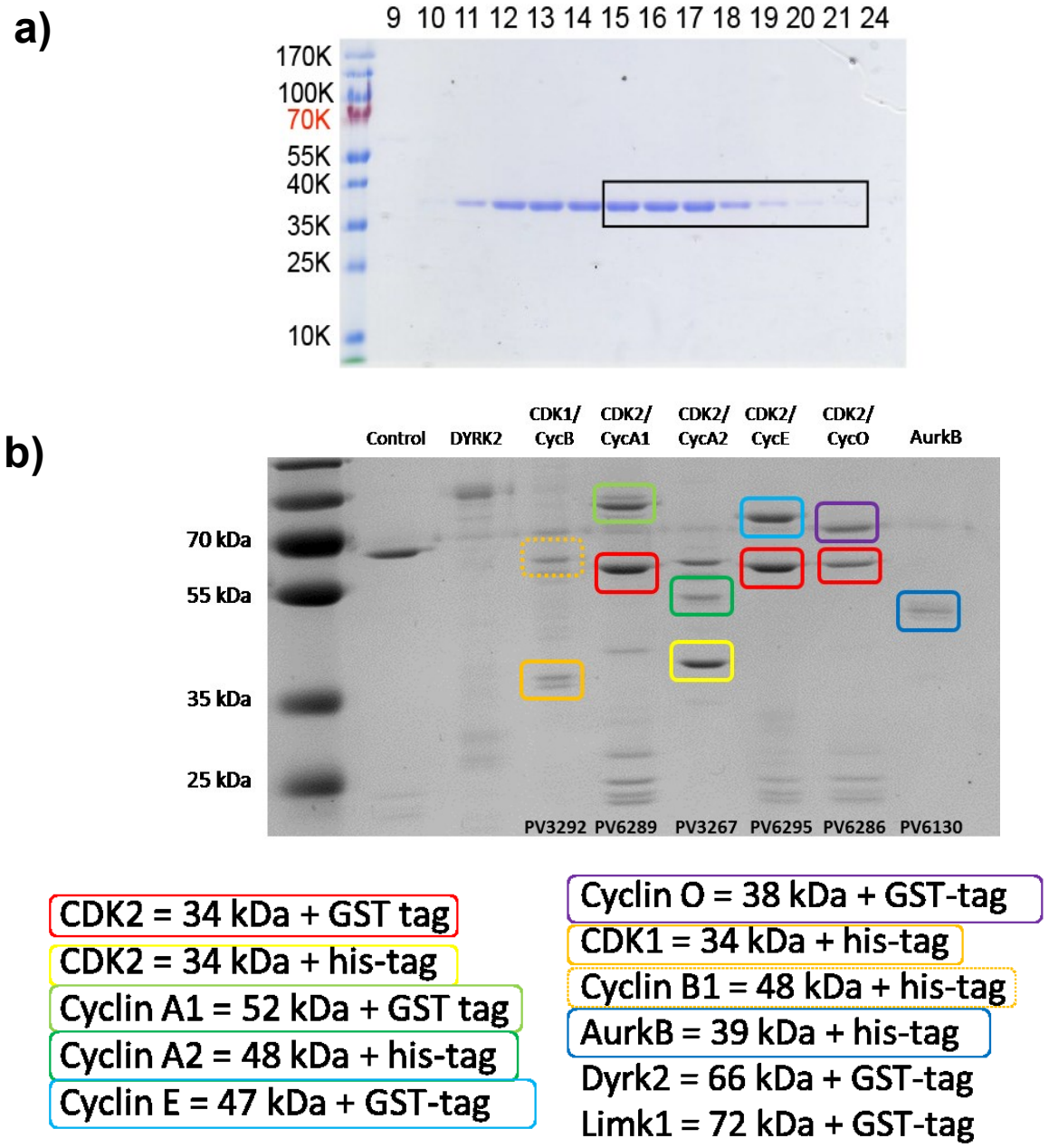

Figure 5.13. CDK1/2 complexes can phosphorylate JMJD7 T37 *in vitro*. a) Coomassie gel showing the recombinant His_6-tagged JMJD7 protein donated by Dr. Malkolovic, Oxford University. The protein fractions marked by the blue box were pooled for use in kinase assays. b) coomassie gel of recombinant kinases purchased from Thermo. Kinase concentrations were equalised for future experiments.

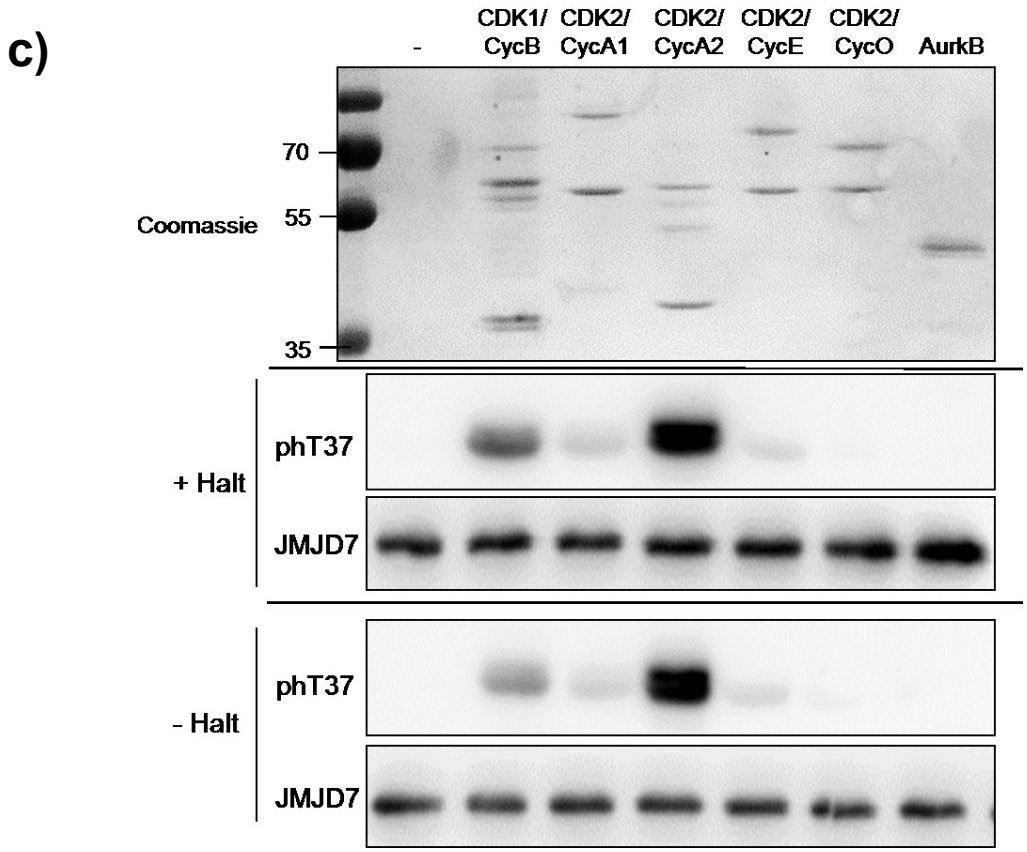

Figure 5.13. CDK1/2 complexes can phosphorylate JMJD7 T37 *in vitro*. c) Western blot after kinase assay. "Kinase only" coomassie gel shows equal loading of kinases, it was run alongside kinase assay sample without JMJD7 because the JMJD7 protein confounded the kinase bands. His_6-JMJD7 was incubated in kinase assay buffer with or without recombinant kinases. The samples were split into two, one set with phosphatase inhibitor, and one set without and then incubated at 30°C for 10 minutes. Western blot shows that CDK1/CycB, CDK2/CycA1, CDK2/CycA2 and CDK2/CycE are able to catalyse JMJD7 T37 phosphorylation *in vitro* with CDK1/CycB and CDK2/CycA2 displaying highest activity. Halt was used as a phosphatase inhibitor as the recombinant kinases were all grown in insect cells. n=2.

d)

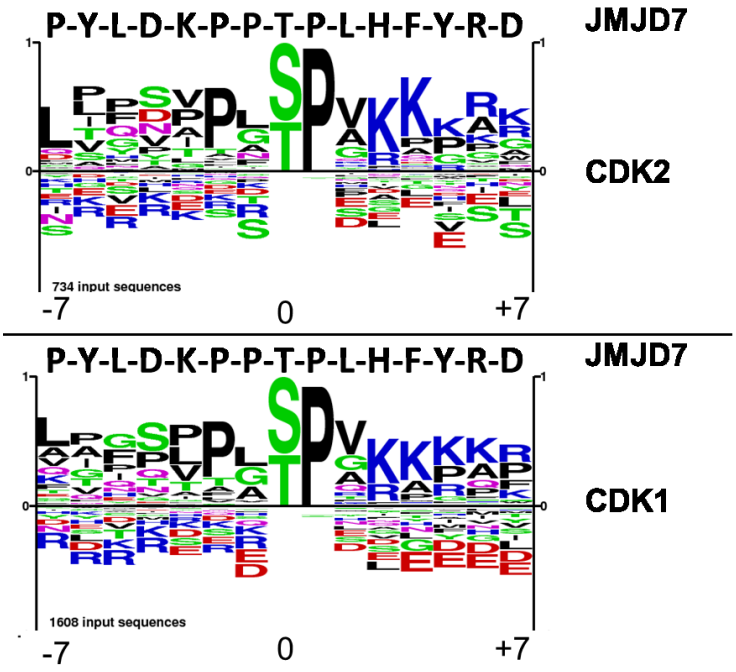

e)

CDK1

JMJD7 - T37 : PYLDKPP[Tph]PLHFYRD
SIRT1 - T530: YLSELPP[Tph]PLHVSED
TP73 - T86 : AASASPY[Tph]PEHAASV
MDM2 - T216: SSSESTE[Tph]PSHQDLD
EPB41 - T60 : LKASNGD[Tph]PTHEDLT

CDK2

JMJD7 - T37 : PYLDKPP[Tph]PLHFYRD
NOBI - T121: SSIQHPE[Tph]PLHISGF
TP73 - T86 : AASASPY[Tph]PEHAASV
MDM2 - T216: SSSESTE[Tph]PSHQDLD

Figure 5.13. d) JMJD7 T37 sequence compared with CDK1 and CDK2 recognition sequences generated by PhosphositePlus (Hornbeck et al., 2015). e) The CDK1 and CDK2 substrates with a Histidine at +3 without any other lysine or arginine residues within 5 residues C-terminal. SIRT1 T530 is the most similar to JMJD7 and is phosphorylated by CDK1/CycB *in vivo* and *in vitro* (Sasaki et al., 2008).

Discussion

Within this chapter, we have investigated a role for JMJD7 within the cell cycle. We found that while T37 phosphorylation levels did not respond to other cell stresses, serum starvation was able to significantly reduce phosphorylation. Consistently, T37 phosphorylation was regulated throughout various stages of the cell cycle. We then began to explore what the upstream kinases might be through experimental approaches including kinase inhibitors, kinase assays (both in house and external) and mass spectrometry. Here, we have determined candidate kinases within the CDK family of kinases and corroborated our findings with bioinformatic analysis.

To explore how JMJD7 phosphorylation was regulated we first commissioned the production of a T37 phospho-specific antibody. We found that although the antibody works well with over expressed JMJD7, the limits of detection were reached when using endogenous JMJD7. There may be several reasons for the lack of sensitivity of the phT37 towards endogenous JMJD7. Firstly, the affinity of the phT37 antibody to the antigen could be lower for JMJD7 than that of other “non-specific” bands seen in the western blots. Second, if endogenous JMJD7 is not expressed as highly as the cross-reactive bands this would interfere with sensitivity and detection. Furthermore, the total amount of endogenous JMJD7 that is phosphorylated in cells is unknown: If total JMJD7 expression is low and phT37 is minimal under ‘basal’ conditions this could also account for issues with sensitivity. While exploring how JMJD7 is phosphorylated during the cell cycle this background band was also observed. In Figures 5.5b and 5.6b it is possible that the background band is partly causing the apparent increase or reduction in phosphorylation. Therefore, any future experiments

should include an immunoprecipitation of the overexpressed JMJD7 to dissect the over expressed from any endogenous bands.

Although proteins cross-reacting with the phT37 antibody were problematic, they were of interest because they were often regulated similarly (e.g. Figure 5.4, and data not shown). We hypothesise that these proteins may in fact be targeted by the same kinase that modifies JMJD7 T37, which might be consistent with an abundant kinase with multiple substrates. Although we attempted to identify these cross-reacting proteins and their phosphorylation site by mass spectrometry, the phT37 antibody did not work well enough for immunoprecipitation.

Cell cycle analysis indicated that JMJD7 phT37 is upregulated at around early to mid S-phase, down regulated at late S and then potentially upregulated again in G2/M. Kinase inhibitor profiling experiments and an unbiased proteomic screen suggested the JMJD7 T37 kinase was related to a CDK, particularly CDK2. CDK2 activity is cell cycle regulated, and can be found associated with CycE towards the end of G1 and into early/mid S phase (Dyson, 1998). The CDK/CycA2 complex forms during mid-S-phase and is active until the early stages of Mitosis (De Boer et al., 2008). Consistent with this, we found that CDK2/CycA2 was able to phosphorylate JMJD7 *in vitro*. Furthermore, we also observed CDK1/CycB1 activity towards phT37, highlighting that JMJD7 could perhaps be phosphorylated by multiple CDK/Cyclin complexes, similar to other *bona fide* CDK1/CDK2 substrates (Zeng et al., 2011, Errico et al., 2010). Indeed, this may also be indicative of functional compensation by different CDK1/2 complexes, as previously demonstrated (L'Italien et al., 2006).

Although our studies in this Chapter have focussed on characterising the JMJD7 T37 kinase, our findings might have implications for our understanding of JMJD7 biology. For example, the observation that phT37 levels oscillate during S-, G2- and M- phase of the cell cycle could suggest that the JMJD7 pathway is linked to the cell cycle for some reason. Interestingly, both JMJD7 substrates, DRG1 and DRG2, have been implicated in the cell cycle (Jang et al., 2016, Lu et al., 2016, Schellhaus et al., 2017). DRG1 knockdown is reported to cause a G2/M phase cell cycle arrest due to altered microtubule stability (Lu et al., 2016, Schellhaus et al., 2017). Furthermore, DRG2 protein expression is upregulated during G2/M and DRG2 knockdown causes a G2/M arrest (Song et al., 2004a). Consistently, DRG2 upregulation was observed after double thymidine block in line with phT37 regulation in mid S-phase and G2/M phase (Figure 5.4b). The mechanisms by which DRG2 might regulate the cell cycle are not yet fully understood, though it is has been proposed to function upstream of the CDK1/CycB1 inhibitors, p21, Wee1 and Myt1 to regulate CDK1/CycB1-mediated progression through mitosis (Jang et al., 2016).

Although the work presented here points towards CDK1/2 activity being involved in catalysing JMJD7 T37 phosphorylation the experiments come with some limitations that will need to be addressed in future work. Firstly, one of the major flaws of inhibitor studies is specificity. In the case presented here, although SNS032 and RO-3306 were able to significantly inhibit JMJD7 phosphorylation, an alternative CDK2 inhibitor, BMS265246, did not recapitulate this in the conditions tested. While it is possible that BMS265246 is not targeting CDK2 or CDK1, it is also possible that both RO-3306 and SNS032 are targeting different kinases that are responsible for JMJD7 phosphorylation. Indeed, lack of specificity is an accepted problem with

kinase inhibitors, including for CDKs (Asghar et al., 2015). That being said, we did test RO-3306 under conditions which are considered appropriate for CDK1-specific inhibition (Yang et al., 2013, Marceaux et al., 2018).

Time course experiments involving RO-3306 highlighted that JMJD7 T37 phosphorylation might be very dynamically regulated. For example, T37 phosphorylation was rapidly restored following the removal of RO-3306 (Figure 5.11c). Likewise, T37 phosphorylation was rapidly lost following treatment with RO-3306 (Figure 5.11a and 5.11b). One possible explanation for such a rapid loss of JMJD7 phosphorylation following RO-3306 treatment is that the modification is rapidly reversed. This raises the possibility that there is an as yet unidentified JMJD7 phospho-T37 phosphatase. The importance of protein phosphatases in cell cycle control is widely accepted (Barr et al., 2011). The tight balance between phosphorylation and dephosphorylation on cell cycle associated proteins keeps enzyme activation and proper transition under control (Asghar et al., 2015, Hunter, 1995). Furthermore, positive and negative feedback loops involving kinases and phosphatase are seen throughout cell cycle biology. Of note, CDK1/CycB1 is predominantly regulated by two positive feedback loops in preparation for mitosis (Lindqvist et al., 2009). The inhibitory phosphorylation of CDK1 on T14 and Y15 is catalysed by kinases Wee1 and Myt1. Simultaneously, T14 and Y15 are dephosphorylated by Cdc25. Active CDK1/CycB1 mediates the inactivating phosphorylation of both Wee1 and Myt1, which in turn reduces CDK1/CycB1 inhibitory phosphorylation. Moreover, active CDK1/CycB1 targets Cdc25 which promotes its activity, and in turn, decreases CDK1/CycB1 phosphorylation (O'Farrell,

2001). It might be interesting in light of the data and discussion above to test whether Cdc25 is able to dephosphorylate JMJD7 T37.

In the absence of a validated proteomic method to identify upstream kinases of a novel phospho-protein, we adapted an RO-3306 treatment and release protocol to try and identify 'stimulus'-induced JMJD7 kinases. The RO-3306 MS identified two potential kinases bound to JMJD7 whose binding was increased upon release (CDK2 and AurkB) that, according to the MRC inhibitor database, are effectively inhibited by RO-3306. Although the approach might be valid, it was not without limitations. For example, on this occasion the release from RO-3306 was sub-optimal, possibly owing to ineffective wash out or loss of phosphorylation after lysis. Furthermore, given that all CDKs require cyclins for substrate recognition and activity (Swaffer et al., 2016), it was anticipated that a cyclin would be detected in complex with the CDK2 that was co-purified with JMJD7. However, no cyclin was detected specifically bound to JMJD7. Due to the transient and dynamic nature of kinase/substrate interactions it could be that the cyclin was lost during lysis or IP. Furthermore, high background binding of CDK1 to the "Empty vector" control sample may have confounded any specific detection of cyclin binding to JMJD7 in this screen (data not shown). Future work should focus on optimising the release and investigating the presence of cyclins and CDK1 by IP-western blotting.

Finally, we confirmed the activity of recombinant CDK2/CycA2 and CDK1/CycB1 towards phT37 in an *in vitro* kinase assay and compared the recognition motifs of other CDK substrates and JMJD7. The amino acid sequence spanning JMJD7 T37 fits with the previously described recognition motif P-X-Tph-P-X-B-X-X (where B is a basic amino acid), further strengthening evidence that JMJD7 may be

phosphorylated by CDK1 and/or CDK2 (Higashi et al., 1995). Interestingly, there is significant crossover found between CDK1 and CDK2 targets, perhaps consistent with JMJD7 being phosphorylated by both CDK1 and CDK2 at different stages of the cell cycle, or under different contexts. However, we cannot rule out Aurora kinase B as having kinase activity on JMJD7. Similar to other enzymes described within this thesis, AurkB is regulated by upstream modification. To the best of our knowledge all recombinant kinases purchased herein were active (shown by activity assay on ThermoFisher datasheet). However, activation and substrate specificity of AurkB is dependent upon its modification (Petsalaki et al., 2011, Pike et al., 2016), therefore, if AurkB was insufficiently modified prior to use it could have caused a false negative.

Future experiments could include over-expression of candidate kinases to identify those that are sufficient to promote JMJD7 phosphorylation. However, caution should be taken with interpretation of overexpression data as it is possible for a kinase to overcome specificity stringency and become delocalised when over-expressed (Moriya, 2015). Importantly, loss-of-function approaches targeting endogenous CDK1 and CDK2 levels will be critical for confirming the identity of the JMJD7 T37 kinase. Such experiments are not without their own caveats however, as CDK1 or CDK2 knockdown cause cell cycle arrest (Long et al., 2010, Satyanarayana and Kaldis, 2009), and CDK1 and CDK2 can compensate for each other, both of which could complicate interpretation of the results.

Chapter 6
Final Discussion

6. Overview

The overall objective of this Thesis was to contribute to our understanding of the regulation and function of the poorly characterised lysyl hydroxylase, JMJD7. In Chapter 2 we defined the cellular localisation and oligomerisation state of JMJD7, explored its functional conservation, and demonstrated that it is required for cellular growth control. Chapter 3 presented bioinformatic analyses of online cancer databases which, although complex, highlighted a potential role for JMJD7, DRG1 and DFRP1 as novel tumour suppressors. Analysis of JMJD7 cancer mutants highlighted a potential N-terminal regulatory domain in which we identified and characterised a novel phosphorylation site: In Chapter 4 we showed that mutation of this phosphorylation site inhibits the role of JMJD7 in growth. This led us to explore the regulation of JMJD7 T37 phosphorylation in Chapter 5, and to investigate the kinase responsible. Our results suggested that JMJD7 phosphorylation is likely mediated by CDK1 and/or CDK2 (or related) complexes and at multiple stages of the cell cycle. Here in this Final Discussion we discuss potential limitations of the work, suggest future directions, and explore the wider implications of our findings.

6.1 JMJD7 in Growth Control

In Chapter 2 we showed that shRNA knockdown of JMJD7 slowed the proliferation of multiple different cell lines, indicating that JMJD7 is required for growth control. This observation may be consistent with the findings of others. Recently, Liu et al. (2017a) reported that CRISPR-mediated knockout of JMJD7 resulted in fewer colonies in a soft agar assay. Furthermore, Ding et al. (2013) previously observed, in an siRNA screen for histone modifiers regulating metastasis, that JMJD7 was required for the invasion of squamous cell carcinoma cells. How JMJD7 might support cell

proliferation and whether such mechanisms are also involved in supporting cell invasion and 3D growth is unclear. However, since the only clear function of JMJD7 thus far is as a protein lysyl hydroxylase, one hypothesis is that these JMJD7-associated phenotypes may be mediated by its substrates, DRG1 and DRG2. Interestingly, both DRG1 and DRG2 have both been associated with growth control via links with mitosis and the G2/M checkpoint of the cell cycle (Lu et al., 2016, Jang et al., 2016). Furthermore, over-expression of DRG1 is able to promote cell transformation by the Ras and Myc oncogenes (Mahajan et al., 1996), and high expression correlates with poor survival in hepatocellular carcinoma (Jiang et al. (2016). These reports would suggest that JMJD7 substrates may be good candidates acting downstream of JMJD7 in growth control. However, it is not yet clear whether the role of JMJD7 in growth in our cell models is 'activity-dependent', which would be necessary to support the hypothesis that DRG1/2 modification is involved. Future work could address this question using the type of 'rescue' models developed in Chapter 4. Such work would complement future efforts to more exhaustively investigate the role of T37 phosphorylation in DRG1 versus DRG2 hydroxylation (discussed further below).

6.2 Paradox? JMJD7 supports cell growth but may be a tumour suppressor

In Chapter 3 we explored a role for JMJD7 in cancer. Using a bioinformatics approach we interrogated publically available databases to identify any associations between altered expression of JMJD7 pathway components and the prognosis of gastric cancer patients and collated data on genetic alterations across cancer types. Unsurprisingly perhaps, considering the difference in tumour genetics between cancer types (Vogelstein et al., 2013), and the heterogeneity of tumours even within

a single cancer (Hanahan and Weinberg, 2011), the findings were not clear cut. That being said, the available evidence may support a role for JMJD7, DRG1 and DFRP1 as tumour suppressors. We observed reduced mRNA expression in patients with worse prognosis, and a variety of missense mutations that were distributed throughout the genes in a pattern that might indicate functional significance. Preliminary analyses indicated that a significant proportion of JMJD7 cancer mutants prevent the normal expression of the JMJD7 protein.

Our data supporting a potential tumour suppressor role of JMJD7 may appear at odds with observations highlighting that JMJD7 is required for growth, consistent with a more oncogenic role. Likewise, any potential involvement of DRG1/DFRP1 downstream of JMJD7 may appear to be in conflict with the role of this complex in supporting growth and promoting transformation (see above). A simple explanation for these apparent contradictions might be that these genes have complex and context-dependent roles in different tumours and cancer types. Although this is almost certainly true, it is also possible that this apparent paradox is a reflection of the biological function of JMJD7 and the DRG1/DFRP1 versus DRG2/DFRP2 pathways, and the consequence of their deregulation. Next we will explore potential scenarios that could account for the paradoxical roles of the JMJD7 pathway in cancer.

In the first example, a cancer-associated gene functions in a cell process that supports growth, but partial loss of function can initiate tumourigenesis in some contexts due to deregulation of other fundamental cellular processes, such as genome stability. For example, DNA Polymerase Delta (POLD) is part of the machinery responsible for DNA replication and repair, and is therefore required for

normal cell division (Nicolas et al., 2016, Song et al., 2015). However, because of its critical role in DNA replication and repair, loss of POLD1 (the catalytic subunit of POLD) is associated with genome instability and cancer progression (Albert et al., 2014, Nicolas et al., 2016, Song et al., 2015, Tumini et al., 2016, Prindle and Loeb, 2012).

In the second scenario, a cancer-associated gene regulates two or more downstream pathways, some of which have opposing roles in tumourigenesis. For example, one pathway might be oncogenic, whilst another pathway is tumour suppressive: In different contexts or tissue types one pathway could be more dominant than another. For example, E2F1 is a transcription factor involved in cell cycle progression, DNA synthesis, checkpoint control, apoptosis, DNA repair, metabolism and development (Johnson and Degregori, 2006, Poppy Roworth et al., 2015). Evidence has shown that inactivation of E2F, in different contexts and different tissue types can have varying effects on tumorigenesis due to the activation and inactivation of specific downstream pathways that operate in a context-dependent manner (Johnson, 2000, Johnson and Degregori, 2006, Pierce et al., 1999, Poppy Roworth et al., 2015, Dubrez, 2017). As such, inactivation of E2F1 can suppress lymphoma development, while in squamous epithelial cells E2F1 inactivation accelerates tumorigenesis (Baudino et al., 2003, Rounbehler et al., 2002).

The possibility that such scenarios could be relevant to the apparent paradoxical roles of the JMJD7 pathway in cancer may be supported by similar observations on closely related protein hydroxylases. For example, the arginyl hydroxylase JMJD5 has been implicated in tumour progression *and* suppression (Chen et al., 2014, Zhang et al., 2015). Perhaps similar to the POLD1 example presented above, JMJD5

functions in homologous recombination and genome integrity (Amendola et al., 2017, Suzuki et al., 2006), and is also required for normal cell growth and development (Ishimura et al., 2012, Oh and Janknecht, 2012). The histidyl hydroxylase MINA53 is reported to be required for tumour cell proliferation, yet has also been implicated as a tumour suppressor gene (TSG) that suppresses metastasis (Yu et al., 2014, Teye et al., 2004, Tsuneoka et al., 2004, Tsuneoka et al., 2002). It has been proposed that the pro-growth role of MINA53 is explained by a role for its activity in ribosome biogenesis, whereas the tumour suppressor function is explained by a different substrate with a function in the epithelial-mesenchymal transition (EMT) pathway (Geng et al., 2017, Yu et al., 2014) (M. Coleman, personal communication).

Can the biological functions of DRG1 and DRG2 potentially explain the paradoxical role of the JMJD7 pathway in cancer? Which of the two scenarios above could explain this paradox? Although these are important questions, further consideration could require a more detailed understanding of the precise functions of DRG1 and DRG2. In general, the available DRG literature assumes that DRG1 and DRG2 are highly-related and -conserved homologs that are functionally redundant (Daugeron et al., 2011, Li and Trueb, 2000). Human DRG1 and DRG2 show similar sequence identity (57%), and their yeast orthologues are both associated with the translating ribosome, with at least one study reporting functional redundancy (Li and Trueb, 2000, Francis et al., 2012, Daugeron et al., 2011). Whether DRG1 and DRG2 are functionally redundant in higher eukaryotes is unclear however, although our own observations might suggest that independent biological roles might (also) exist. For example, we showed differential sub-cellular localisation of DRG1 and DRG2 in Chapter 2: Although both proteins were expressed in the cytoplasm (perhaps

consistent with a role in translation), DRG1 and DFRP1 were also detected in the nucleus, possibly indicating an additional function. To explore the function of DRG1 and DRG2 in an unbiased manner (for the first time), Dr Qinqin Zhuang (Coleman group) performed a proteomic screen using FLAG-tagged DRG1 or DRG2 as bait. Interestingly, he identified that DRG1 and DRG2 have very different interactomes that are largely non-overlapping, again consistent with non-redundant functions of these JMJD7 substrates. Specifically, Dr Zhuang found that DRG1 associates with components of a nuclear histone chaperone complex involved in DNA replication, transcriptional elongation, and cell proliferation. In contrast, DRG2 was found to associate with components of a cytoplasmic translation factor complex that is essential for cell growth and protein synthesis. The exact roles of DRG1 and DRG2 in these respective complexes are still being investigated. However, we hypothesise that JMJD7's role in cancer may fit with a model similar to the scenarios described above. We propose that JMJD7-mediated hydroxylation of DRG1 and DRG2 supports their pro-growth roles in histone chaperone activity (DRG1) and protein translation (DRG2). However, in some contexts, inactivation of JMJD7 or DRG1/DFRP1 could limit the activity of the nuclear histone chaperone pathway, potentially leading to replication and/or transcription 'stress', processes now heavily implicated in causing DNA damage and genome instability in cancer (Hanahan and Weinberg, 2011, Silvera et al., 2010).

6.3 JMJD7 mutation and phosphorylation

Our cancer bioinformatics analyses identified recurrent and 'hot-spot' missense mutations in JMJD7 and downstream pathway components. Such mutational patterns are often indicative of functional consequences that provide a selective

advantage (Miller et al., 2015). As such, 'driver' mutations often occur in functional domains and regulatory motifs. For example, p53 is a transcription factor whose tumour suppressor functions are inactivated by recurrent and hot-spot missense mutations that cluster in its DNA binding domain (Pavletich et al., 1993). Furthermore, recent global analysis of single nucleotide variants has identified mutational hot-spots in TSGs and oncogenes within regions regulated by phosphorylation (Reimand et al., 2013). For example, Reimand et al. (2013) found beta-catein (CTNNB1) was mutated 73 times in the region spanning the phosphosite, S37, leading to constitutive activation and tumour progression. Therefore, identifying enrichment of cancer mutations in poorly characterised cancer-associated genes could help to highlight novel functional and regulatory domains. Indeed, we observed mutation hot-spots in JMJD7 pathway components that fell outside of currently assigned functional domains. One of these, at the very N-terminus of JMJD7, was of particular interest because it was centred round a site that proteomic screens had identified as being phosphorylated. We went on to confirm phosphorylation of JMJD7 T37 by mass spectrometry and antibody-based detection. To test the potential function of T37 phosphorylation, in the absence of having identified the relevant kinase(s), we focussed on the use of blocking (T37A) and mimetic (T37E) mutations. We found that T37 mutation did not significantly affect dimerisation, subcellular localisation, or DRG binding. Our MS analysis did not identify any difference between the capacity of JMJD7 WT or T37A to hydroxylate DRG2. As previously discussed, this assay presented limitations with respect to DRG1. Future work should focus on quantification of DRG1 and DRG2 hydroxylation in the presence of JMJD7 WT, T37A and T37E, possibly using epitope-tagged DRG expression constructs (to overcome

problems of endogenous antibody-based DRG1 purification). Additionally, sensitive (non-saturated) *in vitro* assays could be useful to identify any small differences in JMJD7 activity. Overall, it remains possible that JMJD7 T37 phosphorylation controls substrate specificity, regulating hydroxylation of a given DRG protein under specific conditions. This possibility would be analogous to a report that phosphorylation of the HIF prolyl hydroxylase PHD1 by CDK1 switches its specificity towards an alternative substrate: PHD1-mediated hydroxylation of CEP192, an essential component of centrosomal maturation machinery, is proposed to regulate CEP192 ubiquitination and, in turn, degradation during interphase (Moser et al., 2013, Ortmann et al., 2016).

Generally, the approach taken in this Thesis, and discussed above, to study the function of T37 phosphorylation has taken a 'candidate' approach: Testing hypothesise based on existing knowledge of JMJD7 biochemistry. Future work could be complemented by taking a more 'unbiased' approach, possibly using proteomics. For example, MS-analyses of the interactomes of WT versus T37A and T37E JMJD7 might identify one or more proteins whose binding is regulated by T37 phosphorylation. Preliminary work in this area suggested that it might be a worthwhile line of investigation in the future (data not shown).

In the absence of identifying a substantial role for T37 phosphorylation in regulating functions 'proximal' to JMJD7 (e.g. activity, dimerisation etc), we turned our analyses to investigating its role in the JMJD7-mediated growth control identified in Chapter 2. We found that the expression of JMJD7 T37A was unable to rescue the reduced growth phenotype of cells following endogenous JMJD7 knockdown. How T37 phosphorylation supports the function of JMJD7 in growth control is not yet clear, but the simplest hypothesis might be that it is via effects on enzyme activity. As

discussed above, a critical experiment for the future therefore would be to determine the role of enzyme activity in JMJD7-mediated growth control, possibly by reconstituting JMJD7 knockdown cells with an H178A inactive mutant.

The analysis of less proximal JMJD7 phenotypes such as growth was useful in order to understand its potential importance. Therefore, it might be fruitful during future investigation if the effect of T37 mutants are also tested in other similarly 'global' phenotypes. For example, because of the potential role of the JMJD7 pathway in translational control it would be interesting to test the effect of reconstituting T37 mutants in JMJD7 loss-of-function models on protein synthesis. Our preliminary experiments indeed confirmed that JMJD7 is positively regulating translation (data not shown). However, due to time limitations we were unable to perform the necessary biological replicates to pinpoint the effect of T37 mutation.

6.4 phT37 Kinase Identification

Investigating the function of JMJD7 T37 phosphorylation will be greatly supported by identification of the kinase involved, for two main reasons. Firstly, modulating phosphorylation levels by up- and down-regulating kinase activity will allow functional studies in the absence of JMJD7 mutation. Secondly, the identity of the kinase might provide some further insight into the biological role of JMJD7 T37 phosphorylation, which could help guide new lines of investigation. To this end, we took multiple approaches to try and identify the T37 kinase, including an *in vitro* kinase screen, focussed analyses of kinase inhibitors, and an unbiased proteomic screen. Overall, our data suggested that CDK1 and/or CDK2 might be responsible for the phosphorylation of JMJD7 T37 (many of the limitations and urgent future directions in relation to these findings were already described in detail in the discussion of

Chapter 5). The preliminary assignment of CDK1 is of particular interest with respect to its role in regulating PHD1 activity (Ortmann et al., 2016). Together with the work presented here, this raises the intriguing possibility that regulation of hydroxylase function might be an emerging role of CDK1.

Our assignment of CDK1/2 as potential JMJD7 T37 kinases is also of interest with respect to our other data on JMJD7 localisation and novel localisations and function of DRG1 versus DRG2. Our data in Chapter 2 highlighted that JMJD7 is localised predominantly within the cytoplasm, with a small amount present in the nucleus, similar to DRG1. Interestingly, both of our candidate kinase complexes, CDK2/CycA and CDK1/CycB can shuttle between the nucleus and the cytoplasm throughout interphase until mitosis, when they are rapidly translocated into the nucleus (Jackman et al., 2002). Neither CDK2 nor CyclinA2 has a consensus NLS and it is predicted that they 'piggy back' into the nucleus via the NLS of binding proteins (Jackman et al., 2002). In Chapter 4 we used bioinformatic prediction analysis to determine if JMJD7 contained any NLS or NES sequences. Although, one potential NES sequence was found proximal to T37 we did not observe any major effects of T37 mutation of JMJD7 localisation. However, it would be interesting to identify where in the cell JMJD7 T37 is being phosphorylated, perhaps using methods available to block nuclear export and import (Bedard et al., 2007). It would be interesting to integrate such studies with those on DRG binding and hydroxylation.

6.5 JMJD7 T37 phosphorylation and Cancer

Since T37 phosphorylation positively contributes to the role of JMJD7 in promoting cell proliferation it could perhaps also play a role in supporting tumourigenesis. This hypothesis might predict that JMJD7 T37 kinases were themselves pro-growth

kinases with oncogene-like properties. Indeed, CDKs are essential for cell division and are heavily implicated in tumourigenesis: CDKs and their regulatory proteins are often deregulated in cancer (Canavese et al., 2012, Asghar et al., 2015, Hall and Peters, 1996). Mechanisms of deregulation include ectopic localisation, gene over expression, constitutive activation, and upstream regulator deregulation i.e. kinases, phosphatases and cyclins. For example, high CDK1 *activity* correlated with poor prognosis in colon cancer (Zeestraten et al., 2012). Interestingly, the association between expression of CDK1 and CDK2 has been assessed in breast cancer patients (Kim et al., 2008). Kim et al. (2008) showed that when the ratio of CDK2 *activity* is high compared to CDK1 the prognosis is poor, although the mechanisms are unclear. Furthermore, the impact of individual CDK activity was also analysed in patient prognosis and they found that high activity of both CDK1 and CDK2 were unfavourable to survival (Kim et al., 2008). Similarly, the expression levels of the CDK regulators CycA and CycB have also be assessed in the context of cancer prognosis (Florenes et al., 2001, Fang et al., 2014, Nimeus-Malmstrom et al., 2010, Zhou et al., 2014). For example, high CycB and CycA expression correlated with poor prognosis breast cancer (Winters et al., 2001, Bukholm et al., 2001, Sun et al., 2017). On the other hand, CycA siRNA depletion was associated with abnormal spindle formation during mitosis, suggestive of opposing roles in this context (Li et al., 2018a). As a result of their importance in cancer, CDKs have become attractive targets for therapeutic intervention both alone and in combination with other treatments (Ardito et al., 2017, Canavese et al., 2012, Garrett and Fattaey, 1999). As such, there are 31 active clinical trials worldwide (www.clinicaltrials.gov) and three FDA approved CDK inhibitors for the treatment of breast cancer (de Groot et al.,

2017). Of the CDK inhibitors screened in this Thesis flavopiridol, RO-3306 and SNS032 were able to inhibit JMJD7 phosphorylation. Interestingly, flavopiridol was the first CDK inhibitor to enter clinical trials and currently an orphan drug designation by the FDA for the treatment of rare diseases (Wiernik, 2016). Furthermore flavopiridol is in phase II clinical trials for the treatment of various lymphomas (Tong et al., 2010, Boffo et al., 2018). Similarly, SNS032 is also in clinical trial for multiple myeloma and chronic lymphomatic leukemia and solid tumours (www.clinicaltrials.gov) (Balakrishnan et al., 2016). It would be interesting to explore what role altered JMJD7 T37 phosphorylation might play in the efficacy of such inhibitors.

With respect to the potentially paradoxical roles of JMJD7 in cancer, it is also interesting to consider the functional consequences of cancer mutations in the hot-spot surrounding T37. For example, if T37 phosphorylation supports JMJD7 function (as in growth), and loss of function promotes tumourigenesis, then one role of these cancer mutations could be to prevent T37 phosphorylation. Future work should test whether cancer mutations surrounding T37 inhibit phosphorylation by CDK1/2.

Taken together, we predict that JMJD7 is being phosphorylated at two distinct stages of the cell cycle (Figure 7.1). A G1/S phase block with thymidine, and mitotic block using nocodozole indicate that JMJD7 phosphorylation is increased at these stages. This is consistent with our observation that CDK1/CycA2 and CDK1/CycB1 complexes can phosphorylate JMJD7 *in vitro* (Figure 7.1). Interestingly, CDK2/CycA2 is a *bona fide* S-phase kinase complex with a multitude of substrates involved in transcription and translation. Similarly, CDK1/CycB1 is known as the master regulator of the cell cycle and is most active during G2/M and throughout

mitosis. We hypothesise that this phosphorylation event could be acting as a molecular switch to define substrate specificity between DRG1 and DRG2 (Figure 7.1). In turn, hydroxylation of DRG1 and DRG2 by JMJD7 is regulating their roles in the cell cycle and transcription or translation, respectively (Figure 7.1). How hydroxylation is regulating the role of the DRGs is yet unknown, but of interest.

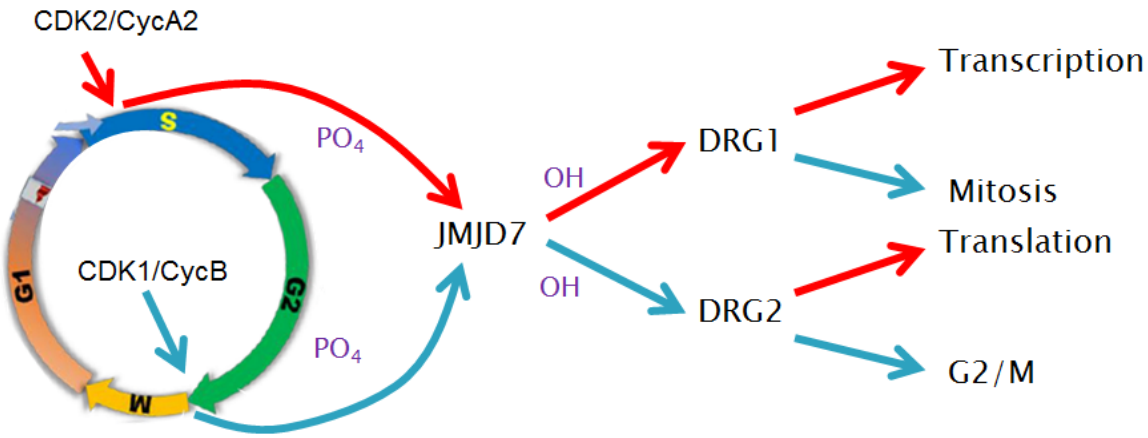

Figure 6.1 A Model to Demonstrate Our JMJD7 Hypothesis. We hypothesise that JMJD7 is phosphorylated during different phases of the cells cycle, specifically that S phase kinase complex CDK2/CycinA2 and G2/M kinase complex CDK1/CyclinB act upon JMJD7. This phosphorylation event mediates JMJD7's enzymatic activity towards DRG1 and DRG2, thereby regulating the function of DRG1 and DRG2 in transcription or translation, respectively, and their roles in the cell cycle.

6.6 Conclusion

The work presented in this Thesis has contributed to the characterisation of JMJD7 as a novel lysyl-hydroxylase, explored its genetic alteration in cancer, and identified a conserved phospho-threonine residue that is necessary for full JMJD7 function. We show that JMJD7 T37 phosphorylation is mitogen- and cell cycle-regulated, and potentially catalysed by cyclin-dependent kinases 1 and 2. Future efforts are necessary to fully understand the mechanism(s) by which JMJD7 is controlling growth, to clarify the effect of phosphorylation on JMJD7 hydroxylase activity, and to confirm CDK1/2 as physiologically relevant JMJD7 T37 kinases. It will be of interest to consider the findings in light of existing and emerging evidence that JMJD7 might act in a novel tumour suppressor pathway.

Chapter 7

Materials and Methods

7.1 Reagents

Where not specified, reagents were purchased from Sigma-Aldrich. Common laboratory solvents (e.g. ethanol, methanol) were purchased from Thermo-Fisher-Scientific.

7.1.1 Solutions

Phosphate Buffered Saline (PBS; 10X): 43 mM Na_2HPO_4, 14 mM KH_2PO_4, 1.37 M NaCl, 27 mM KCl, (ensure pH 7.4). This solution was diluted 1:10 with ultrapure H_2O to make 1x PBS

Phosphate Buffered Saline + Tween (PBST): 0.1% Tween20 (v/v) diluted in 1x PBS

Tris Buffered Saline (TBS): 20mM Tris, 150mM NaCl

Tris Buffered Saline + Tween (TBST): 20mM Tris, 150mM NaCl, 0.1% Tween20 (v/v)

SDS-PAGE Buffer: A 10x solution was purchased from GeneFlow (0.25M Tris, 1.92M Glycine and 1% w/v SDS). The 10x solution was diluted 1:10 for experimental use.

Western blot Transfer Buffer: A 10x solution was purchased from GeneFlow (0.25M Tris, 1.92M Glycine). To make a 1L solution: 100ml of 10x buffer was diluted with 200ml methanol and 700ml ultrapure H_2O.

Tris-Borate-EDTA (TBE) Buffer: 10x solution was purchased from Thermofisher and diluted 1:10 with ultrapure H_2O to make 1x TBE solution with the final concentration of 100mM Tris, 90mM boric acid, 1mM EDTA.

SDS-PAGE Resolving Gel Buffer (4X): 1.5M Tris-HCl pH 8.8, 0.4% (w/v) SDS.

SDS-PAGE Stacking Gel Buffer (4X): 0.5M Tris-HCl pH 6.8, 0.4% (w/v) SDS.

Laemlli buffer (6X): 125mM Tris pH6.8, 6% W/V SDS, 50% glycerol, 225mM DTT

JIES Lysis Buffer: 100mM $NaCl_2$ 20mM TrisHcl pH7.4, 5mM $MgCl_2$, 0.5% w/v Igepal

RIPA Buffer: 150mM $NaCl_2$ 5M EDTA, 1M Tris, 1% NP40, 0.5% NaDoxycholate, 0.1% SDS

3-(4,5-dimethyl-2-yl)-5-(3-carboxymethoxyphenyl)-2-(4-sulfophenyl)-2H-tetrazolium, inner salt (MTS) solution: 42mg MTS powder in 21ml DPBS, pH6-6.5, sterile filtered (0.2μM)

Phenazine methosulfate (PMS) solution: 0.92mg, 1ml DPBS, sterile filter (0.2μM)

Kinase assay buffer: 20 mM Tris (pH7.4), 10mM $MgCl_2$, 100 μM ATP, 0.25x Halt phosphatase inhibitor, 0.2 mM DTT, 1 μg 6-His JMJD7, 200 ng kinase.

7.1.2 Bacterial Reagents

Media and Reagents

Luria-Bertani media: 25g in 1L H_2O

Ampicillin: 50mg/ml dissolved in EtOH

7.2 Methods

7.2.1 Extraction of Bioinformatic Data from Online Tools

Genetic Alteration Frequency Graphs

cBioportal was used to identify mutations of JMJD7, DRG1, DRG2, ZC3H15 in all cancer types. The list was refined by cancer databases with more than 25 samples.

Kaplan Mayer Alteration Frequency Survival Graphs

Survival curves colorectal and lung adenocarcinoma were modified from online database cBioPortal (Cerami et al., 2012, Gao et al., 2013).

Kaplan Mayer High and Low Expression Survival Graphs
Survival curves in breast, lung, gastric and ovarian cancer were modified from online database KM Plotter (kmplot.com).

Genetic Mutation Maps
Mutation data was collected from public online databases (cBioPortal, COSMIC and COSMIC cell lines project) and extrapolated onto protein sequences downloaded from Uniprot (www.uniprot.org) (Cerami et al., 2012, Gao et al., 2013, Forbes et al., 2017).

7.2.2 Primer design
All custom primers generated by Sigma. For cloning primers the coding sequences (CDS) were obtained from online database (NCBI Nucleotide database) and analysed by NEB cutter online software to identify restriction enzymes that did not cut within the sequence. Epitope tag (FLAG or HA) was inserted into the coding sequence either after the initiating Methionine or before the stop codon. Each primer was no more than 99 bp long.

For overlapping SDM primers the sequences were between 27-35 bp long with the mutation in the middle of the primer. The primers were generated to be exactly complimentary and therefore efficiency of PCR was lower due to primer dimers forming. The primers were designed to have no more than a 60% GC content and a melting temperature not exceeding 78˚C and a G or C at the 3' end.

Phusion Site-Directed Mutagenesis primers were designed between 24-30 bp long. The mutation was in either the forward or the reverse primer close to the centre of the sequence. Primers were designed so that the 3' end of the reverse ends where

the 5' end of the forward starts with no overlap and no missing bases. See below for all primer sequences.

7.2.3 Polymerase Chain Reaction (PCR) for Cloning into Plasmid

Cloning PCR was achieved using Phusion High-Fidelity DNA polymerase (NEB: M0530) with primers designed for the specific gene and cloning strategy (Custom primers generated by Sigma). Annealing temperature of 58˚C was applied as standard. Extension times of 40 second per kb for cloning from cDNA, and 15 seconds per kb for less complex plasmid samples. The appropriate positive and negative controls were used for each PCR reaction.

7.2.4 Site Directed Mutagenesis (SDM)

Two SDM protocols were applied in this thesis:

The first used short overlapping primers (see below for primer sequences). Phusion High-fidelity polymerase standard protocol was used for PCR using 15 seconds extension time per kb of DNA with and without 3% DMSO. DpnI was used to digest any contaminating plasmid DNA. The PCR product was then imaged on a 1% agarose gel and subsequently PCR purified using the SIGMA GenElute™ PCR Clean-up Kit (Cat no: NA1020) and eluted in 50µl of elution buffer.

The second SDM approach followed the methods for Phusion Site-Directed Mutagenesis Kit (Thermofisher cat no: F541). The primers were HPLC purified and phosphorylated by the manufacturer (Thermofisher).

7.2.5 Restriction Digest

Restriction digest was carried out using High Fidelity Restriction Endonucleases (NEB) following manufacturer's protocol on plasmid and insert. For plasmid alone Calf Intestinal Phosphatase (NEB cat no: 0290S) digestion was done for 10 minutes

at 37 ˚C. Negative control included an undigested plasmid and positive control was plasmid cut with each enzyme alone.

7.2.6 Ligation

Insert was ligated into the plasmid using T4 DNA Ligase from NEB (cat no: M0202) using the equation:

$$\frac{size\ of\ insert\ (kb)\ \times ng\ of\ vector}{size\ of\ plasmid\ (kb)} \times\ Vector{:}\ insert\ ratio = ng\ of\ insert\ in\ reaction$$

A range of vector : insert ratios was used for each insert. Self-ligation control was a ligation without insert, and positive control re-ligated the insert which was cut out of the vector in the previous Restriction Digest step

7.2.7 Transformation

DH5α high competency *E.coli* (NEB Cat no: C2987) was thawed on ice and 10% ligation or SDM mix was incubated with the bacteria for 30 minutes. Each tube was then heat shocked in a water bath at 42˚C for 30 seconds followed by recovery on ice before adding SOC media and shaking at 37˚C. After one hour the cultures were spread on LB Agar plates containing 50µg/ml Ampicillin. Agar plates were left in a bacterial incubator overnight at 37 ˚C. PUC19 plasmid is provided with NEB DH5α High competency *E.coli* and was used as a positive control, *E.coli* with no plasmid was used as a negative control.

7.2.8 Plasmid DNA Isolation

Colonies were picked from LB agar plates using 5µl plastic inoculation loops,cultured for approximately 16 hours in 10ml LB broth containing 50µg/ml ampicillin. Cultures were then pelleted at 10,000 rpm in a bench top centrifuge for 10 minutes before isolation of plasmid DNA using the Sigma GenElute™ Plasmid Miniprep Kit (Cat no: PLN70) or, Sigma GenElute™ HP Plasmid Midiprep Kit (Cat no: NA0200).

7.2.9 DNA Sequencing

All DNA sequencing was sent to SourceBioscience in 100 ng/µl sample concentrations. Sequencing primers were provided by SourceBioscience, or plasmid specific primers were used.

7.2.10 RNA extraction and cDNA Synthesis

RNA was isolated from whole cell extracts using the Sigma GenElute™ Mammalian Total RNA Miniprep Kit (Cat no: RTN70). Sample was eluted in 50µl of elution buffer as supplied and quantified. cDNA was synthesised used the High Capacity cDNA Reverse Transcription kit (Applied Biosystems, Cat.no: 4368814) using 1µg of RNA starting material. A master mix was made of Reverse Transcriptase kit and added to a T100 thermocycler (BioRad) with amplification conditions: 25°C (10 min), 37°C (120 min), 85°C (5 min).

7.2.11 Real-Time Quantitative PCR (RT-qPCR)

SYBR® Green

qPCR primers were designed using the Eurofins Online Primer Design Tool (www.eurofinsgenomics.eu/). The JMJD7 sequence (NM_001114632.1) was used to target the 3'UTR sequence of JMJD7 mRNA. The forward primer spanned exon 7 and 8 and the reverse was embedded into the 3'UTR sequence. Two separate primer pairs were designed and after validation the best pair was chosen for experimental use. Validation of primers was achieved using a primer concentration titration PCR, a melt curve and agarose gel electrophoresis. SYBR® Green qPCR reactions were completed using the Applied Biosystems Master Mix (Cat no. 4309155) following the manufacturer's protocol.

7.2.12 DNA/RNA Quantification

DNA and RNA quantification was measured using a tabletop Nanodrop (Thermo, Nanodroplite Spectrophotometer) and the 260/280, 260/230 and ng/µl values were calculated. For DNA the 260/280 ratios should be 1.80-2, and 2-2.2 for RNA.

7.2.13 Agarose Gel Electrophoresis

Agarose was purchased from (MercMillipore Cat no: 9012-36-6) and weighed out to 1% (w/v) in TBE buffer with 1:30,000 (v/v) SYBRsafe DNA stain (Invitrogen Cat no: S33102). The solution was microwaved until agarose had completely dissolved and left to set in a casting tray until completely solid. DNA samples were prepared in loading dye (Thermo Scientific™ Cat no: B72) then electrophoresed at 100 V. Bands were observed under UV light in a Vilba Lourmat FusionFX.

Table 7.1 Primers used throughout thesis

Name	Primer (5'-3')
hJMJD7 A18V_F	CGAGAATTCCCGGTCGCTGCAAGGGAG
hJMJD7 A18V_R	CTCCCTTGCAGCGACCGGGAATTCTCG
hJMJD7 R43W_F	CTCCACTTCTACTGGGACTGGGTCTGC
hJMJD7 R43W_R	GCAGACCCAGTCCCAGTAGAAGTGGAG
hJMJD7 A63V_F	CAGCACTGGCCGGTCCTCCAGAAGTGG
hJMJD7 A63V_R	CCACTTCTGGAGGACCGGCCAGTGCTG
hJMJD7 W67R_F	CTCCAGAAGCGGTCCCTCCCCTATTTC
hJMJD7 W67R_R	GAAATAGGGGAGGGACCGCTTCTGGAG

hJMJD7 P70S_F	GTGGTCCCTCTCCTATTTCAGAGCCAC
hJMJD7 P70S_R	GTGGCTCTGAAATAGGAGAGGGACCAC
hJMJD7 Y71C_F	GTGGTCCCTCCCCTGTTTCAGAGCCAC
hJMJD7 Y71C_R	GTGGCTCTGAAACAGGGGAGGGACCAC
hJMJD7 A103T_F	CTTCATGATGCCAACTGAGCGCCGCCTG
hJMJD7 A103T_R	CAGGCGGCGCTCAGTTGGCATCATGAAG
hJMJD7 R105C_F	GATGCCAGCTGAGTGCCGCCTGCCCCTG
hJMJD7 R105C_R	CAGGGGCAGGCGGCACTCAGCTGGCATC
hJMJD7 R106C_F	CCAGCTGAGCGCTGCCTGCCCCTGAGC
hJMJD7 R106C_R	GCTCAGGGGCAGGCAGCGCTCAGCTGG
hJMJD7 L135V_F	CAGTGCTCCAACCGGCCCAGCGAGCTG
hJMJD7 L135V_R	CAGCTCGCTGGGCCGGTTGGAGCACTG
hJMJD7 L143R_F	CTGCCCCAGCTGCGGCCTGATCTGGAATC
hJMJD7 L143R_R	GATTCCAGATCAGGCCGCAGCTGGGGCAG
hJMJD7 M160V_F	GCCCTGGGAAAGGTGCCCGATGCTGTG
hJMJD7 M160V_R	CACAGCATCGGGCACCTTTCCCAGGGC
hJMJD7 R203W_F	CCGCCCAGCGACTGGCCCTTCATCCCC
hJMJD7 R203W_R	GGGGATGAAGGGCCAGTCGCTGGGCGG

hJMJD7 T223I_F	CTAACTGAAGAGGGCATCTTTAAGGTGGTG
hJMJD7 T223I_R	CACCACCTTAAAGATGCCCTCTTCAGTTAG
hJMJD7 R260C_F	GCCCAGGCCCTTTGCTGCACGGTGCGG
hJMJD7 R260C_R	CCGCACCGTGCAGCAAAGGGCCTGGGC
hJMJD7 R264W_F	CGCTGCACGGTGTGGGCCGGTGAGATG
hJMJD7 R264W_R	CATCTCACCGGCCCACACCGTGCAGCG
hJMJD7 E267K_F	GTGCGGGCCGGTAAGATGCTCTATCTG
hJMJD7 E267K_R	CAGATAGAGCATCTTACCGGCCCGCAC
hJMJD7 P272S_F	GATGCTCTATCTGTCGGCTCTGTGGTTC
hJMJD7 P272S_R	GAACCACAGAGCCGACAGATAGAGCATC
hJMJD7 C285W_F	CAGTCCCAGGGCTGGATCGCAGTGAATTTC
hJMJD7 C285W_R	GAAATTCACTGCGATCCAGCCCTGGGACTG
hJMJD7 D297N_F	GACATGGAATACAACCTCAAGTATAGTTAC
hJMJD7 D297N_R	GTAACTATACTTGAGGTTGTATTCCATGTC
hJMJD7 FLAG pIPZ_F	TTTATCATCGATATGGACTACAAAGACCATGATGGTGATTATAAAGATCATGACATTGATTACAAGGATGACGATGATAAGGCGGAGGCGGC
hJMJD7 pIPZ_R	TGCATAGCGGCCGCTCAGTCAAGGCCTGAAG
hJMJD7_HA pcDNA3_F	GTCATTAAGCTTATGGATTACCCATACGATGTTCCAGATTACGCTGCGGAGGCGGCTTTG
hJMJD7_FLAG	GTCATTAAGCTTATGGACTACAAAGACCATGATGGTGATTATAAAGATCATGACATCGATTACAAGGATGACGAT

pcDNA3_F	GATAAGGCGGAGGCGGCTTTG
hJMJD7 pcDNA3_R	TACGACGCGGCCGCTCAGTCAAGGCCTGAAGC
pWZL FLAG JMJD7_F	ttatcaGTCGACATGGACTACAAAGACCATGATG
pWZL NT JMJD7_F	ttatcaGTCGACATGGCGGAGGCGGCTTTGGAAG
pWZL JMJD7_R	ccattgaGTCGACTCAGTCAAGGCCTGAAGC
JMJD7 T37A_F	GACAAACCCCCAGCTCCGCTCCACTTCTACGGGGACTGGGTCTG
JMJD7 T37A_R	GAAGTGGAGCGGAGCTGGGGTTTGTCCAGGTAGGGGCACAGC
JMJD7 T37E_F	GACAAACCCCCAGAACCGCTCCACTTCTACGGGGACTGGGTCTG
JMJD7 T37E_R	GAAGTGGAGCGGTTCTGGGGTTTGTCCAGGTAGGGGCACAGC
SYBR Green qPCR, β-actin_F	CTCTTCCAGCCTTCCTTCCT
SYBR Green qPCR, β-actin_R	GGATGTCCAGGTCACACTTC
SYBR Green qPCR, JMJD7-UTR_F	GCTGCATCGCAGTGAATTTCTG
SYBR Green qPCR, JMJD7-UTR_F	CCTCCAAAGCTGATCTCAAGCC

Mammalian Cell Culture Techniques

7.2.14 Cell Culture

All cell lines were purchased from the ATCC. HeLa and HEK293T cells were cultured in Dulbecco's Modified Eagles Medium (Gibco, Cat no: 41966), and AGS cells cultured in RPMI medium (SIGMA, Cat no: R0883). All cell culture media was supplemented with 10% Fetal Bovine Serum (Sigma, Cat no: F7524) and 1% penicillin/streptomycin (Gibco, Cat no: 15070063). Where applicable media was also supplemented with puromycin (Gibco, Cat no: A1113803) at 2µg/µL (HeLa and HEK293T) or 4µg/µL (AGS), or hygromycin (Gibco, Cat no: 10687010) at 100µg/ml. Cells were split regularly and kept in a humidified incubator at 37ºC, 5% CO_2.

7.2.15 Plasmid Transfection

Cells were seeded at either 2.5 x 10^5 cells /ml (5 X 10^5 cells/well, HEK293T) or 0.5 x 10^5 cells /ml (1 x 10^5 cells/well, HeLa) in one well of a six well plate (See table 7.4). For transfection, plasmid DNA (1µg) was mixed with 100µl Opti-MEM™ (Gibco, Cat no: 31985070) and mixed thoroughly, after the addition of 3µl of FuGENE® (Promega, Cat no: E2691) transfection reagent and vortex, the sample was incubated for 30 minutes at room temperature before adding to 2ml of cells in a 6 well plate. The reaction was scaled appropriately for alternatively sized plates (See Table 7.2).

Table 7. 2 Table showing volumes of regent used for transfection protocol

Size of plate	Volume of Media	Opti-MEM™	FuGENE®	DNA (µg)
12 well	1 ml	50 µl	1.5 µl	500 ng
6 well	2 ml	100 µl	3 µl	1 µg
15 cm	20 ml	1 ml	30 µl	10 µg

7.2.16 siRNA mediated Knockdown

Knockdown of endogenous protein was achieved using Lipofectamine™ RNAimax (Invitrogen, L3000008). The following protocol was used for one well of a 6 well plate (2 ml). Two solutions were made, the first was siRNA at the stated concentrations with 150µl of Opti-MEM. The second was 9µl of Lipofectamine™ RNAimax reagent mixed with 150µl Opti-MEM. Each solution was incubated for 5 minutes at room temperature before pooling, then incubated for another 15 minutes before adding to cells. Mixture was incubated with cells for 4-6 hours before changing media. JMJD7 siRNA used: Sigma, Cat no. SASI_Hs02_00326*04*, SASI_Hs02_00326*05* or Dharmacon J-187551-06 as specified. Control siRNA: Sigma. Cat no: SIC001.

7.2.17 Cell Lysis

Cells were lysed when 90-100% confluent. For cells in one well of a 6-well plate, cells were washed twice in cold PBS to remove traces of DMEM and lysed in either JIES buffer or RIPA buffer, 400µl for HEK293Ts or 200µl for all other cells lines. Cells lysed in RIPA buffer were sonicated for 10 seconds at 8 – and centrifuged in a bench top centrifuge at 4˚C, 14,000rpm, 5 minutes. Cells lysed in JIES were centrifuged at 4˚C, 14,000rpm, 5 minutes. Lysates were kept at -80˚C until required.

7.2.18 Biochemical Sub-Cellular Fractionation

NE-PER Nuclear and Cytoplasmic Extraction Reagents kit was purchased from Thermo Scientific (cat no. 78833). Protocol was altered to replace the nuclear extraction buffer with RIPA buffer plus sonication to allow for better extraction of the insoluble nuclear pellet. In addition, extra wash steps were added between extraction steps to ensure a cleaner extraction.

7.2.19 MTS Cell Proliferation Assay

CellTiter 96 AQueous MTS Reagent Powder was purchased from Promega (cat no. G1112) and Phenazine methosulfate (PMS) reagent was purchased from Sigma (cat no. P9625). Both reagents were dissolved in PBS (Gibco™ Cat no: 14190144) according to manufacturer's protocol and stored at -20˚C, protected from light until further use.

Cells were seeded into 96 well plates in quadruplicates at stated seeding densities in 100µl culture medium. Media only control was used as a blank measurement. Every day for the duration of the assay 100µl of PMS solution was added to 2ml of MTS solution, mixed and 20µl of MTS+PMS solution was pipetted onto cells. To ensure a homogeneous solution the plate was gently mixed, then left in a humidified sterile tissue culture incubator at 37˚C, at 5% CO_2, protected from light. After one or two hours (as stated), the plate was mixed again before measuring absorbance at 490nM a (PerkinElmer EnSpire2300) plate reader.

7.2.20 Antibiotic Kill Curve

To optimise the antibiotic concentration used for each cell line. Target cells were seeded at appropriate densities. Two days later a titration of antibiotic containing

media (as stated) was added to cells cell viability was monitored visually over several days.

7.2.21 Transduction of lenti-viral cell lines

On day 1 HEK293T cells were seeded at $2.5x10^5$ cells/ml into a 6 well plate. The following day lentivirus plasmids pMD2.G (150ng), psPAX2 (350ng) and gene of interest (500ng), were transfected in the presence of Opti-MEM and FuGENE®. On day 3 the host cells were seeded at $1x10^5$ cells/ml for AGS, $0.5x10^5$ cells/ml for HeLa, and $2.5x10^5$ cells/ml for HEK293Ts in a 6 well plate. The following day viral media was removed from HEK293T cells and mixed with an equal volume of with fresh media, filtered through a PES 0.45μM filter, put onto recipient cells then after 24 hours replaced with fresh medium. When recipient cells were 90-100% confluent they were given antibiotic containing media (Puromycin: 1μg/ml HEK293T and HeLa, 2μg/ml AGS). Control (non-viral) cell death was used as a marker of successful transduction. For GFP selection, cells were expanded, seeded into 10cm plates and treated with 1μg/ml doxycycline. 10 hours after treatment cells were resuspended in MACs buffer (PBS with 2% FBS, 1 mM EDTA) and sorted through fluorescence assisted cell sorting (FACS) (CyanB Flow Cytometer). 500,000 cells in the top 10% of GFP expressing cells were selected.

7.2.22 Transduction of retro-viral cell lines

On day 1 HEK293T cells were seeded at $2.5x10^5$ cells/ml into a 6 well plate. On the following day retrovirus plasmids pMD2.G (250ng), GAG-POL (250ng) and gene of interest (500ng), 1μg total, was transfected in the presence of Opti-MEM and FuGENE® as described above. On day 3 the host cells were seeded $1x10^5$ cells/ml for AGS, $0.5x10^5$ cells/ml for HeLa, and $2.5x10^5$ cells/ml for HEK 293Ts. Day 4, viral

media was removed from HEK293T cells and replaced with fresh media. The virus-containing media was sterilised through a PES 0.45μM filter directly on to the host cells, polybrene was added to a final concentration of 8μg/ml, 8 hours later the polybrene-media solution was mixed with an equal volume of fresh DMEM and left overnight. This process was repeated on the following day and the virus packaging HEK293T cells were discarded. When the cells were ~80% confluent hygromycin was added to media to initiate the selection process. The cells were observed until the control (non-viral) cells died. When all control cells were dead the viral cells were assumed to be carrying the gene of interest and grown up into cell culture.

7.2.23 Confocal Microscopy

HeLa cells were seeded onto cover slips in a 12 well plate at $0.3x10^5$ cells/ml, 1ml/ well. For over-expression experiments the plasmid transfection protocol, as described in Section 7.2.15, was used. Cells were fixed after 48 hours: Cover slips were washed in PBS, fixed in 4% paraformaldehyde (PFA) (15 min, room temperature), washed again and permeabilised in PBS with 0.1% (v/v) Tritonx100, (10 min, room temperature). Cover slips were blocked in 1% BSA-PBS for 1 hour at room temperature and primary antibodies were incubated either for 1 hour (room temperature) or overnight (4˚C) in 1%BSA-PBS solution. Cover slips were then washed an additional 3 times in 1%BSA-PBS before probing with secondary antibodies rabbit (Invitrogen™, Cat no: A27034) or mouse (Invitrogen™, Cat no: A28180) for 1 hour at room temperature, shielded from light. Cover slips were mounted onto slides using ProLong™ Gold Antifade Mountant (Invirogen™, Cat no: P36930) and left to dry before sealing with clear nail varnish.

Protein Techniques

7.2.24 Western Blotting

For all western blots 12% SDS page polyacrylamide gels were made in-house and a semi-dry transfer method was performed. The PageRuler™ Prestained Protein Ladder Plus was used as a molecular weight marker (ThermoFisher Scientific cat no: 26616). Absolute protein concentrations were calculated using the BioRad Pierce 600nm assay and all samples were normalised to the lowest concentrations and diluted with 6x laemmli buffer. Protein samples were transferred onto 0.45µm PVDF membrane (GE Healthcare, Cat no: 15289894) at 320mA, 25 minutes per membrane. Membrane was Ponceau (SIGMA, Cat no: P7170) stained to check accurate loading, washed and then blocked in either 5% skimmed milk in PBS-Tween, or 5% BSA in TBS-Tween for 1 hour prior to incubation with primary antibody. Membranes were either incubated with non-HRP tagged primary antibodies overnight at 4ºC followed by species specific HRP labelled secondary antibody. Alternatively, the membranes were incubated with HRP-conjugated antibodies recognising epitope tags (e.g. FLAG or HA) at room temperature for 1 hour. Following antibody incubation the membranes were washed before reading. Chemiluminescence substrate used was either Clarity™ Western ECL Substrate (BioRad, Cat no: 1705061) or SuperSignal™ West Femto (BioRad, Cat no: 34095). Imaged on a Vilba Lourmat FusionFX and densitometry analysis was done on Evolution Capture software.

Table 7. 3 List of catalogue numbers for all the antibodies used in this Thesis

Antigen	Cat no:	Source	Dilution
JMJD7	NBP1-91110	Novus	1:500-1:200
JMJD7	STJ29545	St. John's	1:500
phT37 JMJD7	Custom	Generon	1:1000-1:500
DRG1	13190-1-AP	ProteinTech	1:1,000-1:500
DRG2	14743-1-AP	ProteinTech	1:1,000
DFRP1	HPA031099	Sigma	1:1,000
DFRP2	GTX120331	Gene Tex	1:500
FLAG-HRP	A8592	Sigma M2	1:10,000
HA-HRP	12CA5	Roche	1:5,000
HA	MMS-101P	BioLegend	1:1000
β-actin	ab49900	Abcam	1:25,000
CDK2	E304	Abcam	1:1,1000
Anti rabbit	7074	NEB	1:2000
Anti mouse	7076	NEB	1:2000

7.2.25 Immunoprecipitation

Cells were lysed when 90-100% confluent. For cells in a 6 well plate, cells were lysed in JIES buffer containing 1x protease inhibitors (Sigma, Cat no: S8820) and 1x Halt phosphatase inhibitors (Thermo Scientific, Cat no: 87785) then centrifuged at 14,000rpm for 5 minutes, 4˚C. For FLAG (Sigma, Cat no: M8823) and HA (Sigma, Cat no: A2095) immunoprecipitation, 15µl of beads in slurry were transferred into 1.6ml microcentrifuge tubes and washed 3x in cold JIES buffer before addition of protein lysate. The protein/bead solution was left at 4˚C, overnight rotating on a daisy wheel. The following day, the protein supernatant was discarded and beads were

washed 5 times in JIES buffer containing 1x protease inhibitor (and phosphatase inhibitors where necessary). Protein was eluted by either: FLAG peptide (Sigma, Cat no: F4799) competition (25µg/ml FLAG peptide in TBS) at 21°C, shaking for 10 minutes; or, boiling in 1x laemmli buffer.

7.2.26 Kinase Assay

Kinase buffer was incubated with ATP, His-JMJD7 and recombinant kinase at 30 ˚C for 15 minutes (additional no kinase control included), reaction was stopped by addition of 6x laemmli buffer and boiled for 5 minutes. Samples were run on SDS page polyacrylamide gel for immunoblotting and coomassie staining. CDK recombinant kinases were purchased from Thermo (Cat nos: CDK1/CycB: PV3292, CDK2/CycA1: PV6289, CDK2/CycA2: PV3267, CDK2/CycE:PV6295, CDK2/CycO: PV6286, AurkB: PV6130).

7.2.27 Quantification of DRG Hydroxylation via MS

Eight 15cm plates of HEK 293T cell lines containing pTIPZ alone, or pTIPZ containing WT or T37A JMJD7 (4 plates of parental HEK 293T cells for negative control) were lysed in 4ml of RIPA buffer supplemented with protease inhibitor and 1:2000 TurboNuclease (Thermo, Cat no: T4330-50KU) per plate. After lysis the tubes were left to rotate on a daisy wheel for 30 minutes prior to spinning in a pre-chilled Hettich Rotanta 460R bench top centrifuge at 4,000 rpm. The lysates were divided into two 50 ml falcon tubes and incubated with 50µl protein A sepharose beads slurry and either antibody for DRG1 (8µg) and DRG2 (4µg). The IPs were left to rotate on a daisy wheel overnight at 4˚C. The following day, the 50ml falcon tubes were spun at 1500rpm in a Hettich Rotanta 460R bench top centrifuge for 5 min at 4˚C. After one hour the supernatant was removed and the beads washed five times in JIES buffer +

protease inhibitor. The washed beads were dried by pipetting and proteins were eluted using 50µl 2x Laemmli buffer. IP eluate was run on 12% SDS-page gel and stained for protein using coomassie (BioRad, Cat no: 161-0400). Bands were allocated as DRG1, DFRP1, DRG2 and DFRP2 and cut out for trypsin digest before sending to the Adanced Oxford Proteomics Facility for analysis by LC-MS/MS. A Dionex Ultimate 3000 Ultra Performance Liquid Chromatography (UPLC) system (Thermo-Fisher Scientific) was used as frontend separation. The MS/MS scan modes were FT-ICR/Orbitrap, using an ESI (nanospray) ion source and CID/CAD fragmentation mode. Data analysed using the PEAKS 7.0 software (Bioinformatics Solutions).

Cell Cycle Techniques

7.2.29 RO-3306 block and release for Mass Spectrometry

HEK293T cells were seeded at 3.2 x 10^6 / ml into six 15cm plates in 20ml of DMEM. The following day five plates were transfected with 15ng pcDNA3 FLAG JMJD7 WT + 15ng pcDNA3, the sixth plate was transfected with 30ng pcDNA3 only (EV). Four of the WT transfected plates were treated with 5µM RO-3306 when they reached ~60 % confluence to ensure untreated cells weren't affected by cell cycle pausing due to contact inhibition. The EV plate and one WT plate were treated with the same volume of DMSO (Sigma, Cat no: D2650). 16 hours after treatment cells were washed twice in 37ºC PBS and fresh media was added. Cells were harvested by scraping into the media to avoid loss of metaphase cells during washes. Samples were taken every 15 minutes from 0-45 minutes.

7.2.30 Fluorescence Assisted Cell Sorting (FACS)

Cells used for FACS analysis of cell cycle were washed twice with PBS before fixing in ice cold 70% ethanol for 15 minutes at -20 ºC. Ethanol fixed cells were washed twice more before treating with 1µg/ml RNase (Roche, Cat no: RNASEA-RO), then stained with propidium iodide (Sigma, Cat no: P4864) in PBS at 37ºC for 20 minutes. FACS analysis was carried out on a CyanB flow cytometer and analysed using Summit software.

Table 7. 4 Table presenting the number of cells used per plate for each cell line

Cell Line	No Cells per ml	No Cells per well (/plate)	Plate Size
HEK293T	2.5×10^5	5×10^5	6 well
HEK293T	2×10^4	2000	96 well
HEK293T	3.2×10^5	6.4×10^6	15 cm plate
HeLa	0.5×10^5	1×10^5	6 well
HeLa	0.3×10^5	0.3×10^5	12 well
HeLa	1×10^4	1000	96 well
AGS	1×10^5	2×10^5	6 well
AGS	1×10^4	1000	96 well

Appendices

Appendix i

Statistical Analysis for day 3-5 for MTS assay in AGS cells

Day 3

(I) Cell.line	(J) Cell.line	Mean Difference (I-J)	Std. Error	Sig.	95% Confidence Interval	
					Lower Bound	Upper Bound
1.00	2.00	.29300*	.01484	.000	.2489	.3371
	3.00	.25700*	.01484	.000	.2129	.3011
	4.00	.39250*	.01484	.000	.3484	.4366
2.00	1.00	-.29300*	.01484	.000	-.3371	-.2489
	3.00	-.03600	.01484	.125	-.0801	.0081
	4.00	.09950*	.01484	.000	.0554	.1436
3.00	1.00	-.25700*	.01484	.000	-.3011	-.2129
	2.00	.03600	.01484	.125	-.0081	.0801
	4.00	.13550*	.01484	.000	.0914	.1796
4.00	1.00	-.39250*	.01484	.000	-.4366	-.3484
	2.00	-.09950*	.01484	.000	-.1436	-.0554
	3.00	-.13550*	.01484	.000	-.1796	-.0914

*. The mean difference is significant at the 0.05 level.

Day 4

(I) Cell.line	(J) Cell.line	Mean Difference (I-J)	Std. Error	Sig.	95% Confidence Interval	
					Lower Bound	Upper Bound
1.00	2.00	.69150*	.03046	.000	.5998	.7832
	3.00	.70808*	.03290	.000	.6091	.8071
	4.00	.97150*	.03046	.000	.8798	1.0632
2.00	1.00	-.69150*	.03046	.000	-.7832	-.5998
	3.00	.01658	.03290	.956	-.0824	.1156
	4.00	.28000*	.03046	.000	.1883	.3717
3.00	1.00	-.70808*	.03290	.000	-.8071	-.6091
	2.00	-.01658	.03290	.956	-.1156	.0824
	4.00	.26342*	.03290	.000	.1644	.3624
4.00	1.00	-.97150*	.03046	.000	-1.0632	-.8798
	2.00	-.28000*	.03046	.000	-.3717	-.1883
	3.00	-.26342*	.03290	.000	-.3624	-.1644

*. The mean difference is significant at the 0.05 level.

Day 5

(I) Cell.line	(J) Cell.line	Mean Difference (I-J)	Std. Error	Sig.	95% Confidence Interval	
					Lower Bound	Upper Bound
1.00	2.00	.54575*	.05410	.000	.3851	.7064
	3.00	.44900*	.05410	.000	.2884	.6096
	4.00	1.08625*	.05410	.000	.9256	1.2469
2.00	1.00	-.54575*	.05410	.000	-.7064	-.3851
	3.00	-.09675	.05410	.325	-.2574	.0639
	4.00	.54050*	.05410	.000	.3799	.7011
3.00	1.00	-.44900*	.05410	.000	-.6096	-.2884
	2.00	.09675	.05410	.325	-.0639	.2574
	4.00	.63725*	.05410	.000	.4766	.7979
4.00	1.00	-1.08625*	.05410	.000	-1.2469	-.9256
	2.00	-.54050*	.05410	.000	-.7011	-.3799
	3.00	-.63725*	.05410	.000	-.7979	-.4766

*. The mean difference is significant at the 0.05 level.

Statistical Analysis for day 3-5 for MTS assay in HeLa cells:

Day 3

(I) Cell.line	(J) Cell.line	Mean Difference (I-J)	Std. Error	Sig.	95% Confidence Interval	
					Lower Bound	Upper Bound
1.00	2.00	.09175*	.01711	.001	.0440	.1395
	3.00	.50125*	.01711	.000	.4535	.5490
2.00	1.00	-.09175*	.01711	.001	-.1395	-.0440
	3.00	.40950*	.01711	.000	.3617	.4573
3.00	1.00	-.50125*	.01711	.000	-.5490	-.4535
	2.00	-.40950*	.01711	.000	-.4573	-.3617

*. The mean difference is significant at the 0.05 level.

Day 4

(I) Cell.line	(J) Cell.line	Mean Difference (I-J)	Std. Error	Sig.	95% Confidence Interval	
					Lower Bound	Upper Bound
1.00	2.00	.14450*	.03115	.003	.0575	.2315
	3.00	.56050*	.03115	.000	.4735	.6475
2.00	1.00	-.14450*	.03115	.003	-.2315	-.0575
	3.00	.41600*	.03115	.000	.3290	.5030
3.00	1.00	-.56050*	.03115	.000	-.6475	-.4735
	2.00	-.41600*	.03115	.000	-.5030	-.3290

*. The mean difference is significant at the 0.05 level.

Day 5

(I) Cell.line	(J) Cell.line	Mean Difference (I-J)	Std. Error	Sig.	95% Confidence Interval	
					Lower Bound	Upper Bound
1.00	2.00	.11050*	.02745	.008	.0339	.1871
	3.00	.46525*	.02745	.000	.3886	.5419
2.00	1.00	-.11050*	.02745	.008	-.1871	-.0339
	3.00	.35475*	.02745	.000	.2781	.4314
3.00	1.00	-.46525*	.02745	.000	-.5419	-.3886
	2.00	-.35475*	.02745	.000	-.4314	-.2781

*. The mean difference is significant at the 0.05 level.

Statistical Analysis for day 3-5 for MTS assay in HeLa cells:

Day 3

(I) Cell.line	(J) Cell.line	Mean Difference (I-J)	Std. Error	Sig.	95% Confidence Interval	
					Lower Bound	Upper Bound
1.00	2.00	.05975*	.01317	.004	.0230	.0965
	3.00	.08025*	.01317	.000	.0435	.1170
2.00	1.00	-.05975*	.01317	.004	-.0965	-.0230
	3.00	.02050	.01317	.312	-.0163	.0573
3.00	1.00	-.08025*	.01317	.000	-.1170	-.0435
	2.00	-.02050	.01317	.312	-.0573	.0163

*. The mean difference is significant at the 0.05 level.

Day 4

(I) Cell.line	(J) Cell.line	Mean Difference (I-J)	Std. Error	Sig.	95% Confidence Interval	
					Lower Bound	Upper Bound
1.00	2.00	.27900*	.05219	.001	.1333	.4247
	3.00	.31825*	.05219	.000	.1725	.4640
2.00	1.00	-.27900*	.05219	.001	-.4247	-.1333
	3.00	.03925	.05219	.740	-.1065	.1850
3.00	1.00	-.31825*	.05219	.000	-.4640	-.1725
	2.00	-.03925	.05219	.740	-.1850	.1065

*. The mean difference is significant at the 0.05 level.

Day 5

(I) Cell.line	(J) Cell.line	Mean Difference (I-J)	Std. Error	Sig.	95% Confidence Interval	
					Lower Bound	Upper Bound
1.00	2.00	.57250*	.04851	.000	.4370	.7080
	3.00	.59150*	.04851	.000	.4560	.7270
2.00	1.00	-.57250*	.04851	.000	-.7080	-.4370
	3.00	.01900	.04851	.920	-.1165	.1545
3.00	1.00	-.59150*	.04851	.000	-.7270	-.4560
	2.00	-.01900	.04851	.920	-.1545	.1165

*. The mean difference is significant at the 0.05 level.

Appendix ii

Full Proqinase Screen Data

			A	B		
Kinase (ProQinase Lot #)	**External Vendor Lot #**	**Enzyme, ng/well**	Activity raw values n=1	Substrate-BG, mean of 3 singlicates	**Activity values, corrected (A-B)**	**Normalised to ng/well**
DYRK1A (Lot002)	INV_38993	10	1584	38	**1546**	154.60
DYRK4 (Lot002)	INV_37361	50	4853	38	**4815**	96.30
CDK9/CycK (Lot001)	INV_35774	40	2589	38	**2551**	63.78
DYRK2 (Lot001)	CAR_09CBS-1249B	4	251	38	**213**	53.25
HIPK2 (Lot001)	INV_452552	20	893	38	**855**	42.75
LIMK1 (Lot001)	INV_367810	50	1760	38	**1722**	34.44
MEK2 (Lot001)	INV_32519	100	3465	38	**3427**	34.27
CAMKK1 (Lot001)	INV_406782	30	782	38	**744**	24.80
DYRK3 (Lot001)	INV_290370	3	100	38	**62**	20.67
RPS6KA1 (Lot002)	INV_386267	10	242	38	**204**	20.40
EEF2K (Lot001)	INV_38185	8	151	38	**113**	14.13
IKK-alpha (Lot003)	INV_447027	50	496	38	**458**	9.16
MAP3K9 (Lot002)	INV_762486	15	169	38	**131**	8.73
HIPK1 (Lot001)	INV_37497	20	209	38	**171**	8.55
Aurora-A (Lot004)		50	443	38	**405**	8.10
CAMK2D (Lot001)	INV_31647	1	46	38	**8**	8.00
HIPK4 (Lot001)	INV_719847	20	175	38	**137**	6.85
CLK4 (Lot001)	INV_34379	100	600	38	**562**	5.62
CK1-gamma2 (Lot001)	INV_31770	10	93	38	**55**	5.50
CAMK2G (Lot001)	MIL_D8NN026U	5	64	38	**26**	5.20
MEK5 (Lot005)		100	479	38	**441**	4.41
CDK1/CycA (Lot005)		15	100	38	**62**	4.13
HIPK3 (Lot001)	INV_35332	20	108	38	**70**	3.50
CAMK1D (Lot001)	INV_33214	100	341	38	**303**	3.03
NEK2 (Lot002)		50	178	38	**140**	2.80
MAP3K10 (Lot001)	INV_34554	25	103	38	**65**	2.60
MAP3K11 (Lot001)	INV_34029	25	100	38	**62**	2.48
CK1-alpha1 (Lot001)		100	280	38	**242**	2.42

DNA-PK (Lot001)	INV_727478	10	62	38	**24**	2.40
STK23 (Lot002)	INV_285180	25	97	38	**59**	2.36
CAMK2B (Lot001)	INV_35330	100	267	38	**229**	2.29
SNK (Lot007)		50	150	38	**112**	2.24
CHK1 (Lot002)		50	140	38	**102**	2.04
PKC-zeta (Lot005)		50	139	38	**101**	2.02
CHK2 (Lot002)	INV_31541	10	58	38	**20**	2.00
MAP3K7/MAP3K7IP1 (Lot001)	INV_452618	10	56	38	**18**	1.80
LRRK2 wt (Lot002)	INV_698199	75	172	38	**134**	1.79
ARK5 (Lot002)		100	213	38	**175**	1.75
MEKK2 (Lot003)	INV_34361	15	64	38	**26**	1.73
CDK5/p35NCK (Lot001)		15	62	38	**24**	1.60
MARK4 (Lot001)	INV_304213	5	46	38	**8**	1.60
CLK1 (Lot001)		400	645	38	**607**	1.52
IRAK1 (Lot002)	INV_472069	20	67	38	**29**	1.45
MKNK2 (Lot001)	INV_504229	10	52	38	**14**	1.40
MARK1 (Lot001)		100	158	38	**120**	1.20
MKK4 (Lot004)		50	97	38	**59**	1.18
ACV-R2A (Lot001)	INV_862446	40	85	38	**47**	1.18
ACV-R1 (Lot001)		20	61	38	**23**	1.15
GSK3-alpha (Lot001)	INV_29135	50	94	38	**56**	1.12
PKC-delta (Lot004)		25	66	38	**28**	1.12
VRK2 (Lot001)	CAR_08CBS-0814	20	60	38	**22**	1.10
ACV-R1B (Lot001)	INV_35826	10	49	38	**11**	1.10
CDC42BPB (Lot001)		25	65	38	**27**	1.08
VRK1 (Lot001)		50	90	38	**52**	1.04
PRKG1 (Lot001)	INV_36099	12.5	51	38	**13**	1.04
WEE1 (Lot005)		200	238	38	**200**	1.00
EIF2AK3 (Lot001)	INV_390343Z2C	20	58	38	**20**	1.00
CK1-gamma1 (Lot001)	INV_34360	5	43	38	**5**	1.00
PKC-mu (Lot004)		20	57	38	**19**	0.95
SRPK2 (Lot001)		20	56	38	**18**	0.90
TTK (Lot003)		100	125	38	**87**	0.87
MAP3K1 (Lot001)		10	46	38	**8**	0.80
CK1-epsilon (Lot001)	INV_31778	2.5	40	38	**2**	0.80

STK33 (Lot001)	INV_36048	50	75	38	**37**	0.74
SNARK (Lot001)		200	182	38	**144**	0.72
IKK-beta (Lot005)		100	109	38	**71**	0.71
BMPR1A (Lot002)	INV_834034	50	73	38	**35**	0.70
DAPK2 (Lot001 +CaM)	INV_32159	10	45	38	**7**	0.70
TTBK1 (Lot004)		10	45	38	**7**	0.70
PLK1 (Lot013)		50	72	38	**34**	0.68
STK39 (Lot001)	CAR_08CBS-0864	50	72	38	**34**	0.68
RPS6KA5 (Lot001)	INV_33702	25	54	38	**16**	0.64
PLK3 (Lot001)		30	57	38	**19**	0.63
AMPK-alpha1 (Lot001)		200	163	38	**125**	0.63
TSSK1 (Lot001)	INV_31989	5	41	38	**3**	0.60
MKK7 (Lot002)		150	124	38	**86**	0.57
IKK-epsilon (Lot007)		20	49	38	**11**	0.55
CDK1/CycE (Lot001)		50	65	38	**27**	0.54
MYLK3 (Lot001)	INV_34028	50	64	38	**26**	0.52
PAK4 (Lot004)		50	63	38	**25**	0.50
AKT2 (Lot003)		200	137	38	**99**	0.50
MARK3 (Lot001)		100	83	38	**45**	0.45
PKC-iota (Lot006)		50	60	38	**22**	0.44
LRRK2 I2020T (Lot001)	INV_586693	50	58	38	**20**	0.40
CK2-alpha1 (Lot003)		20	46	38	**8**	0.40
CK1-gamma3 (Lot001)	INV_34380	5	40	38	**2**	0.40
NIK (Lot003)		350	177	38	**139**	0.40
STK25 (Lot001)	INV_33163	20	45	38	**7**	0.35
SAK (Lot003)		100	72	38	**34**	0.34
PKC-nu (Lot002)		50	54	38	**16**	0.32
GSG2 (Lot002)	INV_869949	7	40	38	**2**	0.29
SGK3 (Lot004)		50	52	38	**14**	0.28
Aurora-C (Lot009)		100	64	38	**26**	0.26
PKMYT1 (Lot002)	CAR_09CBS-0180	35	45	38	**7**	0.20
CDK1CycB1 (Lot025)		25	43	38	**5**	0.20
SRPK1 (Lot001)		25	43	38	**5**	0.20
MST4 (Lot001)		100	57	38	**19**	0.19
RIPK2 (Lot003)		50	47	38	**9**	0.18

PCTAIRE1 (Lot004)		400	104	38	**66**	0.17
TAOK3 (Lot005)		50	46	38	**8**	0.16
Aurora-B (Lot008)		100	53	38	**15**	0.15
PAK3 (Lot001)		20	41	38	**3**	0.15
CAMK4 (Lot001)	INV_35391	75	49	38	**11**	0.15
MKNK1 (Lot001)	INV_652363	15	40	38	**2**	0.13
LIMK2 (Lot001)	INV_355434	150	56	38	**18**	0.12
COT (Lot018)		300	68	38	**30**	0.10
PBK (Lot003)		200	57	38	**19**	0.10
WNK1 (Lot001)		50	42	38	**4**	0.08
TSK2 (Lot002)		25	40	38	**2**	0.08
PASK (Lot001)	INV_34883	50	41	38	**3**	0.06
DMPK (Lot001)	INV_34024	80	42	38	**4**	0.05
CDK7CycH (Lot002)		50	40	38	**2**	0.04
CDK8/CycC (Lot002)		50	40	38	**2**	0.04
DAPK1 (Lot002)		40	39	38	**1**	0.03
PRKX (Lot001)	INV_34283	10	38	38	**0**	0.00
CK2-alpha2 (Lot001)		50	37	38	**-1**	-0.02
MLK4 (Lot002)		50	36	38	**-2**	-0.04
S6K-beta (Lot001)	INV_34389	100	32	38	**-6**	-0.06
SLK (Lot001)	INV_34390	25	36	38	**-2**	-0.08
CDK6/CycD1 (Lot004)		200	21	38	**-17**	-0.09
CAMKK2 (Lot001)	INV_35319	10	37	38	**-1**	-0.10
CDC42BPA (Lot001)	INV_36844	10	37	38	**-1**	-0.10
MAPKAPK2 (Lot004)		10	37	38	**-1**	-0.10
mTOR (Lot001)	INV_533404	20	36	38	**-2**	-0.10
PAK6 (Lot001)		25	35	38	**-3**	-0.12
PRK1 (Lot004)		25	35	38	**-3**	-0.12
PIM2 (Lot002)		50	32	38	**-6**	-0.12
LRRK2 R1441C (Lot001)	INV_612366	50	31	38	**-7**	-0.14
PDK1 (Lot002)		20	35	38	**-3**	-0.15
HRI (Lot001)		80	26	38	**-12**	-0.15
GRK2 (Lot001)	INV_31090	50	29	38	**-9**	-0.18
SIK1 aa1-350 (Lot003)		50	29	38	**-9**	-0.18
TBK1 (Lot004)		5	37	38	**-1**	-0.20
RIPK5 (Lot001)	INV_38724	10	36	38	**-2**	-0.20

ERK7 (Lot002)		50	28	38	**-10**	-0.20
S6K (Lot006)		50	28	38	**-10**	-0.20
MST3 (Lot001)	INV_32932	20	33	38	**-5**	-0.25
CDK2/CycA (Lot005)		50	25	38	**-13**	-0.26
B-RAF wt (Lot001)		25	31	38	**-7**	-0.28
RAF1 DYDY (Lot001)		10	35	38	**-3**	-0.30
RPS6KA4 (Lot001)	INV_34070	50	23	38	**-15**	-0.30
MELK (Lot001)		100	4	38	**-34**	-0.34
PAK2 (Lot001)		25	29	38	**-9**	-0.36
GSK3-beta (Lot003)		50	20	38	**-18**	-0.36
JNK2 (Lot003)		5	36	38	**-2**	-0.40
TGFB-R1 (Lot003)		10	34	38	**-4**	-0.40
AKT1 (Lot007)		25	28	38	**-10**	-0.40
MKK6SDTD (Lot001)		50	17	38	**-21**	-0.42
MYLK (Lot001)	INV_36152	25	27	38	**-11**	-0.44
CDK6/CycD3 (Lot003)	CAR_09CBS-0622	20	29	38	**-9**	-0.45
MEK1 wt (Lot002)		50	14	38	**-24**	-0.48
SGK1 (Lot005)		50	13	38	**-25**	-0.50
CDK4/CycD1 (Lot007)		25	25	38	**-13**	-0.52
MEKK3 (Lot001)	INV_34560	15	30	38	**-8**	-0.53
PHKG2 (Lot001)	INV_37321	10	32	38	**-6**	-0.60
PKC-epsilon (Lot006)		10	32	38	**-6**	-0.60
NEK7 (Lot002)		25	23	38	**-15**	-0.60
BUB1B (Lot002)	CAR_08CBS-1281	35	17	38	**-21**	-0.60
CDK9/CycT (Lot004)		15	28	38	**-10**	-0.67
CDK4/CycD3 (Lot001)		10	31	38	**-7**	-0.70
WNK2 (Lot001)	INV_35976	40	9	38	**-29**	-0.73
ACV-R2B (Lot001)	INV_745099	25	19	38	**-19**	-0.76
PAK1 (Lot002)		15	26	38	**-12**	-0.80
STK17A (Lot001)	INV_33789	25	16	38	**-22**	-0.88
CDK5/p25NCK (Lot001)		15	24	38	**-14**	-0.93
BRSK2 (Lot002)	CAR_08CBS-0302	25	14	38	**-24**	-0.96
AKT3 (Lot004)		10	28	38	**-10**	-1.00
B-RAF VE (Lot002)		25	13	38	**-25**	-1.00
NEK11 (Lot001)	INV_38163	25	13	38	**-25**	-1.00

NEK6 (Lot001)		20	17	38	**-21**	-1.05
TAOK2 (Lot001)	INV_622141	20	17	38	**-21**	-1.05
PAK7 (Lot001)		15	22	38	**-16**	-1.07
PHKG1 (Lot001)	INV_34488	5	32	38	**-6**	-1.20
TLK1 (Lot002)		15	20	38	**-18**	-1.20
ACV-RL1 (Lot002)	INV_511550	20	12	38	**-26**	-1.30
DCAMKL2 (Lot001)	INV_35320	20	11	38	**-27**	-1.35
TSF1 (Lot002)		25	4	38	**-34**	-1.36
SGK2 (Lot001)	INV_34433	20	9	38	**-29**	-1.45
PKC-eta (Lot005)		10	23	38	**-15**	-1.50
PKC-gamma (Lot007)		10	23	38	**-15**	-1.50
PKN3 (Lot002)	CAR_09CBS-1290	20	7	38	**-31**	-1.55
RPS6KA2 (Lot001)	INV_34468	10	22	38	**-16**	-1.60
MAP4K5 (Lot001)	INV_33456	3	33	38	**-5**	-1.67
RPS6KA3 (Lot002)	INV_37397	5	29	38	**-9**	-1.80
ERK1 (Lot002)		20	1	38	**-37**	-1.85
MAPKAPK5 (Lot005)		20	1	38	**-37**	-1.85
PRK2 (Lot001)	INV_34557	20	0	38	**-38**	-1.90
CK1-delta (Lot001)	INV_33225	5	28	38	**-10**	-2.00
MAP4K2 (Lot001)	INV_35217	4	29	38	**-9**	-2.25
JNK3 (Lot001)		5	26	38	**-12**	-2.40
CDC7/ASK (Lot001)	CAR_10CBS-0119	10	13	38	**-25**	-2.50
NLK (Lot002)		10	13	38	**-25**	-2.50
TGFB-R2 (Lot001)	CAR_09CBS-0960	10	13	38	**-25**	-2.50
GRK6 (Lot002)	INV_37437	15	0	38	**-38**	-2.53
PKC-zeta wt aa184-592 (Lot001)		10	11	38	**-27**	-2.70
CDK2/CycE (Lot009)		10	10	38	**-28**	-2.80
JNK1 (Lot005)		5	23	38	**-15**	-3.00
GRK3 (Lot001)	INV_34008	10	7	38	**-31**	-3.10
PKA (Lot002)	INV_37377	5	22	38	**-16**	-3.20
ZAK (Lot001)	INV_34603	4	25	38	**-13**	-3.25
MAPKAPK3 (Lot001)		10	4	38	**-34**	-3.40
GRK5 (Lot001)	INV_38284	5	20	38	**-18**	-3.60
DAPK3 (Lot001)	INV_33763	10	1	38	**-37**	-3.70

MINK1 (Lot002)		10	1	38	**-37**	-3.70
CDK3/CycE (Lot001)		10	0	38	**-38**	-3.80
CLK3 (Lot002)		10	0	38	**-38**	-3.80
EIF2AK2 (Lot001)	INV_374655	10	0	38	**-38**	-3.80
ERK2 (Lot004)		10	0	38	**-38**	-3.80
IRAK4 (Lot006)		10	0	38	**-38**	-3.80
MST2 (Lot003)		10	0	38	**-38**	-3.80
NEK3 (Lot001)	INV_34362	10	0	38	**-38**	-3.80
p38-alpha (Lot005)		10	0	38	**-38**	-3.80
TLK2 (Lot002)		10	0	38	**-38**	-3.80
WNK3 (Lot001)	INV_36047	10	0	38	**-38**	-3.80
PKC-beta1 (Lot004)		2.5	28	38	**-10**	-4.00
p38-beta (Lot004)		3	26	38	**-12**	-4.00
GRK4 (Lot002)	INV_401163	5	17	38	**-21**	-4.20
PRKD2 (Lot001)	INV_34015	5	16	38	**-22**	-4.40
NEK9 (Lot001)	INV_38162	2	29	38	**-9**	-4.50
p38-gamma (Lot001)	INV_32881	5	13	38	**-25**	-5.00
PKC-alpha (Lot005)		2.5	25	38	**-13**	-5.20
MARK2 (Lot002)	INV_503177	5	11	38	**-27**	-5.40
ROCK1 (Lot001)	INV_37178	4	16	38	**-22**	-5.50
PRKG2 (Lot002)	INV_273926	1	32	38	**-6**	-6.00
LRRK G2019S (Lot001)	INV_513572	5	4	38	**-34**	-6.80
PKC-beta2 (Lot003)		5	3	38	**-35**	-7.00
PIM3 (Lot001)	MIL_33220U	4	9	38	**-29**	-7.25
NEK1 (Lot001)	INV_35267	5	1	38	**-37**	-7.40
TTBK2 (Lot002)	CAR_08CBS-1131	5	1	38	**-37**	-7.40
PKC-theta (Lot008)		2.5	19	38	**-19**	-7.60
GRK7 (Lot001)	INV_34013	5	0	38	**-38**	-7.60
MAP4K4 (Lot001)	INV_33761	5	0	38	**-38**	-7.60
MST1 (Lot002)		5	0	38	**-38**	-7.60
ROCK2 (Lot002)		2.5	16	38	**-22**	-8.80
SNF1LK2 (Lot001)	INV_279613	2.5	16	38	**-22**	-8.80
CAMK2A (Lot001)	INV_28192	2	19	38	**-19**	-9.50
NEK4 (Lot002)	INV_35817	4	0	38	**-38**	-9.50
p38-delta (Lot001)		2	17	38	**-21**	-10.50
ASK1 (Lot001)	INV_666419	2	16	38	**-22**	-11.00

BRSK1 (Lot001)	INV_36097	3	4	38	**-34**	-11.33
DYRK1B (Lot001)	INV_450178	2	13	38	**-25**	-12.50
CLK2 (Lot001)	INV_271879	2	12	38	**-26**	-13.00
PIM1 (Lot003)		2	10	38	**-28**	-14.00
MYLK2 (Lot001)		2.5	1	38	**-37**	-14.80
RPS6KA6 (Lot001)	INV_37496	2	4	38	**-34**	-17.00

Appendix iii

Full RO-3306 Kinase Mass Spectrometry Screen Data

	Relative binding to JMJD7		
Appears in all samples except EV (DMSO, 0h and 15m)	**DMSO**	**0h**	**15m**
JMJD7	**12865.33**	**6735.16**	**4560.45**
Tubulin beta-4A chain OS=Homo sapiens GN=TUBB4A PE=1 SV=2	31.62	73.3506958	98.2859361
Polyubiquitin-B (Fragment) OS=Homo sapiens GN=UBB PE=1 SV=1	13.21	63.8571291	59.5809119
Isoform B of Phosphate carrier protein, mitochondrial OS=Homo sapiens GN=SLC25A3	11.99	22.9029907	33.8245802
Elongation factor 1-alpha 1 OS=Homo sapiens GN=EEF1A1 PE=1 SV=1	10.33	32.6257782	35.7146943
T-cell receptor alpha joining 56 (Fragment) OS=Homo sapiens GN=TRAJ56 PE=4 SV=1	5.64	10.7733834	15.9108117
Mitochondrial carrier homolog 2 OS=Homo sapiens GN=MTCH2 PE=1 SV=1	5.05	6.85752598	12.0459514
Very-long-chain enoyl-CoA reductase OS=Homo sapiens GN=TECR PE=1 SV=1	3.72	3.45741561	8.85814694
Non-histone chromosomal protein HMG-17 OS=Homo sapiens GN=HMGN2 PE=1 SV=3	3.32	1.20340985	4.65475874

Eukaryotic translation initiation factor 1A, Y-chromosomal OS=Homo sapiens GN=EIF1AY PE=1 SV=4	3.09	5.9024388	5.89602774
Isoform 2 of Polymerase delta-interacting protein 3 OS=Homo sapiens GN=POLDIP3	2.72	10.3531451	4.73939072
Isoform 2 of Programmed cell death protein 6 OS=Homo sapiens GN=PDCD6	2.64	3.68663653	2.56716997
Signal recognition particle receptor subunit beta OS=Homo sapiens GN=SRPRB PE=1 SV=3	2.52	1.68095344	4.42907347
Mitochondrial glutamate carrier 1 OS=Homo sapiens GN=SLC25A22 PE=1 SV=1	2.37	5.46309869	2.70822327
Complex I assembly factor TIMMDC1, mitochondrial OS=Homo sapiens GN=TIMMDC1 PE=1 SV=2	2.2	5.17657254	1.55158625
Derlin OS=Homo sapiens GN=DERL1 PE=1 SV=1	1.98	1.39442729	0.87453043
Serine/threonine-protein phosphatase 2A catalytic subunit beta isoform OS=Homo sapiens GN=PPP2CB PE=1 SV=1	1.84	2.2731075	1.35411163
Isoform CNPI of 2',3'-cyclic-nucleotide 3'-phosphodiesterase OS=Homo sapiens GN=CNP	1.82	0.97418893	0.64884516
Calcium-binding mitochondrial carrier protein Aralar1 OS=Homo sapiens GN=SLC25A12 PE=1 SV=2	1.73	3.64843304	1.83369284
Protein pelota homolog OS=Homo sapiens GN=PELO PE=1 SV=2	1.64	1.73825868	1.52337559
Keratin, type I cytoskeletal 19 OS=Homo sapiens GN=KRT19 PE=1 SV=4	1.62	4.27879059	4.57012676
High mobility group protein B1 OS=Homo sapiens GN=HMGB1	1.55	2.96077027	4.37265215

PE=1 SV=3			
NADH dehydrogenase [ubiquinone] 1 alpha subcomplex assembly factor 3 OS=Homo sapiens GN=NDUFAF3 PE=1 SV=1	1.49	1.10790113	0.73347713
Mitochondrial fission process protein 1 OS=Homo sapiens GN=MTFP1 PE=1 SV=1	1.44	1.54724124	0.98737307
Isoform 2 of Ubiquitin-conjugating enzyme E2 G2 OS=Homo sapiens GN=UBE2G2	1.43	0.64945929	0.95916241
E3 ubiquitin-protein ligase RNF5 OS=Homo sapiens GN=RNF5 PE=1 SV=1	1.42	1.06969765	1.57979691
Secretory carrier-associated membrane protein 3 OS=Homo sapiens GN=SCAMP3 PE=1 SV=3	1.35	3.15178771	3.04675118
Protein S100-A8 OS=Homo sapiens GN=S100A8 PE=1 SV=1	1.34	1.01239242	1.49516493
Heat shock protein HSP 90-alpha A2 OS=Homo sapiens GN=HSP90AA2P PE=1 SV=2	1.31	2.00568309	2.31327404
Monocarboxylate transporter 1 OS=Homo sapiens GN=SLC16A1 PE=1 SV=3	1.18	1.03149416	2.8210659
Sideroflexin-2 OS=Homo sapiens GN=SFXN2 PE=1 SV=2	1.17	1.27981683	1.32590097
Leucine-rich repeat-containing protein 40 OS=Homo sapiens GN=LRRC40 PE=1 SV=1	1.13	1.39442729	1.15663702
Acyl-Coenzyme A dehydrogenase, C-4 to C-12 straight chain, isoform CRA_a OS=Homo sapiens GN=ACADM PE=1 SV=1	1.1	1.41352903	0.90274109
60S ribosomal protein L30 (Fragment) OS=Homo sapiens GN=RPL30 PE=1 SV=1	1.07	3.76304351	1.241269

Selenoprotein H OS=Homo sapiens GN=SELENOH PE=1 SV=1	1.01	1.92927611	1.18484768
Developmentally-regulated GTP-binding protein 2 OS=Homo sapiens GN=DRG2 PE=1 SV=1	0.99	0.80227323	2.79285524
Histone H2A type 1 OS=Homo sapiens GN=HIST1H2AG PE=1 SV=2	0.93	1.77646216	2.62359129
DNA-directed RNA polymerases I and III subunit RPAC1 (Fragment) OS=Homo sapiens GN=POLR1C PE=1 SV=1	0.92	0.744968	0.95916241
Prefoldin subunit 6 OS=Homo sapiens GN=PFDN6 PE=1 SV=1	0.9	0.93598544	1.07200504
Isoform 2 of Pyruvate dehydrogenase E1 component subunit beta, mitochondrial OS=Homo sapiens GN=PDHB	0.87	0.24832267	2.45432734
Solute carrier family 35 member E1 (Fragment) OS=Homo sapiens GN=SLC35E1 PE=1 SV=2	0.84	1.60454647	0.36673857
Isoform 2 of Phosphatidylglycerophosphatase and protein-tyrosine phosphatase 1 OS=Homo sapiens GN=PTPMT1	0.81	1.54724124	0.95916241
Cytochrome c oxidase assembly factor 3 homolog, mitochondrial OS=Homo sapiens GN=COA3 PE=1 SV=1	0.8	1.52813949	3.38527908
Mitochondrial ornithine transporter 1 OS=Homo sapiens GN=SLC25A15 PE=1 SV=1	0.76	2.55963365	0.42315989
Dehydrogenase/reductase SDR family member 7B OS=Homo sapiens GN=DHRS7B PE=1 SV=1	0.75	1.43263078	0.90274109
NADH dehydrogenase [ubiquinone] 1 alpha subcomplex subunit 9, mitochondrial OS=Homo sapiens GN=NDUFA9 PE=1 SV=2	0.74	0.744968	0.33852791

Tetratricopeptide repeat protein 19, mitochondrial OS=Homo sapiens GN=TTC19 PE=1 SV=4	0.74	1.79556391	0.33852791
Isoform 2 of Ubiquitin carboxyl-terminal hydrolase 15 OS=Homo sapiens GN=USP15	0.72	0.89778195	1.89011416
Helicase-like transcription factor OS=Homo sapiens GN=HLTF PE=1 SV=1	0.71	0.4393401	1.1002157
Transmembrane protein 165 OS=Homo sapiens GN=TMEM165 PE=1 SV=1	0.71	1.83376739	1.41053295
Small integral membrane protein 4 OS=Homo sapiens GN=SMIM4 PE=1 SV=2	0.7	1.33712206	1.97474613
Cytochrome c oxidase subunit 6C OS=Homo sapiens GN=COX6C PE=1 SV=2	0.69	1.31802031	1.94653547
Isoform 5 of Minor histocompatibility antigen H13 OS=Homo sapiens GN=HM13	0.66	0.89778195	0.39494923
Estradiol 17-beta-dehydrogenase 11 OS=Homo sapiens GN=HSD17B11 PE=1 SV=2	0.64	1.2225116	1.80548218
COP9 constitutive photomorphogenic-like protein subunit 4 isoform 2 OS=Homo sapiens GN=COPS4 PE=1 SV=1	0.63	0.19101744	0.28210659
Isoform 2 of Eukaryotic translation initiation factor 4E OS=Homo sapiens GN=EIF4E - Other versions in EV	0.63	0.72586626	0.50779186
MICOS complex subunit OS=Homo sapiens GN=APOOL PE=1 SV=1	0.63	1.73825868	1.77727152
Oligosaccharyltransferase complex subunit OSTC OS=Homo	0.63	1.20340985	1.77727152

sapiens GN=OSTC PE=1 SV=1			
Sideroflexin-4 OS=Homo sapiens GN=SFXN4 PE=1 SV=1	0.63	1.2225116	0.78989845
Isoform 2 of Cyclin-dependent kinase 2 OS=Homo sapiens GN=CDK2	0.6	1.6618517	1.69263954
Isoform 2 of Calcium-binding mitochondrial carrier protein SCaMC-1 OS=Homo sapiens GN=SLC25A24	0.58	0.84047672	0.28210659
Long-chain fatty acid transport protein 4 OS=Homo sapiens GN=SLC27A4 PE=1 SV=1	0.57	0.9168837	1.32590097
Protein RER1 (Fragment) OS=Homo sapiens GN=RER1 PE=1 SV=1	0.56	1.06969765	0.70526648
Serine palmitoyltransferase 1 OS=Homo sapiens GN=SPTLC1 PE=1 SV=1	0.56	1.64274996	0.53600252
Small ubiquitin-related modifier 4 OS=Homo sapiens GN=SUMO4 PE=1 SV=2	0.54	1.03149416	1.52337559
Isoform 2 of Endoplasmic reticulum-Golgi intermediate compartment protein 1 OS=Homo sapiens GN=ERGIC1	0.52	1.68095344	1.46695427
Sigma intracellular receptor 2 OS=Homo sapiens GN=TMEM97 PE=1 SV=1	0.52	0.99329067	1.46695427
Isoform Short of Ancient ubiquitous protein 1 OS=Homo sapiens GN=AUP1	0.5	0.21011918	0.31031725
Stromal cell-derived factor 2-like protein 1 OS=Homo sapiens GN=SDF2L1 PE=1 SV=2	0.48	0.42023836	0.6206345

Exportin-T OS=Homo sapiens GN=XPOT PE=1 SV=2	0.47	0.55395057	0.25389593
Pachytene checkpoint protein 2 homolog OS=Homo sapiens GN=TRIP13 PE=1 SV=2	0.47	0.40113662	0.95916241
Cytochrome c oxidase subunit 2 OS=Homo sapiens GN=MT-CO2 PE=1 SV=1	0.44	1.39442729	0.56421318
Isoform 2 of TRPM8 channel-associated factor 1 OS=Homo sapiens GN=TCAF1	0.44	0.09550872	0.1410533
Isoform 3 of Lysophospholipid acyltransferase 7 OS=Homo sapiens GN=MBOAT7	0.44	1.18430811	0.76168779
Prolactin regulatory element-binding protein OS=Homo sapiens GN=PREB PE=1 SV=1	0.43	0.51574708	0.36673857
Transmembrane 9 superfamily member 3 OS=Homo sapiens GN=TM9SF3 PE=1 SV=2	0.41	0.28652616	0.42315989
Isoform 2 of Extended synaptotagmin-2 OS=Homo sapiens GN=ESYT2	0.4	0.28652616	0.59242384
Large neutral amino acids transporter small subunit 1 OS=Homo sapiens GN=SLC7A5 PE=1 SV=2	0.4	0.55395057	0.25389593
Probable glutamate--tRNA ligase, mitochondrial OS=Homo sapiens GN=EARS2 PE=1 SV=1	0.39	0.34383139	0.25389593
Isoform 2 of Adenosine 3'-phospho 5'-phosphosulfate transporter 1 OS=Homo sapiens GN=SLC35B2	0.38	0.21011918	0.31031725
Isoform 2 of Cytochrome c oxidase assembly protein COX15 homolog OS=Homo sapiens GN=COX15	0.38	0.72586626	0.67705582

Isoform 2 of Transmembrane and TPR repeat-containing protein 3 OS=Homo sapiens GN=TMTC3	0.37	0.70676452	0.1410533
DnaJ (Hsp40) homolog, subfamily B, member 12, isoform CRA_c OS=Homo sapiens GN=DNAJB12 PE=1 SV=1	0.36	0.68766277	0.31031725
Sulfhydryl oxidase 2 OS=Homo sapiens GN=QSOX2 PE=1 SV=3	0.35	0.24832267	0.56421318
Isoform 2 of 2-amino-3-ketobutyrate coenzyme A ligase, mitochondrial OS=Homo sapiens GN=GCAT	0.34	1.18430811	0.59242384
Protein-S-isoprenylcysteine O-methyltransferase OS=Homo sapiens GN=ICMT PE=1 SV=1	0.34	0.3056279	0.45137054
Delta(24)-sterol reductase OS=Homo sapiens GN=Nbla03646 PE=1 SV=1	0.33	0.87868021	0.28210659
Isoform 2 of Mitochondrial 2-oxodicarboxylate carrier OS=Homo sapiens GN=SLC25A21	0.33	0.63035754	0.42315989
Protein cornichon homolog 4 OS=Homo sapiens GN=CNIH4 PE=1 SV=1	0.33	0.63035754	0.93095175
Chitobiosyldiphosphodolichol beta-mannosyltransferase OS=Homo sapiens GN=ALG1 PE=1 SV=2	0.3	0.36293313	0.53600252
Solute carrier family 2, facilitated glucose transporter member 1 OS=Homo sapiens GN=SLC2A1 PE=1 SV=2	0.3	0.57305231	0.25389593
Isoform 2 of YTH domain-containing family protein 2 OS=Homo sapiens GN=YTHDF2	0.28	0.53484882	0.50779186
Succinate dehydrogenase [ubiquinone] flavoprotein subunit, mitochondrial OS=Homo sapiens GN=SDHA PE=1 SV=1	0.28	0.53484882	0.25389593

Mitochondrial import inner membrane translocase subunit Tim17-B OS=Homo sapiens GN=TIMM17B PE=1 SV=1	0.26	0.49664534	0.73347713
NADH dehydrogenase [ubiquinone] 1 alpha subcomplex assembly factor 4 OS=Homo sapiens GN=NDUFAF4 PE=1 SV=1	0.26	1.10790113	1.63621822
Protein spinster homolog 1 OS=Homo sapiens GN=SPNS1 PE=1 SV=1	0.26	0.15281395	0.22568527
Armadillo repeat-containing X-linked protein 3 OS=Homo sapiens GN=ARMCX3 PE=1 SV=1	0.25	0.22922092	0.33852791
Cisplatin resistance related protein CRR9p, isoform CRA_c OS=Homo sapiens GN=CLPTM1L PE=1 SV=1	0.24	0.21011918	0.31031725
Aurora kinase B (Fragment) OS=Homo sapiens GN=AURKB PE=1 SV=1	0.18	1.81466565	1.21305834
Dimethyladenosine transferase 2, mitochondrial OS=Homo sapiens GN=TFB2M PE=1 SV=1	0.23	0.68766277	0.31031725
Isoform 2 of Melanoma-associated antigen D1 OS=Homo sapiens GN=MAGED1	0.23	0.21011918	0.31031725
Serine/threonine-protein kinase PLK1 OS=Homo sapiens GN=PLK1 PE=1 SV=1	0.23	0.13371221	0.19747461
Bifunctional methylenetetrahydrofolate dehydrogenase/cyclohydrolase, mitochondrial OS=Homo sapiens GN=MTHFD2 PE=1 SV=1	0.22	0.42023836	1.35411163
ATP synthase subunit a OS=Homo sapiens GN=MT-ATP6 PE=1 SV=1	0.21	0.40113662	0.59242384

Glycerol-3-phosphate acyltransferase 4 OS=Homo sapiens GN=GPAT4 PE=1 SV=1	0.2	0.59215405	0.25389593
Zinc finger BED domain-containing protein 1 OS=Homo sapiens GN=ZBED1 PE=1 SV=1	0.2	0.82137498	0.16926395
mRNA turnover protein 4 homolog OS=Homo sapiens GN=MRTO4 PE=1 SV=2	0.19	0.36293313	0.53600252
Isoform 3 of Atypical kinase COQ8A, mitochondrial OS=Homo sapiens GN=COQ8A	0.24	0.28652616	0.67705582
Splicing factor U2AF 35 kDa subunit-like protein OS=Homo sapiens GN=U2AF1L5 PE=1 SV=1	0.18	0.34383139	1.1002157
Protein SCO2 homolog, mitochondrial OS=Homo sapiens GN=SCO2 PE=1 SV=3	0.17	0.70676452	0.4795812
Pyrroline-5-carboxylate reductase OS=Homo sapiens GN=PYCR3 PE=1 SV=1	0.17	0.32472964	0.4795812
Nitric oxide synthase-interacting protein OS=Homo sapiens GN=NOSIP PE=1 SV=1	0.15	0.28652616	0.42315989
Isoform 2 of Nucleoporin NUP188 homolog OS=Homo sapiens GN=NUP188	0.14	0.09550872	0.08463198
Isoform 2 of Short/branched chain specific acyl-CoA dehydrogenase, mitochondrial OS=Homo sapiens GN=ACADSB	0.14	0.26742441	0.39494923
Isoform 2 of UDP-glucose:glycoprotein glucosyltransferase 1 OS=Homo sapiens GN=UGGT1	0.14	0.15281395	0.08463198
Isoform 2 of Lipase maturation factor 2 OS=Homo sapiens	0.13	0.11461046	0.16926395

GN=LMF2			
Isoform 2 of Nucleoporin NDC1 OS=Homo sapiens GN=NDC1	0.13	0.53484882	0.16926395
Acyl-CoA desaturase OS=Homo sapiens GN=SCD PE=1 SV=2	0.12	1.08879939	0.70526648
Isoform 2 of Mannose-1-phosphate guanyltransferase beta OS=Homo sapiens GN=GMPPB	0.11	0.21011918	0.31031725
Isoform 2 of Probable ATP-dependent RNA helicase DDX47 OS=Homo sapiens GN=DDX47	0.11	0.4393401	0.31031725
Isoleucine--tRNA ligase, mitochondrial OS=Homo sapiens GN=IARS2 PE=1 SV=2	0.09	0.17191569	0.25389593
Isoform 2 of ATP-binding cassette sub-family D member 3 OS=Homo sapiens GN=ABCD3	0.08	0.15281395	0.22568527
Isoform 2 of Eukaryotic translation initiation factor 3 subunit D OS=Homo sapiens GN=EIF3D - isoform 3 in EV	0.08	0.15281395	0.22568527
Isoform 2 of E3 UFM1-protein ligase 1 OS=Homo sapiens GN=UFL1	0.06	0.22922092	0.53600252
DNA mismatch repair protein OS=Homo sapiens GN=MSH2 PE=1 SV=1	0.05	0.09550872	0.28210659
KIAA0368 OS=Homo sapiens GN=KIAA0368 PE=1 SV=1	0.04	0.24832267	0.05642132

Appendix iiii

ARTICLES
https://doi.org/10.1038/s41589-018-0071-y

nature chemical biology

Corrected: Publisher correction

The Jumonji-C oxygenase JMJD7 catalyzes (3*S*)-lysyl hydroxylation of TRAFAC GTPases

Suzana Markolovic[1,7], Qinqin Zhuang[2,7], Sarah E. Wilkins[1], Charlotte D. Eaton[2], Martine I. Abboud[1], Maximiliano J. Katz[3], Helen E. McNeil[2], Robert K. Leśniak[1], Charlotte Hall[2], Weston B. Struwe[1], Rebecca Konietzny[4], Simon Davis[4], Ming Yang[4,5], Wei Ge[1], Justin L. P. Benesch[1], Benedikt M. Kessler[4], Peter J. Ratcliffe[4,5], Matthew E. Cockman[4,5], Roman Fischer[4], Pablo Wappner[3], Rasheduzzaman Chowdhury[1,6]*, Mathew L. Coleman[2,8]* and Christopher J. Schofield[1,8]*

Biochemical, structural and cellular studies reveal Jumonji-C (JmjC) domain-containing 7 (JMJD7) to be a 2-oxoglutarate (2OG)-dependent oxygenase that catalyzes (3*S*)-lysyl hydroxylation. Crystallographic analyses reveal JMJD7 to be more closely related to the JmjC hydroxylases than to the JmjC demethylases. Biophysical and mutation studies show that JMJD7 has a unique dimerization mode, with interactions between monomers involving both N- and C-terminal regions and disulfide bond formation. A proteomic approach identifies two related members of the translation factor (TRAFAC) family of GTPases, developmentally regulated GTP-binding proteins 1 and 2 (DRG1/2), as activity-dependent JMJD7 interactors. Mass spectrometric analyses demonstrate that JMJD7 catalyzes Fe(II)- and 2OG-dependent hydroxylation of a highly conserved lysine residue in DRG1/2; amino-acid analyses reveal that JMJD7 catalyzes (3*S*)-lysyl hydroxylation. The functional assignment of JMJD7 will enable future studies to define the role of DRG hydroxylation in cell growth and disease.

Following their initial identification as pro-collagen prolyl and lysyl hydroxylases, Fe(II)- and 2-oxoglutarate (2OG)-dependent oxygenases have emerged as widespread regulators of protein biosynthesis[1,2]. The hypoxia-inducible factor (HIF) prolyl and asparaginyl hydroxylases regulate the levels and transcriptional activity of the αβ-HIFs. Prolyl hydroxylation, by the prolyl hydroxylase domain oxygenases (PHDs; also known as EGLNs), regulates HIF-α subunit levels by signaling for degradation, while asparaginyl hydroxylation (catalyzed by factor inhibiting hypoxia-inducible factor, FIH) regulates HIF transcriptional activity; the sensitivity of the PHDs and FIH catalysis to cellular oxygen availability enable them to act as hypoxia sensors[3]. FIH, but not the PHDs, is a member of the Jumonji-C (JmjC) subfamily of 2OG oxygenases[4], other members of which regulate transcription via demethylation of the three histone lysine N^{ε}-methylation states. JmjC histone demethylase (KDM) catalysis proceeds via hydroxylation to give a hemiaminal intermediate, which fragments to give the demethylated product and formaldehyde[5]. There are about six human JmjC KDM subfamilies, which are being studied due to their roles in transcription and links to cancer and genetic disorders resulting from their mutation[6]. 2OG oxygenases are current therapeutic targets with compounds being developed for clinical applications in cancer (for example, KDM5 inhibitors)[7] and anemia (PHD inhibitors)[8].

With the exception of FIH, there are limited reports on the ~10 human JmjC oxygenases that catalyze the formation of stable alcohol products ('JmjC hydroxylases'), which are less well studied than the JmjC KDMs. In addition to HIF-α isoforms, FIH catalyzes modification of ankyrin repeat domains[9], and Jumonji domain-containing 6 (JMJD6) catalyzes hydroxylation of splicing regulatory proteins[10]. JmjC hydroxylases also have ancient roles in the regulation of protein biosynthesis by modifying the translational machinery[11]. The ribosomal oxygenases MYC-induced nuclear antigen (MINA53) and nucleolar protein 66 (NO66) catalyze histidinyl hydroxylation of Rpl27a and Rpl8, respectively[12]. Transfer RNA yW-synthesizing enzyme 5 (TYW5) is a tRNA hydroxylase[13], and Jumonji domain-containing 4 (JMJD4) catalyzes hydroxylation of eukaryotic release factor 1 (eRF1), a reaction increasing stop codon recognition efficiency[14]. In eukaryotes ranging from yeasts to humans, a 2OG oxygenase that is not a JmjC protein (human: OGFOD1; *Drosophila*: Sudestada1), but which is related to the HIF PHDs, catalyzes hydroxylation of a prolyl residue in close contact with messenger RNA in ribosomes[15]. Overall, these results indicate that multiple 2OG oxygenases are involved in the regulation of protein synthesis at both the transcriptional and translational levels[2,15].

Jumonji domain-containing 7 (JMJD7) is one of the few remaining biochemically uncharacterized human JmjC oxygenases; structure-based bioinformatics predicts that it is an Fe(II)- and 2OG-dependent oxygenase containing a JmjC catalytic domain (Supplementary Fig. 1). We report biochemical, crystallographic and cellular studies revealing JMJD7 to be a structurally distinct JmjC hydroxylase that catalyzes (3*S*)-lysyl hydroxylation in two related members of the translation factor (TRAFAC) GTPase family. The results will enable future work to elucidate

[1]Chemistry Research Laboratory, Department of Chemistry, University of Oxford, Oxford, UK. [2]Institute of Cancer and Genomic Sciences, University of Birmingham, Birmingham, UK. [3]Instituto Leloir, Buenos Aires, Argentina. [4]Target Discovery Institute, University of Oxford, Oxford, UK. [5]The Francis Crick Institute, London, UK. [6]Present address: Department of Molecular and Cellular Physiology, Stanford University School of Medicine, Clark Center, Stanford, CA, USA. [7]These authors contributed equally: Suzana Markolovic, Qinqin Zhuang. [8]These authors jointly supervised this work: Mathew L. Coleman, Christopher J. Schofield. *e-mail: rashed.chowdhury@stanford.edu; m.coleman@bham.ac.uk; christopher.schofield@chem.ox.ac.uk

the biological roles of JMJD7 in protein synthesis, the regulation of cell growth and disease.

Results

JMJD7 suppresses cell growth in *Drosophila*. In an RNAi-based screen for variations in the size of the *Drosophila* posterior wing compartment, we observed that knockdown of *CG10133* mRNA, the *Drosophila* orthologue of human *JMJD7* (*dmJMJD7*, 45% sequence identity), correlates with increased posterior wing compartment size, probably through an increase in cell size (Supplementary Fig. 2). Among human JmjC proteins, structure-based bioinformatics predicts that JMJD7 is most closely related to FIH[4], TYW5[15], Jumonji domain-containing 5 (JMJD5)[16] and the ribosomal oxygenases MINA53 and NO66[11], all of which are JmjC hydroxylases with roles in protein biosynthesis regulation (in some cases, they are also reported to have KDM activities). As the catalytic activities and structures of the JmjC oxygenases can relate to their physiological roles[17], we undertook biochemical studies on JMJD7.

JMJD7 is structurally similar to JmjC hydroxylases. Analysis of the activity of recombinant JMJD7 using ^{1}H NMR reveals slow Fe(II)-stimulated conversion of 2OG to succinate in the absence of a substrate (Supplementary Fig. 3). As observed for some other 2OG oxygenases, this conversion was reduced by the broad-spectrum inhibitor *N*-oxalylglycine (NOG)[18]; alanine substitution of one of the predicted Fe(II)-binding residues (His178) also reduces 2OG turnover (Supplementary Figs. 1 and 3b,c). To support the biochemical characterization of JMJD7 and to investigate whether it functions as a hydroxylase and/or KDM, we then worked to solve crystal structures for human JMJD7.

A structure of full-length His_6-tagged JMJD7 complexed with 2OG and Mn(II), an inert Fe(II) substitute, was solved by molecular replacement (Fig. 1). We obtained a higher-resolution (2.2 Å) structure of a JMJD7 variant arising from a missense mutation (R260C) present in endometrial cancer[19] and autism[20] (Supplementary Fig. 1), the fold of which is very similar to the wild type (0.35 Å Cα r.m.s. deviation; Supplementary Fig. 4 and Supplementary Table 1). JMJD7 crystallizes as an oligomer with two or four molecules in each asymmetric unit (Fig. 1 and Supplementary Fig. 4). Biophysical analyses reveal JMJD7 to be dimeric in solution, consistent with immunoprecipitation studies in cells (Supplementary Fig. 5a–c). Uniquely among the characterized JmjC proteins, JMJD7 dimerization involves hydrophobic interactions between α-helices from both N- and C-terminal regions (α1, α2 and α9, respectively) and a disulfide bond involving Cys47 from two monomers (Fig. 1a and Supplementary Figs. 5d,e and 6). The dimeric state of JMJD7 suggests a closer structural similarity to the JmjC hydroxylases, rather than the demethylases[17], since the former are commonly observed as dimers: FIH[21] and TYW5[15] oligomerize via C-terminal α-helical bundles, while MINA53 and NO66 oligomerize via α-helical bundles located between their JmjC and winged-helix domains[11] (Supplementary Fig. 5e).

The structures reveal that each JMJD7 molecule is comprised of nine α-helices, eighteen β-strands and two 3_{10} helices. The catalytic domain contains the characteristic 2OG oxygenase distorted double-stranded β-helix (DSBH) core barrel, formed from eight β-strands, arranged as two antiparallel major (βI, βVIII, βIII, βVI) and minor (βII, βVII, βIV and βV) sheets[17]. The DSBH houses the active site, where the 2OG oxalyl group, water and the metal-binding triad (His178, Asp180 and His277) coordinate the metal in an octahedral geometry (Fig. 1b). The 2OG C1 carboxylate is positioned to make a hydrogen-bonding network with the amides of Asn184 and Asn289. As with most structurally characterized JmjC oxygenases, the 2OG C5 carboxylate interacts via electrostatic and hydrogen-bonding interactions with a lysine (Lys193) on βIV[17]. Most 2OG oxygenases have two or three polar side chains

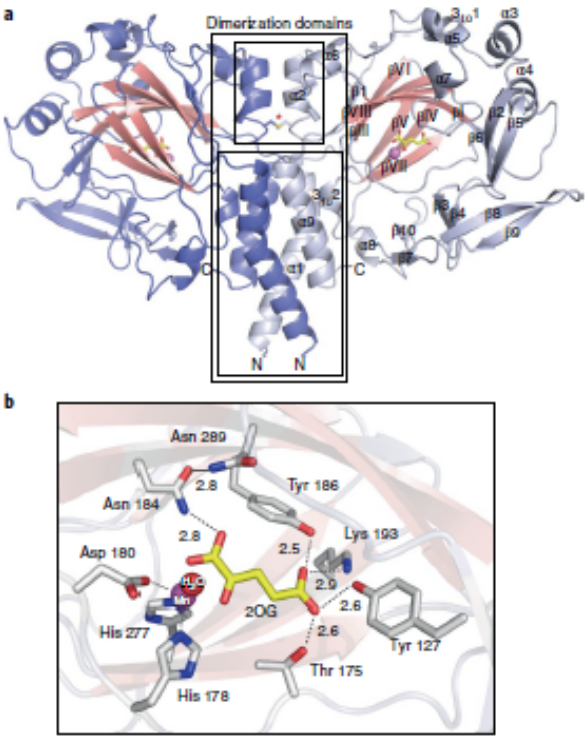

Fig. 1 | Structural analyses of the JmjC hydroxylase, JMJD7. a, View from a crystal structure of human JMJD7 complexed with Mn(II) (violet sphere) and 2OG (yellow) showing the unique dimerization interface, which involves regions both N- and C-terminal to the DSBH core fold and the disulfide bond between Cys 47 of each monomer (red asterisk). β-Strands comprising the distorted 8-stranded (I–VIII) DSBH, conserved in 2OG oxygenases, are in pink. **b**, At the active site, Mn (substituting for Fe(II), violet sphere) is octahedrally coordinated by His178, Asp180, His277, the 2OG oxalyl group (yellow) and water (red sphere). 2OG is apparently tightly bound by hydrogen bonding/electrostatic interactions between its C5 carboxylate and Tyr127, Thr175, Tyr186 and Lys193, and its C1 carboxylate with Asn184 and Asn289 (dotted lines, numerical values represent hydrogen-bond distances in ångströms).

positioned to interact with the 2OG C5 carboxylate group; notably, JMJD7 has four such side chains. In addition to Lys193, the hydroxyls of Tyr127, Thr175 and Tyr186 form additional hydrogen bonds with the 2OG C5 carboxylate group (Fig. 1b). The apparently tight binding of 2OG is consistent with the observed slow substrate uncoupled 2OG turnover (Supplementary Fig. 3).

Comparison of the JMJD7 active site with those of other JmjC oxygenases reveals closer structural similarity with JmjC hydroxylases than KDMs. Notably, binding of the 2OG C1 carboxylate, involving hydrogen bonds with the Asn-184 and Asn-289 side-chain amides, emulates interactions made by FIH[4] (that is, with the Asn-205_{FIH} and Asn-294_{FIH} side chains; Supplementary Fig. 7a). Importantly, JMJD7 lacks a hydrophobic region crucial in binding the N^{ε}-methyl lysine group of the JmjC KDMs[17]. Most JmjC KDMs tend to have an extended loop at the N terminus of DSBH βI that is involved in substrate binding; this is shortened in JMJD7, as in other JmjC hydroxylases (Supplementary Fig. 7b)[17]. Consistent with the absence of structural domains associated with KDM activity (for example, characteristic histone- and nucleic acid-binding

domains; Supplementary Fig. 7c), a panel of histone H3.1 fragments known to be JmjC KDM substrates were not modified by JMJD7 (Supplementary Fig. 8). Overall, the combined biophysical analyses reveal JMJD7 to have greater structural similarity to the JmjC hydroxylases than to the JmjC KDMs.

Proteomics identifies TRAFAC GTPases as JMJD7 interactors. To identify potential JMJD7 substrates, we used mass spectrometry (MS) to compare the proteins interacting with wild-type and (near) inactive (H178A) JMJD7, using dimethyl-*N*-oxalylglycine (DMOG), a cell-penetrating precursor of NOG[14], to trap substrates. Immunoaffinity purifications from extracts of DMOG-treated cells expressing FLAG-tagged wild-type or JMJD7 H178A were analyzed. JMJD7-specific interactions ablated by the H178A mutation included two closely related GTPases, developmentally regulated GTP-binding proteins 1 and 2 (DRG1/2), and their respective binding partners, DRG family regulatory proteins 1 and 2 (DFRP1/2) (Fig. 2a and Supplementary Fig. 9a)[22]. Known JmjC hydroxylase substrates (for example, eRF1, splicing factors, HIFα and Rpl27a/Rpl8), ankyrins or KDM substrates (for example, histones) were not detected. Activity-dependent interactions of JMJD7 with DRG1 and DRG2 were confirmed in different cell lines (Supplementary Fig. 9b–d). Reciprocal immunoprecipitations using FLAG-tagged DRGs confirmed the interaction with endogenous JMJD7, but not the related hydroxylase JMJD4 (Supplementary Fig. 9e). Importantly, purification of endogenous DRG–DFRP complexes also co-precipitated endogenous JMJD7 (but not JMJD4; Fig. 2b). To investigate whether JMJD7 and DRG1/2 co-localize, immunofluorescence staining of co-expressed JMJD7 and DRG1 or DRG2 was performed in HeLa cells (Fig. 2c). Consistent with the proteomic and co-immunoprecipitation data, we observed significant co-localization of JMJD7 with DRG1 and DRG2 in both nuclear and cytoplasmic compartments. Overall, the combined interaction and localization data support the assignment of DRG1 and DRG2 as JMJD7 interactors and potential substrates.

JMJD7 catalyzes DRG lysyl hydroxylation. To investigate whether DRG–DFRP complexes are JMJD7 substrates, HA–DRG1/2 and V5–DFRP1/2 were purified from cells overproducing control or FLAG–JMJD7, hydrolyzed by trypsin and then analyzed by MS. The results identified a single lysyl hydroxylation site in a highly conserved region in both DRG1 and DRG2 (that is, at Lys22/Lys21, respectively; Fig. 3a,b and Supplementary Fig. 10). Notably, in cells overexpressing JMJD7, we reproducibly observed increases in hydroxylated peptides corresponding to a 'missed' trypsin cleavage site in DRG1 (NK(OH)ATAHHLGLLK) and DRG2 (NK(OH)ATEYHLGLLK), suggesting that JMJD7-catalyzed hydroxylation hinders trypsin-catalyzed hydrolysis (Fig. 3b).

We then tested the cellular assignment of JMJD7-mediated DRG1/2 lysyl hydroxylation by assaying 20-mer peptide fragments spanning the DRG1 sequence as substrates (Supplementary Table 2; a 25-mer peptide, $DRG1_{16–40}$, was also used for biochemical characterization as described later in the text). Consistent with the cell results (Fig. 3a,b and Supplementary Fig. 9), the only peptide undergoing a JMJD7-dependent +16 Da shift was $DRG1_{21–40}$ (NKATAHHLGLLKARLAKLRR-NH_2; Fig. 3c). Peptide hydroxylation was impaired by the absence of 2OG and Fe(II) and inhibited by NOG[18] or the use of a JMJD7-H178A variant (Fig. 3d). Incubation under $^{18}O_2$ revealed that JMJD7 catalyzes incorporation of ^{18}O into its product, as observed for other 2OG protein hydroxylases (Supplementary Fig. 11). Alanine substitution at the hydroxylation site prevented hydroxylation and blocked the interaction between isolated JMJD7 and DRG1/2 (Supplementary Figs. 12 and 13). Interestingly, the DRG-hydroxylation sites are highly conserved in almost all animals including *Drosophila* (Fig. 3a). Recombinant dmJMJD7 hydroxylates human DRG1 and 2 peptides with similar

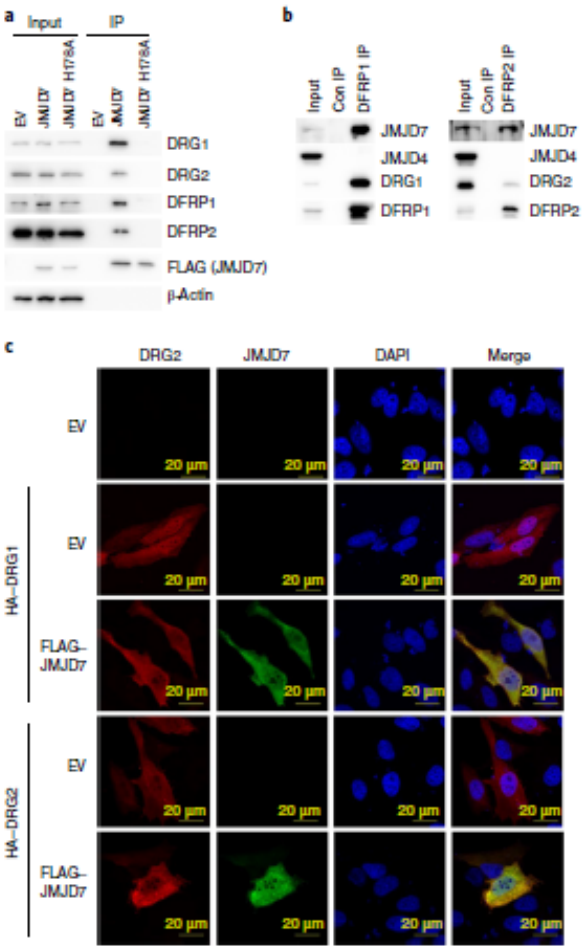

Fig. 2 | JMJD7 interacts with DRG–DFRP complexes in an active-site-dependent manner. a, Interaction of JMJD7 and DRG–DFRP is consistent with proteomic analyses (Supplementary Fig. 9a). 3× FLAG wild-type or inactive (H178A) JMJD7 was produced in doxycycline-inducible HEK293T cells before anti-FLAG immunopurification (IP) and western blotting with the indicated antibodies. Note the lack of interaction of DRG and DFRP proteins with JMJD7 H178A. The specificity of endogenous DRG antibodies was verified by siRNA knockdown (Supplementary Fig. 9f). Immunoprecipitation experiments validating proteomic data were repeated three times, with similar results. Uncropped western blots are provided in Supplementary Fig. 27. **b**, Endogenous DRG–DFRP complexes contain endogenous JMJD7. Endogenous DFRP1 (left) or DFRP2 (right) complexes were immunopurified from HEK293T cells before western blotting with the indicated antibodies. Note that immunoprecipitation samples were diluted 1:10 before analyses of 'bait' (DFRP/DRG levels). This interaction experiment was repeated three times, with similar results. Uncropped western blots are provided in Supplementary Fig. 28. **c**, Co-localization of DRG1/2 and JMJD7. HeLa cells were transfected with control (empty vector, EV), FLAG–JMJD7 and/or HA–DRG1/2 before immunostaining for HA (red) and JMJD7 (green) and labeling nuclei with DAPI. This experiment was repeated three times, with similar results.

efficiency as human JMJD7 (Supplementary Fig. 14a, compare to Supplementary Fig. 15). Furthermore, dmJMJD7 is able to reconstitute activity-dependent interactions with endogenous DRG1 and DRG2 in human cells (Supplementary Fig. 14b). These analyses

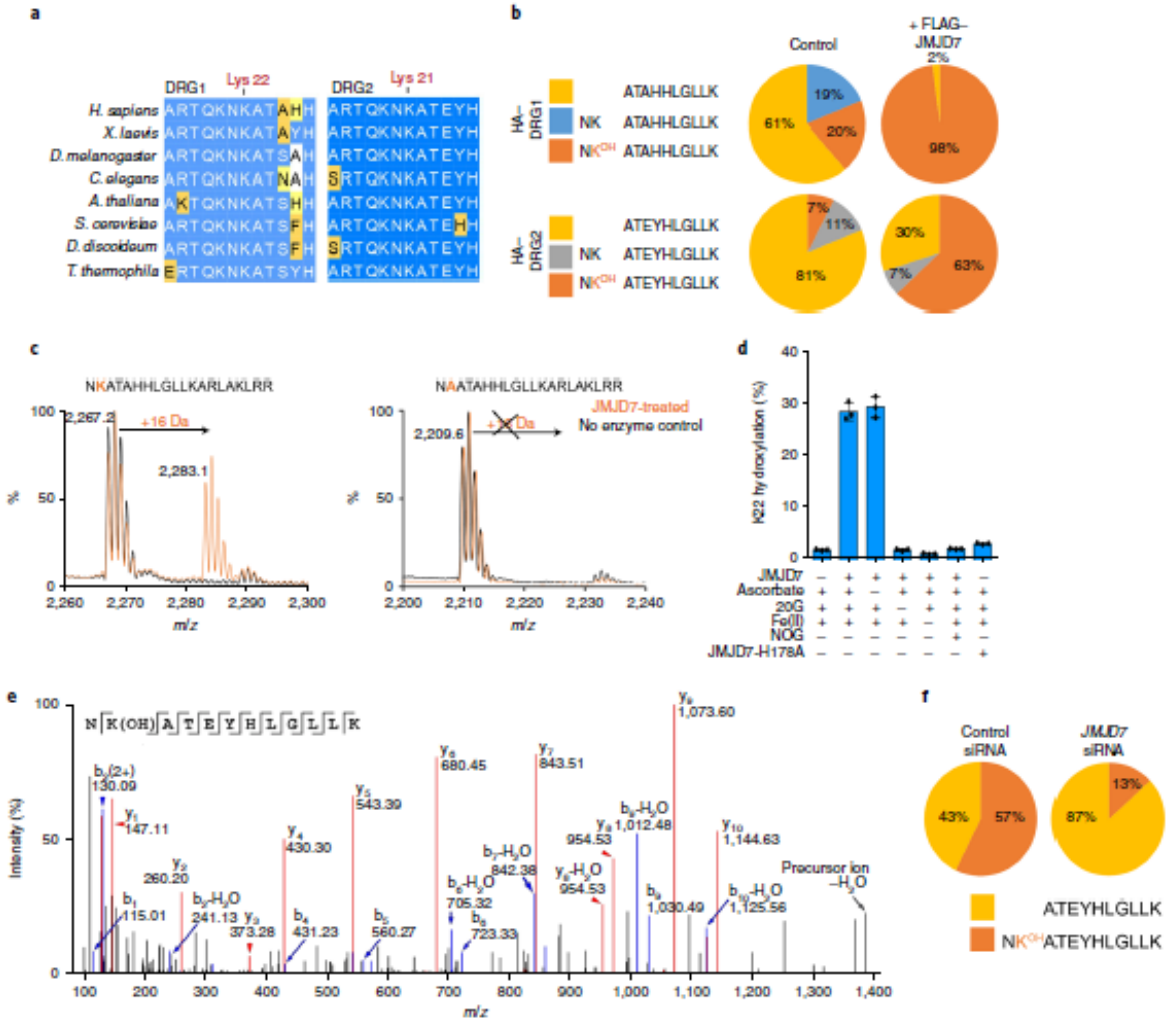

Fig. 3 | JMJD7 catalyzes lysyl hydroxylation of the DRG1/2 GTPases. a, Alignment of the conserved DRG1/2 sequences hydroxylated by JMJD7 in different eukaryotes (Protein BLAST; the figure was prepared using Clustal Omega and GeneDoc). **b**, Qualitative analysis of the extent of DRG1 Lys-22 (upper) and DRG2 Lys-21 (lower) hydroxylation in the absence (left) or presence (right) of JMJD7 overexpression. Trypsinolysis at Lys 22 of DRG1 and Lys 21 of DRG2 is impeded by hydroxylation, complicating quantification: precursor signal intensities of the indicated tryptic fragments, as judged by precursor ion chromatogram analysis, were used; a shift in proportion of the fully trypsinized peptide signal to the uncleaved trypsinized lysyl-hydroxylated peptide signal is indicative of increased hydroxylation. See Supplementary Fig. 10 for MS/MS fragments detected. **c**, Representative MALDI mass spectra for wild-type $DRG1_{21-40}$ (left) and K22A $DRG1_{21-40}$ (right) in the absence (black) or presence (orange) of JMJD7. The K22A substitution nearly ablates peptide hydroxylation. This experiment was repeated three times, with similar results. **d**, Representative MALDI-MS assays with $DRG1_{16-40}$ in the presence/absence of co-factors/substrates and inhibitor. Ascorbate has no effect on JMJD7 activity in the linear range (the activity of some 2OG oxygenases is promoted by ascorbate[18]). The JMJD7-H178A variant has reduced activity. The data represent the mean ± standard deviation ($n = 3$ replicates with a single biological sample) after incubation for 5 min at 37 °C. This assay was repeated twice, with similar results. **e**, MS/MS spectra of the Lys-21-hydroxylated tryptic peptide fragment from endogenous DRG2 (see Supplementary Fig 17a–c for extended data, and Supplementary Fig. 17d–f for DRG1). Note that fragments of the hydroxylated peptide lose water (−18 Da, probably to give a C2/C3 dehydro species, consistent with C3 hydroxylation), so most b ions appear as pairs. Similar spectra were identified in multiple samples from two independent experiments. **f**, Quantification of endogenous DRG2 Lys-21 hydroxylation following control or *JMJD7* siRNA. This experiment was repeated twice, with similar results.

suggest that JMJD7-catalyzed DRG hydroxylation is highly conserved in animals, possibly in a manner linked to the growth phenotype observed on *dmJMJD7* knockdown in *Drosophila* (Supplementary Fig. 2).

The DRG2 peptide ($DRG2_{20-39}$; NKATEYHLGLLKAKLAKY RA-NH_2) was a less efficient substrate than the analogous $DRG1_{21-40}$ substrate (Supplementary Fig. 15a,b). A structure of the DRG1 homologue from *Saccharomyces cerevisiae* (ribosome-interacting GTPase 1 (RBG1), 66% sequence identity, Protein Data Bank (PDB) ID: 4A9A) reveals that the Lys-22 side chain protrudes from a loop on a highly conserved region of a helix-turn-helix (HTH) motif (Fig. 3a and Supplementary Fig. 15c)[23]. Strikingly, the

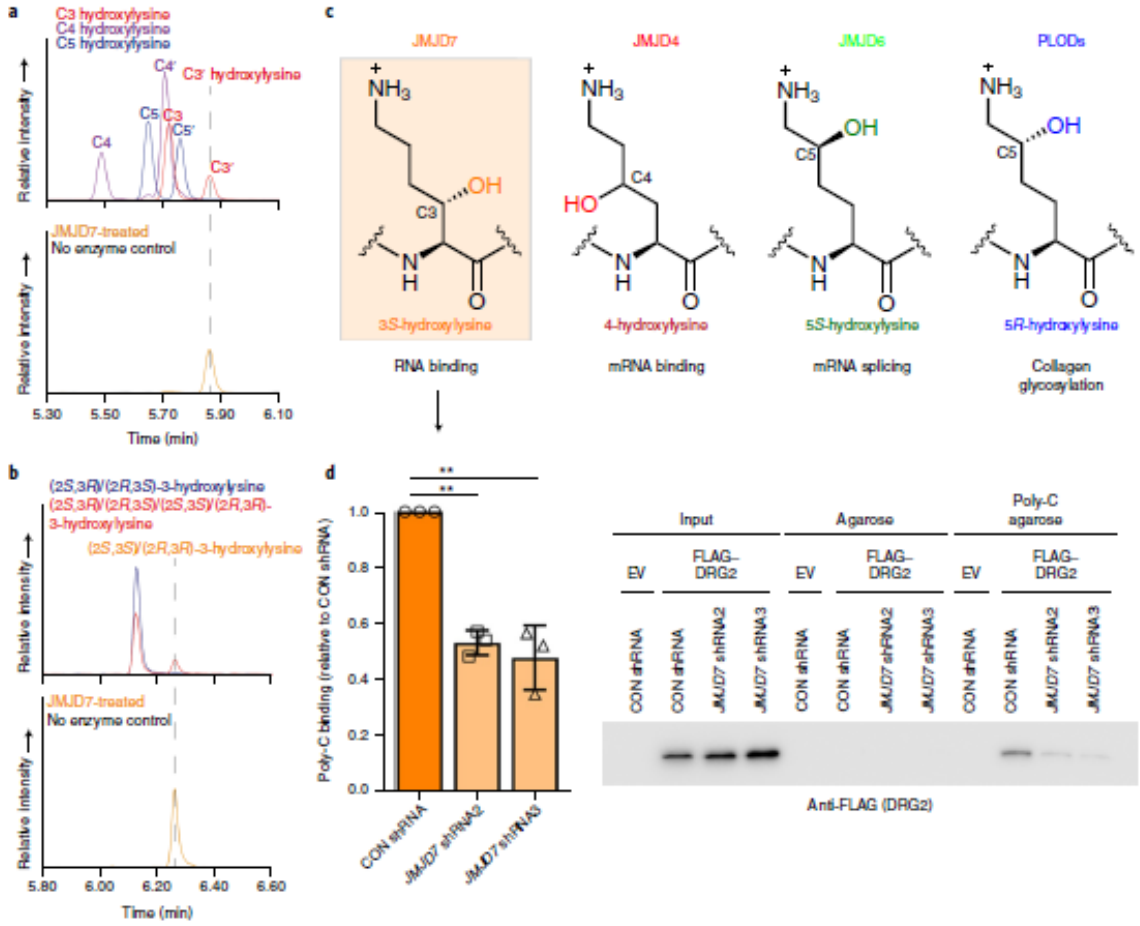

Fig. 4 | JMJD7 is a (3S)-lysyl hydroxylase that promotes DRG ribonucleic acid binding. a, Overlaid extracted ion chromatograms ($m/z = 503.2$) corresponding to: (top) C3 (red), C4 (violet) and C5 (dark blue) hydroxylysine standards post-derivatization (two peaks are observed because each standard is a mixture of stereoisomers—(2*S*,X*R*)/(2*R*,X*S*) and (2*S*,X*S*)/(2*R*,X*R*); X is the hydroxylation site; see Supplementary Fig. 19); (bottom) hydrolyzed $DRG1_{21-40}$ peptide incubated with (orange) or without (black) JMJD7 before hydrolysis. The new product in the JMJD7-treated sample (orange) elutes at the same retention time as one of the C3 stereoisomeric pairs (C3'). **b**, Overlaid extracted ion chromatograms ($m/z = 503.2$) corresponding to: (top) C3 hydroxylysine standard sample (dark blue) and (2*S*,3*R*)/(2*R*,3*S*)-3-hydroxylysine standard (red) indicates the (2*S*,3*R*)/(2*R*,3*S*)-3-hydroxylysine enantiomeric pair co-elutes with the first peak of the C3 standard; (bottom) hydrolyzed $DRG1_{21-40}$ peptide incubated with (orange) or without (black) JMJD7. The new peak in JMJD7-treated sample (orange) elutes at the same retention time as the standard corresponding to (2*S*,3*S*)/(2*R*,3*R*)-3-hydroxylysine (see Supplementary Fig. 19). Amino-acid analyses were repeated two or three times, with similar results. **c**, Currently described forms of lysyl hydroxylation and their functions. PLODs, procollagen lysyl hydroxylases. **d**, *JMJD7* knockdown reduces the affinity of purified DRG2 for an RNA poly-C (cytidine nucleotide) agarose column. 3× FLAG DRG2 was purified from doxycycline-inducible control shRNA cells (CON shRNA) or two independent *JMJD7* shRNA cell lines (no. 2 and no. 3) before anti-FLAG purification and incubation with poly-C agarose. Captured FLAG–DRG2 was detected by anti-FLAG western blotting (right; uncropped western blots are provided in Supplementary Fig. 39) and quantified in three independent experiments, with similar results (left): the data represent the mean ± s.e.m. ($n = 3$ biologically independent experiments) analyzed by two-sided Student's *t*-test (**$P < 0.01$; $P = 0.0016$ for *JMJD7* shRNA2 and 0.0082 for *JMJD7* shRNA3).

position of Lys 22 in the HTH of RBG1, and by implication DRG1/2, resembles that of the lysyl hydroxylation site of a JMJD4 substrate, eRF1[14] (Supplementary Fig. 15c,d). The location of Lys 22 protruding from a turn between two α-helices suggests that secondary structure may be important in JMJD7-substrate recognition, as for JMJD4[14]. Increasing the DRG1 fragment length at its N-terminus to include other conserved residues in the HTH ($DRG1_{16-40}$; *ARTQK*NKATAHHLGLLKARLAKLRR-NH_2) results in more efficient hydroxylation (Supplementary Fig. 15a,b). Importantly, the N-terminally extended $DRG2_{15-39}$ fragment (*ARTQK*NKAT EYHLGLLKAKLAKYRA-NH_2) undergoes efficient hydroxylation. To investigate how JMJD7 interacts with DRG1/2, we attempted to obtain JMJD7-DRG1/2 crystal structures, but have as yet been unsuccessful. We therefore modelled JMJD7-Fe-2OG-DRG1 complexes based on the crystal structures of JMJD7-Mn-2OG (PDB: 5NFO) and *S. cerevisiae* RBG1 (PDB: 4A9A). The modeling and cysteine substitution studies (Supplementary Fig. 16) support the combined biochemical observations implying that long-range interactions involving conserved residues distant from those immediately surrounding the hydroxylated lysine are important in

productive JMJD7 binding. Overall, the combined cellular and isolated protein studies define JMJD7 as a lysyl hydroxylase acting on both DRG1 and DRG2.

To investigate whether JMJD7 is necessary for hydroxylation of DRGs, we immunopurified endogenous DRG1/2 from HEK293T cells (Supplementary Fig. 17); MS analyses identified substantial levels of both Lys 22 (Supplementary Fig. 17d) and Lys 21 (Fig. 3e,f) hydroxylation, respectively. Importantly, endogenous levels of DRG2 Lys-21 hydroxylation were dependent on the presence of JMJD7 expression (Fig. 3f and Supplementary Fig. 17b). Consistent with the overexpression analyses (Fig. 3b and Supplementary Fig. 10), the ability of trypsin to cleave endogenous DRGs at the C-terminal side of Lys 22/Lys 21 was reduced following hydroxylation (Fig. 3f). We also observed inhibition of DRG hydrolysis by hydroxylation with Lys-N, which cleaves at the N-terminal side of lysyl residues (Supplementary Fig. 18). This phenomenon has not been reported following hydroxylation of lysine at the C4 or C5 positions by protein hydroxylases[14,24,25], implying that JMJD7 catalyzes a novel form of lysyl hydroxylation.

JMJD7 is a (3*S*)-lysyl hydroxylase. To date, characterized 2OG oxygenases catalyze hydroxylation at the C4 (for example, JMJD4[14]) and C5 (for example, JMJD6 and the procollagen lysyl hydroxylases[10,26]) positions of lysyl side chains. To investigate the regio- and stereo-selectivity of JMJD7, a DRG1 peptide was hydroxylated, and then hydrolyzed and subjected to amino-acid analysis. Following derivatization, LC–MS revealed a new peak, not present in controls, with a mass corresponding to derivatized hydroxylysine (observed 503.2162 Da; calculated 503.2037 Da). Comparison using C3, C4 and C5 hydroxylysine standards[14] reveals that the product co-elutes with one of the C3 hydroxylysine enantiomeric pairs (Fig. 4a and Supplementary Fig. 19); C3 hydroxylation is supported by NMR analyses of hydroxylated DRG1 and DRG2 peptides (Supplementary Fig. 20). Comparison with a diastereomeric mixture of C3 hydroxylysine isomers and synthetic (2*S*,3*R*)/(2*R*,3*S*)-hydroxylysine standard[27] identified (2*S*,3*S*)-hydroxylysine as the JMJD7-catalyzed product (Fig. 4b and Supplementary Fig. 19c,d). No evidence for other isomers was observed within detection limits, revealing that JMJD7 stereospecifically catalyzes (3*S*)-hydroxylation (Fig. 4a–c; assuming retention of (2*S*)-stereochemistry).

DRG hydroxylation promotes ribonucleic acid binding. The effect of C3 lysyl hydroxylation on *in vitro* proteolysis suggests that this post-translational modification can regulate intramolecular interactions with functional consequences. We therefore explored potential biological roles of DRG C3 lysyl hydroxylation. Unlike HIF hydroxylases, JMJD7 did not significantly regulate substrate levels: Overexpression of wild-type or H178A JMJD7 (Fig. 2a and Supplementary Fig. 9b–d), treatment with DMOG (Supplementary Fig. 9b–d) or DRG hydroxylation site mutation (Supplementary Figs. 21 and 22) did not consistently affect the expression of DRG or DFRP proteins in cells. Furthermore, hydroxylation did not, within detection limits, change the thermal stability of full-length, isolated DRG1 (using differential scanning calorimetry; Supplementary Fig. 23). Consistent with the lack of effect on cellular stability, hydroxylation site substituted DRGs did not affect their ability to co-precipitate DFRPs, which are major regulators of DRG protein turnover[22] (Supplementary Fig. 21). Hydroxylation also did not consistently affect GTPase activity, as determined by ^{1}H NMR or phosphate release assays using recombinant DRG1 in vitro (Supplementary Fig. 24), or using DRG1/2 purified from cells exposed to JMJD7 overexpression, short hairpin RNA (shRNA) knockdown or DMOG treatment (Supplementary Fig. 25).

As described above, the lysine residue targeted by JMJD7 is located at the apex of a highly conserved HTH motif within the N-terminal regions of DRG1/2 (Supplementary Fig. 15c). Although the role of this domain has not previously been reported, yeast complementation studies reveal that it is critical for DRG function[28]. JMJD7-mediated DRG hydroxylation is analogous to JMJD4-mediated eRF1 hydroxylation (Supplementary Fig. 15c,d), in the sense that both are lysyl hydroxylation events targeting HTH domains. eRF1 lysyl hydroxylation is thought to promote translation termination by supporting the interaction of eRF1 with the mRNA stop codon[14], raising the possibility that DRG lysyl hydroxylation catalyzed by JMJD7 has a related function. Indeed, we observed significant binding of DRG2 to RNA affinity columns (Supplementary Fig. 22; consistent with previous reports[29]). Furthermore, a DRG2 Lys-21 variant had reduced affinity for RNA, thus localizing RNA-binding activity to the HTH domain (Supplementary Fig. 22). Importantly, shRNA-mediated *JMJD7* knockdown also reduced the RNA binding affinity of purified DRG2 (Fig. 4d and Supplementary Fig. 22d). These data support a role for JMJD7-mediated C3 lysyl hydroxylation in promoting the interaction of the DRG TRAFAC GTPases with RNA. Future work can focus on defining the precise nature of the JMJD7–DRG–DFRP ribonucleoprotein complexes and their biological roles.

Discussion

The combined cellular and biochemical results demonstrate that JMJD7 targets highly conserved lysine residues within two closely related TRAFAC GTPase proteins. The finding that JMJD7 catalyzes (3*S*)-lysyl hydroxylation expands the repertoire of 2OG oxygenase-catalyzed modifications of basic residues, which also include histidinyl hydroxylation[12,30], lysyl C4 hydroxylation[14], lysyl (5*S*)- and (5*R*)-hydroxylation[24,26], N^{ε}-methyl lysyl demethylation[31], argininyl C3 hydroxylation[12] and, possibly, *N*-methyl argininyl demethylation[32]. The extent of 2OG oxygenase-catalyzed lysyl hydroxylation is striking. With the discovery of JMJD7-catalyzed C3 lysyl hydroxylation, a total of seven different sites of lysine side chain oxidations is now known to be catalyzed by 2OG oxygenases. Aside from the 'not (yet) observed' C3 and C4 stereoisomers, oxidation reactions at the C2 and C6 positions are unidentified exceptions; although the products of such reactions are probably unstable, they have precedence in 2OG oxygenase-catalyzed protein fragmentation (albeit not at lysine residues as yet) via C2 hydroxylation[33].

In most cases, the detailed biochemical roles of lysyl hydroxylations are unclear, with the enablement of glycosylation by procollagen (5*R*)-lysyl hydroxylation[26] and improved stop codon decoding by C4 lysyl hydroxylation[14,34,35] being exceptions. Our experiments indicate that JMJD7-catalyzed hydroxylation does not substantially affect the intrinsic stability, protein expression or GTPase activity of DRGs. Interestingly, however, we observed that JMJD7-catalyzed C3 lysyl hydroxylation clearly impairs experimental proteolysis, at either the C- or N-terminal sides of the target lysyl residue. While inhibition of the tested proteases is probably not biologically relevant, this observation raises the possibility of a wider role for protein hydroxylation in directly modulating protease hydrolysis. This is particularly attractive for C3 lysyl hydroxylation and nucleophilic serine/threonine protease inhibition, where work with proteases and bacterial cell wall biosynthesis enzymes employing nucleophilic serine catalysis has revealed that substrate/inhibitor substitutions that perturb hydrolysis (or formation) of the acyl–enzyme complex can lead to inhibition[36].

In addition to effects on protease hydrolysis, we observed JMJD7- and hydroxylation site-dependent regulation of RNA binding, analogous to the role of JMJD4 in promoting mRNA stop codon decoding by eRF1[14]. Although future work is required to address the physiological RNA targets, the presence of DRGs in ribosome fractions from diverse species including yeasts, plants and humans[28,37,38] could be consistent with an interaction with messenger or ribosomal RNA. Although the biochemical role of the DRGs in protein translation is unclear, it is consistent with their similarity

to other OBG GTPases of the TRAFAC family, which have roles in ribosome biogenesis and translation control[23,39]. A prokaryotic 2OG-dependent prolyl hydroxylase homologous with the animal HIF prolyl hydroxylases, elongation factor thermo unstable (EF-Tu), has also been found to catalyze hydroxylation of a loop region of a translation-associated GTPase[40]; thus, physical and functional interactions between 2OG oxygenases, translation factors and RNA may have ancient origins.

The discovery of JMJD7-catalyzed DRG hydroxylation contributes to growing evidence on the importance of the dynamic interactions between 2OG oxygenases and their substrates/interacting partners in disease[6,41]. Both JMJD7 and DRG1/DRG2 are linked to cell growth in diverse cell types and species[29,37,42–44]. JMJD7 and DRG1/2 may also have context-dependent roles in diseases including cancer and mental disorders; the *DRG2* gene is located in a chromosomal region implicated in the Smith–Magenis neurobehavioral syndrome[45], and DRG1/2 SNPs have been identified in a screen of candidate genes for autism spectrum disorders[46]. In support of this, genetic studies in high-risk autism families and people with severe intellectual disabilities have identified two substitutions in the *JMJD7* gene[20,47]. Future work can now address whether JMJD7-catalyzed hydroxylation of DRG1/2 regulates protein synthesis and how this underlies the role of this novel pathway in growth control and disease.

Methods

Methods, including statements of data availability and any associated accession codes and references, are available at https://doi.org/10.1038/s41589-018-0071-y.

Received: 7 March 2017; Accepted: 3 April 2018;
Published online: 18 June 2018

References

1. Markolovic, S., Wilkins, S. E. & Schofield, C. J. Protein hydroxylation catalyzed by 2-oxoglutarate-dependent oxygenases. *J. Biol. Chem.* **290**, 20712–20722 (2015).
2. Ploumakis, A. & Coleman, M. L. OH, the places you'll go! Hydroxylation, gene expression, and cancer. *Mol. Cell* **58**, 729–741 (2015).
3. Semenza, G. L. Oxygen sensing, hypoxia-inducible factors, and disease pathophysiology. *Annu. Rev. Pathol.* **9**, 47–71 (2014).
4. Elkins, J. M. et al. Structure of factor-inhibiting hypoxia-inducible factor (HIF) reveals mechanism of oxidative modification of HIF-1α. *J. Biol. Chem.* **278**, 1802–1806 (2003).
5. Walport, L. J., Hopkinson, R. J. & Schofield, C. J. Mechanisms of human histone and nucleic acid demethylases. *Curr. Opin. Chem. Biol.* **16**, 525–534 (2012).
6. Johansson, C. et al. The roles of Jumonji-type oxygenases in human disease. *Epigenomics* **6**, 89–120 (2014).
7. Morera, L., Lübbert, M. & Jung, M. Targeting histone methyltransferases and demethylases in clinical trials for cancer therapy. *Clin. Epigenetics* **8**, 57 (2016).
8. Chan, M. C., Holt-Martyn, J. P., Schofield, C. J. & Ratcliffe, P. J. Pharmacological targeting of the HIF hydroxylases – A new field in medicine development. *Mol. Aspects Med.* **47–48**, 54–75 (2016).
9. Cockman, M. E., Webb, J. D. & Ratcliffe, P. J. FIH-dependent asparaginyl hydroxylation of ankyrin repeat domain-containing proteins. *Ann. NY Acad. Sci.* **1177**, 9–18 (2009).
10. Webby, C. J. et al. Jmjd6 catalyses lysyl-hydroxylation of U2AF65, a protein associated with RNA splicing. *Science* **325**, 90–93 (2009).
11. Chowdhury, R. et al. Ribosomal oxygenases are structurally conserved from prokaryotes to humans. *Nature* **510**, 422–426 (2014).
12. Ge, W. et al. Oxygenase-catalyzed ribosome hydroxylation occurs in prokaryotes and humans. *Nat. Chem. Biol.* **8**, 960–962 (2012).
13. Kato, M. et al. Crystal structure of a novel JmjC-domain-containing protein, TYW5, involved in tRNA modification. *Nucleic Acids Res.* **39**, 1576–1585 (2011).
14. Feng, T. et al. Optimal translational termination requires C4 lysyl hydroxylation of eRF1. *Mol. Cell* **53**, 645–654 (2014).
15. Zhuang, Q., Feng, T. & Coleman, M. L. Modifying the maker: Oxygenases target ribosome biology. *Translation* **3**, e1009331 (2015).
16. Del Rizzo, P. A., Krishnan, S. & Trievel, R. C. Crystal structure and functional analysis of JMJD5 indicate an alternate specificity and function. *Mol. Cell. Biol.* **32**, 4044–4052 (2012).
17. Markolovic, S. et al. Structure–function relationships of human JmjC oxygenases—demethylases versus hydroxylases. *Curr. Opin. Struct. Biol.* **41**, 62–72 (2016).
18. Rose, N. R., McDonough, M. A., King, O. N. F., Kawamura, A. & Schofield, C. J. Inhibition of 2-oxoglutarate dependent oxygenases. *Chem. Soc. Rev.* **40**, 4364–4397 (2011).
19. Kandoth, C. et al. Integrated genomic characterization of endometrial carcinoma. *Nature* **497**, 67–73 (2013).
20. Matsunami, N. et al. Identification of rare DNA sequence variants in high-risk autism families and their prevalence in a large case/control population. *Mol. Autism* **5**, 5 (2014).
21. Lancaster, D. E. et al. Disruption of dimerization and substrate phosphorylation inhibit factor inhibiting hypoxia-inducible factor (FIH) activity. *Biochem. J.* **383**, 429–437 (2004).
22. Ishikawa, K., Azuma, S., Ikawa, S., Semba, K. & Inoue, J. I. Identification of DRG family regulatory proteins (DFRPs): Specific regulation of DRG1 and DRG2. *Genes Cells* **10**, 139–150 (2005).
23. Francis, S. M., Gas, M.-E., Daugeron, M.-C., Bravo, J. & Seraphin, B. Rbg1-Tma46 dimer structure reveals new functional domains and their role in polysome recruitment. *Nucleic Acids Res.* **40**, 11100–11114 (2012).
24. Mantri, M. et al. The 2-oxoglutarate-dependent oxygenase JMJD6 catalyses oxidation of lysine residues to give 5S-hydroxylysine residues. *ChemBioChem* **12**, 531–534 (2011).
25. Witkop, B. The application of Hudson's lactone rule to γ- and δ-hydroxyamino acids and the question of the configuration of δ-hydroxy-L-lysine from collagen. *Experientia* **XII**, 372–374 (1956).
26. Myllyharju, J. & Kivirikko, K. I. Collagens and collagen-related diseases. *Ann. Med.* **33**, 7–21 (2001).
27. Leśniak, R. K., Markolovic, S., Tars, K. & Schofield, C. J. Human carnitine biosynthesis proceeds via (2*S*,3*S*)-3-hydroxy-N^{ε}-trimethyllysine. *Chem. Commun.* **53**, 440–442 (2017).
28. Daugeron, M.-C., Prouteau, M., Lacroute, F. & Séraphin, B. The highly conserved eukaryotic DRG factors are required for efficient translation in a manner redundant with the putative RNA helicase Slh1. *Nucleic Acids Res.* **39**, 2221–2233 (2011).
29. Ishikawa, K. et al. Cloning and characterization of *Xenopus laevis drg2*, a member of the developmentally regulated GTP-binding protein subfamily. *Gene* **322**, 105–112 (2003).
30. Yang, M. et al. Factor-inhibiting hypoxia-inducible factor (FIH) catalyses the post-translational hydroxylation of histidinyl residues within ankyrin repeat domains. *FEBS J.* **278**, 1086–1097 (2011).
31. Klose, R. J., Kallin, E. M. & Zhang, Y. JmjC-domain-containing proteins and histone demethylation. *Nat. Rev. Genet.* **7**, 715–727 (2006).
32. Walport, L. J. et al. Arginine demethylation is catalysed by a subset of JmjC histone lysine demethylases. *Nat. Commun.* **7**, 11974 (2016).
33. Mantri, M., Zhang, Z., McDonough, M. A. & Schofield, C. J. Autocatalysed oxidative modifications to 2-oxoglutarate dependent oxygenases. *FEBS J.* **279**, 1563–1575 (2012).
34. Mathetsl, S., Berninghausen, O., Becker, T. & Beckmann, R. Structure of a human translation termination complex. *Nucleic Acids Res.* **43**, 8615–8626 (2015).
35. Brown, A., Shao, S., Murray, J., Hegde, R. S. & Ramakrishnan, V. Structural basis for stop codon recognition in eukaryotes. *Nature* **524**, 493–496 (2015).
36. Powers, J. C., Asgian, J. L., Ekici, O. D. & James, K. E. Irreversible inhibitors of serine, cysteine, and threonine proteases. *Chem. Rev.* **102**, 4639–4750 (2002).
37. Nelson, B. J., Maas, K. J., Dekeyser, J. L. & Stafstrom, J. P. Association of DRG1 and DRG2 with ribosomes from pea, *Arabidopsis*, and yeast. *Int. J. Plant Sci.* **170**, 834–844 (2009).
38. Ishikawa, K., Akiyama, T., Ito, K., Semba, K. & Inoue, J. Independent stabilizations of polysomal Drg1/Dfrp1 complex and non-polysomal Drg2/Dfrp2 complex in mammalian cells. *Biochem. Biophys. Res. Commun.* **390**, 552–556 (2009).
39. Leipe, D. D., Wolf, Y. I., Koonin, E. V. & Aravind, L. Classification and evolution of P-loop GTPases and related ATPases. *J. Mol. Biol.* **317**, 41–72 (2002).
40. Scotti, J. S. et al. Human oxygen sensing may have origins in prokaryotic elongation factor Tu prolyl-hydroxylation. *Proc. Natl Acad. Sci. USA* **111**, 13331–13336 (2014).
41. Christopher J. Schofield, C. J. & Hausinger, R. P. (eds.). *2-Oxoglutarate-Dependent Oxygenases* RSC Metallobiology Series No. 3 (Royal Society of Chemistry, Cambridge, UK, 2015).
42. Jang, S. H., Kim, A.-R., Park, N.-H., Park, J. W. & Han, I.-S. DRG2 regulates G2/M progression via the cyclin B1-Cdk1 complex. *Mol. Cells* **39**, 699–704 (2016).
43. Lu, L., Lv, Y., Dong, J., Hu, S. & Peng, R. DRG1 is a potential oncogene in lung adenocarcinoma and promotes tumor progression via spindle checkpoint signaling regulation. *Oncotarget* **7**, 72795–72806 (2016).

44. Wei, D. et al. Molecular cloning and expression of two closely related GTP-binding proteins from zebrafish. *DNA Seq.* **15**, 246–250 (2004).
45. Vlangos, C. N., Das, P., Patel, P. I. & Elsea, S. H. Assignment of developmentally regulated GTP-binding protein (DRG2) to human chromosome band 17p11.2 with somatic cell hybrids and localization to the Smith–Magenis syndrome critical interval. *Cytogenet. Cell Genet.* **88**, 283–285 (2000).
46. de Krom, M. et al. A common variant in DRD3 receptor is associated with autism spectrum disorder. *Biol. Psychiatry* **65**, 625–630 (2009).
47. de Ligt, J. et al. Diagnostic exome sequencing in persons with severe intellectual disability. *N. Engl. J. Med.* **367**, 1921–1929 (2012).

Acknowledgements

We thank the Biotechnology and Biological Sciences Research Council (BB/L009846/1, C.J.S.), the Medical Research Council (MR/N021053/1, M.L.C.), the Wellcome Trust (106244/Z/14/Z, C.J.S.), Cancer Research UK (24552, M.L.C.), the University of Oxford Clarendon Fund (S.M.) and Kellogg College, University of Oxford (through a Junior Research Fellowship; M.I.A.) for support. We thank E. Flashman (Department of Chemistry, University of Oxford) for assistance with the $^{18}O_2$ experiment and K. Connolly (Institute of Cancer and Genomics Sciences, University of Birmingham) for *Drosophila* cDNA.

Author contributions

The following 'second authors' contributed equally: S.E.W., C.D.E., M.I.A. and M.J.K. S.M., Q.Z., S.E.W., M.J.K., P.W., R.C., M.L.C. and C.J.S. designed and conceived the research; S.M. prepared all recombinant JMJD7 constructs and performed and analyzed CD experiments and all enzyme activity assays by MALDI-MS and NMR; Q.Z. performed substrate discovery proteomics, enzyme–substrate interaction assays, all JMJD7 loss-of-function experiments, and DRG–DFRP interaction, GTPase and RNA-binding assays; S.M. and R.C. performed the crystallography in which R.C. played both an experimental and supervisory role; C.D.E. performed confocal microscopy, cellular dimerization, and dmJMJD7 interaction experiments; Q.Z., C.H. and H.E.M. prepared mammalian expression constructs used by Q.Z.; W.G. and S.M. prepared plasmids for recombinant protein production; S.M. performed and analyzed amino-acid analyses with guidance from S.E.W.; M.I.A. performed and analyzed peptide NMR work, produced and purified recombinant DRG1, performed DRG1 stability and activity assays, and analyzed data; Q.Z. purified exogenous and endogenous proteins for MS and analyzed data with help from M.L.C.; R.K., S.D. and R.F. performed MS and analyzed data; B.M.K. provided MS instrument use. R.K.L. prepared hydroxylysine standards; S.M. and W.B.S. performed and analyzed native MS/SEC-MALS; J.L.P.B. provided SEC-MALS instrument use. M.J.K. and P.W. performed and analyzed Drosophila experiments; R.C. performed enzyme–substrate modeling, prepared recombinant dmJMJD7 and performed proteolysis assays; M.Y., M.E.C. and P.J.R. performed preliminary immunoprecipitations; S.M., Q.Z., S.E.W., C.D.E., R.C., M.L.C. and C.J.S. analyzed data; S.M., Q.Z., R.C., M.L.C. and C.J.S. wrote the manuscript.

Competing interests

The authors declare no competing interests.

Additional information

Supplementary information is available for this paper at https://doi.org/10.1038/s41589-018-0071-y.

Reprints and permissions information is available at www.nature.com/reprints.

Correspondence and requests for materials should be addressed to R.C. or M.L.C. or C.J.S.

Publisher's note: Springer Nature remains neutral with regard to jurisdictional claims in published maps and institutional affiliations.

Bibliography

ABU-FARHA, M., ELISMA, F. & FIGEYS, D. 2008. Identification of protein-protein interactions by mass spectrometry coupled techniques. *Adv Biochem Eng Biotechnol,* 110**,** 67-80.
ADZHUBEI, I. A., SCHMIDT, S., PESHKIN, L., RAMENSKY, V. E., GERASIMOVA, A., BORK, P., KONDRASHOV, A. S. & SUNYAEV, S. R. 2010. A method and server for predicting damaging missense mutations. *Nat Methods,* 7**,** 248-9.
AL-NABHANI, M., AL-RASHDI, S., AL-MURSHEDI, F., AL-KINDI, A., AL-THIHLI, K., AL-SAEGH, A., AL-FUTAISI, A., AL-MAMARI, W., ZADJALI, F. & AL-MAAWALI, A. 2018. Reanalysis of exome sequencing data of intellectual disability samples: Yields and benefits. *Clin Genet*.
ALAHARI, S., POST, M., ROLFO, A., WEKSBERG, R. & CANIGGIA, I. 2018. Compromised JMJD6 Histone Demethylase Activity Affects VHL Gene Repression in Preeclampsia. *J Clin Endocrinol Metab,* 103**,** 1545-1557.
ALBERT, T. K., RIGAULT, C., EICKHOFF, J., BAUMGART, K., ANTRECHT, C., KLEBL, B., MITTLER, G. & MEISTERERNST, M. 2014. Characterization of molecular and cellular functions of the cyclin-dependent kinase CDK9 using a novel specific inhibitor. *Br J Pharmacol,* 171**,** 55-68.
ALBERTSON, D. G. 2006. Gene amplification in cancer. *Trends Genet,* 22**,** 447-55.
AMENDOLA, P. G., ZAGHET, N., RAMALHO, J. J., VILSTRUP JOHANSEN, J., BOXEM, M. & SALCINI, A. E. 2017. JMJD-5/KDM8 regulates H3K36me2 and is required for late steps of homologous recombination and genome integrity. *PLoS Genet,* 13**,** e1006632.
APRELIKOVA, O., CHEN, K., EL TOUNY, L. H., BRIGNATZ-GUITTARD, C., HAN, J., QIU, T., YANG, H. H., LEE, M. P., ZHU, M. & GREEN, J. E. 2016. The epigenetic modifier JMJD6 is amplified in mammary tumors and cooperates with c-Myc to enhance cellular transformation, tumor progression, and metastasis. *Clin Epigenetics,* 8**,** 38.
ARCHAMBAULT, V., BUCHLER, N. E., WILMES, G. M., JACOBSON, M. D. & CROSS, F. R. 2005. Two-faced cyclins with eyes on the targets. *Cell Cycle,* 4**,** 125-30.
ARDITO, F., GIULIANI, M., PERRONE, D., TROIANO, G. & LO MUZIO, L. 2017. The crucial role of protein phosphorylation in cell signaling and its use as targeted therapy (Review). *Int J Mol Med,* 40**,** 271-280.
ASGHAR, U., WITKIEWICZ, A. K., TURNER, N. C. & KNUDSEN, E. S. 2015. The history and future of targeting cyclin-dependent kinases in cancer therapy. *Nat Rev Drug Discov,* 14**,** 130-46.
AYOUB, N., NOMA, K., ISAAC, S., KAHAN, T., GREWAL, S. I. & COHEN, A. 2003. A novel jmjC domain protein modulates heterochromatization in fission yeast. *Mol Cell Biol,* 23**,** 4356-70.
BABA, A., OHTAKE, F., OKUNO, Y., YOKOTA, K., OKADA, M., IMAI, Y., NI, M., MEYER, C. A., IGARASHI, K., KANNO, J., BROWN, M. & KATO, S. 2011. PKA-dependent regulation of the histone lysine demethylase complex PHF2-ARID5B. *Nat Cell Biol,* 13**,** 668-75.
BARDWELL, A. J., ABDOLLAHI, M. & BARDWELL, L. 2003. Docking sites on mitogen-activated protein kinase (MAPK) kinases, MAPK phosphatases and the Elk-1 transcription factor compete for MAPK binding and are crucial for enzymic activity. *Biochem J,* 370**,** 1077-85.
BARR, F. A., ELLIOTT, P. R. & GRUNEBERG, U. 2011. Protein phosphatases and the regulation of mitosis. *J Cell Sci,* 124**,** 2323-34.
BAUDINO, T. A., MACLEAN, K. H., BRENNAN, J., PARGANAS, E., YANG, C., ASLANIAN, A., LEES, J. A., SHERR, C. J., ROUSSEL, M. F. & CLEVELAND, J. L. 2003. Myc-mediated proliferation and lymphomagenesis, but not apoptosis, are compromised by E2f1 loss. *Mol Cell,* 11**,** 905-14.
BEDARD, J. E., PURNELL, J. D. & WARE, S. M. 2007. Nuclear import and export signals are essential for proper cellular trafficking and function of ZIC3. *Hum Mol Genet,* 16**,** 187-98.
BENEVOLENSKAYA, E. V., MURRAY, H. L., BRANTON, P., YOUNG, R. A. & KAELIN, W. G., JR. 2005. Binding of pRB to the PHD protein RBP2 promotes cellular differentiation. *Mol Cell,* 18**,** 623-35.
BENSIMON, A., AEBERSOLD, R. & SHILOH, Y. 2011. Beyond ATM: the protein kinase landscape of the DNA damage response. *FEBS Lett,* 585**,** 1625-39.
BERRY, W. L. & JANKNECHT, R. 2013. KDM4/JMJD2 histone demethylases: epigenetic regulators in cancer cells. *Cancer Res,* 73**,** 2936-42.

BI, W., YAN, J., STANKIEWICZ, P., PARK, S. S., WALZ, K., BOERKOEL, C. F., POTOCKI, L., SHAFFER, L. G., DEVRIENDT, K., NOWACZYK, M. J., INOUE, K. & LUPSKI, J. R. 2002. Genes in a refined Smith-Magenis syndrome critical deletion interval on chromosome 17p11.2 and the syntenic region of the mouse. *Genome Res,* 12**,** 713-28.
BIONDI, R. M. & NEBREDA, A. R. 2003. Signalling specificity of Ser/Thr protein kinases through docking-site-mediated interactions. *Biochem J,* 372**,** 1-13.
BJORNSTAD, L. G., MEZA, T. J., OTTERLEI, M., OLAFSRUD, S. M., MEZA-ZEPEDA, L. A. & FALNES, P. O. 2012. Human ALKBH4 interacts with proteins associated with transcription. *PLoS One,* 7**,** e49045.
BOECKEL, J. N., DERLET, A., GLASER, S. F., LUCZAK, A., LUCAS, T., HEUMULLER, A. W., KRUGER, M., ZEHENDNER, C. M., KALUZA, D., DODDABALLAPUR, A., OHTANI, K., TREGUER, K. & DIMMELER, S. 2016. JMJD8 Regulates Angiogenic Sprouting and Cellular Metabolism by Interacting With Pyruvate Kinase M2 in Endothelial Cells. *Arterioscler Thromb Vasc Biol,* 36**,** 1425-33.
BOECKEL, J. N., GUARANI, V., KOYANAGI, M., ROEXE, T., LENGELING, A., SCHERMULY, R. T., GELLERT, P., BRAUN, T., ZEIHER, A. & DIMMELER, S. 2011. Jumonji domain-containing protein 6 (Jmjd6) is required for angiogenic sprouting and regulates splicing of VEGF-receptor 1. *Proc Natl Acad Sci U S A,* 108**,** 3276-81.
BOSE, J., GRUBER, A. D., HELMING, L., SCHIEBE, S., WEGENER, I., HAFNER, M., BEALES, M., KONTGEN, F. & LENGELING, A. 2004. The phosphatidylserine receptor has essential functions during embryogenesis but not in apoptotic cell removal. *J Biol,* 3**,** 15.
BOTTGER, A., ISLAM, M. S., CHOWDHURY, R., SCHOFIELD, C. J. & WOLF, A. 2015. The oxygenase Jmjd6--a case study in conflicting assignments. *Biochem J,* 468**,** 191-202.
BRAUCHLE, M., YAO, Z., ARORA, R., THIGALE, S., CLAY, I., INVERARDI, B., FLETCHER, J., TASLIMI, P., ACKER, M. G., GERRITS, B., VOSHOL, J., BAUER, A., SCHUBELER, D., BOUWMEESTER, T. & RUFFNER, H. 2013. Protein complex interactor analysis and differential activity of KDM3 subfamily members towards H3K9 methylation. *PLoS One,* 8**,** e60549.
BUNDRED, J. R., HENDRIX, E. & COLEMAN, M. L. 2018. The emerging roles of ribosomal histidyl hydroxylases in cell biology, physiology and disease. *Cell Mol Life Sci*.
BURCHFIELD, J. S., LI, Q., WANG, H. Y. & WANG, R. F. 2015. JMJD3 as an epigenetic regulator in development and disease. *Int J Biochem Cell Biol,* 67**,** 148-57.
BURG, J. M., LINK, J. E., MORGAN, B. S., HELLER, F. J., HARGROVE, A. E. & MCCAFFERTY, D. G. 2015. KDM1 class flavin-dependent protein lysine demethylases. *Biopolymers,* 104**,** 213-46.
CANAVESE, M., SANTO, L. & RAJE, N. 2012. Cyclin dependent kinases in cancer: potential for therapeutic intervention. *Cancer Biol Ther,* 13**,** 451-7.
CASTRO-GINER, F., RATCLIFFE, P. & TOMLINSON, I. 2015. The mini-driver model of polygenic cancer evolution. *Nat Rev Cancer,* 15**,** 680-5.
CASTRO, A., BERNIS, C., VIGNERON, S., LABBE, J. C. & LORCA, T. 2005. The anaphase-promoting complex: a key factor in the regulation of cell cycle. *Oncogene,* 24**,** 314-25.
CERAMI, E., GAO, J., DOGRUSOZ, U., GROSS, B. E., SUMER, S. O., AKSOY, B. A., JACOBSEN, A., BYRNE, C. J., HEUER, M. L., LARSSON, E., ANTIPIN, Y., REVA, B., GOLDBERG, A. P., SANDER, C. & SCHULTZ, N. 2012. The cBio cancer genomics portal: an open platform for exploring multidimensional cancer genomics data. *Cancer Discov,* 2**,** 401-4.
CERVERA, A. M., APOSTOLOVA, N., LUNA-CRESPO, F., SANJUAN-PLA, A., GARCIA-BOU, R. & MCCREATH, K. J. 2006. An alternatively spliced transcript of the PHD3 gene retains prolyl hydroxylase activity. *Cancer Lett,* 233**,** 131-8.
CHANG, B., CHEN, Y., ZHAO, Y. & BRUICK, R. K. 2007. JMJD6 is a histone arginine demethylase. *Science,* 318**,** 444-7.
CHANG, L. & KARIN, M. 2001. Mammalian MAP kinase signalling cascades. *Nature,* 410**,** 37-40.
CHEN, C. F., FENG, X., LIAO, H. Y., JIN, W. J., ZHANG, J., WANG, Y., GONG, L. L., LIU, J. J., YUAN, X. H., ZHAO, B. B., ZHANG, D., CHEN, G. F., WAN, Y., GUO, J., YAN, H. P. & HE, Y. W. 2014. Regulation of T cell proliferation by JMJD6 and PDGF-BB during chronic hepatitis B infection. *Sci Rep,* 4**,** 6359.

CHEN, J., SAHA, P., KORNBLUTH, S., DYNLACHT, B. D. & DUTTA, A. 1996. Cyclin-binding motifs are essential for the function of p21CIP1. *Mol Cell Biol,* 16**,** 4673-82.
CHEN, J., SHEN, B. Y., DENG, X. X., ZHAN, Q. & PENG, C. H. 2012. SKP1-CULLIN1-F-box (SCF)-mediated DRG2 degradation facilitated chemotherapeutic drugs induced apoptosis in hepatocellular carcinoma cells. *Biochem Biophys Res Commun,* 420**,** 651-5.
CHEN, N., RINNER, O., CZERNIK, D., NYTKO, K. J., ZHENG, D., STIEHL, D. P., ZAMBONI, N., GSTAIGER, M. & FREI, C. 2011a. The oxygen sensor PHD3 limits glycolysis under hypoxia via direct binding to pyruvate kinase. *Cell Res,* 21**,** 983-6.
CHEN, Q., SINHA, K., DENG, J. M., YASUDA, H., KRAHE, R., BEHRINGER, R. R. & DE CROMBRUGGHE, B. 2015. Mesenchymal Deletion of Histone Demethylase NO66 in Mice Promotes Bone Formation. *J Bone Miner Res,* 30**,** 1608-17.
CHEN, Y., TERAJIMA, M., BANERJEE, P., GUO, H., LIU, X., YU, J., YAMAUCHI, M. & KURIE, J. M. 2017. FKBP65-dependent peptidyl-prolyl isomerase activity potentiates the lysyl hydroxylase 2-driven collagen cross-link switch. *Sci Rep,* 7**,** 46021.
CHEN, Y., YANG, X., HUANG, Y., LIU, E. & WANG, L. 2011b. Associations of the single-nucleotide polymorphisms of the Mina gene with the development of asthma in Chinese Han children: a case-control study. *Genet Test Mol Biomarkers,* 15**,** 531-6.
CHEN, Z., ZANG, J., WHETSTINE, J., HONG, X., DAVRAZOU, F., KUTATELADZE, T. G., SIMPSON, M., MAO, Q., PAN, C. H., DAI, S., HAGMAN, J., HANSEN, K., SHI, Y. & ZHANG, G. 2006. Structural insights into histone demethylation by JMJD2 family members. *Cell,* 125**,** 691-702.
CHENG, H. C., QI, R. Z., PAUDEL, H. & ZHU, H. J. 2011. Regulation and function of protein kinases and phosphatases. *Enzyme Res,* 2011**,** 794089.
CHENG, Q. & CHEN, J. 2010. Mechanism of p53 stabilization by ATM after DNA damage. *Cell Cycle,* 9**,** 472-8.
CHENG, Y., WANG, Y., LI, J., CHANG, I. & WANG, C. Y. 2017. A novel read-through transcript JMJD7-PLA2G4B regulates head and neck squamous cell carcinoma cell proliferation and survival. *Oncotarget,* 8**,** 1972-1982.
CHOWDHURY, R., SEKIRNIK, R., BRISSETT, N. C., KROJER, T., HO, C. H., NG, S. S., CLIFTON, I. J., GE, W., KERSHAW, N. J., FOX, G. C., MUNIZ, J. R. C., VOLLMAR, M., PHILLIPS, C., PILKA, E. S., KAVANAGH, K. L., VON DELFT, F., OPPERMANN, U., MCDONOUGH, M. A., DOHERTY, A. J. & SCHOFIELD, C. J. 2014. Ribosomal oxygenases are structurally conserved from prokaryotes to humans. *Nature,* 510**,** 422-426.
CHRISTENSEN, J., AGGER, K., CLOOS, P. A., PASINI, D., ROSE, S., SENNELS, L., RAPPSILBER, J., HANSEN, K. H., SALCINI, A. E. & HELIN, K. 2007. RBP2 belongs to a family of demethylases, specific for tri-and dimethylated lysine 4 on histone 3. *Cell,* 128**,** 1063-76.
CIKALA, M., ALEXANDROVA, O., DAVID, C. N., PROSCHEL, M., STIENING, B., CRAMER, P. & BOTTGER, A. 2004. The phosphatidylserine receptor from Hydra is a nuclear protein with potential Fe(II) dependent oxygenase activity. *BMC Cell Biol,* 5**,** 26.
CIOFFI, C. L., LIU, X. Q., KOSINSKI, P. A., GARAY, M. & BOWEN, B. R. 2003. Differential regulation of HIF-1 alpha prolyl-4-hydroxylase genes by hypoxia in human cardiovascular cells. *Biochem Biophys Res Commun,* 303**,** 947-53.
CLARKE, T. L., SANCHEZ-BAILON, M. P., CHIANG, K., REYNOLDS, J. J., HERRERO-RUIZ, J., BANDEIRAS, T. M., MATIAS, P. M., MASLEN, S. L., SKEHEL, J. M., STEWART, G. S. & DAVIES, C. C. 2017. PRMT5-Dependent Methylation of the TIP60 Coactivator RUVBL1 Is a Key Regulator of Homologous Recombination. *Mol Cell,* 65**,** 900-916 e7.
CLISSOLD, P. M. & PONTING, C. P. 2001. JmjC: cupin metalloenzyme-like domains in jumonji, hairless and phospholipase A2beta. *Trends Biochem Sci,* 26**,** 7-9.
COCKMAN, M. E., MASSON, N., MOLE, D. R., JAAKKOLA, P., CHANG, G. W., CLIFFORD, S. C., MAHER, E. R., PUGH, C. W., RATCLIFFE, P. J. & MAXWELL, P. H. 2000. Hypoxia inducible factor-alpha binding and ubiquitylation by the von Hippel-Lindau tumor suppressor protein. *J Biol Chem,* 275**,** 25733-41.

COLE, A. R., CAUSERET, F., YADIRGI, G., HASTIE, C. J., MCLAUCHLAN, H., MCMANUS, E. J., HERNANDEZ, F., EICKHOLT, B. J., NIKOLIC, M. & SUTHERLAND, C. 2006. Distinct priming kinases contribute to differential regulation of collapsin response mediator proteins by glycogen synthase kinase-3 in vivo. *J Biol Chem,* 281**,** 16591-8.
CORBETT, A. H. 2018. Post-transcriptional regulation of gene expression and human disease. *Curr Opin Cell Biol,* 52**,** 96-104.
COZZA, G., ZANIN, S., DETERMANN, R., RUZZENE, M., KUNICK, C. & PINNA, L. A. 2014. Synthesis and properties of a selective inhibitor of homeodomain-interacting protein kinase 2 (HIPK2). *PLoS One,* 9**,** e89176.
CUMMINS, E. P., BERRA, E., COMERFORD, K. M., GINOUVES, A., FITZGERALD, K. T., SEEBALLUCK, F., GODSON, C., NIELSEN, J. E., MOYNAGH, P., POUYSSEGUR, J. & TAYLOR, C. T. 2006. Prolyl hydroxylase-1 negatively regulates IkappaB kinase-beta, giving insight into hypoxia-induced NFkappaB activity. *Proc Natl Acad Sci U S A,* 103**,** 18154-9.
DAUGERON, M. C., PROUTEAU, M., LACROUTE, F. & SERAPHIN, B. 2011. The highly conserved eukaryotic DRG factors are required for efficient translation in a manner redundant with the putative RNA helicase Slh1. *Nucleic Acids Res,* 39**,** 2221-33.
DE BOER, L., OAKES, V., BEAMISH, H., GILES, N., STEVENS, F., SOMODEVILLA-TORRES, M., DESOUZA, C. & GABRIELLI, B. 2008. Cyclin A/cdk2 coordinates centrosomal and nuclear mitotic events. *Oncogene,* 27**,** 4261-8.
DE KROM, M., STAAL, W. G., OPHOFF, R. A., HENDRIKS, J., BUITELAAR, J., FRANKE, B., DE JONGE, M. V., BOLTON, P., COLLIER, D., CURRAN, S., VAN ENGELAND, H. & VAN REE, J. M. 2009. A common variant in DRD3 receptor is associated with autism spectrum disorder. *Biol Psychiatry,* 65**,** 625-30.
DE LIGT, J., WILLEMSEN, M. H., VAN BON, B. W., KLEEFSTRA, T., YNTEMA, H. G., KROES, T., VULTO-VAN SILFHOUT, A. T., KOOLEN, D. A., DE VRIES, P., GILISSEN, C., DEL ROSARIO, M., HOISCHEN, A., SCHEFFER, H., DE VRIES, B. B., BRUNNER, H. G., VELTMAN, J. A. & VISSERS, L. E. 2012. Diagnostic exome sequencing in persons with severe intellectual disability. *N Engl J Med,* 367**,** 1921-9.
DECLERCQ, W., VANDEN BERGHE, T. & VANDENABEELE, P. 2009. RIP kinases at the crossroads of cell death and survival. *Cell,* 138**,** 229-32.
DEL RIZZO, P. A., KRISHNAN, S. & TRIEVEL, R. C. 2012. Crystal structure and functional analysis of JMJD5 indicate an alternate specificity and function. *Mol Cell Biol,* 32**,** 4044-52.
DELASSUS, G. S., CHO, H. & ELICEIRI, G. L. 2011. New signaling pathways from cancer progression modulators to mRNA expression of matrix metalloproteinases in breast cancer cells. *J Cell Physiol,* 226**,** 3378-84.
DELGADO, M. D. & LEON, J. 2006. Gene expression regulation and cancer. *Clin Transl Oncol,* 8**,** 780-7.
DEPHOURE, N., HOWSON, R. W., BLETHROW, J. D., SHOKAT, K. M. & O'SHEA, E. K. 2005. Combining chemical genetics and proteomics to identify protein kinase substrates. *Proc Natl Acad Sci U S A,* 102**,** 17940-5.
DEVER, T. E. & GREEN, R. 2012. The elongation, termination, and recycling phases of translation in eukaryotes. *Cold Spring Harb Perspect Biol,* 4**,** a013706.
DEY, B. K., STALKER, L., SCHNERCH, A., BHATIA, M., TAYLOR-PAPIDIMITRIOU, J. & WYNDER, C. 2008. The histone demethylase KDM5b/JARID1b plays a role in cell fate decisions by blocking terminal differentiation. *Mol Cell Biol,* 28**,** 5312-27.
DHILLON, A. S., HAGAN, S., RATH, O. & KOLCH, W. 2007. MAP kinase signalling pathways in cancer. *Oncogene,* 26**,** 3279-90.
DI CONZA, G., TRUSSO CAFARELLO, S., LOROCH, S., MENNERICH, D., DESCHOEMAEKER, S., DI MATTEO, M., EHLING, M., GEVAERT, K., PRENEN, H., ZAHEDI, R. P., SICKMANN, A., KIETZMANN, T., MORETTI, F. & MAZZONE, M. 2017. The mTOR and PP2A Pathways Regulate PHD2 Phosphorylation to Fine-Tune HIF1alpha Levels and Colorectal Cancer Cell Survival under Hypoxia. *Cell Rep,* 18**,** 1699-1712.

DI MARO, G., ORLANDELLA, F. M., BENCIVENGA, T. C., SALERNO, P., UGOLINI, C., BASOLO, F., MAESTRO, R. & SALVATORE, G. 2014. Identification of targets of Twist1 transcription factor in thyroid cancer cells. *J Clin Endocrinol Metab,* 99**,** E1617-26.
DINCHUK, J. E., FOCHT, R. J., KELLEY, J. A., HENDERSON, N. L., ZOLOTARJOVA, N. I., WYNN, R., NEFF, N. T., LINK, J., HUBER, R. M., BURN, T. C., RUPAR, M. J., CUNNINGHAM, M. R., SELLING, B. H., MA, J., STERN, A. A., HOLLIS, G. F., STEIN, R. B. & FRIEDMAN, P. A. 2002. Absence of post-translational aspartyl beta-hydroxylation of epidermal growth factor domains in mice leads to developmental defects and an increased incidence of intestinal neoplasia. *J Biol Chem,* 277**,** 12970-7.
DING, X., PAN, H., LI, J., ZHONG, Q., CHEN, X., DRY, S. M. & WANG, C. Y. 2013. Epigenetic activation of AP1 promotes squamous cell carcinoma metastasis. *Sci Signal,* 6**,** ra28.1-13, S0-15.
DIRIL, M. K., RATNACARAM, C. K., PADMAKUMAR, V. C., DU, T., WASSER, M., COPPOLA, V., TESSAROLLO, L. & KALDIS, P. 2012. Cyclin-dependent kinase 1 (Cdk1) is essential for cell division and suppression of DNA re-replication but not for liver regeneration. *Proc Natl Acad Sci U S A,* 109**,** 3826-31.
DONG, S., NUTT, C. L., BETENSKY, R. A., STEMMER-RACHAMIMOV, A. O., DENKO, N. C., LIGON, K. L., ROWITCH, D. H. & LOUIS, D. N. 2005. Histology-based expression profiling yields novel prognostic markers in human glioblastoma. *J Neuropathol Exp Neurol,* 64**,** 948-55.
DONG, X., LIN, Q., AIHARA, A., LI, Y., HUANG, C. K., CHUNG, W., TANG, Q., CHEN, X., CARLSON, R., NADOLNY, C., GABRIEL, G., OLSEN, M. & WANDS, J. R. 2015. Aspartate beta-Hydroxylase expression promotes a malignant pancreatic cellular phenotype. *Oncotarget,* 6**,** 1231-48.
DOREE, M. & HUNT, T. 2002. From Cdc2 to Cdk1: when did the cell cycle kinase join its cyclin partner? *J Cell Sci,* 115**,** 2461-4.
DUAN, G. & WALTHER, D. 2015. The roles of post-translational modifications in the context of protein interaction networks. *PLoS Comput Biol,* 11**,** e1004049.
DUBREZ, L. 2017. Regulation of E2F1 Transcription Factor by Ubiquitin Conjugation. *Int J Mol Sci,* 18.
DURONIO, R. J. & XIONG, Y. 2013. Signaling pathways that control cell proliferation. *Cold Spring Harb Perspect Biol,* 5**,** a008904.
DUTTA, A., LE MAGNEN, C., MITROFANOVA, A., OUYANG, X., CALIFANO, A. & ABATE-SHEN, C. 2016. Identification of an NKX3.1-G9a-UTY transcriptional regulatory network that controls prostate differentiation. *Science,* 352**,** 1576-80.
DYSON, N. 1998. The regulation of E2F by pRB-family proteins. *Genes Dev,* 12**,** 2245-62.
ECHALIER, A., COT, E., CAMASSES, A., HODIMONT, E., HOH, F., JAY, P., SHEINERMAN, F., KRASINSKA, L. & FISHER, D. 2012. An integrated chemical biology approach provides insight into Cdk2 functional redundancy and inhibitor sensitivity. *Chem Biol,* 19**,** 1028-40.
EILBRACHT, J., REICHENZELLER, M., HERGT, M., SCHNOLZER, M., HEID, H., STOHR, M., FRANKE, W. W. & SCHMIDT-ZACHMANN, M. S. 2004. NO66, a highly conserved dual location protein in the nucleolus and in a special type of synchronously replicating chromatin. *Mol Biol Cell,* 15**,** 1816-32.
EISINGER-MATHASON, T. S., ZHANG, M., QIU, Q., SKULI, N., NAKAZAWA, M. S., KARAKASHEVA, T., MUCAJ, V., SHAY, J. E., STANGENBERG, L., SADRI, N., PURE, E., YOON, S. S., KIRSCH, D. G. & SIMON, M. C. 2013. Hypoxia-dependent modification of collagen networks promotes sarcoma metastasis. *Cancer Discov,* 3**,** 1190-205.
EPSTEIN, A. C., GLEADLE, J. M., MCNEILL, L. A., HEWITSON, K. S., O'ROURKE, J., MOLE, D. R., MUKHERJI, M., METZEN, E., WILSON, M. I., DHANDA, A., TIAN, Y. M., MASSON, N., HAMILTON, D. L., JAAKKOLA, P., BARSTEAD, R., HODGKIN, J., MAXWELL, P. H., PUGH, C. W., SCHOFIELD, C. J. & RATCLIFFE, P. J. 2001. C. elegans EGL-9 and mammalian homologs define a family of dioxygenases that regulate HIF by prolyl hydroxylation. *Cell,* 107**,** 43-54.
ERRICO, A., DESHMUKH, K., TANAKA, Y., POZNIAKOVSKY, A. & HUNT, T. 2010. Identification of substrates for cyclin dependent kinases. *Adv Enzyme Regul,* 50**,** 375-99.

ESTEY, M. P., DI CIANO-OLIVEIRA, C., FROESE, C. D., FUNG, K. Y., STEELS, J. D., LITCHFIELD, D. W. & TRIMBLE, W. S. 2013. Mitotic regulation of SEPT9 protein by cyclin-dependent kinase 1 (Cdk1) and Pin1 protein is important for the completion of cytokinesis. *J Biol Chem,* 288**,** 30075-86.
FADOK, V. A., BRATTON, D. L., ROSE, D. M., PEARSON, A., EZEKEWITZ, R. A. & HENSON, P. M. 2000. A receptor for phosphatidylserine-specific clearance of apoptotic cells. *Nature,* 405**,** 85-90.
FALNES, P. O., JOHANSEN, R. F. & SEEBERG, E. 2002. AlkB-mediated oxidative demethylation reverses DNA damage in Escherichia coli. *Nature,* 419**,** 178-82.
FANG, Y., YU, H., LIANG, X., XU, J. & CAI, X. 2014. Chk1-induced CCNB1 overexpression promotes cell proliferation and tumor growth in human colorectal cancer. *Cancer Biol Ther,* 15**,** 1268-79.
FENG, T., YAMAMOTO, A., WILKINS, S. E., SOKOLOVA, E., YATES, L. A., MUNZEL, M., SINGH, P., HOPKINSON, R. J., FISCHER, R., COCKMAN, M. E., SHELLEY, J., TRUDGIAN, D. C., SCHODEL, J., MCCULLAGH, J. S., GE, W., KESSLER, B. M., GILBERT, R. J., FROLOVA, L. Y., ALKALAEVA, E., RATCLIFFE, P. J., SCHOFIELD, C. J. & COLEMAN, M. L. 2014. Optimal translational termination requires C4 lysyl hydroxylation of eRF1. *Mol Cell,* 53**,** 645-54.
FERNANDES, R. J., FARNAND, A. W., TRAEGER, G. R., WEIS, M. A. & EYRE, D. R. 2011. A role for prolyl 3-hydroxylase 2 in post-translational modification of fibril-forming collagens. *J Biol Chem,* 286**,** 30662-9.
FERREIRA, S. I., MATOSO, E., VENANCIO, M., SARAIVA, J., MELO, J. B. & CARREIRA, I. M. 2012. Critical region in 2q31.2q32.3 deletion syndrome: Report of two phenotypically distinct patients, one with an additional deletion in Alagille syndrome region. *Mol Cytogenet,* 5**,** 25.
FERRERO, M., FERRAGUD, J., ORLANDO, L., VALERO, L., SANCHEZ DEL PINO, M., FARRAS, R. & FONT DE MORA, J. 2011. Phosphorylation of AIB1 at mitosis is regulated by CDK1/CYCLIN B. *PLoS One,* 6**,** e28602.
FILARSKY, M., ZILLNER, K., ARAYA, I., VILLAR-GAREA, A., MERKL, R., LANGST, G. & NEMETH, A. 2015. The extended AT-hook is a novel RNA binding motif. *RNA Biol,* 12**,** 864-76.
FINN, R. S., DERING, J., CONKLIN, D., KALOUS, O., COHEN, D. J., DESAI, A. J., GINTHER, C., ATEFI, M., CHEN, I., FOWST, C., LOS, G. & SLAMON, D. J. 2009. PD 0332991, a selective cyclin D kinase 4/6 inhibitor, preferentially inhibits proliferation of luminal estrogen receptor-positive human breast cancer cell lines in vitro. *Breast Cancer Res,* 11**,** R77.
FLAHERTY, K. T., ROBERT, C., HERSEY, P., NATHAN, P., GARBE, C., MILHEM, M., DEMIDOV, L. V., HASSEL, J. C., RUTKOWSKI, P., MOHR, P., DUMMER, R., TREFZER, U., LARKIN, J. M., UTIKAL, J., DRENO, B., NYAKAS, M., MIDDLETON, M. R., BECKER, J. C., CASEY, M., SHERMAN, L. J., WU, F. S., OUELLET, D., MARTIN, A. M., PATEL, K. & SCHADENDORF, D. 2012. Improved survival with MEK inhibition in BRAF-mutated melanoma. *N Engl J Med,* 367**,** 107-14.
FLORENES, V. A., MAELANDSMO, G. M., FAYE, R., NESLAND, J. M. & HOLM, R. 2001. Cyclin A expression in superficial spreading malignant melanomas correlates with clinical outcome. *J Pathol,* 195**,** 530-6.
FORBES, S. A., BEARE, D., BOUTSELAKIS, H., BAMFORD, S., BINDAL, N., TATE, J., COLE, C. G., WARD, S., DAWSON, E., PONTING, L., STEFANCSIK, R., HARSHA, B., KOK, C. Y., JIA, M., JUBB, H., SONDKA, Z., THOMPSON, S., DE, T. & CAMPBELL, P. J. 2017. COSMIC: somatic cancer genetics at high-resolution. *Nucleic Acids Res,* 45**,** D777-D783.
FRANCIS, S. M., GAS, M. E., DAUGERON, M. C., BRAVO, J. & SERAPHIN, B. 2012. Rbg1-Tma46 dimer structure reveals new functional domains and their role in polysome recruitment. *Nucleic Acids Res,* 40**,** 11100-14.
FREEDMAN, S. J., SUN, Z. Y., POY, F., KUNG, A. L., LIVINGSTON, D. M., WAGNER, G. & ECK, M. J. 2002. Structural basis for recruitment of CBP/p300 by hypoxia-inducible factor-1 alpha. *Proc Natl Acad Sci U S A,* 99**,** 5367-72.
FU, D., BROPHY, J. A., CHAN, C. T., ATMORE, K. A., BEGLEY, U., PAULES, R. S., DEDON, P. C., BEGLEY, T. J. & SAMSON, L. D. 2010. Human AlkB homolog ABH8 Is a tRNA methyltransferase required for wobble uridine modification and DNA damage survival. *Mol Cell Biol,* 30**,** 2449-59.

FU, D., SAMSON, L. D., HUBSCHER, U. & VAN LOON, B. 2015. The interaction between ALKBH2 DNA repair enzyme and PCNA is direct, mediated by the hydrophobic pocket of PCNA and perturbed in naturally-occurring ALKBH2 variants. *DNA Repair (Amst),* 35**,** 13-8.
FU, Y., DOMINISSINI, D., RECHAVI, G. & HE, C. 2014. Gene expression regulation mediated through reversible m(6)A RNA methylation. *Nat Rev Genet,* 15**,** 293-306.
FUJINO, S., KINUGASA, T., SUDO, T., MIZOBE, T., YOSHIDA, T., YOSHIDA, N., OHCHI, T., TAJIRI, K., YUGE, K., NAGASU, S., KATAGIRI, M. & AKAGI, Y. 2018. Mina53 nuclear localization is an important indicator of prognosis in patients with colorectal cancer after adjuvant chemotherapy. *Oncol Rep,* 40**,** 101-110.
GAO, J., AKSOY, B. A., DOGRUSOZ, U., DRESDNER, G., GROSS, B., SUMER, S. O., SUN, Y., JACOBSEN, A., SINHA, R., LARSSON, E., CERAMI, E., SANDER, C. & SCHULTZ, N. 2013. Integrative analysis of complex cancer genomics and clinical profiles using the cBioPortal. *Sci Signal,* 6**,** pl1.
GARNIS, C., BUYS, T. P. & LAM, W. L. 2004. Genetic alteration and gene expression modulation during cancer progression. *Mol Cancer,* 3**,** 9.
GARRETT, M. D. & FATTAEY, A. 1999. CDK inhibition and cancer therapy. *Curr Opin Genet Dev,* 9**,** 104-11.
GATEI, M., SCOTT, S. P., FILIPPOVITCH, I., SORONIKA, N., LAVIN, M. F., WEBER, B. & KHANNA, K. K. 2000. Role for ATM in DNA damage-induced phosphorylation of BRCA1. *Cancer Res,* 60**,** 3299-304.
GAVET, O. & PINES, J. 2010. Progressive activation of CyclinB1-Cdk1 coordinates entry to mitosis. *Dev Cell,* 18**,** 533-43.
GE, W., WOLF, A., FENG, T., HO, C. H., SEKIRNIK, R., ZAYER, A., GRANATINO, N., COCKMAN, M. E., LOENARZ, C., LOIK, N. D., HARDY, A. P., CLARIDGE, T. D. W., HAMED, R. B., CHOWDHURY, R., GONG, L., ROBINSON, C. V., TRUDGIAN, D. C., JIANG, M., MACKEEN, M. M., MCCULLAGH, J. S., GORDIYENKO, Y., THALHAMMER, A., YAMAMOTO, A., YANG, M., LIU-YI, P., ZHANG, Z., SCHMIDT-ZACHMANN, M., KESSLER, B. M., RATCLIFFE, P. J., PRESTON, G. M., COLEMAN, M. L. & SCHOFIELD, C. J. 2012. Oxygenase-catalyzed ribosome hydroxylation occurs in prokaryotes and humans. *Nat Chem Biol,* 8**,** 960-962.
GELSE, K., POSCHL, E. & AIGNER, T. 2003. Collagens--structure, function, and biosynthesis. *Adv Drug Deliv Rev,* 55**,** 1531-46.
GENG, F., JIANG, Z., SONG, X., ZHOU, H. & ZHAO, H. 2017. Mdig suppresses epithelial-mesenchymal transition and inhibits the invasion and metastasis of nonsmall cell lung cancer via regulating GSK-3beta/beta-catenin signaling. *Int J Oncol,* 51**,** 1898-1908.
GIBCUS, J. H. & DEKKER, J. 2012. The context of gene expression regulation. *F1000 Biol Rep,* 4**,** 8.
GIET, R. & GLOVER, D. M. 2001. Drosophila aurora B kinase is required for histone H3 phosphorylation and condensin recruitment during chromosome condensation and to organize the central spindle during cytokinesis. *J Cell Biol,* 152**,** 669-82.
GILKES, D. M., BAJPAI, S., CHATURVEDI, P., WIRTZ, D. & SEMENZA, G. L. 2013. Hypoxia-inducible factor 1 (HIF-1) promotes extracellular matrix remodeling under hypoxic conditions by inducing P4HA1, P4HA2, and PLOD2 expression in fibroblasts. *J Biol Chem,* 288**,** 10819-29.
GILLETTE, T. G. & HILL, J. A. 2015. Readers, writers, and erasers: chromatin as the whiteboard of heart disease. *Circ Res,* 116**,** 1245-53.
GJALTEMA, R. A. & BANK, R. A. 2017. Molecular insights into prolyl and lysyl hydroxylation of fibrillar collagens in health and disease. *Crit Rev Biochem Mol Biol,* 52**,** 74-95.
GUERRA-CASTELLANO, A., DIAZ-MORENO, I., VELAZQUEZ-CAMPOY, A., DE LA ROSA, M. A. & DIAZ-QUINTANA, A. 2016. Structural and functional characterization of phosphomimetic mutants of cytochrome c at threonine 28 and serine 47. *Biochim Biophys Acta,* 1857**,** 387-95.
GUTKIND, J. S. 2000. Regulation of mitogen-activated protein kinase signaling networks by G protein-coupled receptors. *Sci STKE,* 2000**,** re1.

GYORFFY, B., LANCZKY, A., EKLUND, A. C., DENKERT, C., BUDCZIES, J., LI, Q. & SZALLASI, Z. 2010. An online survival analysis tool to rapidly assess the effect of 22,277 genes on breast cancer prognosis using microarray data of 1,809 patients. *Breast Cancer Res Treat,* 123**,** 725-31.
HAHN, P., BOSE, J., EDLER, S. & LENGELING, A. 2008. Genomic structure and expression of Jmjd6 and evolutionary analysis in the context of related JmjC domain containing proteins. *BMC Genomics,* 9**,** 293.
HALL, M. & PETERS, G. 1996. Genetic alterations of cyclins, cyclin-dependent kinases, and Cdk inhibitors in human cancer. *Adv Cancer Res,* 68**,** 67-108.
HANAHAN, D. & WEINBERG, R. A. 2011. Hallmarks of cancer: the next generation. *Cell,* 144**,** 646-74.
HARREMAN, M. T., KLINE, T. M., MILFORD, H. G., HARBEN, M. B., HODEL, A. E. & CORBETT, A. H. 2004. Regulation of nuclear import by phosphorylation adjacent to nuclear localization signals. *J Biol Chem,* 279**,** 20613-21.
HARVEY, B. M. & HALTIWANGER, R. S. 2018. Regulation of Notch Function by O-Glycosylation. *Adv Exp Med Biol,* 1066**,** 59-78.
HARVEY, S. L., CHARLET, A., HAAS, W., GYGI, S. P. & KELLOGG, D. R. 2005. Cdk1-dependent regulation of the mitotic inhibitor Wee1. *Cell,* 122**,** 407-20.
HATZIMICHAEL, E., LO NIGRO, C., LATTANZIO, L., SYED, N., SHAH, R., DASOULA, A., JANCZAR, K., VIVENZA, D., MONTEVERDE, M., MERLANO, M., PAPOUDOU-BAI, A., BAI, M., SCHMID, P., STEBBING, J., BOWER, M., DYER, M. J., KARRAN, L. E., ELGUETAKARSTEGL, C., FARRELL, P. J., THOMPSON, A., BRIASOULIS, E. & CROOK, T. 2012. The collagen prolyl hydroxylases are novel transcriptionally silenced genes in lymphoma. *Br J Cancer,* 107**,** 1423-32.
HAUTALA, T., BYERS, M. G., EDDY, R. L., SHOWS, T. B., KIVIRIKKO, K. I. & MYLLYLA, R. 1992. Cloning of human lysyl hydroxylase: complete cDNA-derived amino acid sequence and assignment of the gene (PLOD) to chromosome 1p36.3----p36.2. *Genomics,* 13**,** 62-9.
HEARD, M. E., BESIO, R., WEIS, M., RAI, J., HUDSON, D. M., DIMORI, M., ZIMMERMAN, S. M., KAMYKOWSKI, J. A., HOGUE, W. R., SWAIN, F. L., BURDINE, M. S., MACKINTOSH, S. G., TACKETT, A. J., SUVA, L. J., EYRE, D. R. & MORELLO, R. 2016. Sc65-Null Mice Provide Evidence for a Novel Endoplasmic Reticulum Complex Regulating Collagen Lysyl Hydroxylation. *PLoS Genet,* 12**,** e1006002.
HEIKKINEN, J., RISTELI, M., WANG, C., LATVALA, J., ROSSI, M., VALTAVAARA, M. & MYLLYLA, R. 2000. Lysyl hydroxylase 3 is a multifunctional protein possessing collagen glucosyltransferase activity. *J Biol Chem,* 275**,** 36158-63.
HENDERSON, B. R. 2012. The BRCA1 Breast Cancer Suppressor: Regulation of Transport, Dynamics, and Function at Multiple Subcellular Locations. *Scientifica (Cairo),* 2012**,** 796808.
HEWITSON, K. S., MCNEILL, L. A., RIORDAN, M. V., TIAN, Y. M., BULLOCK, A. N., WELFORD, R. W., ELKINS, J. M., OLDHAM, N. J., BHATTACHARYA, S., GLEADLE, J. M., RATCLIFFE, P. J., PUGH, C. W. & SCHOFIELD, C. J. 2002. Hypoxia-inducible factor (HIF) asparagine hydroxylase is identical to factor inhibiting HIF (FIH) and is related to the cupin structural family. *J Biol Chem,* 277**,** 26351-5.
HIGASHI, H., SUZUKI-TAKAHASHI, I., TAYA, Y., SEGAWA, K., NISHIMURA, S. & KITAGAWA, M. 1995. Differences in substrate specificity between Cdk2-cyclin A and Cdk2-cyclin E in vitro. *Biochem Biophys Res Commun,* 216**,** 520-5.
HILLRINGHAUS, L., YUE, W. W., ROSE, N. R., NG, S. S., GILEADI, C., LOENARZ, C., BELLO, S. H., BRAY, J. E., SCHOFIELD, C. J. & OPPERMANN, U. 2011. Structural and evolutionary basis for the dual substrate selectivity of human KDM4 histone demethylase family. *J Biol Chem,* 286**,** 41616-25.
HIMPEL, S., PANZER, P., EIRMBTER, K., CZAJKOWSKA, H., SAYED, M., PACKMAN, L. C., BLUNDELL, T., KENTRUP, H., GROTZINGER, J., JOOST, H. G. & BECKER, W. 2001. Identification of the autophosphorylation sites and characterization of their effects in the protein kinase DYRK1A. *Biochem J,* 359**,** 497-505.
HIRSILA, M., KOIVUNEN, P., GUNZLER, V., KIVIRIKKO, K. I. & MYLLYHARJU, J. 2003. Characterization of the human prolyl 4-hydroxylases that modify the hypoxia-inducible factor. *J Biol Chem,* 278**,** 30772-80.

HO, J. R., CHAPEAUBLANC, E., KIRKWOOD, L., NICOLLE, R., BENHAMOU, S., LEBRET, T., ALLORY, Y., SOUTHGATE, J., RADVANYI, F. & GOUD, B. 2012. Deregulation of Rab and Rab effector genes in bladder cancer. *PLoS One,* 7**,** e39469.
HOLLAND, P. M. & COOPER, J. A. 1999. Protein modification: docking sites for kinases. *Curr Biol,* 9**,** R329-31.
HOLLERN, D. P., HONEYSETT, J., CARDIFF, R. D. & ANDRECHEK, E. R. 2014. The E2F transcription factors regulate tumor development and metastasis in a mouse model of metastatic breast cancer. *Mol Cell Biol,* 34**,** 3229-43.
HOMAN, E. P., LIETMAN, C., GRAFE, I., LENNINGTON, J., MORELLO, R., NAPIERALA, D., JIANG, M. M., MUNIVEZ, E. M., DAWSON, B., BERTIN, T. K., CHEN, Y., LUA, R., LICHTARGE, O., HICKS, J., WEIS, M. A., EYRE, D. & LEE, B. H. 2014. Differential effects of collagen prolyl 3-hydroxylation on skeletal tissues. *PLoS Genet,* 10**,** e1004121.
HONG, J. R., LIN, G. H., LIN, C. J., WANG, W. P., LEE, C. C., LIN, T. L. & WU, J. L. 2004. Phosphatidylserine receptor is required for the engulfment of dead apoptotic cells and for normal embryonic development in zebrafish. *Development,* 131**,** 5417-27.
HONG, S., CHO, Y. W., YU, L. R., YU, H., VEENSTRA, T. D. & GE, K. 2007. Identification of JmjC domain-containing UTX and JMJD3 as histone H3 lysine 27 demethylases. *Proc Natl Acad Sci U S A,* 104**,** 18439-44.
HORNBECK, P. V., ZHANG, B., MURRAY, B., KORNHAUSER, J. M., LATHAM, V. & SKRZYPEK, E. 2015. PhosphoSitePlus, 2014: mutations, PTMs and recalibrations. *Nucleic Acids Res,* 43**,** D512-20.
HORTON, J. R., ENGSTROM, A., ZOELLER, E. L., LIU, X., SHANKS, J. R., ZHANG, X., JOHNS, M. A., VERTINO, P. M., FU, H. & CHENG, X. 2016. Characterization of a Linked Jumonji Domain of the KDM5/JARID1 Family of Histone H3 Lysine 4 Demethylases. *J Biol Chem,* 291**,** 2631-46.
HSIA, D. A., TEPPER, C. G., POCHAMPALLI, M. R., HSIA, E. Y., IZUMIYA, C., HUERTA, S. B., WRIGHT, M. E., CHEN, H. W., KUNG, H. J. & IZUMIYA, Y. 2010. KDM8, a H3K36me2 histone demethylase that acts in the cyclin A1 coding region to regulate cancer cell proliferation. *Proc Natl Acad Sci U S A,* 107**,** 9671-6.
HU, B., MITRA, J., VAN DEN HEUVEL, S. & ENDERS, G. H. 2001. S and G2 phase roles for Cdk2 revealed by inducible expression of a dominant-negative mutant in human cells. *Mol Cell Biol,* 21**,** 2755-66.
HU, D., ANSARI, D., PAWLOWSKI, K., ZHOU, Q., SASOR, A., WELINDER, C., KRISTL, T., BAUDEN, M., REZELI, M., JIANG, Y., MARKO-VARGA, G. & ANDERSSON, R. 2018. Proteomic analyses identify prognostic biomarkers for pancreatic ductal adenocarcinoma. *Oncotarget,* 9**,** 9789-9807.
HU, Y. J. & IMBALZANO, A. N. 2016. Global gene expression profiling of JMJD6- and JMJD4-depleted mouse NIH3T3 fibroblasts. *Sci Data,* 3**,** 160022.
HUANG, C., XIANG, Y., WANG, Y., LI, X., XU, L., ZHU, Z., ZHANG, T., ZHU, Q., ZHANG, K., JING, N. & CHEN, C. D. 2010. Dual-specificity histone demethylase KIAA1718 (KDM7A) regulates neural differentiation through FGF4. *Cell Res,* 20**,** 154-65.
HUDSON, D. M., JOENG, K. S., WERTHER, R., RAJAGOPAL, A., WEIS, M., LEE, B. H. & EYRE, D. R. 2015. Post-translationally abnormal collagens of prolyl 3-hydroxylase-2 null mice offer a pathobiological mechanism for the high myopia linked to human LEPREL1 mutations. *J Biol Chem,* 290**,** 8613-22.
HUDSON, D. M., WEIS, M., RAI, J., JOENG, K. S., DIMORI, M., LEE, B. H., MORELLO, R. & EYRE, D. R. 2017. P3h3-null and Sc65-null Mice Phenocopy the Collagen Lysine Under-hydroxylation and Cross-linking Abnormality of Ehlers-Danlos Syndrome Type VIA. *J Biol Chem,* 292**,** 3877-3887.
HUNTER, T. 1995. Protein kinases and phosphatases: the yin and yang of protein phosphorylation and signaling. *Cell,* 80**,** 225-36.
HWANG, I., CHO, S. W. & AHN, J. Y. 2018. Chaperone-E3 Ligase Complex HSP70-CHIP Mediates Ubiquitination of Ribosomal Protein S3. *Int J Mol Sci,* 19.
INTERNATIONAL HUMAN GENOME SEQUENCING, C. 2004. Finishing the euchromatic sequence of the human genome. *Nature,* 431**,** 931-45.

ISHIHAMA, Y., ODA, Y., TABATA, T., SATO, T., NAGASU, T., RAPPSILBER, J. & MANN, M. 2005. Exponentially modified protein abundance index (emPAI) for estimation of absolute protein amount in proteomics by the number of sequenced peptides per protein. *Mol Cell Proteomics,* 4**,** 1265-72.
ISHIKAWA, K., AKIYAMA, T., ITO, K., SEMBA, K. & INOUE, J. 2009a. Independent stabilizations of polysomal Drg1/Dfrp1 complex and non-polysomal Drg2/Dfrp2 complex in mammalian cells. *Biochem Biophys Res Commun,* 390**,** 552-6.
ISHIKAWA, K., AZUMA, S., IKAWA, S., MORISHITA, Y., GOHDA, J., AKIYAMA, T., SEMBA, K. & INOUE, J. 2003. Cloning and characterization of Xenopus laevis drg2, a member of the developmentally regulated GTP-binding protein subfamily. *Gene,* 322**,** 105-12.
ISHIKAWA, K., AZUMA, S., IKAWA, S., SEMBA, K. & INOUE, J. 2005. Identification of DRG family regulatory proteins (DFRPs): specific regulation of DRG1 and DRG2. *Genes Cells,* 10**,** 139-50.
ISHIKAWA, K., ITO, K., INOUE, J. & SEMBA, K. 2013. Cell growth control by stable Rbg2/Gir2 complex formation under amino acid starvation. *Genes Cells,* 18**,** 859-72.
ISHIKAWA, Y., WIRZ, J., VRANKA, J. A., NAGATA, K. & BACHINGER, H. P. 2009b. Biochemical characterization of the prolyl 3-hydroxylase 1.cartilage-associated protein.cyclophilin B complex. *J Biol Chem,* 284**,** 17641-7.
ISHIMURA, A., MINEHATA, K., TERASHIMA, M., KONDOH, G., HARA, T. & SUZUKI, T. 2012. Jmjd5, an H3K36me2 histone demethylase, modulates embryonic cell proliferation through the regulation of Cdkn1a expression. *Development,* 139**,** 749-59.
ITO, S., SHEN, L., DAI, Q., WU, S. C., COLLINS, L. B., SWENBERG, J. A., HE, C. & ZHANG, Y. 2011. Tet proteins can convert 5-methylcytosine to 5-formylcytosine and 5-carboxylcytosine. *Science,* 333**,** 1300-3.
ITO, T., MATSUBARA, D., TANAKA, I., MAKIYA, K., TANEI, Z. I., KUMAGAI, Y., SHIU, S. J., NAKAOKA, H. J., ISHIKAWA, S., ISAGAWA, T., MORIKAWA, T., SHINOZAKI-USHIKU, A., GOTO, Y., NAKANO, T., TSUCHIYA, T., TSUBOCHI, H., KOMURA, D., ABURATANI, H., DOBASHI, Y., NAKAJIMA, J., ENDO, S., FUKAYAMA, M., SEKIDO, Y., NIKI, T. & MURAKAMI, Y. 2016. Loss of YAP1 defines neuroendocrine differentiation of lung tumors. *Cancer Sci,* 107**,** 1527-1538.
IZARD, J. W. & KENDALL, D. A. 1994. Signal peptides: exquisitely designed transport promoters. *Mol Microbiol,* 13**,** 765-73.
JACKMAN, M., KUBOTA, Y., DEN ELZEN, N., HAGTING, A. & PINES, J. 2002. Cyclin A- and cyclin E-Cdk complexes shuttle between the nucleus and the cytoplasm. *Mol Biol Cell,* 13**,** 1030-45.
JANG, S. H., KIM, A. R., PARK, N. H., PARK, J. W. & HAN, I. S. 2016. DRG2 Regulates G2/M Progression via the Cyclin B1-Cdk1 Complex. *Mol Cells,* 39**,** 699-704.
JENSEN, O. N. 2004. Modification-specific proteomics: characterization of post-translational modifications by mass spectrometry. *Curr Opin Chem Biol,* 8**,** 33-41.
JIA, G., FU, Y., ZHAO, X., DAI, Q., ZHENG, G., YANG, Y., YI, C., LINDAHL, T., PAN, T., YANG, Y. G. & HE, C. 2011. N6-methyladenosine in nuclear RNA is a major substrate of the obesity-associated FTO. *Nat Chem Biol,* 7**,** 885-7.
JIANG, B. G., WAN, Z. H., HUANG, J., LI, L. M., LIU, H., FU, S. Y., YANG, Y., ZHANG, J., YUAN, S. X., WANG, R. Y., YANG, Y., GU, F. M., DONG, L. W., PAN, Z. Y. & ZHOU, W. P. 2016. Elevated ZC3H15 increases HCC growth and predicts poor survival after surgical resection. *Oncotarget,* 7**,** 37238-37249.
JIANG, M., MA, Y., CHENG, H., NI, X., GUO, L., XIE, Y. & MAO, Y. 2001. Molecular cloning and characterization of a novel human gene (HSPBAP1) from human fetal brain. *Cytogenet Cell Genet,* 95**,** 48-51.
JIANG, W., ZHOU, X., LI, Z., LIU, K., WANG, W., TAN, R., CONG, X., SHAN, J., ZHAN, Y., CUI, Z., JIANG, L., LI, Q., SHEN, S., BAI, M., CHENG, Y., LI, B., TAN, M., MA, D. K., LIU, J. O. & DANG, Y. 2018. Prolyl 4-hydroxylase 2 promotes B-cell lymphoma progression via hydroxylation of Carabin. *Blood,* 131**,** 1325-1336.

JIANG, Y. & PRICE, D. H. 2004. Rescue of the TTF2 knockdown phenotype with an siRNA-resistant replacement vector. *Cell Cycle,* 3**,** 1151-3.
JOHANSSON, C., TUMBER, A., CHE, K., CAIN, P., NOWAK, R., GILEADI, C. & OPPERMANN, U. 2014. The roles of Jumonji-type oxygenases in human disease. *Epigenomics,* 6**,** 89-120.
JOHNSON, D. G. 2000. The paradox of E2F1: oncogene and tumor suppressor gene. *Mol Carcinog,* 27**,** 151-7.
JOHNSON, D. G. & DEGREGORI, J. 2006. Putting the Oncogenic and Tumor Suppressive Activities of E2F into Context. *Curr Mol Med,* 6**,** 731-8.
JOHNSON, L. N. 2009. The regulation of protein phosphorylation. *Biochem Soc Trans,* 37**,** 627-41.
JONES, M. A., COVINGTON, M. F., DITACCHIO, L., VOLLMERS, C., PANDA, S. & HARMER, S. L. 2010. Jumonji domain protein JMJD5 functions in both the plant and human circadian systems. *Proc Natl Acad Sci U S A,* 107**,** 21623-8.
KAFER, G. R., LI, X., HORII, T., SUETAKE, I., TAJIMA, S., HATADA, I. & CARLTON, P. M. 2016. 5-Hydroxymethylcytosine Marks Sites of DNA Damage and Promotes Genome Stability. *Cell Rep,* 14**,** 1283-1292.
KANAKKANTHARA, A., JEGANATHAN, K. B., LIMZERWALA, J. F., BAKER, D. J., HAMADA, M., NAM, H. J., VAN DEURSEN, W. H., HAMADA, N., NAYLOR, R. M., BECKER, N. A., DAVIES, B. A., VAN REE, J. H., MER, G., SHAPIRO, V. S., MAHER, L. J., 3RD, KATZMANN, D. J. & VAN DEURSEN, J. M. 2016. Cyclin A2 is an RNA binding protein that controls Mre11 mRNA translation. *Science,* 353**,** 1549-1552.
KATO, J., MATSUSHIME, H., HIEBERT, S. W., EWEN, M. E. & SHERR, C. J. 1993. Direct binding of cyclin D to the retinoblastoma gene product (pRb) and pRb phosphorylation by the cyclin D-dependent kinase CDK4. *Genes Dev,* 7**,** 331-42.
KATO, M., ARAISO, Y., NOMA, A., NAGAO, A., SUZUKI, T., ISHITANI, R. & NUREKI, O. 2011. Crystal structure of a novel JmjC-domain-containing protein, TYW5, involved in tRNA modification. *Nucleic Acids Res,* 39**,** 1576-85.
KATZ, M. J., ACEVEDO, J. M., LOENARZ, C., GALAGOVSKY, D., LIU-YI, P., PEREZ-PEPE, M., THALHAMMER, A., SEKIRNIK, R., GE, W., MELANI, M., THOMAS, M. G., SIMONETTA, S., BOCCACCIO, G. L., SCHOFIELD, C. J., COCKMAN, M. E., RATCLIFFE, P. J. & WAPPNER, P. 2014. Sudestada1, a Drosophila ribosomal prolyl-hydroxylase required for mRNA translation, cell homeostasis, and organ growth. *Proc Natl Acad Sci U S A,* 111**,** 4025-30.
KE, K., SUL, O. J., KIM, W. K., LEE, M. H., KO, M. S., SUH, J. H., KIM, H. J., KIM, S. Y., PARK, J. W. & CHOI, H. S. 2013. Overexpression of developmentally regulated GTP-binding protein-2 increases bone loss. *Am J Physiol Endocrinol Metab,* 304**,** E703-10.
KENNEDY, R. D. & D'ANDREA, A. D. 2005. The Fanconi Anemia/BRCA pathway: new faces in the crowd. *Genes Dev,* 19**,** 2925-40.
KHO, Y., KIM, S. C., JIANG, C., BARMA, D., KWON, S. W., CHENG, J., JAUNBERGS, J., WEINBAUM, C., TAMANOI, F., FALCK, J. & ZHAO, Y. 2004. A tagging-via-substrate technology for detection and proteomics of farnesylated proteins. *Proc Natl Acad Sci U S A,* 101**,** 12479-84.
KHOUEIRY, R., SOHNI, A., THIENPONT, B., LUO, X., VELDE, J. V., BARTOCCETTI, M., BOECKX, B., ZWIJSEN, A., RAO, A., LAMBRECHTS, D. & KOH, K. P. 2017. Lineage-specific functions of TET1 in the postimplantation mouse embryo. *Nat Genet,* 49**,** 1061-1072.
KHOURY-HADDAD, H., NADAR-PONNIAH, P. T., AWWAD, S. & AYOUB, N. 2015. The emerging role of lysine demethylases in DNA damage response: dissecting the recruitment mode of KDM4D/JMJD2D to DNA damage sites. *Cell Cycle,* 14**,** 950-8.
KHOURY, G. A., BALIBAN, R. C. & FLOUDAS, C. A. 2011. Proteome-wide post-translational modification statistics: frequency analysis and curation of the swiss-prot database. *Sci Rep,* 1.
KIM, S. J., NAKAYAMA, S., MIYOSHI, Y., TAGUCHI, T., TAMAKI, Y., MATSUSHIMA, T., TORIKOSHI, Y., TANAKA, S., YOSHIDA, T., ISHIHARA, H. & NOGUCHI, S. 2008. Determination of the specific activity of CDK1 and CDK2 as a novel prognostic indicator for early breast cancer. *Ann Oncol,* 19**,** 68-72.

KIM, S. M., KIM, J. Y., CHOE, N. W., CHO, I. H., KIM, J. R., KIM, D. W., SEOL, J. E., LEE, S. E., KOOK, H., NAM, K. I., KOOK, H., BHAK, Y. Y. & SEO, S. B. 2010. Regulation of mouse steroidogenesis by WHISTLE and JMJD1C through histone methylation balance. *Nucleic Acids Res,* 38**,** 6389-403.
KIVIRIKKO, K. I. & MYLLYHARJU, J. 1998. Prolyl 4-hydroxylases and their protein disulfide isomerase subunit. *Matrix Biol,* 16**,** 357-68.
KIVIRIKKO, K. I. & PROCKOP, D. J. 1972. Partial purification and characterization of protocollagen lysine hydroxylase from chick embryos. *Biochim Biophys Acta,* 258**,** 366-79.
KLOSE, R. J., KALLIN, E. M. & ZHANG, Y. 2006. JmjC-domain-containing proteins and histone demethylation. *Nat Rev Genet,* 7**,** 715-27.
KNORRE, D. G., KUDRYASHOVA, N. V. & GODOVIKOVA, T. S. 2009. Chemical and functional aspects of posttranslational modification of proteins. *Acta Naturae,* 1**,** 29-51.
KO, M. S., KIM, H. J., KIM, H. K., YOON, N. A., LEE, U. H., LEE, S. C., CHUNG, D. K., LEE, B. J., SUH, J. H., CHO, W. J. & PARK, J. W. 2014. Developmentally regulated GTP-binding protein 2 ameliorates EAE by suppressing the development of TH17 cells. *Clin Immunol,* 150**,** 225-35.
KO, M. S., LEE, U. H., KIM, S. I., KIM, H. J., PARK, J. J., CHA, S. J., KIM, S. B., SONG, H., CHUNG, D. K., HAN, I. S., KWACK, K. & PARK, J. W. 2004. Overexpression of DRG2 suppresses the growth of Jurkat T cells but does not induce apoptosis. *Arch Biochem Biophys,* 422**,** 137-44.
KOIVUNEN, P., HIRSILA, M., GUNZLER, V., KIVIRIKKO, K. I. & MYLLYHARJU, J. 2004. Catalytic properties of the asparaginyl hydroxylase (FIH) in the oxygen sensing pathway are distinct from those of its prolyl 4-hydroxylases. *J Biol Chem,* 279**,** 9899-904.
KOYAMA, K., FUKUSHIMA, Y., INAZAWA, J., TOMOTSUNE, D., TAKAHASHI, N. & NAKAMURA, Y. 1996. The human homologue of the murine Llglh gene (LLGL) maps within the Smith-Magenis syndrome region in 17p11.2. *Cytogenet Cell Genet,* 72**,** 78-82.
KUHNS, K. J., ZHANG, G., WANG, Z. & LIU, W. 2018. ARD1/NAA10 acetylation in prostate cancer. *Exp Mol Med,* 50**,** 89.
KUIPER, C. & VISSERS, M. C. 2014. Ascorbate as a co-factor for fe- and 2-oxoglutarate dependent dioxygenases: physiological activity in tumor growth and progression. *Front Oncol,* 4**,** 359.
KUKKOLA, L., HIETA, R., KIVIRIKKO, K. I. & MYLLYHARJU, J. 2003. Identification and characterization of a third human, rat, and mouse collagen prolyl 4-hydroxylase isoenzyme. *J Biol Chem,* 278**,** 47685-93.
KUMAR, S., IWAO, M., YAMAGISHI, T., NODA, M. & ASASHIMA, M. 1993. Expression of GTP-binding protein gene drg during Xenopus laevis development. *Int J Dev Biol,* 37**,** 539-46.
KUMAR, S. & REDDY, P. H. 2018. MicroRNA-455-3p as a Potential Biomarker for Alzheimer's Disease: An Update. *Front Aging Neurosci,* 10**,** 41.
KUMAR, S., TOMOOKA, Y. & NODA, M. 1992. Identification of a set of genes with developmentally down-regulated expression in the mouse brain. *Biochem Biophys Res Commun,* 185**,** 1155-61.
KUNISAKI, Y., MASUKO, S., NODA, M., INAYOSHI, A., SANUI, T., HARADA, M., SASAZUKI, T. & FUKUI, Y. 2004. Defective fetal liver erythropoiesis and T lymphopoiesis in mice lacking the phosphatidylserine receptor. *Blood,* 103**,** 3362-4.
L'ITALIEN, L., TANUDJI, M., RUSSELL, L. & SCHEBYE, X. M. 2006. Unmasking the redundancy between Cdk1 and Cdk2 at G2 phase in human cancer cell lines. *Cell Cycle,* 5**,** 984-93.
LA COUR, T., KIEMER, L., MOLGAARD, A., GUPTA, R., SKRIVER, K. & BRUNAK, S. 2004. Analysis and prediction of leucine-rich nuclear export signals. *Protein Eng Des Sel,* 17**,** 527-36.
LANCASTER, D. E., MCNEILL, L. A., MCDONOUGH, M. A., APLIN, R. T., HEWITSON, K. S., PUGH, C. W., RATCLIFFE, P. J. & SCHOFIELD, C. J. 2004. Disruption of dimerization and substrate phosphorylation inhibit factor inhibiting hypoxia-inducible factor (FIH) activity. *Biochem J,* 383**,** 429-37.
LANDFORS, M., NAKKEN, S., FUSSER, M., DAHL, J. A., KLUNGLAND, A. & FEDORCSAK, P. 2016. Sequencing of FTO and ALKBH5 in men undergoing infertility work-up identifies an infertility-associated variant and two missense mutations. *Fertil Steril,* 105**,** 1170-1179.e5.

LANDO, D., PEET, D. J., GORMAN, J. J., WHELAN, D. A., WHITELAW, M. L. & BRUICK, R. K. 2002a. FIH-1 is an asparaginyl hydroxylase enzyme that regulates the transcriptional activity of hypoxia-inducible factor. *Genes Dev,* 16**,** 1466-71.
LANDO, D., PEET, D. J., WHELAN, D. A., GORMAN, J. J. & WHITELAW, M. L. 2002b. Asparagine hydroxylation of the HIF transactivation domain a hypoxic switch. *Science,* 295**,** 858-61.
LAU, Y. F. & ZHANG, J. 2000. Expression analysis of thirty one Y chromosome genes in human prostate cancer. *Mol Carcinog,* 27**,** 308-21.
LEE, C. R., LEE, S. H., RIGAS, N. K., KIM, R. H., KANG, M. K., PARK, N. H. & SHIN, K. H. 2016. Elevated expression of JMJD6 is associated with oral carcinogenesis and maintains cancer stemness properties. *Carcinogenesis,* 37**,** 119-128.
LEE, H. J., CHUA, G. H., KRISHNAN, A., LANE, D. P. & VERMA, C. S. 2007. Substrate specificity of cyclins determined by electrostatics. *Cell Cycle,* 6**,** 2219-26.
LEE, Y. F., MILLER, L. D., CHAN, X. B., BLACK, M. A., PANG, B., ONG, C. W., SALTO-TELLEZ, M., LIU, E. T. & DESAI, K. V. 2012. JMJD6 is a driver of cellular proliferation and motility and a marker of poor prognosis in breast cancer. *Breast Cancer Res,* 14**,** R85.
LEVIN, M., STARK, M. & ASSARAF, Y. G. 2018. The JmjN domain as a dimerization interface and a targeted inhibitor of KDM4 demethylase activity. *Oncotarget,* 9**,** 16861-16882.
LI, B. & TRUEB, B. 2000. DRG represents a family of two closely related GTP-binding proteins. *Biochim Biophys Acta,* 1491**,** 196-204.
LI, M. O., SARKISIAN, M. R., MEHAL, W. Z., RAKIC, P. & FLAVELL, R. A. 2003. Phosphatidylserine receptor is required for clearance of apoptotic cells. *Science,* 302**,** 1560-3.
LI, N., DHAR, S. S., CHEN, T. Y., KAN, P. Y., WEI, Y., KIM, J. H., CHAN, C. H., LIN, H. K., HUNG, M. C. & LEE, M. G. 2016. JARID1D Is a Suppressor and Prognostic Marker of Prostate Cancer Invasion and Metastasis. *Cancer Res,* 76**,** 831-43.
LI, Y., CHEN, Y., MA, Y., NENKOV, M., HAASE, D. & PETERSEN, I. 2018. Collagen prolyl hydroxylase 3 has a tumor suppressive activity in human lung cancer. *Exp Cell Res,* 363**,** 121-128.
LIM, H. J., DIMOVA, N. V., TAN, M. K., SIGOILLOT, F. D., KING, R. W. & SHI, Y. 2013. The G2/M regulator histone demethylase PHF8 is targeted for degradation by the anaphase-promoting complex containing CDC20. *Mol Cell Biol,* 33**,** 4166-80.
LIN, J.-R., MONDAL, A. M., LIU, R. & HU, J. 2012. Minimalist ensemble algorithms for genome-wide protein localization prediction. *BMC Bioinformatics,* 13**,** 157.
LINDQVIST, A., RODRIGUEZ-BRAVO, V. & MEDEMA, R. H. 2009. The decision to enter mitosis: feedback and redundancy in the mitotic entry network. *J Cell Biol,* 185**,** 193-202.
LIU, C., GILMONT, R. R., BENNDORF, R. & WELSH, M. J. 2000. Identification and characterization of a novel protein from Sertoli cells, PASS1, that associates with mammalian small stress protein hsp27. *J Biol Chem,* 275**,** 18724-31.
LIU, F., CLARK, W., LUO, G., WANG, X., FU, Y., WEI, J., WANG, X., HAO, Z., DAI, Q., ZHENG, G., MA, H., HAN, D., EVANS, M., KLUNGLAND, A., PAN, T. & HE, C. 2016. ALKBH1-Mediated tRNA Demethylation Regulates Translation. *Cell,* 167**,** 816-828.e16.
LIU, H., WANG, C., LEE, S., DENG, Y., WITHER, M., OH, S., NING, F., DEGE, C., ZHANG, Q., LIU, X., JOHNSON, A. M., ZANG, J., CHEN, Z., JANKNECHT, R., HANSEN, K., MARRACK, P., LI, C. Y., KAPPLER, J. W., HAGMAN, J. & ZHANG, G. 2017a. Clipping of arginine-methylated histone tails by JMJD5 and JMJD7. *Proc Natl Acad Sci U S A,* 114**,** E7717-e7726.
LIU, H., WANG, C., LEE, S., NING, F., WANG, Y., ZHANG, Q., CHEN, Z., ZANG, J., NIX, J., DAI, S., MARRACK, P., HAGMAN, J., KAPPLER, J. & ZHANG, G. 2018a. Specific Recognition of Arginine Methylated Histone Tails by JMJD5 and JMJD7. *Sci Rep,* 8**,** 3275.
LIU, L., KIM, H., CASTA, A., KOBAYASHI, Y., SHAPIRO, L. S. & CHRISTIANO, A. M. 2014. Hairless is a histone H3K9 demethylase. *Faseb j,* 28**,** 1534-42.

LIU, M., LIU, Y., DENG, L., WANG, D., HE, X., ZHOU, L., WICHA, M. S., BAI, F. & LIU, S. 2018b. Transcriptional profiles of different states of cancer stem cells in triple-negative breast cancer. *Mol Cancer,* 17**,** 65.
LIU, N. A., JIANG, H., BEN-SHLOMO, A., WAWROWSKY, K., FAN, X. M., LIN, S. & MELMED, S. 2011. Targeting zebrafish and murine pituitary corticotroph tumors with a cyclin-dependent kinase (CDK) inhibitor. *Proc Natl Acad Sci U S A,* 108**,** 8414-9.
LIU, W., MA, Q., WONG, K., LI, W., OHGI, K., ZHANG, J., AGGARWAL, A. & ROSENFELD, M. G. 2013. Brd4 and JMJD6-associated anti-pause enhancers in regulation of transcriptional pause release. *Cell,* 155**,** 1581-1595.
LIU, W., TANASA, B., TYURINA, O. V., ZHOU, T. Y., GASSMANN, R., LIU, W. T., OHGI, K. A., BENNER, C., GARCIA-BASSETS, I., AGGARWAL, A. K., DESAI, A., DORRESTEIN, P. C., GLASS, C. K. & ROSENFELD, M. G. 2010a. PHF8 mediates histone H4 lysine 20 demethylation events involved in cell cycle progression. *Nature,* 466**,** 508-12.
LIU, X., SI, W., LIU, X., HE, L., REN, J., YANG, Z., YANG, J., LI, W., LIU, S., PEI, F., YANG, X. & SUN, L. 2017b. JMJD6 promotes melanoma carcinogenesis through regulation of the alternative splicing of PAK1, a key MAPK signaling component. *Mol Cancer,* 16**,** 175.
LIU, Y., HUO, Z., YAN, B., LIN, X., ZHOU, Z. N., LIANG, X., ZHU, W., LIANG, D., LI, L., LIU, Y., ZHAO, H., SUN, Y. & CHEN, Y. H. 2010b. Prolyl hydroxylase 3 interacts with Bcl-2 to regulate doxorubicin-induced apoptosis in H9c2 cells. *Biochem Biophys Res Commun,* 401**,** 231-7.
LOENARZ, C., GE, W., COLEMAN, M. L., ROSE, N. R., COOPER, C. D., KLOSE, R. J., RATCLIFFE, P. J. & SCHOFIELD, C. J. 2010. PHF8, a gene associated with cleft lip/palate and mental retardation, encodes for an Nepsilon-dimethyl lysine demethylase. *Hum Mol Genet,* 19**,** 217-22.
LOENARZ, C., SEKIRNIK, R., THALHAMMER, A., GE, W., SPIVAKOVSKY, E., MACKEEN, M. M., MCDONOUGH, M. A., COCKMAN, M. E., KESSLER, B. M., RATCLIFFE, P. J., WOLF, A. & SCHOFIELD, C. J. 2014. Hydroxylation of the eukaryotic ribosomal decoding center affects translational accuracy. *Proc Natl Acad Sci U S A,* 111**,** 4019-24.
LOLLI, G. & JOHNSON, L. N. 2005. CAK-Cyclin-dependent Activating Kinase: a key kinase in cell cycle control and a target for drugs? *Cell Cycle,* 4**,** 572-7.
LONG, X. E., GONG, Z. H., PAN, L., ZHONG, Z. W., LE, Y. P., LIU, Q., GUO, J. M. & ZHONG, J. C. 2010. Suppression of CDK2 expression by siRNA induces cell cycle arrest and cell proliferation inhibition in human cancer cells. *BMB Rep,* 43**,** 291-6.
LOTHROP, A. P., TORRES, M. P. & FUCHS, S. M. 2013. Deciphering post-translational modification codes. *FEBS Lett,* 587**,** 1247-57.
LU, L., LV, Y., DONG, J., HU, S. & PENG, R. 2016. DRG1 is a potential oncogene in lung adenocarcinoma and promotes tumor progression via spindle checkpoint signaling regulation. *Oncotarget,* 7**,** 72795-72806.
LU, Y., CHANG, Q., ZHANG, Y., BEEZHOLD, K., ROJANASAKUL, Y., ZHAO, H., CASTRANOVA, V., SHI, X. & CHEN, F. 2009. Lung cancer-associated JmjC domain protein mdig suppresses formation of tri-methyl lysine 9 of histone H3. *Cell Cycle,* 8**,** 2101-9.
LUTFUL KABIR, F. M., ALVAREZ, C. E. & BIRD, R. C. 2015. Canine Mammary Carcinomas: A Comparative Analysis of Altered Gene Expression. *Vet Sci,* 3.
MA, H. T. & POON, R. Y. 2011. Synchronization of HeLa cells. *Methods Mol Biol,* 761**,** 151-61.
MAHAJAN, M. A., PARK, S. T. & SUN, X. H. 1996. Association of a novel GTP binding protein, DRG, with TAL oncogenic proteins. *Oncogene,* 12**,** 2343-50.
MAHON, P. C., HIROTA, K. & SEMENZA, G. L. 2001. FIH-1: a novel protein that interacts with HIF-1alpha and VHL to mediate repression of HIF-1 transcriptional activity. *Genes Dev,* 15**,** 2675-86.
MAITI, A. & DROHAT, A. C. 2011. Thymine DNA glycosylase can rapidly excise 5-formylcytosine and 5-carboxylcytosine: potential implications for active demethylation of CpG sites. *J Biol Chem,* 286**,** 35334-8.
MALUMBRES, M. 2014. Cyclin-dependent kinases. *Genome Biol,* 15**,** 122.

MALUMBRES, M. & BARBACID, M. 2001. To cycle or not to cycle: a critical decision in cancer. *Nat Rev Cancer,* 1**,** 222-31.
MANI, M., LEE, U. H., YOON, N. A., KIM, H. J., KO, M. S., SEOL, W., JOE, Y., CHUNG, H. T., LEE, B. J., MOON, C. H., CHO, W. J. & PARK, J. W. 2016. Developmentally regulated GTP-binding protein 2 coordinates Rab5 activity and transferrin recycling. *Mol Biol Cell,* 27**,** 334-48.
MANI, M., LEE, U. H., YOON, N. A., YOON, E. H., LEE, B. J., CHO, W. J. & PARK, J. W. 2017. Developmentally regulated GTP-binding protein 2 is required for stabilization of Rac1-positive membrane tubules. *Biochem Biophys Res Commun,* 493**,** 758-764.
MARCEAUX, C., PETIT, D., BERTOGLIO, J. & DAVID, M. D. 2018. Phosphorylation of ARHGAP19 by CDK1 and ROCK regulates its subcellular localization and function during mitosis. *J Cell Sci,* 131.
MARKOLOVIC, S., LEISSING, T. M., CHOWDHURY, R., WILKINS, S. E., LU, X. & SCHOFIELD, C. J. 2016. Structure-function relationships of human JmjC oxygenases-demethylases versus hydroxylases. *Curr Opin Struct Biol,* 41**,** 62-72.
MARKOLOVIC, S., WILKINS, S. E. & SCHOFIELD, C. J. 2015. Protein Hydroxylation Catalyzed by 2-Oxoglutarate-dependent Oxygenases. *J Biol Chem,* 290**,** 20712-22.
MARKOLOVIC, S., ZHUANG, Q., WILKINS, S. E., EATON, C. D., ABBOUD, M. I., KATZ, M. J., MCNEIL, H. E., LESNIAK, R. K., HALL, C., STRUWE, W. B., KONIETZNY, R., DAVIS, S., YANG, M., GE, W., BENESCH, J. L. P., KESSLER, B. M., RATCLIFFE, P. J., COCKMAN, M. E., FISCHER, R., WAPPNER, P., CHOWDHURY, R., COLEMAN, M. L. & SCHOFIELD, C. J. 2018. The Jumonji-C oxygenase JMJD7 catalyzes (3S)-lysyl hydroxylation of TRAFAC GTPases. *Nat Chem Biol,* 14**,** 688-695.
MARTINEZ, S. & HAUSINGER, R. P. 2015. Catalytic Mechanisms of Fe(II)- and 2-Oxoglutarate-dependent Oxygenases. *J Biol Chem,* 290**,** 20702-11.
MATHEISL, S., BERNINGHAUSEN, O., BECKER, T. & BECKMANN, R. 2015. Structure of a human translation termination complex. *Nucleic Acids Res,* 43**,** 8615-26.
MATSUNAMI, N., HENSEL, C. H., BAIRD, L., STEVENS, J., OTTERUD, B., LEPPERT, T., VARVIL, T., HADLEY, D., GLESSNER, J. T., PELLEGRINO, R., KIM, C., THOMAS, K., WANG, F., OTIENO, F. G., HO, K., CHRISTENSEN, G. B., LI, D., PREKERIS, R., LAMBERT, C. G., HAKONARSON, H. & LEPPERT, M. F. 2014. Identification of rare DNA sequence variants in high-risk autism families and their prevalence in a large case/control population. *Mol Autism,* 5**,** 5.
MCDONOUGH, M. A., LOENARZ, C., CHOWDHURY, R., CLIFTON, I. J. & SCHOFIELD, C. J. 2010. Structural studies on human 2-oxoglutarate dependent oxygenases. *Curr Opin Struct Biol,* 20**,** 659-72.
MERKLER, D. J. 1994. C-terminal amidated peptides: production by the in vitro enzymatic amidation of glycine-extended peptides and the importance of the amide to bioactivity. *Enzyme Microb Technol,* 16**,** 450-6.
METZEN, E., BERCHNER-PFANNSCHMIDT, U., STENGEL, P., MARXSEN, J. H., STOLZE, I., KLINGER, M., HUANG, W. Q., WOTZLAW, C., HELLWIG-BURGEL, T., JELKMANN, W., ACKER, H. & FANDREY, J. 2003. Intracellular localisation of human HIF-1 alpha hydroxylases: implications for oxygen sensing. *J Cell Sci,* 116**,** 1319-26.
MILLER, C. J. & TURK, B. E. 2018. Homing in: Mechanisms of Substrate Targeting by Protein Kinases. *Trends Biochem Sci,* 43**,** 380-394.
MILLER, M. L., REZNIK, E., GAUTHIER, N. P., AKSOY, B. A., KORKUT, A., GAO, J., CIRIELLO, G., SCHULTZ, N. & SANDER, C. 2015. Pan-Cancer Analysis of Mutation Hotspots in Protein Domains. *Cell Syst,* 1**,** 197-209.
MILLER, T. E., LIAU, B. B., WALLACE, L. C., MORTON, A. R., XIE, Q., DIXIT, D., FACTOR, D. C., KIM, L. J. Y., MORROW, J. J., WU, Q., MACK, S. C., HUBERT, C. G., GILLESPIE, S. M., FLAVAHAN, W. A., HOFFMANN, T., THUMMALAPALLI, R., HEMANN, M. T., PADDISON, P. J., HORBINSKI, C. M., ZUBER, J., SCACHERI, P. C., BERNSTEIN, B. E., TESAR, P. J. & RICH, J. N. 2017. Transcription elongation factors represent in vivo cancer dependencies in glioblastoma. *Nature,* 547**,** 355-359.
MISRA, R. N., XIAO, H. Y., KIM, K. S., LU, S., HAN, W. C., BARBOSA, S. A., HUNT, J. T., RAWLINS, D. B., SHAN, W., AHMED, S. Z., QIAN, L., CHEN, B. C., ZHAO, R., BEDNARZ, M. S., KELLAR, K. A., MULHERON,

J. G., BATORSKY, R., ROONGTA, U., KAMATH, A., MARATHE, P., RANADIVE, S. A., SACK, J. S., TOKARSKI, J. S., PAVLETICH, N. P., LEE, F. Y., WEBSTER, K. R. & KIMBALL, S. D. 2004. N-(cycloalkylamino)acyl-2-aminothiazole inhibitors of cyclin-dependent kinase 2. N-[5-[[[5-(1,1-dimethylethyl)-2-oxazolyl]methyl]thio]-2-thiazolyl]-4- piperidinecarboxamide (BMS-387032), a highly efficacious and selective antitumor agent. *J Med Chem,* 47**,** 1719-28.
MONTECUCCO, A., ZANETTA, F. & BIAMONTI, G. 2015. Molecular mechanisms of etoposide. *Excli j,* 14**,** 95-108.
MOON, H. G., OH, K., LEE, J., LEE, M., KIM, J. Y., YOO, T. K., SEO, M. W., PARK, A. K., RYU, H. S., JUNG, E. J., KIM, N., JEONG, S., HAN, W., LEE, D. S. & NOH, D. Y. 2015. Prognostic and functional importance of the engraftment-associated genes in the patient-derived xenograft models of triple-negative breast cancers. *Breast Cancer Res Treat,* 154**,** 13-22.
MORDECHAI, S., GRADSTEIN, L., PASANEN, A., OFIR, R., EL AMOUR, K., LEVY, J., BELFAIR, N., LIFSHITZ, T., JOSHUA, S., NARKIS, G., ELBEDOUR, K., MYLLYHARJU, J. & BIRK, O. S. 2011. High myopia caused by a mutation in LEPREL1, encoding prolyl 3-hydroxylase 2. *Am J Hum Genet,* 89**,** 438-45.
MORELLO, R., BERTIN, T. K., CHEN, Y., HICKS, J., TONACHINI, L., MONTICONE, M., CASTAGNOLA, P., RAUCH, F., GLORIEUX, F. H., VRANKA, J., BACHINGER, H. P., PACE, J. M., SCHWARZE, U., BYERS, P. H., WEIS, M., FERNANDES, R. J., EYRE, D. R., YAO, Z., BOYCE, B. F. & LEE, B. 2006. CRTAP is required for prolyl 3- hydroxylation and mutations cause recessive osteogenesis imperfecta. *Cell,* 127**,** 291-304.
MORI, T., OKAMOTO, K., TANAKA, Y., TEYE, K., UMATA, T., OHNEDA, K., TOKUYAMA, K., OKABE, M. & TSUNEOKA, M. 2013. Ablation of Mina53 in mice reduces allergic response in the airways. *Cell Struct Funct,* 38**,** 155-67.
MORIMOTO, T., LOH, P. C., HIRAI, T., ASAI, K., KOBAYASHI, K., MORIYA, S. & OGASAWARA, N. 2002. Six GTP-binding proteins of the Era/Obg family are essential for cell growth in Bacillus subtilis. *Microbiology,* 148**,** 3539-52.
MORIYA, H. 2015. Quantitative nature of overexpression experiments. *Mol Biol Cell,* 26**,** 3932-9.
MORO, M. L., PHILLIPS, A. S., GAIMSTER, K., PAUL, C., MUDHER, A., NICOLL, J. A. R. & BOCHE, D. 2018. Pyroglutamate and Isoaspartate modified Amyloid-Beta in ageing and Alzheimer's disease. *Acta Neuropathol Commun,* 6**,** 3.
MOSER, S. C., BENSADDEK, D., ORTMANN, B., MAURE, J. F., MUDIE, S., BLOW, J. J., LAMOND, A. I., SWEDLOW, J. R. & ROCHA, S. 2013. PHD1 links cell-cycle progression to oxygen sensing through hydroxylation of the centrosomal protein Cep192. *Dev Cell,* 26**,** 381-92.
MUELLER, J. W., IDKOWIAK, J., GESTEIRA, T. F., VALLET, C., HARDMAN, R., VAN DEN BOOM, J., DHIR, V., KNAUER, S. K., ROSTA, E. & ARLT, W. 2018. Human DHEA sulfation requires direct interaction between PAPS synthase 2 and DHEA sulfotransferase SULT2A1. *J Biol Chem,* 293**,** 9724-9735.
MULLER, A. C., GIAMBRUNO, R., WEISSER, J., MAJEK, P., HOFER, A., BIGENZAHN, J. W., SUPERTI-FURGA, G., JESSEN, H. J. & BENNETT, K. L. 2016. Identifying Kinase Substrates via a Heavy ATP Kinase Assay and Quantitative Mass Spectrometry. *Sci Rep,* 6**,** 28107.
MULLERS, E., SILVA CASCALES, H., BURDOVA, K., MACUREK, L. & LINDQVIST, A. 2017. Residual Cdk1/2 activity after DNA damage promotes senescence. *Aging Cell,* 16**,** 575-584.
MYLLYHARJU, J. 2003. Prolyl 4-hydroxylases, the key enzymes of collagen biosynthesis. *Matrix Biol,* 22**,** 15-24.
NAKAMINE, A., OUCHANOV, L., JIMENEZ, P., MANGHI, E. R., ESQUIVEL, M., MONGE, S., FALLAS, M., BURTON, B. K., SZOMJU, B., ELSEA, S. H., MARSHALL, C. R., SCHERER, S. W. & MCINNES, L. A. 2008. Duplication of 17(p11.2p11.2) in a male child with autism and severe language delay. *Am J Med Genet A,* 146a**,** 636-43.
NEBBIOSO, A., TAMBARO, F. P., DELL'AVERSANA, C. & ALTUCCI, L. 2018. Cancer epigenetics: Moving forward. *PLoS Genet,* 14**,** e1007362.
NICOLAS, E., GOLEMIS, E. A. & ARORA, S. 2016. POLD1: Central mediator of DNA replication and repair, and implication in cancer and other pathologies. *Gene,* 590**,** 128-41.
NIELSEN, H. 2017. Predicting Secretory Proteins with SignalP. *Methods Mol Biol,* 1611**,** 59-73.

NIMEUS-MALMSTROM, E., KOLIADI, A., AHLIN, C., HOLMQVIST, M., HOLMBERG, L., AMINI, R. M., JIRSTROM, K., WARNBERG, F., BLOMQVIST, C., FERNO, M. & FJALLSKOG, M. L. 2010. Cyclin B1 is a prognostic proliferation marker with a high reproducibility in a population-based lymph node negative breast cancer cohort. *Int J Cancer,* 127**,** 961-7.
NISHI, H., HASHIMOTO, K. & PANCHENKO, A. R. 2011. Phosphorylation in protein-protein binding: effect on stability and function. *Structure,* 19**,** 1807-15.
NISHIZAWA, Y., NISHIDA, N., KONNO, M., KAWAMOTO, K., ASAI, A., KOSEKI, J., TAKAHASHI, H., HARAGUCHI, N., NISHIMURA, J., HATA, T., MATSUDA, C., MIZUSHIMA, T., SATOH, T., DOKI, Y., MORI, M. & ISHII, H. 2017. Clinical Significance of Histone Demethylase NO66 in Invasive Colorectal Cancer. *Ann Surg Oncol,* 24**,** 841-849.
NODA, T., YAMAMOTO, H., TAKEMASA, I., YAMADA, D., UEMURA, M., WADA, H., KOBAYASHI, S., MARUBASHI, S., EGUCHI, H., TANEMURA, M., UMESHITA, K., DOKI, Y., MORI, M. & NAGANO, H. 2012. PLOD2 induced under hypoxia is a novel prognostic factor for hepatocellular carcinoma after curative resection. *Liver Int,* 32**,** 110-8.
NOMA, A., ISHITANI, R., KATO, M., NAGAO, A., NUREKI, O. & SUZUKI, T. 2010. Expanding role of the jumonji C domain as an RNA hydroxylase. *J Biol Chem,* 285**,** 34503-7.
O'FARRELL, P. H. 2001. Triggering the all-or-nothing switch into mitosis. *Trends Cell Biol,* 11**,** 512-9.
O'ROURKE, J. F., DACHS, G. U., GLEADLE, J. M., MAXWELL, P. H., PUGH, C. W., STRATFORD, I. J., WOOD, S. M. & RATCLIFFE, P. J. 1997. Hypoxia response elements. *Oncol Res,* 9**,** 327-32.
OGAWA, Y., NONAKA, Y., GOTO, T., OHNISHI, E., HIRAMATSU, T., KII, I., YOSHIDA, M., IKURA, T., ONOGI, H., SHIBUYA, H., HOSOYA, T., ITO, N. & HAGIWARA, M. 2010. Development of a novel selective inhibitor of the Down syndrome-related kinase Dyrk1A. *Nat Commun,* 1**,** 86.
OH, S. & JANKNECHT, R. 2012. Histone demethylase JMJD5 is essential for embryonic development. *Biochem Biophys Res Commun,* 420**,** 61-5.
OHSHIO, I., KAWAKAMI, R., TSUKADA, Y., NAKAJIMA, K., KITAE, K., SHIMANOE, T., SAIGO, Y., HASE, H., UEDA, Y., JINGUSHI, K. & TSUJIKAWA, K. 2016. ALKBH8 promotes bladder cancer growth and progression through regulating the expression of survivin. *Biochem Biophys Res Commun,* 477**,** 413-8.
OLSON, E. N., ARNOLD, H. H., RIGBY, P. W. & WOLD, B. J. 1996. Know your neighbors: three phenotypes in null mutants of the myogenic bHLH gene MRF4. *Cell,* 85**,** 1-4.
ORTMANN, B., BENSADDEK, D., CARVALHAL, S., MOSER, S. C., MUDIE, S., GRIFFIS, E. R., SWEDLOW, J. R., LAMOND, A. I. & ROCHA, S. 2016. CDK-dependent phosphorylation of PHD1 on serine 130 alters its substrate preference in cells. *J Cell Sci,* 129**,** 191-205.
OUGLAND, R., LANDO, D., JONSON, I., DAHL, J. A., MOEN, M. N., NORDSTRAND, L. M., ROGNES, T., LEE, J. T., KLUNGLAND, A., KOUZARIDES, T. & LARSEN, E. 2012. ALKBH1 is a histone H2A dioxygenase involved in neural differentiation. *Stem Cells,* 30**,** 2672-82.
PARK, J. B., AGNIHOTRI, S., GOLBOURN, B., BERTRAND, K. C., LUCK, A., SABHA, N., SMITH, C. A., BYRON, S., ZADEH, G., CROUL, S., BERENS, M. & RUTKA, J. T. 2014. Transcriptional profiling of GBM invasion genes identifies effective inhibitors of the LIM kinase-Cofilin pathway. *Oncotarget,* 5**,** 9382-95.
PASSOJA, K., RAUTAVUOMA, K., ALA-KOKKO, L., KOSONEN, T. & KIVIRIKKO, K. I. 1998. Cloning and characterization of a third human lysyl hydroxylase isoform. *Proc Natl Acad Sci U S A,* 95**,** 10482-6.
PAVLETICH, N. P., CHAMBERS, K. A. & PABO, C. O. 1993. The DNA-binding domain of p53 contains the four conserved regions and the major mutation hot spots. *Genes Dev,* 7**,** 2556-64.
PETSALAKI, E., AKOUMIANAKI, T., BLACK, E. J., GILLESPIE, D. A. & ZACHOS, G. 2011. Phosphorylation at serine 331 is required for Aurora B activation. *J Cell Biol,* 195**,** 449-66.
PETTERSEN, E. F., GODDARD, T. D., HUANG, C. C., COUCH, G. S., GREENBLATT, D. M., MENG, E. C. & FERRIN, T. E. 2004. UCSF Chimera--a visualization system for exploratory research and analysis. *J Comput Chem,* 25**,** 1605-12.
PICKARD, R. T., STRIFLER, B. A., KRAMER, R. M. & SHARP, J. D. 1999. Molecular cloning of two new human paralogs of 85-kDa cytosolic phospholipase A2. *J Biol Chem,* 274**,** 8823-31.

PICKART, C. M. 2004. Back to the future with ubiquitin. *Cell,* 116**,** 181-90.
PIERCE, A. M., SCHNEIDER-BROUSSARD, R., GIMENEZ-CONTI, I. B., RUSSELL, J. L., CONTI, C. J. & JOHNSON, D. G. 1999. E2F1 has both oncogenic and tumor-suppressive properties in a transgenic model. *Mol Cell Biol,* 19**,** 6408-14.
PIKE, T., BROWNLOW, N., KJAER, S., CARLTON, J. & PARKER, P. J. 2016. PKCvarepsilon switches Aurora B specificity to exit the abscission checkpoint. *Nat Commun,* 7**,** 13853.
PILLAI, M. R., LIAN, S. & BIX, M. 2014. Mina: a Th2 response regulator meets TGFbeta. *Curr Opin Immunol,* 31**,** 38-43.
PIRES-LUIS, A. S., VIEIRA-COIMBRA, M., VIEIRA, F. Q., COSTA-PINHEIRO, P., SILVA-SANTOS, R., DIAS, P. C., ANTUNES, L., LOBO, F., OLIVEIRA, J., GONCALVES, C. S., COSTA, B. M., HENRIQUE, R. & JERONIMO, C. 2015. Expression of histone methyltransferases as novel biomarkers for renal cell tumor diagnosis and prognostication. *Epigenetics,* 10**,** 1033-43.
PLOUMAKIS, A. & COLEMAN, M. L. 2015. OH, the Places You'll Go! Hydroxylation, Gene Expression, and Cancer. *Mol Cell,* 58**,** 729-41.
POKIDYSHEVA, E., BOUDKO, S., VRANKA, J., ZIENTEK, K., MADDOX, K., MOSER, M., FASSLER, R., WARE, J. & BACHINGER, H. P. 2014. Biological role of prolyl 3-hydroxylation in type IV collagen. *Proc Natl Acad Sci U S A,* 111**,** 161-6.
POPPY ROWORTH, A., GHARI, F. & LA THANGUE, N. B. 2015. To live or let die - complexity within the E2F1 pathway. *Mol Cell Oncol,* 2**,** e970480.
POULARD, C., RAMBAUD, J., LAVERGNE, E., JACQUEMETTON, J., RENOIR, J. M., TREDAN, O., CHABAUD, S., TREILLEUX, I., CORBO, L. & LE ROMANCER, M. 2015. Role of JMJD6 in Breast Tumourigenesis. *PLoS One,* 10**,** e0126181.
PRAKASH, T., SHARMA, V. K., ADATI, N., OZAWA, R., KUMAR, N., NISHIDA, Y., FUJIKAKE, T., TAKEDA, T. & TAYLOR, T. D. 2010. Expression of conjoined genes: another mechanism for gene regulation in eukaryotes. *PLoS One,* 5**,** e13284.
PRINDLE, M. J. & LOEB, L. A. 2012. DNA polymerase delta in DNA replication and genome maintenance. *Environ Mol Mutagen,* 53**,** 666-82.
PUCA, R., NARDINOCCHI, L., SACCHI, A., RECHAVI, G., GIVOL, D. & D'ORAZI, G. 2009. HIPK2 modulates p53 activity towards pro-apoptotic transcription. *Mol Cancer,* 8**,** 85.
QI, L. & ZHANG, Y. 2015. Alisertib (MLN8237), a selective Aurora-A kinase inhibitor, induces apoptosis in human tongue squamous cell carcinoma cell both in vitro and in vivo. *Tumour Biol,* 36**,** 1797-802.
RASMUSSEN, K. D. & HELIN, K. 2016. Role of TET enzymes in DNA methylation, development, and cancer. *Genes Dev,* 30**,** 733-50.
RATOVITSKI, T., ARBEZ, N., STEWART, J. C., CHIGHLADZE, E. & ROSS, C. A. 2015. PRMT5- mediated symmetric arginine dimethylation is attenuated by mutant huntingtin and is impaired in Huntington's disease (HD). *Cell Cycle,* 14**,** 1716-29.
REED, S. M. & QUELLE, D. E. 2014. p53 Acetylation: Regulation and Consequences. *Cancers (Basel),* 7**,** 30-69.
REIMAND, J., WAGIH, O. & BADER, G. D. 2013. The mutational landscape of phosphorylation signaling in cancer. *Sci Rep,* 3**,** 2651.
REN, S. & ROLLINS, B. J. 2004. Cyclin C/cdk3 promotes Rb-dependent G0 exit. *Cell,* 117**,** 239-51.
ROUNBEHLER, R. J., ROGERS, P. M., CONTI, C. J. & JOHNSON, D. G. 2002. Inactivation of E2f1 enhances tumorigenesis in a Myc transgenic model. *Cancer Res,* 62**,** 3276-81.
RUBINSZTEIN, D. C. 2010. Cdks regulate autophagy via Vps34. *Mol Cell,* 38**,** 483-4.
RUE, P. & MARTINEZ ARIAS, A. 2015. Cell dynamics and gene expression control in tissue homeostasis and development. *Mol Syst Biol,* 11**,** 792.
SAEED, K., OSTLING, P., BJORKMAN, M., MIRTTI, T., ALANEN, K., VESTERINEN, T., SANKILA, A., LUNDIN, J., LUNDIN, M., RANNIKKO, A., NORDLING, S., MPINDI, J. P., KOHONEN, P., ILJIN, K., KALLIONIEMI, O. & RANTALA, J. K. 2015. Androgen receptor-interacting protein HSPBAP1 facilitates growth of prostate cancer cells in androgen-deficient conditions. *Int J Cancer,* 136**,** 2535-45.

SAMPLE, P. J., KORENY, L., PARIS, Z., GASTON, K. W., RUBIO, M. A., FLEMING, I. M., HINGER, S., HORAKOVA, E., LIMBACH, P. A., LUKES, J. & ALFONZO, J. D. 2015. A common tRNA modification at an unusual location: the discovery of wyosine biosynthesis in mitochondria. *Nucleic Acids Res,* 43**,** 4262-73.
SARENEVA, T., PIRHONEN, J., CANTELL, K. & JULKUNEN, I. 1995. N-glycosylation of human interferon-gamma: glycans at Asn-25 are critical for protease resistance. *Biochem J,* 308 (Pt 1)**,** 9-14.
SASAKI, T., MAIER, B., KOCLEGA, K. D., CHRUSZCZ, M., GLUBA, W., STUKENBERG, P. T., MINOR, W. & SCRABLE, H. 2008. Phosphorylation regulates SIRT1 function. *PLoS One,* 3**,** e4020.
SATYANARAYANA, A. & KALDIS, P. 2009. Mammalian cell-cycle regulation: several Cdks, numerous cyclins and diverse compensatory mechanisms. *Oncogene,* 28**,** 2925-39.
SAZUKA, T., KINOSHITA, M., TOMOOKA, Y., IKAWA, Y., NODA, M. & KUMAR, S. 1992. Expression of DRG during murine embryonic development. *Biochem Biophys Res Commun,* 189**,** 371-7.
SCHELLHAUS, A. K., MORENO-ANDRES, D., CHUGH, M., YOKOYAMA, H., MOSCHOPOULOU, A., DE, S., BONO, F., HIPP, K., SCHAFFER, E. & ANTONIN, W. 2017. Developmentally Regulated GTP binding protein 1 (DRG1) controls microtubule dynamics. *Sci Rep,* 7**,** 9996.
SCHENKER, T., LACH, C., KESSLER, B., CALDERARA, S. & TRUEB, B. 1994. A novel GTP-binding protein which is selectively repressed in SV40 transformed fibroblasts. *J Biol Chem,* 269**,** 25447-53.
SCHOFIELD, C. J. & RATCLIFFE, P. J. 2004. Oxygen sensing by HIF hydroxylases. *Nat Rev Mol Cell Biol,* 5**,** 343-54.
SEDGWICK, B. 2004. Repairing DNA-methylation damage. *Nat Rev Mol Cell Biol,* 5**,** 148-57.
SEPE, P. S., LAHOUSSE, S. A., GEMELLI, B., CHANG, H., MAEDA, T., WANDS, J. R. & DE LA MONTE, S. M. 2002. Role of the aspartyl-asparaginyl-beta-hydroxylase gene in neuroblastoma cell motility. *Lab Invest,* 82**,** 881-91.
SHAH, R., SMITH, P., PURDIE, C., QUINLAN, P., BAKER, L., AMAN, P., THOMPSON, A. M. & CROOK, T. 2009. The prolyl 3-hydroxylases P3H2 and P3H3 are novel targets for epigenetic silencing in breast cancer. *Br J Cancer,* 100**,** 1687-96.
SHARMA, A., SINGH, K. & ALMASAN, A. 2012. Histone H2AX phosphorylation: a marker for DNA damage. *Methods Mol Biol,* 920**,** 613-26.
SHARMA, S., KELLY, T. K. & JONES, P. A. 2010. Epigenetics in cancer. *Carcinogenesis,* 31**,** 27-36.
SHEN, J., XIANG, X., CHEN, L., WANG, H., WU, L., SUN, Y., MA, L., GU, X., LIU, H., WANG, L., YU, Y. N., SHAO, J., HUANG, C. & CHIN, Y. E. 2017. JMJD5 cleaves monomethylated histone H3 N-tail under DNA damaging stress. *EMBO Rep,* 18**,** 2131-2143.
SHI, Y., LAN, F., MATSON, C., MULLIGAN, P., WHETSTINE, J. R., COLE, P. A., CASERO, R. A. & SHI, Y. 2004. Histone demethylation mediated by the nuclear amine oxidase homolog LSD1. *Cell,* 119**,** 941-53.
SHIMADA, K., NAKAMURA, M., ANAI, S., DE VELASCO, M., TANAKA, M., TSUJIKAWA, K., OUJI, Y. & KONISHI, N. 2009. A novel human AlkB homologue, ALKBH8, contributes to human bladder cancer progression. *Cancer Res,* 69**,** 3157-64.
SHOULDERS, M. D. & RAINES, R. T. 2009. Collagen structure and stability. *Annu Rev Biochem,* 78**,** 929-58.
SHPARGEL, K. B., SENGOKU, T., YOKOYAMA, S. & MAGNUSON, T. 2012. UTX and UTY demonstrate histone demethylase-independent function in mouse embryonic development. *PLoS Genet,* 8**,** e1002964.
SILVERA, D., FORMENTI, S. C. & SCHNEIDER, R. J. 2010. Translational control in cancer. *Nat Rev Cancer,* 10**,** 254-66.
SINGH, B. & EYRAS, E. 2017. The role of alternative splicing in cancer. *Transcription,* 8**,** 91-98.
SINGLETON, R. S., LIU-YI, P., FORMENTI, F., GE, W., SEKIRNIK, R., FISCHER, R., ADAM, J., POLLARD, P. J., WOLF, A., THALHAMMER, A., LOENARZ, C., FLASHMAN, E., YAMAMOTO, A., COLEMAN, M. L., KESSLER, B. M., WAPPNER, P., SCHOFIELD, C. J., RATCLIFFE, P. J. & COCKMAN, M. E. 2014. OGFOD1

catalyzes prolyl hydroxylation of RPS23 and is involved in translation control and stress granule formation. *Proc Natl Acad Sci U S A,* 111**,** 4031-6.
SINHA, K. M., YASUDA, H., COOMBES, M. M., DENT, S. Y. & DE CROMBRUGGHE, B. 2010. Regulation of the osteoblast-specific transcription factor Osterix by NO66, a Jumonji family histone demethylase. *Embo j,* 29**,** 68-79.
SONG, C., CHANG, X. J., BEAN, K. M., PROIA, M. S., KNOPF, J. L. & KRIZ, R. W. 1999. Molecular characterization of cytosolic phospholipase A2-beta. *J Biol Chem,* 274**,** 17063-7.
SONG, H., KIM, S. I., KO, M. S., KIM, H. J., HEO, J. C., LEE, H. J., LEE, H. S., HAN, I. S., KWACK, K. & PARK, J. W. 2004a. Overexpression of DRG2 increases G2/M phase cells and decreases sensitivity to nocodazole-induced apoptosis. *J Biochem,* 135**,** 331-5.
SONG, J., HONG, P., LIU, C., ZHANG, Y., WANG, J. & WANG, P. 2015. Human POLD1 modulates cell cycle progression and DNA damage repair. *BMC Biochem,* 16**,** 14.
SONG, Y., KESUMA, D., WANG, J., DENG, Y., DUAN, J., WANG, J. H. & QI, R. Z. 2004b. Specific inhibition of cyclin-dependent kinases and cell proliferation by harmine. *Biochem Biophys Res Commun,* 317**,** 128-32.
SONG, Y., ZHENG, S., WANG, J., LONG, H., FANG, L., WANG, G., LI, Z., QUE, T., LIU, Y., LI, Y., ZHANG, X., FANG, W. & QI, S. 2017. Hypoxia-induced PLOD2 promotes proliferation, migration and invasion via PI3K/Akt signaling in glioma. *Oncotarget,* 8**,** 41947-41962.
SONGE-MOLLER, L., VAN DEN BORN, E., LEIHNE, V., VAGBO, C. B., KRISTOFFERSEN, T., KROKAN, H. E., KIRPEKAR, F., FALNES, P. O. & KLUNGLAND, A. 2010. Mammalian ALKBH8 possesses tRNA methyltransferase activity required for the biogenesis of multiple wobble uridine modifications implicated in translational decoding. *Mol Cell Biol,* 30**,** 1814-27.
STENFLO, J., HOLME, E., LINDSTEDT, S., CHANDRAMOULI, N., HUANG, L. H., TAM, J. P. & MERRIFIELD, R. B. 1989. Hydroxylation of aspartic acid in domains homologous to the epidermal growth factor precursor is catalyzed by a 2-oxoglutarate-dependent dioxygenase. *Proc Natl Acad Sci U S A,* 86**,** 444-7.
STEVENSON-LINDERT, L. M., FOWLER, P. & LEW, J. 2003. Substrate specificity of CDK2-cyclin A. What is optimal? *J Biol Chem,* 278**,** 50956-60.
STRATTON, M. R., CAMPBELL, P. J. & FUTREAL, P. A. 2009. The cancer genome. *Nature,* 458**,** 719-24.
SU, P., WEN, S., ZHANG, Y., LI, Y., XU, Y., ZHU, Y., LV, H., ZHANG, F., WANG, M. & TIAN, Z. 2016. Identification of the Key Genes and Pathways in Esophageal Carcinoma. *Gastroenterol Res Pract,* 2016**,** 2968106.
SUN, L., HUANG, Y., WEI, Q., TONG, X., CAI, R., NALEPA, G. & YE, X. 2015. Cyclin E-CDK2 protein phosphorylates plant homeodomain finger protein 8 (PHF8) and regulates its function in the cell cycle. *J Biol Chem,* 290**,** 4075-85.
SUPEK, F., MINANA, B., VALCARCEL, J., GABALDON, T. & LEHNER, B. 2014. Synonymous mutations frequently act as driver mutations in human cancers. *Cell,* 156**,** 1324-1335.
SUZUKI, K., SAKO, K., AKIYAMA, K., ISODA, M., SENOO, C., NAKAJO, N. & SAGATA, N. 2015. Identification of non-Ser/Thr-Pro consensus motifs for Cdk1 and their roles in mitotic regulation of C2H2 zinc finger proteins and Ect2. *Sci Rep,* 5**,** 7929.
SUZUKI, T., MINEHATA, K., AKAGI, K., JENKINS, N. A. & COPELAND, N. G. 2006. Tumor suppressor gene identification using retroviral insertional mutagenesis in Blm-deficient mice. *EMBO J,* 25**,** 3422-31.
SWAFFER, M. P., JONES, A. W., FLYNN, H. R., SNIJDERS, A. P. & NURSE, P. 2016. CDK Substrate Phosphorylation and Ordering the Cell Cycle. *Cell,* 167**,** 1750-1761 e16.
TAHILIANI, M., KOH, K. P., SHEN, Y., PASTOR, W. A., BANDUKWALA, H., BRUDNO, Y., AGARWAL, S., IYER, L. M., LIU, D. R., ARAVIND, L. & RAO, A. 2009. Conversion of 5-methylcytosine to 5-hydroxymethylcytosine in mammalian DNA by MLL partner TET1. *Science,* 324**,** 930-5.

TAIRA, N., NIHIRA, K., YAMAGUCHI, T., MIKI, Y. & YOSHIDA, K. 2007. DYRK2 is targeted to the nucleus and controls p53 via Ser46 phosphorylation in the apoptotic response to DNA damage. *Mol Cell,* 25**,** 725-38.
TAIRA, N. & YOSHIDA, K. 2012. Post-translational modifications of p53 tumor suppressor: determinants of its functional targets. *Histol Histopathol,* 27**,** 437-43.
TAKALUOMA, K., HYRY, M., LANTTO, J., SORMUNEN, R., BANK, R. A., KIVIRIKKO, K. I., MYLLYHARJU, J. & SOININEN, R. 2007. Tissue-specific changes in the hydroxylysine content and cross-links of collagens and alterations in fibril morphology in lysyl hydroxylase 1 knock-out mice. *J Biol Chem,* 282**,** 6588-96.
TAKEDA, D. Y., WOHLSCHLEGEL, J. A. & DUTTA, A. 2001. A bipartite substrate recognition motif for cyclin-dependent kinases. *J Biol Chem,* 276**,** 1993-7.
TAKEUCHI, T., YAMAZAKI, Y., KATOH-FUKUI, Y., TSUCHIYA, R., KONDO, S., MOTOYAMA, J. & HIGASHINAKAGAWA, T. 1995. Gene trap capture of a novel mouse gene, jumonji, required for neural tube formation. *Genes Dev,* 9**,** 1211-22.
TAN, X. P., DONG, W. G., ZHANG, Q., YANG, Z. R., LEI, X. F. & AI, M. H. 2014. Potential effects of Mina53 on tumor growth in human pancreatic cancer. *Cell Biochem Biophys,* 69**,** 619-25.
TEYE, K., TSUNEOKA, M., ARIMA, N., KODA, Y., NAKAMURA, Y., UETA, Y., SHIROUZU, K. & KIMURA, H. 2004. Increased expression of a Myc target gene Mina53 in human colon cancer. *Am J Pathol,* 164**,** 205-16.
THAKUR, C., WOLFARTH, M., SUN, J., ZHANG, Y., LU, Y., BATTELLI, L., PORTER, D. W. & CHEN, F. 2015. Oncoprotein mdig contributes to silica-induced pulmonary fibrosis by altering balance between Th17 and Treg T cells. *Oncotarget,* 6**,** 3722-36.
THE UNIPROT, C. 2017. UniProt: the universal protein knowledgebase. *Nucleic Acids Res,* 45**,** D158-D169.
THEODOSIOU, A. & ASHWORTH, A. 2002. MAP kinase phosphatases. *Genome Biol,* 3**,** REVIEWS3009.
TIAINEN, P., PASANEN, A., SORMUNEN, R. & MYLLYHARJU, J. 2008. Characterization of recombinant human prolyl 3-hydroxylase isoenzyme 2, an enzyme modifying the basement membrane collagen IV. *J Biol Chem,* 283**,** 19432-9.
TIAN, Y. M., MOLE, D. R., RATCLIFFE, P. J. & GLEADLE, J. M. 2006. Characterization of different isoforms of the HIF prolyl hydroxylase PHD1 generated by alternative initiation. *Biochem J,* 397**,** 179-86.
TIBBETTS, R. S., CORTEZ, D., BRUMBAUGH, K. M., SCULLY, R., LIVINGSTON, D., ELLEDGE, S. J. & ABRAHAM, R. T. 2000. Functional interactions between BRCA1 and the checkpoint kinase ATR during genotoxic stress. *Genes Dev,* 14**,** 2989-3002.
TONG, W. G., CHEN, R., PLUNKETT, W., SIEGEL, D., SINHA, R., HARVEY, R. D., BADROS, A. Z., POPPLEWELL, L., COUTRE, S., FOX, J. A., MAHADOCON, K., CHEN, T., KEGLEY, P., HOCH, U. & WIERDA, W. G. 2010. Phase I and pharmacologic study of SNS-032, a potent and selective Cdk2, 7, and 9 inhibitor, in patients with advanced chronic lymphocytic leukemia and multiple myeloma. *J Clin Oncol,* 28**,** 3015-22.
TREWICK, S. C., HENSHAW, T. F., HAUSINGER, R. P., LINDAHL, T. & SEDGWICK, B. 2002. Oxidative demethylation by Escherichia coli AlkB directly reverts DNA base damage. *Nature,* 419**,** 174-8.
TSAI, C. K., HUANG, L. C., TSAI, W. C., HUANG, S. M., LEE, J. T. & HUENG, D. Y. 2018. Overexpression of PLOD3 promotes tumor progression and poor prognosis in gliomas. *Oncotarget,* 9**,** 15705-15720.
TSUKADA, Y., FANG, J., ERDJUMENT-BROMAGE, H., WARREN, M. E., BORCHERS, C. H., TEMPST, P. & ZHANG, Y. 2006. Histone demethylation by a family of JmjC domain-containing proteins. *Nature,* 439**,** 811-6.
TSUKADA, Y., ISHITANI, T. & NAKAYAMA, K. I. 2010. KDM7 is a dual demethylase for histone H3 Lys 9 and Lys 27 and functions in brain development. *Genes Dev,* 24**,** 432-7.

TSUNEOKA, M., FUJITA, H., ARIMA, N., TEYE, K., OKAMURA, T., INUTSUKA, H., KODA, Y., SHIROUZU, K. & KIMURA, H. 2004. Mina53 as a potential prognostic factor for esophageal squamous cell carcinoma. *Clin Cancer Res,* 10**,** 7347-56.
TSUNEOKA, M., KODA, Y., SOEJIMA, M., TEYE, K. & KIMURA, H. 2002. A novel myc target gene, mina53, that is involved in cell proliferation. *J Biol Chem,* 277**,** 35450-9.
TUMINI, E., BARROSO, S., CALERO, C. P. & AGUILERA, A. 2016. Roles of human POLD1 and POLD3 in genome stability. *Sci Rep,* 6**,** 38873.
TURNER, B. M. 2012. The adjustable nucleosome: an epigenetic signaling module. *Trends Genet,* 28**,** 436-44.
UNOKI, M., MASUDA, A., DOHMAE, N., ARITA, K., YOSHIMATSU, M., IWAI, Y., FUKUI, Y., UEDA, K., HAMAMOTO, R., SHIRAKAWA, M., SASAKI, H. & NAKAMURA, Y. 2013. Lysyl 5-hydroxylation, a novel histone modification, by Jumonji domain containing 6 (JMJD6). *J Biol Chem,* 288**,** 6053-62.
VAN BUGGENHOUT, G., VAN RAVENSWAAIJ-ARTS, C., MC MAAS, N., THOELEN, R., VOGELS, A., SMEETS, D., SALDEN, I., MATTHIJS, G., FRYNS, J. P. & VERMEESCH, J. R. 2005. The del(2)(q32.2q33) deletion syndrome defined by clinical and molecular characterization of four patients. *Eur J Med Genet,* 48**,** 276-89.
VAN DER HEIDE, L. P., HOEKMAN, M. F. & SMIDT, M. P. 2004. The ins and outs of FoxO shuttling: mechanisms of FoxO translocation and transcriptional regulation. *Biochem J,* 380**,** 297-309.
VAN DER KELEN, K., BEYAERT, R., INZE, D. & DE VEYLDER, L. 2009. Translational control of eukaryotic gene expression. *Crit Rev Biochem Mol Biol,* 44**,** 143-68.
VAN DER SLOT, A. J., ZUURMOND, A. M., BARDOEL, A. F., WIJMENGA, C., PRUIJS, H. E., SILLENCE, D. O., BRINCKMANN, J., ABRAHAM, D. J., BLACK, C. M., VERZIJL, N., DEGROOT, J., HANEMAAIJER, R., TEKOPPELE, J. M., HUIZINGA, T. W. & BANK, R. A. 2003. Identification of PLOD2 as telopeptide lysyl hydroxylase, an important enzyme in fibrosis. *J Biol Chem,* 278**,** 40967-72.
VARJOSALO, M., KESKITALO, S., VAN DROGEN, A., NURKKALA, H., VICHALKOVSKI, A., AEBERSOLD, R. & GSTAIGER, M. 2013. The protein interaction landscape of the human CMGC kinase group. *Cell Rep,* 3**,** 1306-20.
VASSILEV, L. T. 2006. Cell cycle synchronization at the G2/M phase border by reversible inhibition of CDK1. *Cell Cycle,* 5**,** 2555-6.
VASSILEV, L. T., TOVAR, C., CHEN, S., KNEZEVIC, D., ZHAO, X., SUN, H., HEIMBROOK, D. C. & CHEN, L. 2006. Selective small-molecule inhibitor reveals critical mitotic functions of human CDK1. *Proc Natl Acad Sci U S A,* 103**,** 10660-5.
VOGELSTEIN, B., PAPADOPOULOS, N., VELCULESCU, V. E., ZHOU, S., DIAZ, L. A., JR. & KINZLER, K. W. 2013. Cancer genome landscapes. *Science,* 339**,** 1546-58.
VRANKA, J. A., SAKAI, L. Y. & BACHINGER, H. P. 2004. Prolyl 3-hydroxylase 1, enzyme characterization and identification of a novel family of enzymes. *J Biol Chem,* 279**,** 23615-21.
VUONG, H., CHENG, F., LIN, C. C. & ZHAO, Z. 2014. Functional consequences of somatic mutations in cancer using protein pocket-based prioritization approach. *Genome Med,* 6**,** 81.
WALPORT, L. J., HOPKINSON, R. J., CHOWDHURY, R., SCHILLER, R., GE, W., KAWAMURA, A. & SCHOFIELD, C. J. 2016. Arginine demethylation is catalysed by a subset of JmjC histone lysine demethylases. *Nat Commun,* 7**,** 11974.
WALPORT, L. J., HOPKINSON, R. J., VOLLMAR, M., MADDEN, S. K., GILEADI, C., OPPERMANN, U., SCHOFIELD, C. J. & JOHANSSON, C. 2014. Human UTY(KDM6C) is a male-specific N-methyl lysyl demethylase. *J Biol Chem,* 289**,** 18302-13.
WANG, C., ZHANG, Q., HANG, T., TAO, Y., MA, X., WU, M., ZHANG, X. & ZANG, J. 2015a. Structure of the JmjC domain-containing protein NO66 complexed with ribosomal protein Rpl8. *Acta Crystallogr D Biol Crystallogr,* 71**,** 1955-64.
WANG, D., ZHANG, S. & CHEN, F. 2018. High Expression of PLOD1 Drives Tumorigenesis and Affects Clinical Outcome in Gastrointestinal Carcinoma. *Genet Test Mol Biomarkers,* 22**,** 366-373.

WANG, F., HE, L., HUANGYANG, P., LIANG, J., SI, W., YAN, R., HAN, X., LIU, S., GUI, B., LI, W., MIAO, D., JING, C., LIU, Z., PEI, F., SUN, L. & SHANG, Y. 2014. JMJD6 promotes colon carcinogenesis through negative regulation of p53 by hydroxylation. *PLoS Biol,* 12**,** e1001819.
WANG, H., HAN, H., MOUSSES, S. & VON HOFF, D. D. 2006. Targeting loss-of-function mutations in tumor-suppressor genes as a strategy for development of cancer therapeutic agents. *Semin Oncol,* 33**,** 513-20.
WANG, J., XU, X., LIU, Z., WEI, X., ZHUANG, R., LU, D., ZHOU, L., XIE, H. & ZHENG, S. 2013. LEPREL1 Expression in Human Hepatocellular Carcinoma and Its Suppressor Role on Cell Proliferation. *Gastroenterol Res Pract,* 2013**,** 109759.
WANG, X., ZHAO, B. S., ROUNDTREE, I. A., LU, Z., HAN, D., MA, H., WENG, X., CHEN, K., SHI, H. & HE, C. 2015b. N(6)-methyladenosine Modulates Messenger RNA Translation Efficiency. *Cell,* 161**,** 1388-99.
WEBB, J. D., COLEMAN, M. L. & PUGH, C. W. 2009. Hypoxia, hypoxia-inducible factors (HIF), HIF hydroxylases and oxygen sensing. *Cell Mol Life Sci,* 66**,** 3539-54.
WEBBY, C. J., WOLF, A., GROMAK, N., DREGER, M., KRAMER, H., KESSLER, B., NIELSEN, M. L., SCHMITZ, C., BUTLER, D. S., YATES, J. R., 3RD, DELAHUNTY, C. M., HAHN, P., LENGELING, A., MANN, M., PROUDFOOT, N. J., SCHOFIELD, C. J. & BOTTGER, A. 2009. Jmjd6 catalyses lysyl-hydroxylation of U2AF65, a protein associated with RNA splicing. *Science,* 325**,** 90-3.
WEI, D., YAO, J., YANG, X., CHENG, L., LU, D. & XUE, J. 2004. Molecular cloning and expression of two closely related GTP-binding proteins from zebrafish. *DNA Seq,* 15**,** 246-50.
WESTBYE, M. P., FEYZI, E., AAS, P. A., VAGBO, C. B., TALSTAD, V. A., KAVLI, B., HAGEN, L., SUNDHEIM, O., AKBARI, M., LIABAKK, N. B., SLUPPHAUG, G., OTTERLEI, M. & KROKAN, H. E. 2008. Human AlkB homolog 1 is a mitochondrial protein that demethylates 3-methylcytosine in DNA and RNA. *J Biol Chem,* 283**,** 25046-56.
WILKINS, S. E., ISLAM, M. S., GANNON, J. M., MARKOLOVIC, S., HOPKINSON, R. J., GE, W., SCHOFIELD, C. J. & CHOWDHURY, R. 2018. JMJD5 is a human arginyl C-3 hydroxylase. *Nat Commun,* 9**,** 1180.
WILKINSON, B. & GILBERT, H. F. 2004. Protein disulfide isomerase. *Biochim Biophys Acta,* 1699**,** 35-44.
WILLIAMS, S. T., WALPORT, L. J., HOPKINSON, R. J., MADDEN, S. K., CHOWDHURY, R., SCHOFIELD, C. J. & KAWAMURA, A. 2014. Studies on the catalytic domains of multiple JmjC oxygenases using peptide substrates. *Epigenetics,* 9**,** 1596-603.
WINSLOW, S., LINDQUIST, K. E., EDSJO, A. & LARSSON, C. 2016. The expression pattern of matrix-producing tumor stroma is of prognostic importance in breast cancer. *BMC Cancer,* 16**,** 841.
WOHLSCHLEGEL, J. A., DWYER, B. T., TAKEDA, D. Y. & DUTTA, A. 2001. Mutational analysis of the Cy motif from p21 reveals sequence degeneracy and specificity for different cyclin-dependent kinases. *Mol Cell Biol,* 21**,** 4868-74.
WOLF, A., MANTRI, M., HEIM, A., MULLER, U., FICHTER, E., MACKEEN, M. M., SCHERMELLEH, L., DADIE, G., LEONHARDT, H., VENIEN-BRYAN, C., KESSLER, B. M., SCHOFIELD, C. J. & BOTTGER, A. 2013. The polyserine domain of the lysyl-5 hydroxylase Jmjd6 mediates subnuclear localization. *Biochem J,* 453**,** 357-70.
WOUT, P. K., SATTLEGGER, E., SULLIVAN, S. M. & MADDOCK, J. R. 2009. Saccharomyces cerevisiae Rbg1 protein and its binding partner Gir2 interact on Polyribosomes with Gcn1. *Eukaryot Cell,* 8**,** 1061-71.
WOUTERS, M. A., RIGOUTSOS, I., CHU, C. K., FENG, L. L., SPARROW, D. B. & DUNWOODIE, S. L. 2005. Evolution of distinct EGF domains with specific functions. *Protein Sci,* 14**,** 1091-103.
WU, B. H., CHEN, H., CAI, C. M., FANG, J. Z., WU, C. C., HUANG, L. Y., WANG, L. & HAN, Z. G. 2016. Epigenetic silencing of JMJD5 promotes the proliferation of hepatocellular carcinoma cells by down-regulating the transcription of CDKN1A 686. *Oncotarget,* 7**,** 6847-63.

WU, T. F., YAO, Y. L., LAI, I. L., LAI, C. C., LIN, P. L. & YANG, W. M. 2015. Loading of PAX3 to Mitotic Chromosomes Is Mediated by Arginine Methylation and Associated with Waardenburg Syndrome. *J Biol Chem,* 290**,** 20556-64.
WYNDER, C., STALKER, L. & DOUGHTY, M. L. 2010. Role of H3K4 demethylases in complex neurodevelopmental diseases. *Epigenomics,* 2**,** 407-18.
XI, Z. Q., SUN, J. J., WANG, X. F., LI, M. W., LIU, X. Z., WANG, L. Y., ZHU, X., XIAO, F., LI, J. M., GONG, Y. & GUAN, L. F. 2007. HSPBAP1 is found extensively in the anterior temporal neocortex of patients with intractable epilepsy. *Synapse,* 61**,** 741-7.
XI, Z. Q., XIAO, F., YUAN, J., WANG, X. F., WANG, L., QUAN, F. Y. & LIU, G. W. 2009. Gene expression analysis on anterior temporal neocortex of patients with intractable epilepsy. *Synapse,* 63**,** 1017-28.
XIE, L., PI, X., MISHRA, A., FONG, G., PENG, J. & PATTERSON, C. 2012. PHD3-dependent hydroxylation of HCLK2 promotes the DNA damage response. *J Clin Invest,* 122**,** 2827-36.
XIONG, G., DENG, L., ZHU, J., RYCHAHOU, P. G. & XU, R. 2014. Prolyl-4-hydroxylase alpha subunit 2 promotes breast cancer progression and metastasis by regulating collagen deposition. *BMC Cancer,* 14**,** 1.
XU, Y., ZHANG, L., WEI, Y., ZHANG, X., XU, R., HAN, M., HUANG, B., CHEN, A., LI, W., ZHANG, Q., LI, G., WANG, J., ZHAO, P. & LI, X. 2017. Procollagen-lysine 2-oxoglutarate 5-dioxygenase 2 promotes hypoxia-induced glioma migration and invasion. *Oncotarget,* 8**,** 23401-23413.
XUE, L. & TAO, W. A. 2013. Current technologies to identify protein kinase substrates in high throughput. *Front Biol (Beijing),* 8**,** 216-227.
YANAGIHARA, T., TOMINO, T., URUNO, T. & FUKUI, Y. 2017. Thymic epithelial cell-specific deletion of Jmjd6 reduces Aire protein expression and exacerbates disease development in a mouse model of autoimmune diabetes. *Biochem Biophys Res Commun,* 489**,** 8-13.
YANG, M., SU, H., SOGA, T., KRANC, K. R. & POLLARD, P. J. 2014. Prolyl hydroxylase domain enzymes: important regulators of cancer metabolism. *Hypoxia (Auckl),* 2**,** 127-142.
YANG, S., ZHANG, L., LIU, M., CHONG, R., DING, S. J., CHEN, Y. & DONG, J. 2013. CDK1 phosphorylation of YAP promotes mitotic defects and cell motility and is essential for neoplastic transformation. *Cancer Res,* 73**,** 6722-33.
YANG, Z., ZHUANG, L., SZATMARY, P., WEN, L., SUN, H., LU, Y., XU, Q. & CHEN, X. 2015. Upregulation of heat shock proteins (HSPA12A, HSP90B1, HSPA4, HSPA5 and HSPA6) in tumour tissues is associated with poor outcomes from HBV-related early-stage hepatocellular carcinoma. *Int J Med Sci,* 12**,** 256-63.
YEO, K. S., TAN, M. C., LIM, Y. Y. & EA, C. K. 2017. JMJD8 is a novel endoplasmic reticulum protein with a JmjC domain. *Sci Rep,* 7**,** 15407.
YEO, K. S., TAN, M. C., WONG, W. Y., LOH, S. W., LAM, Y. L., TAN, C. L., LIM, Y. Y. & EA, C. K. 2016. JMJD8 is a positive regulator of TNF-induced NF-kappaB signaling. *Sci Rep,* 6**,** 34125.
YEOWELL, H. N. & WALKER, L. C. 1999. Tissue specificity of a new splice form of the human lysyl hydroxylase 2 gene. *Matrix Biol,* 18**,** 179-87.
YOO, H., SON, D., LEE, Y. J. & HONG, K. 2016. Mouse JMJD4 is dispensable for embryogenesis. *Mol Reprod Dev,* 83**,** 588-93.
YOSEF, N., SHALEK, A. K., GAUBLOMME, J. T., JIN, H., LEE, Y., AWASTHI, A., WU, C., KARWACZ, K., XIAO, S., JORGOLLI, M., GENNERT, D., SATIJA, R., SHAKYA, A., LU, D. Y., TROMBETTA, J. J., PILLAI, M. R., RATCLIFFE, P. J., COLEMAN, M. L., BIX, M., TANTIN, D., PARK, H., KUCHROO, V. K. & REGEV, A. 2013. Dynamic regulatory network controlling TH17 cell differentiation. *Nature,* 496**,** 461-8.
YOUN, M. Y., YOKOYAMA, A., FUJIYAMA-NAKAMURA, S., OHTAKE, F., MINEHATA, K., YASUDA, H., SUZUKI, T., KATO, S. & IMAI, Y. 2012. JMJD5, a Jumonji C (JmjC) domain-containing protein, negatively regulates osteoclastogenesis by facilitating NFATc1 protein degradation. *J Biol Chem,* 287**,** 12994-3004.
YU, M., SUN, J., THAKUR, C., CHEN, B., LU, Y., ZHAO, H. & CHEN, F. 2014. Paradoxical roles of mineral dust induced gene on cell proliferation and migration/invasion. *PLoS One,* 9**,** e87998.

ZEESTRATEN, E. C., MAAK, M., SHIBAYAMA, M., SCHUSTER, T., NITSCHE, U., MATSUSHIMA, T., NAKAYAMA, S., GOHDA, K., FRIESS, H., VAN DE VELDE, C. J., ISHIHARA, H., ROSENBERG, R., KUPPEN, P. J. & JANSSEN, K. P. 2012. Specific activity of cyclin-dependent kinase I is a new potential predictor of tumour recurrence in stage II colon cancer. *Br J Cancer,* 106**,** 133-40.
ZENG, X., CHEN, S. & HUANG, H. 2011. Phosphorylation of EZH2 by CDK1 and CDK2: a possible regulatory mechanism of transmission of the H3K27me3 epigenetic mark through cell divisions. *Cell Cycle,* 10**,** 579-83.
ZHANG, J., NI, S. S., ZHAO, W. L., DONG, X. C. & WANG, J. L. 2013. High expression of JMJD6 predicts unfavorable survival in lung adenocarcinoma. *Tumour Biol,* 34**,** 2397-401.
ZHANG, R., HUANG, Q., LI, Y., SONG, Y. & LI, Y. 2015. JMJD5 is a potential oncogene for colon carcinogenesis. *Int J Clin Exp Pathol,* 8**,** 6482-9.
ZHAO, X. F. & APLAN, P. D. 1998. SCL binds the human homologue of DRG in vivo. *Biochim Biophys Acta,* 1448**,** 109-14.
ZHAO, Y., BRICKNER, J. R., MAJID, M. C. & MOSAMMAPARAST, N. 2014. Crosstalk between ubiquitin and other post-translational modifications on chromatin during double-strand break repair. *Trends Cell Biol,* 24**,** 426-34.
ZHENG, G., DAHL, J. A., NIU, Y., FEDORCSAK, P., HUANG, C. M., LI, C. J., VAGBO, C. B., SHI, Y., WANG, W. L., SONG, S. H., LU, Z., BOSMANS, R. P., DAI, Q., HAO, Y. J., YANG, X., ZHAO, W. M., TONG, W. M., WANG, X. J., BOGDAN, F., FURU, K., FU, Y., JIA, G., ZHAO, X., LIU, J., KROKAN, H. E., KLUNGLAND, A., YANG, Y. G. & HE, C. 2013. ALKBH5 is a mammalian RNA demethylase that impacts RNA metabolism and mouse fertility. *Mol Cell,* 49**,** 18-29.
ZHOU, L., LI, J., ZHAO, Y. P., CUI, Q. C., ZHOU, W. X., GUO, J. C., YOU, L., WU, W. M. & ZHANG, T. P. 2014. The prognostic value of Cyclin B1 in pancreatic cancer. *Med Oncol,* 31**,** 107.
ZHOU, Y., JIN, G., MI, R., ZHANG, J., ZHANG, J., XU, H., CHENG, S., ZHANG, Y., SONG, W. & LIU, F. 2017. Knockdown of P4HA1 inhibits neovascularization via targeting glioma stem cell-endothelial cell transdifferentiation and disrupting vascular basement membrane. *Oncotarget,* 8**,** 35877-35889.